Biomechanics of Limb Prostheses Directly Attached to Bone

Lindsay Kathleen Newcombe

University College London

A dissertation submitted in fulfilment of the requirements for the degree of

Doctor of Philosophy of the University of London

September 2008

ProQuest LLC
789 East Eisenhower Parkway
P.O. Box 1346
Ann Arbor, MI 48106-1346

I, Lindsay Kathleen Newcombe, confirm that the work presented in this thesis is my own. Where information has been derived from other sources, I confirm that this has been indicated in the thesis.

Abstract

The technique of attaching a limb directly to the skeleton has clear benefits, when compared with socket-attachment, for the many amputees who encounter skin problems. A potential risk of attaching a limb to the skeleton is the wound where the implant breaches the skin. At the Centre for Biomedical Engineering in the Institute of Orthopædics and Musculoskeletal Science at UCL, a method has been devised which enhances epithelial attachment to the implant, resisting infection, and this has been used to develop a system for attaching a limb to the skeleton: *Intraosseous Transcutaneous Amputation Prosthesis*, or ITAP.

In a transfemoral prosthesis, protection of bone from external loading is anticipated and in this thesis a fail-safe component is designed to prevent fracture. It has adjustable activation levels and has been tested to the appropriate International Standards. In order to determine loads that are to be allowed and prevented, normal loading of the femur during ordinary activities is researched failure modes of femoral bone are investigated.

Finite element analysis is employed to investigate the stress distribution throughout the femur with the attachment of a prosthetic leg. A cylindrical model is used to assess the effect of varying geometry and material properties of the bone and implant. An anatomical model, derived from a CT scan, is used to analyse the effect of stump length.

There are three risk groups that the amputee can be allocated depending on the level of amputation, the size of the bone, and the amount of bone contact with the implant. At the beginning of rehabilitation the fail-safe is set low to protect the poorer bone and bone-implant interface. The settings are gradually increased during rehabilitation to 60Nm, 80Nm or 100Nm in bending and 10Nm, 15Nm and 25Nm in torsion for high, medium and low risk amputees respectively.

Acknowledgments

I am privileged to have been surrounded by intelligent, friendly and helpful people at the Centre for Biomedical Engineering and the Department of Mechanical Engineering. Thank you to all who have helped me to finish this work.

Dr Mike Dewar

Mike, I am grateful to you for your support as my tutor when I was an undergraduate and for your patience in sticking with me until I finished writing this thesis. Also, thank you for devising the excellent course that attracted me to UCL in the first place. It must be just about time for that retirement now...

Dr Paul Fromme

Paul, thank you for adopting me and being my supervisor. Your clear way of thinking has helped me to examine my work critically, and has inspired me to be more thoughtful and thorough.

Professor Gordon Blunn

Gordon, you have given me confidence by your deep understanding of a vast range of topics. You care for your students exhaustively, thank you for your encouragement.

Mr Keith Rayner

Keith, you are dependable and your logical way of thinking has prevented me getting excessively muddled. Thank you for making my 'bits' and then helping to mod them out of recognition, and for restoring my sight.

Mr Mark Harrison

Thank you to Mark for helping with setting-up my tests, and for lifts that prevented long cross-country journeys.

Acknowledgments

Dr Sunita Ahir

Sunita, thank you for teaching me how to use MARC, and for your companionship. I wish you all the best for your future.

Dr Kevin Drake

Thank you for setting me out on the path of FEA, and for your solid advice.

Dr Jay Meswania

Thank you, Jay, for all of your work with the calibration.

It has been a pleasure to work in the Zimmer lab: Thank you to: Jonathan for intelligent answers to questions, and unusual questions that beg answers; Carolina for your kindness and hot lunches; Elena for your smile and being a source of information about things biological; Sorousheh for your attentiveness and for not producing a sign to ban me; Kevin for reminding me that there is life out there; Michelle for crosswords and cake; Kunalun for encouraging my progress 'ehem'; Rohit for enlightening me in the ways of the NHS; and Priya for encouragement to just get up there an present something. Thank you to Haleh for the work you did while you were here. Anyone for a *Rich Tea*?

Thank you to Josie, Jarmilla and Annie, the steadfast secretarial team, always on-hand with stationery and friendly words.

To Mum and Dad, thank you for support of all kinds. You are such attentive parents, always ready to abandon yourselves and be there for me. I am deeply grateful for being your child.

To Andrew, my husband, thank you for consistently loving me. Thank you for supporting me in all this and in everything I do.

Contents

Contents

Contents

Contents

Contents

Contents

Figures

Figures

Figures

Figures

Figures

Figures

Figures

Figures

Figures

Figures

Figures

Figures

Tables

Tables

1 Introduction and Literature Review

1.1 Traditional Prosthetic Legs

Amputation of part of a leg is a profoundly disabling event. The senses, control and strength of the original leg are lost and, without assistance, the means for ambulation is removed. Mobility can be restored by the use of a wheelchair, crutches or a prosthetic leg. Prostheses are the method of choice for many amputees: they are versatile and look natural.

Prosthetic legs are designed to support the amputee's weight and dynamic loads as comfortably as possible and to facilitate ambulation. A prosthetic limb for a transfemoral amputation involves a foot component, shin, knee mechanism and a means for attaching to the body that dictates how the load is transmitted.

In general, amputees regard comfort and control as the most important features of a prosthetic leg (Czerniecki and Gitter, 1995; Klute *et al.*, 2001; Marks and Michael, 2001). The interface between the residual limb and the prosthesis is critical: it is the key to comfort and control (Haberman, 1995; Marks and Michael, 2001). Modern trans-femoral socket prostheses are kept on either by establishing a vacuum between the stump and the socket or with straps (Barsby, 1995; Michael, 1989). In both cases most of the load is taken through the *ischial tuberosity* (the part of the pelvis that takes the body's weight while sitting) and the soft tissue around the stump. This manner of loading requires the skin to bear the

body weight. Unlike the skin on the sole of the foot, the skin of the leg is not adapted to bear these loads.

It is a design requirement of sockets to have high friction against the skin in order to support the body weight during the stance phase of gait and prevent slipping of the prosthesis during the swing phase (Zhang *et al.*, 1996). Friction necessarily results in the application of a shear force to the skin which causes occlusion of blood flow (which may already be poor in the case of amputations that have been carried out due to vascular disease), it can also result in abrasion and sometimes breaking of the skin (Zhang *et al.*, 1996).

1.2 Direct Skeletal Attachment of Prostheses

To overcome the problems associated with the stump/socket interface, the idea of applying the load straight to the skeleton, *through* (as opposed to *across*) the skin, has clear attractions. The proposed benefits of skeletal attachment of a prosthetic leg are:

- skin problems and blood occlusion from a rubbing socket will be eliminated,
- the hip joint will no longer be obstructed by a solid socket, allowing free movement (Sullivan *et al.*, 2003),
- better control because the forces are no longer being transmitted through a cushion of soft tissue.

The first systems to explore the possibility of transcutaneous prosthetic implants were dental implants, which have become widely accepted and available (Adell *et al.*, 1990). An anchor that is designed to encourage bone growth for stability is implanted into the maxilla or mandible and, usually some time later, a prosthetic tooth is attached to it (Brånemark *et al.*, 1977). The attachment of bone to the anchor is regarded as the reason for long-term success of dental implants (Albrektsson, 1981). Dental implants hold some of the keys to

the biological aspects of direct-attached limb prostheses, as do percutaneous craniofacial prostheses (such as hearing aids) and epitheses (such as auricle replacements).

Extremity prostheses must withstand very different loading from craniofacial prostheses. A number of patents have been granted for percutaneous implant fixation for trans-humeral and trans-femoral amputations (Owens, 1976; Restwick *et al.*; 1979 Grundei, 2001; Grundei, 2002), and subsequently bone-anchored limb replacements have finally started to be researched, designed, and trialled. Three trans-femoral designs are currently being piloted and the technology has also been applied to arm, finger and maxillofacial prostheses.

1.2.1 Various Projects for Limb Attachment

The current design with the longest clinical experience has been developed at the University of Gothenburg, Sweden, in association with *Integrum AB*, Gothenburg (Sullivan *et al.*, 2003). The design is based on dental implants patented by Rickard Brånemark in 1977. The rehabilitation programme for this has been given the acronym OPRA (Osseointegrated Prosthesis for the Rehabilitation of Amputees). It was devised in 1990 and, as well as being piloted in Gothenburg, is used in two other centres: at Monash University in Melbourne and, since 1997, at the University of Surrey.

Another design is being developed at the University of Lübeck, Germany, in association with ESKA GmbH, Lübeck, Germany. The first 'Endo-Exo Prosthesis' was implanted in 2000 (Grundei, 2002), and twenty amputees have had surgery, however little has been published regarding this design and follow-up of the patients.

This thesis is part of a project at the Centre for Biomedical Engineering, at the Institute of Orthopædics and Musculoskeletal Science, University College London, to improve on the two attachment techniques mentioned above. The system has the acronym 'ITAP':

'Intraosseous Transcutaneous Amputation Prosthesis'. It aims to improve the success of direct skeletal attachment of limb prostheses by combating infection and reducing rehabilitation time. The technique is currently undergoing a clinical trial for finger amputees, has been used to treat a patient with a transhumeral amputation, and pets with amputated limbs. Figures 1.1(a) and 1.2 (a) show abutments protruding through the skin for attaching prostheses and figures 1.1(b) and 1.2(c) show the ITAP prostheses attached.

(a) (b)

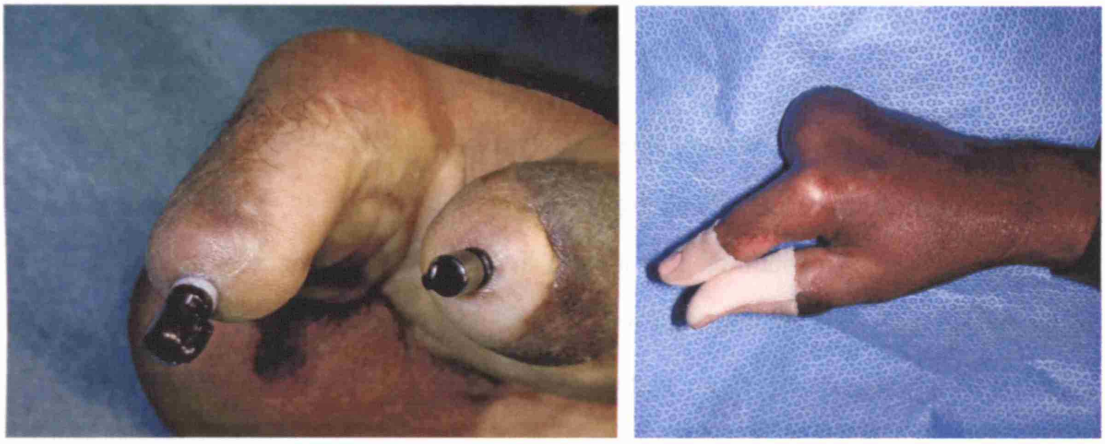

Figure 1.1 ITAP digit prostheses (a) percutaneous abutments for attachment (b) prostheses attached before the cosmetic appearance has been completed. Photographs courtesy of Prof. Gordon Blunn, Centre for Biomedical Engineering, University College London.

(a) (b) (c)

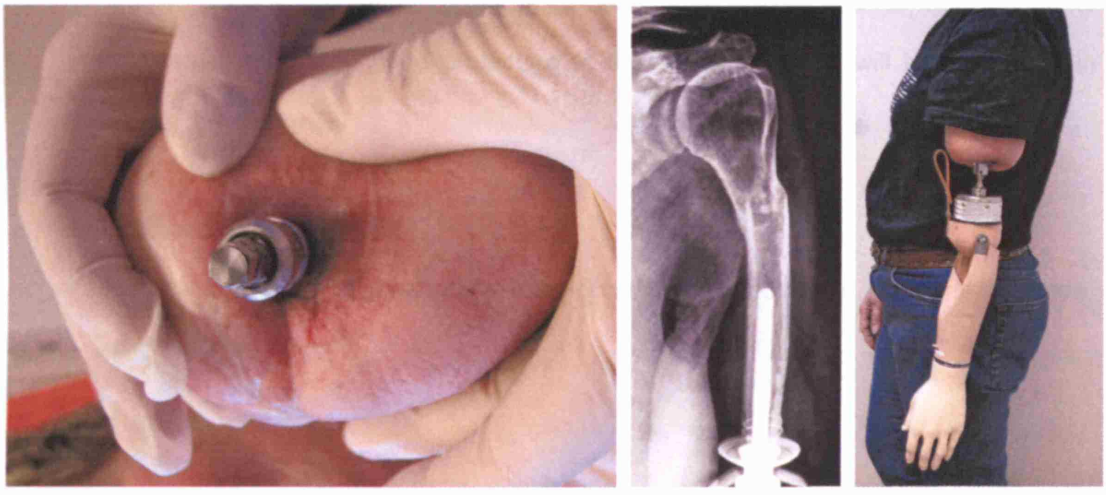

Figure 1.2 ITAP arm prosthesis (a) percutaneous abutment for attachment (b) radiograph of implant in bone (c) prosthesis attached. Photographs courtesy of Prof. Gordon Blunn, Centre for Biomedical Engineering, University College London.

1.2.2 Construction

The following is an outline of the components of the OPRA and ITAP structures for a leg prosthesis. Figure 1.3 shows a diagram of the components.

1. Intramedullary Anchor

   This is implanted first. It is designed to encourage bone growth to enhance fixation. The fixation of bone to the implant will be discussed in section 1.3.

2. Percutaneous Part

   In the OPRA prosthesis this is implanted in a second round of surgery (Sullivan, 2003), but may be implanted at the same time as the intramedullary anchor, as with ITAP. It is attached to the first component and protrudes through the skin. The distal end of this component attaches to the third component. The percutaneous part of the prosthesis will be discussed in section 1.4.

3. Fail-Safe Mechanism

   A fail-safe mechanism protects the bone from excessive loads. In the OPRA prosthesis there is a torque limiting device but nothing to prevent damage due to bending loads and component number 2 has broken or bent in a number of patients (Sullivan *et al.* 2003). The protection of the implanted bone will be discussed in section 1.5.

4. Prosthesis

   The rest of the leg is assembled from conventional prosthetic components: knee, shin, ankle and foot.

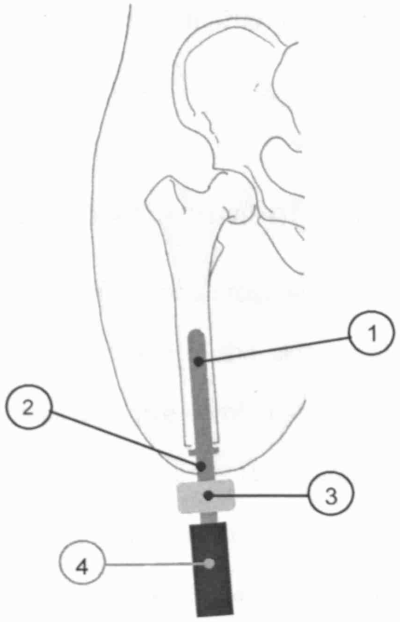

Figure 1.3 A simplified diagram of a bone-anchored trans-femoral prosthesis.

1.2.3 Rehabilitation Procedures

Bone is a material consisting of living cells so, unlike engineering materials, it adapts to the stresses applied and the strains experienced. When a transfemoral amputee uses a socket prosthesis the loads through the femur are lower than normal and the femur becomes weaker. The strength of the bone is linked to the density and Sherk et al. (2008) and Rush et al. (1994) measured the density of amputees' femurs and found them to be significantly lower than the non-amputated femur (This is discussed in greater detail in chapter 3). The ITAP implant is inserted into this weaker bone so the loads applied to it must be increased gradually to allow it to strengthen.

The OPRA rehabilitation procedure includes the gradual loading of the prosthesis and this will take place with ITAP as well. In OPRA, the amputee is first fitted with a short 'training' prosthesis and is instructed to apply 200N axial load to the prosthesis daily by leaning on a set of bathroom scales. When this load is comfortable for the amputee they are to increase the load the following week by 100N force, and gradually increase in this manner until they

reach their own body weigh (Sullivan et al. 2003). At this point they are fitted with a full-length prosthesis and begin gait training.

1.2.4 Benefits of Skeletal Attachment of Leg Prostheses

The main benefit of skeletal attachment of a prosthetic leg is that it can allow amputees, who are unable to wear prostheses because of the skin problems they encounter with socket prostheses, to wear a prosthesis and give comfort and greater mobility to those who are able to use their prosthesis for only short time (Sullivan, 2003; Marks and Michael 2001). Patients in the OPRA programme have also reported easier attachment and removal of the prosthesis and improved function (Ax, 2004) since there is no socket to restrict hip movement. Further benefits are discussed in the following sections.

1.2.4.1 Stump Size Variation

Socket prostheses, since they need to form a vacuum around the residual limb, must fit the amputee precisely. They must be remade from time-to-time when the amputee gains or loses weight or if the residual limb swells due to trauma, and as it gradually reduces in size after amputation due to reduction in swelling and muscle wastage. This remaking is not necessary for an amputee wearing an ITAP prosthesis.

1.2.4.2 Osseoperception

When a device is connected to bone through the skin, the two sensory connections between the external device and the nervous system are with the bone and with the soft tissue at the implant interface. It was observed in 1999 that a person wearing a dental implant compared with a dentally-anchored bridge had restored masticatory awareness, and the biting sensation was attributed to the activation of the nerves in the bone surrounding the implant (Dahlstrom, 1999)

To investigate the magnitude of this 'periprosthetic perception', patients with bone-attached limb prostheses were asked to identify whether or not they felt vibrations applied to their prostheses (Branemark 1997; Ysander *et al.*, 2001). The perception of vibration was found to be comparable to that for a normal limb. Patients in the OPRA trial are often able to identify the type of surface on which they are walking (Rydevik, 1997). Brånemark considers the sense of proprioception in the bone to be significant enough to be termed 'osseoperception'.

There are two types of nerve in bone: one is thought to regulate blood flow and the other network is thought to provide a sense of pain and proprioception (Buma *et al.*, 1995). An histochemical analysis of tibia implants in rats has shown that when bone remodels around an implant both types of nerve are present (Ysander *et al.*, 2001).

One of the most useful applications of osseoperception might be to prevent overloading of an extremity. Joints in the body are surrounded by proprioceptors which detect extreme joint extension (Rydevik, 1997), the sense of loading provided by osseoperception may provide a similar service for the transcutaneous implant. There is continuing research into the physiological basis for osseoperception (Ysander *et al.*, 2001).

1.2.4.3 Gait

Trans-femoral amputation introduces more mechanical disadvantages than the loss of the knee, ankle, foot and the muscles distal to the amputation. Removal of the distal femur also removes the insertions of a number of retained muscles; these are re-attached to the bone in a technique known as myodesis or myoplasty. Often the *adductor magnus* and the *quadriceps* are wrapped around the resected femur and attached at the other side (Murdoch and Bennet Wilson Jr, 1990). Other muscles are re-attached at points proximal to their physiological positions, reducing their lever arms, thus their strength. As a result, an

amputee with a shorter residual limb will use more energy for the same movement of their prosthesis than another with a longer stump.

The gait is no longer a series of muscular contractions to manoeuvre the hip, knee, ankle and toes because the hip is now the only manipulable articulation. Prosthetic gait is a process of swinging the leg forwards, moving over it, and letting the advancing body weight bend the knee (if a knee mechanism is incorporated) (Popovic, 1995). In calculating the forces affecting the bone/implant interface this revised gait pattern must be taken into account.

It has been qualitatively observed that the absence of the socket results in improved control of the prosthesis, with the movement being dictated directly by the femur and with the hip free to move in all directions. But it doesn't appear to make the gait of an amputee any better *quantitatively*: using data from gait analysis (Sullivan *et al.*, 2003). Improved gait is not one of the proposed benefits of ITAP, although a greater range of movement is achievable at the hip because of the loss of the socket.

1.3 Fixation of Bone to the Implant

Attachment of skin to the implant is vital to the success of ITAP, and attachment of the bone to the implant is also very important. There are risks in attaching any implant to bone, and a number of different factors influence the stresses that are experienced by the skeleton as a result of implantation: the material properties of the materials that are used, the biological reaction to the materials, the geometry of bone and of the implant, the loads applied to the prosthesis and the amount of bone fixation to the implant.

1.3.1 Design of the Intramedullary Implant

The intramedullary implants on which the ITAP design is based have a long history of encouraging bone to remodel in a beneficial manner without excessive resorption. In 1949 Stanmore Implants Worldwide, at the Centre for Biomedical Engineering, University College London, implanted their first massive prosthesis for osteosarcoma, the most common primary malignant tumour in children (Schindler 1996). A 'massive prosthesis' replaces the diseased femoral diaphysis and any affected joint. Since then the Centre has worked extensively on the design of massive implants custom-made for each patient (Rougraff 1994; Simon 1986). It is from this expertise that ITAP is developed.

Some of the features of massive implants that are used in the design of ITAP are: short radial flutes on the intramedullary stem cut into the cortical bone to limit rotation; the stem will be coated with an *osseoconductive* coating, encouraging bone to grow onto it and increasing the bone density; and a collar at the distal end of the resected femur has been shown to encourage increased bone growth (Walker and Robinson, 1998). Using these principles, the design of the internal part of the implant is based on years of experience of massive implant design. Figure 1.4 shows a selection of massive prostheses.

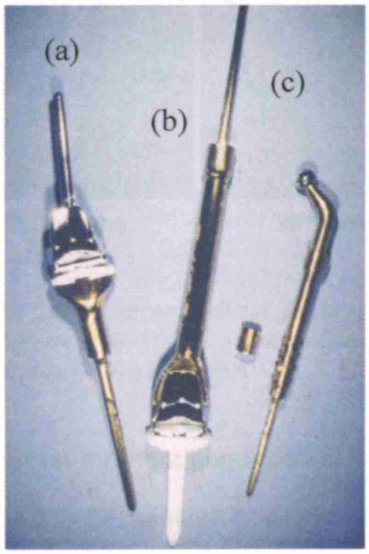

Figure 1.4 Massive prostheses for osteosarcoma: (a) proximal tibia, (b) distal femur and (c) proximal femur. Photograph courtesy Prof. Gordon Blunn at the Centre for Biomedical Engineering, University College London.

1.3.2 Remodelling of Bone

It was mentioned in section 1.2.2 that the femoral bone of an amputee is weaker than normal because the bone is subjected to much lower loading. Bone responds to a changed loading pattern by remodelling to better withstand the forces applied to it (Wolff, 1986). When a directly attached prosthesis is used to apply forces the bone will adapt to the new loading pattern provided that the force is increased gradually. This has been found in knee and hip prostheses where the bone has remodelled as a response to the new loading pattern brought about by the prosthesis.

As the load from the prosthesis is often transmitted in a non-physiological way regions where the stresses are reduced will cause bone to reduce in mass and density (Prendergast, 1997). This is known as stress shielding. Figure 1.5 shows radiographs of a femur implanted with a distal femur prosthesis over 72 months after implantation showing bone remodelling and stress shielding.

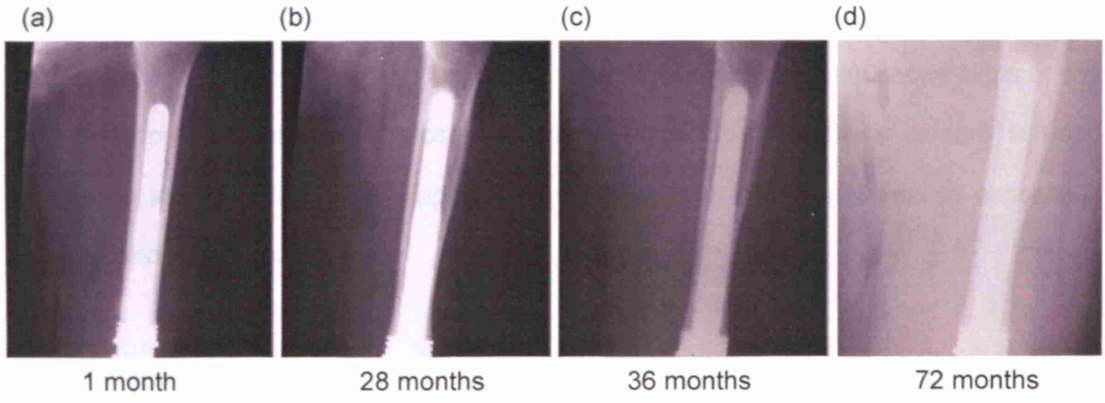

Figure 1.5 Radiographs of remodelling around distal femur prosthesis at (a) one month after implantation (b) 28 months, (c) 36 months and (d) 72 months. Courtesy of Professor G. Blunn, Centre for Biomedical Engineering, University College London.

In figure 1.5 the femur is thicker on the right hand side at 28 months than at 1 month, and appears to have further thickened by 72 months. Stress shielding is apparent by the thinning of the femur toward the end of the bone. The implant has a collar abutting the cut end of the bone to encourage remodelling, resulting in an hourglass shape.

The shape of a limb bone is optimal for the loads normally applied to it (Wolff, 1986). An implant designed to apply these loads through the bone is restricted to the same overall dimensions and also to replicating the force vectors as closely as possible.

1.3.3 Biomaterials and Immune Response

When a prosthesis is implanted into bone an acute immune response is triggered. Inflammatory tissue surrounds the implant and attracts monocytes. The monocytes turn into macrophages and attempt to break down the foreign body (Martini and Bartholomew, 2000), this is a chronic process. The soft tissue surrounding the implant can grow thicker and loosen it from the site of implantation.

In 1960, Charnley introduced the use of polymethylmethacralate (PMMA or 'bone cement') for the fixation of bone-attached prostheses (Heimke, 1989). A layer of cement between the implant and the bone creates an intimate attachment and delays the biological response. Despite good results with PMMA, after about five to ten years the cement shows signs of soft tissue encapsulation and thus loosening (Dalby *et al.*, 2001). Bone cement is used extensively and techniques that apply it under pressure to fill the surrounding cancellous tissue extend its life *in vivo*.

Other materials have been applied to the problem of long-term implants. Branemark (1977) discovered that titanium induces an intimate contact with bone and elicits a lesser immune response than the biomaterials that had been used up to that point. Experiments with glasses and ceramics containing calcium phosphate (Hench, 1973) led to the development of calcium hydroxyapatite (HA) as an agent to improve the fixation of implants without cement (Heimke, 1989).

The design of an implant and surgical methods depend on the needs of the prosthesis. Heimke (1989) described the essential issue in all attempts to replace bone as "the reliable fixation of the substitute in its environment for the intended lifetime". A longer intended lifetime indicates a need for a reliable and longer-lasting fixation method.

Success rates of implants are usually measured in years. For example, an elderly patient might be given a hip prosthesis and fixation method that have been tested to last up to ten years but an active, young, patient would require a system that was expected to last longer. The term 'osseointegration' has been proposed to relate to an intimate connection between the bone and the implant that lasts a lifetime and is summarised as follows by Branemark and Skalak (1998):

- an osseointegrated fixture will provide a stable support for a prosthesis under functional loads;
- new bone grows right up to the surface of the metal fixture and there is no fibrous capsule surrounding it (only bone and marrow tissue is found at the implant surface).
- there is no mechanism of rejection;
- and there is no relative motion between the implant and the bone at physiological loads throughout the patient's lifetime.

The concept of osseointegration has been mostly applied to dental prostheses. In dental implants osseointegration is not always achieved at the interface. In one study 4.3% of implants were found to not be osseointegrated (Cheung and Leung, 2003). With the OPRA prosthesis it is claimed that all amputees achieve osseointegration (Sullivan *et al.*, 2003).

If ITAP is to successfully allow the patient to take their weight through the mid diaphysis of the femur, the connection between metal and bone must be very immobile and long lasting.

The criteria used to define osseointegration, above, might be a useful tool in assessing the success or otherwise of the implant fixation.

1.3.4 Biocompatability of Titanium

Titanium has been shown to possess excellent biocompatibility. Titanium oxide, which is present on all titanium surfaces, appears to allow proteins to adsorb onto it. It is thought that the immune system recognises the proteins covering the implant surface and so recognises the implant as part of the body, lessening the immune response (Jansson *et al.*, 2001).

The titanium oxide must be preserved and, if possible, increased during sterilisation of an implant before surgery. It is important to regulate the oxidation because different sterilisation techniques result in different thicknesses of oxide (Breme and Biehl, 1998). Titanium must be treated carefully at high temperatures because a thick oxide layer can develop, which makes it harder and more difficult to machine (Black and Hastings, 1998).

If the oxide is scratched *in vivo*, oxygen in the body will cause the exposed titanium to oxidise, releasing titanium ions into the body. Their effects are not completely understood, but metal ions have been found to interfere with the differentiation of pre osteoblast cells and osteoclasts (Puelo and Nanci, 1999). It is, therefore, important that the surface is protected in the body. For this reason titanium is seldom used in the design of implants with sliding or rolling contact such as knees and hips.

A further benefit of using titanium is that its stiffness is closer to that of bone than stainless steel or cobalt chrome, common in the manufacture of prosthetic hips and knees, resulting in less stress shielding. Titanium has half the stiffness of stainless steel or cobalt chrome.

Material	Young's Modulus (GPa)
Cobalt Chrome	210-330
Stainless Steel 216	216
Titanium	100-105
Diaphesial Cortical Bone	20

Table 1.1 Comparison of the stiffness of bone and various biocompatible materials (Black and Hastings, 1998).

Titanium, in its commercially pure form (known as cp-Ti), is comparatively soft, it has a yield strength of 200 to 390 MPa) (Breme and Biehl, 1998). This is the material used for the implant and percutaneous abutment in OPRA, and implants in the OPRA programme have bent under apparently normal loading (Moore, 2003).

For many biomedical applications titanium is alloyed with aluminium and vanadium to create a similarly biocompatible, but stronger, material with a yield strength of 830 MPa and a slightly higher Young's Modulus of 113-120GPa (Breme and Biehl, 1998). The alloy is called Ti6Al4V. The properties of this alloy are well known because it has been used since the first dental implants in 1967 (Branemark, 1997), and it has been studied and accepted as a biomaterial (Breme and Biehl, 1998). This alloy is used in ITAP.

1.4 Epithelial Adhesion to Percutaneous Implant

A drawback to the OPRA system is the incidence of infection (Arcuri, 1995): infections have occurred in over half of the patients in the British clinical trial (Robinson, 2007).

1.4.1 Wound Healing of Skin

Epithelial attachment to the implant is one way in which limb prostheses differ from dental implants. The gum, unlike the skin, is designed to be breached: when the crown of a

growing tooth presses against it, it is naturally absorbed (Gray, 1858a). The purpose of the gingiva is to allow penetration and prevent infection.

In contrast, the only protection the skin has when being permanently penetrated is its normal wound healing mechanism which is described in figure 1.6. When skin is pierced, a scab forms (figure 1.6(a)), and the epithelial layer grows down and around the scab to isolate it and attempt to re-establish epithelial continuity (figure 1.6(b)). This process is known as *downgrowth*. With a permanent percutaneous implant downgrowth still occurs, attempting to expel the implant from the body, but cannot result in epithelial continuity and, if no attempt is made to attach the skin to the implant a route is left for possible bacterial infection.

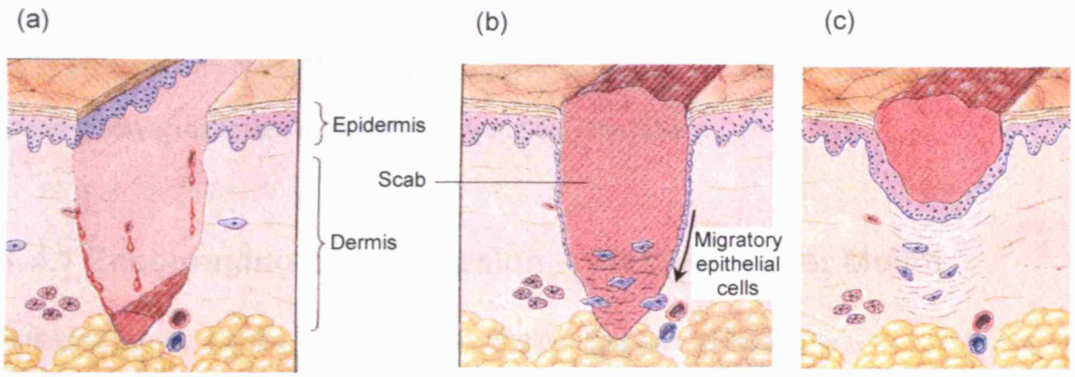

Figure 1.6 The sequence of wound healing of skin. (a) formation of the scab; (b) epithelial downgrowth; (c) internal healing of the wound. Adapted from Martini 1992.

Neither the ESKA nor the OPRA percutaneous limb prosthesis results in any skin adhesion between the dermis and the implanted device. The OPRA programme encourages epithelial attachment to the end of the resected bone to prevent continuation of downgrowth (Brånemark, 1997; Sullivan *et al.*, 2003) but a gap is still evident between the implant and the skin, creating a channel for infection.

A study of commercially-pure titanium, bone-anchored, auricular epitheses and hearing aids found no attachment of connective tissue to the percutaneous components in healthy patients (Holgers *et al.* 1995). The investigators discovered an increased number of inflammatory cells at the tissue/titanium interface which were not attached to the metal.

They also noted that there was no undesirable downgrowth either working to enclose or expel the percutaneous implant from the body and its absence suggests that the inflammatory cells are inhibiting epithelialisation. The conclusion was that the inflammatory cells are actually beneficial to the clinical performance of the implant, so the success of the implant is dependent on a continuous immune response.

In the OPRA percutaneous prosthesis the dermis has not formed a reasonable barrier to infection and inflammatory cells are required at the wound site to prevent downgrowth. If a prosthetic limb is to be reliably attached to a bone through the skin, attempts must be made to defend the wound, one method of defence is to encourage growth of the dermis onto the prosthetic surface. It is undesirable to rely on antibiotic treatment for long-term management as is the case with the OPRA system (Sullivan *et al.*, 2003). A technique is used in ITAP to prevent downgrowth and to seal the skin-implant interface.

1.4.1 Encouraging Skin Adhesion – the Deer Antler Model

Research at the Centre for Biomedical Engineering has looked at ways of protecting the patient from infection caused by the permanent epithelial breach. An intimate connection of the skin to the implant would act as a seal, and to achieve this, downgrowth and inflammation need to be prevented.

Studying the natural analogy of a red deer antler, which is heavily loaded for some months of the year yet seldom infected (Blunn *et al.* 2001), the traits on the left of table 1.2 have been identified as important factors in the stability of the bone/skin interface and applicable to ITAP and in order to emulate the red deer analogy, the ITAP system incorporates the features on the right of table 1.2.

Red Deer Antler	ITAP Prosthesis
The antler is an integral part of the skeleton, there is no relative movement between the antler and the skull.	The bone-anchor of the implant will be securely embedded using techniques developed in massive implants: it will have an hydroxyapatite and/or porous surface and will be made from titanium to encourage bone growth onto and into it.
The dermis is intimately attached to the bone.	The internal part of the implant will be covered with an adhesion promoting protein.
The skin epithelium becomes thinner towards the antler, and is only one cell thick at the bone interface.	Surgical removal of the hypodermis will promote attachment to the implant.
The part of the antler under the skin is covered with pores of diameter 18-40 microns which allows for collagen fibre ingrowth into the pores and attachment of the dermis.	The internal part of the implant in the soft tissue region between the bone and skin will be flattened to a mushroom-shape, increasing the surface area for attachment. This will be porous and also include small holes suitable for suturing the soft tissue to prevent movement. It will be coated with adhesion proteins.

Table 1.2 Traits of the deer antler and the features of ITAP used to emulate them from the patent application (Blum et al. 2001).

To achieve the above features, a special surgical procedure has been developed. The surgical procedure used for implanting auricular epitheses and bone-anchored hearing aids at Gothenburg University included the removal of subcutaneous soft tissue to ensure close

contact between the skin and the bone (Holgers *et al.* 1995); the removal of this subcutaneous cushion has also been found to relieve 'tremendous problems' in craniofacial prostheses (Branemark, 1997). The removal of this tissue would expose the bone to mechanical injury and the skin to a reduced blood supply so in the ITAP prosthesis a dermal soft tissue layer will be retrieved but it is necessary to keep it as immobile as possible to encourage a good seal at the skin-metal interface. This is achieved by providing a porous platform for the soft tissue to grow on to and into. Figures 1.1(a) and 1.2 (a) show the percutaneous part of the implants for attachment of digital prostheses and a transhumeral prosthesis.

1.5 Protection of the Implant and Bone from Loading

Attaching a prosthetic leg directly to the bone puts the body at increased risk by removing some of the protection from extraneous forces in the form of the cartilage and viscoelastic properties of bone and tendon.

1.5.1 Fail-Safe Component for Prosthesis

The OPRA system of prosthetic leg replacement includes a device to protect the bone form torsional loading. When a force becomes dangerous in bending, however, the abutment passing through the skin bends; this 'weak point' is replaceable in an out-patient procedure (Rydevik, 1997). In one centre, five out of nine patients had to undergo at least one abutment replacement in six years (Sullivan *et al.*, 2003) and one amputee has had sixteen replacements in eight years of use (Robinson, 2007). A means of protection like this is not possible for the ITAP prosthesis because the success of the system is dependent on the maintenance of the skin attachment to the implant. Therefore a fail-safe device must be located external to the body. The design and testing of this component has been an important part of the work contained in this thesis.

The importance of including a protective mechanism is highlighted by the experience of one of the pets that have been implanted with an ITAP device. The prosthesis provided for the dog 'Storm' included a fail-safe capability which comprised a weak section of the prosthesis designed to break under high loading. This weak section broke almost immediately so he was issued with a stronger one. His owner, fearing the prosthesis would 'break' again, strengthened the weak point in the prosthesis and the implant fractured inside the dog's stump and he had to have further surgery to replace the implant. Figure 1.7 shows a radiograph of Storm's fractured implant.

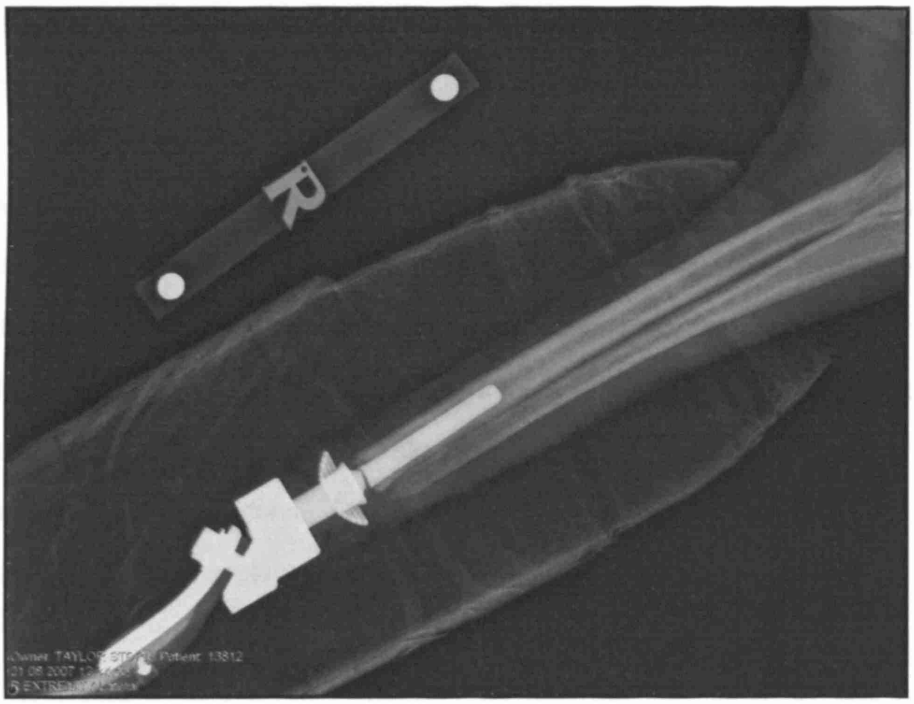

Figure 1.7 Radiograph of Storm's fractured implant. Courtesy of Professor Blunn, University College London.

Storm's story highlights the importance of including a fail-safe device in the prosthesis. For the soft tissue attachment to be maintained it is important that this is situated external to the body.

1.5.2 Finite Element Analysis of Transfemoral Implants for prosthetic Attachment

In order to design a fail-safe device it is vital to know the loads which may be withstood during normal activity and the loads that will cause the bone or the implant to break. The loads experienced during normal activity were investigated from published research into the loading of prostheses.

The loads that could cause the bone to break are dependent on a number of factors: the strength and size of the bone of the amputee; the size, geometry and material of the implant; the level of amputation; and the amount of bone-implant contact. A method of calculation is required that can take into account the many different factors that influence strength.

Finite element analysis is a computational method that can be used to find the stresses and strains throughout a complex geometry. The geometry is split into blocks and each 'element' is assigned material properties. Boundary conditions such as forces, moments or supports are applied and the finite element analysis programme is used to solve the simultaneous equations that will give the stresses and strains throughout the structure due to the applied boundary conditions. Finite element analysis has been used extensively for investigating the effect of implants on surrounding bone.

In order to create a finite element model, material properties, geometry and boundary conditions are required. The material properties were found from published literature, and the geometry was obtained from scanning a femur using computed tomography. In order to investigate the many geometric variables a simpler model was first used, comprising a tubular bone, and then the model created from the scanned femur was used to investigate the relative risk to the bone caused by amputating at different levels.

A team working with the Brånemark OPRA implant have published two papers on FEA of the implanted femur (Xu et al. 2000) and (Xu et al. 2006) based on the geometry of the Brånemark implant. The implant is different from the ITAP implant in that it is threaded so that it is screwed into the bone, it is also shorter than the ITAP implant and is manufactured from commercially-pure titanium and the ITAP implant is Ti6Al4V.

The first study (Xu *et al.*, 2000) was an axisymmetric model that was used to investigate geometric variables of the implant and bone for the purpose of aiding future modifications to the design of the implant. They studied the outer and inner diameter of the thread, the pitch size and the implant length under combined loading. They found that the there were stress concentrations in the bone near the implant tip and at the end of the bone.

Xu *et al.* (2006) used the data from a CT scan to model the OPRA implant in-situ. The purpose of this was to compare two implant diameters to inform the best choice of implant for a particular amputee. They found that the implant of smaller diameter caused less stress shielding in the bone because the narrower implant is more flexible.

When Xu *et al.* compared their two papers they found that there were some differences between the two models due to the geometry used in each. Their results are not directly relevant to ITAP because the geometry and material of the implant are different.

Xu *et al.* used von Mises stress in the bone to measure the effect of changing implant variables. It was adequate for them to use a scalar representation of the stresses in the bone to see the relative effect of altering the geometry but the von Mises stress neglects the stress orientations in the bone and is therefore not sufficient for analysing the risk of fracture of an anisotropic material. So in this study the stresses in the three normal axes and three shear planes were considered to assess the risk to the bone of geometry variations.

1.6 Structure of the Thesis

A need for protection of the bone from excessive external loading is anticipated and in this study the risks to the bone are evaluated by investigating the material properties and geometry of the bone. A fail-safe device is designed and a protocol is proposed for setting it to protect the femur of different amputees. Table 1.3 shows an outline of the chapter organisation.

Research into Loads for Fail-Safe Device	Finite Element Analysis	Design of Fail-Safe Device
Chapter 2 Normal Loads in the Femur	Chapter 4 The Effect of Geometric and Material Variables on the Stress Transferred to the Femur	Chapter 6 Recommendations for Setting the Fail-Safe
Chapter 3 Material Properties of the Human Femur	Chapter 5 Effect of Amputation Level on the Stress Transferred to the Femur	Chapter 7 Design of a Fail-Safe Device to Protect the Bone

Table 1.3 Plan of chapters in this dissertation.

In order to know what loads are to be resisted and allowed by the fail-safe mechanism, both normal loads experienced by the femur and loads that might damage it need to be established. In chapter two the loads that are expected to be experienced by the femur implanted with ITAP are reviewed. Particular attention is paid to ordinary activities that produce high loads in the femur such as stair climbing.

To assess the loads at which a femur might break, the material properties of the femur must first be described. A review of literature in chapter three details previous research into the

material properties of the human femur. In section 3.1 the elastic properties of femoral bone are investigated. In section 3.2 a failure model is chosen that takes into account the anisotropic nature of bone. Section 3.3 contains research into the strength of the bone-implant interface. Chapter 3 concludes with material properties for use in the FEA models in subsequent chapters.

There are two chapters which investigate the behaviour of an implanted femur using finite element analysis. The first finite element analysis study is a parametric investigation: a simple, cylindrical, model of a bone and implant is used and different variables of bone and implant geometry are investigated to discover which effect the highest stresses in the femur. The material properties used are taken from chapter three and the applied loads are from chapter two.

The second finite element analysis model is a more detailed representation of a femur and implant. The femur shape is taken from a CT scan, and the varying density in the bone, calculated from the CT images is used to model the material properties throughout the femur. Three different resection levels are modelled to investigate the effect of amputation level on the stresses in the femur.

The conclusions of the previous four chapters are compiled in chapter six and settings for the fail-safe mechanism are recommended and advice is given about whether they need to be altered for amputees of different stump length, bone quality or duration of rehabilitation.

In chapter seven the design and testing of a fail-safe mechanism is recorded which allows the amputee to use the prosthesis without hindrance at safe loads and prevent the bone from being damaged during an incident of high loading.

2 Normal Loads in the Femur

2.1 Introduction

The fail-safe mechanism is required to protect the femur from excessive forces and moments but it must also allow the amputee to carry out normal daily activities without being interrupted by the activation of the mechanism. In this chapter the loads experienced in the femur during normal activities are investigated so that the fail-safe can be designed to remain rigid unless a load occurs that may cause fracture.

There are two ways to measure the loads applied to the femur during walking on a skeletally-attached prosthesis: by calculating the loads from forces and moments measured externally by gait analysis; or measuring directly from an instrumented prosthesis.

At this time, those working on the OPRA prosthesis have published two papers that describe the loading applied to the abutment during walking and other activities (Lee *et al.*, 2007a; Lee *et al.*, 2007b). Both studies use a load cell to record the forces in three axes and the moments about these axes. These publications will be reviewed and then further studies will be investigated to find the loads expected during other activities: jogging, running and cycling.

2.2 Human Gait

Prior to investigating the loads that act on the ITAP implant it is essential to have an understanding of the forces and moments that are encountered during gait and of the nomenclature relating to the description of gait. Figure 2.1 shows the phases of the gait cycle. The gait cycle is described from the time at which the heel of one foot hits the ground, known as heel-strike, to the moment when that heel touches the ground subsequently. Stance phase is the time during which the foot is in contact with the ground and swing phase is when the foot is not in contact with the ground. Mid-stance, toe-off and mid-swing describe different positions of the foot and occur at about 30%, 60% and 80% of the gait cycle.

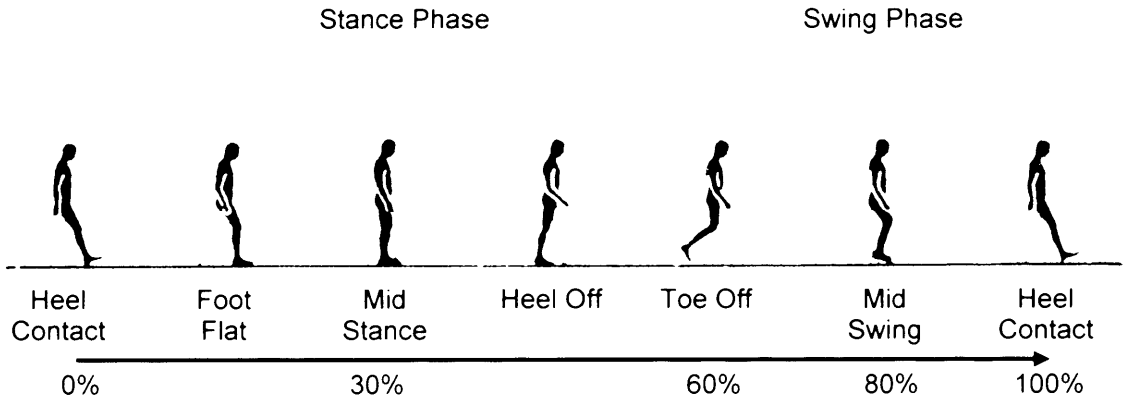

Figure 2.1 The gait cycle from heel contact to heel contact of the right leg. Adapted from (Whittle.M., 1993)).

Figure 2.2 shows the ground reaction force against the feet during a gait cycle for a normal subject, with the components in the medial-lateral direction, anterior–posterior direction and in the axial direction. These measurements can be made using an instrumented force transducer, or 'force plate', set into the floor of a gait laboratory. The loads measured by the force plate are equal to the loads experienced by the foot, as defined by Newton's Third Law.

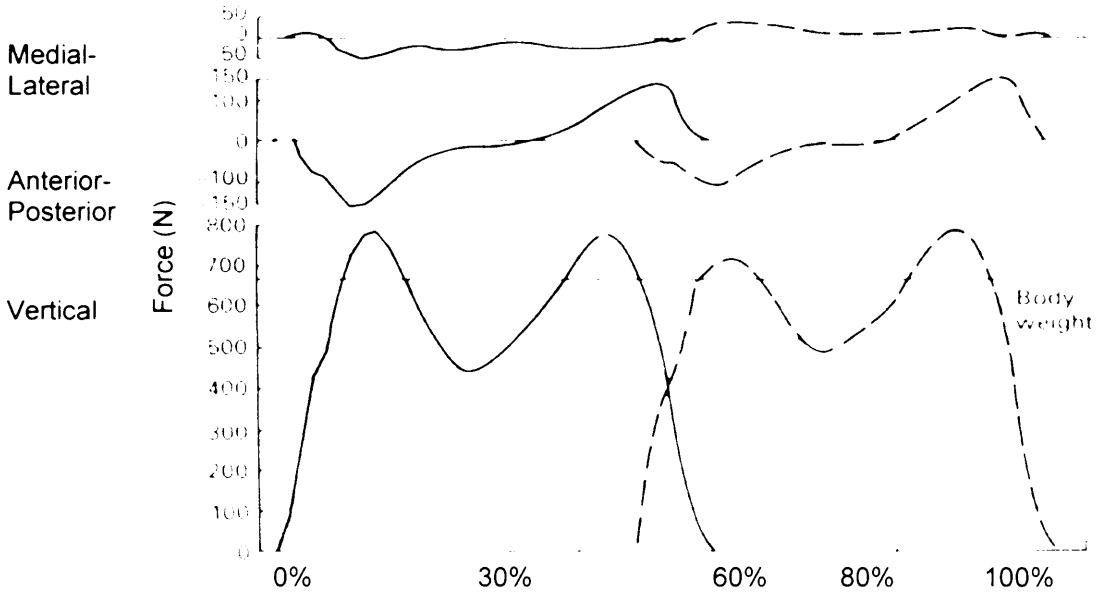

Figure 2.2 The ground reaction force in Newtons measured during a typical gait cycle for the right leg (solid) and the left leg (dashed). Adapted from Whittle (1993)

No loads are recorded for the right foot after 60% of the gait cycle because the leg is in swing phase, and not in contact with the ground. Vertical force has a higher value than medial-lateral force and anterior-posterior force. Two peak axial forces of similar magnitude are recorded during the stance phase and there is a dip between them. The force in the anterior-posterior (A-P) direction peaks at similar times in the gait cycle, in the anterior direction at the beginning of the stance phase and in the posterior direction at the end of the stance phase. The medial-lateral (M-L) force is approximately constant throughout the stance phase.

The ground reaction force measured for an amputee wearing a prosthetic leg differs slightly from that seen in figure 2.2, although it is similar in form. The vertical load is more constant during stance phase, with the peaks lower and the trough shallower. The shape and magnitude of the graphs are dependent on the componentry of the prosthesis, the length and musculature of the stump and the amputee's ability to control the prosthesis.

2.3 Evaluation of a Study into Loading of a Skeletally-Attached Prosthesis

Two papers have been published in which a load cell is mounted in series with the OPRA prosthesis to measure the loads applied to the abutment. The load cell is situated proximal to the knee mechanism, as shown in figure 2.3, as described by Frossard *et al.* (2008).

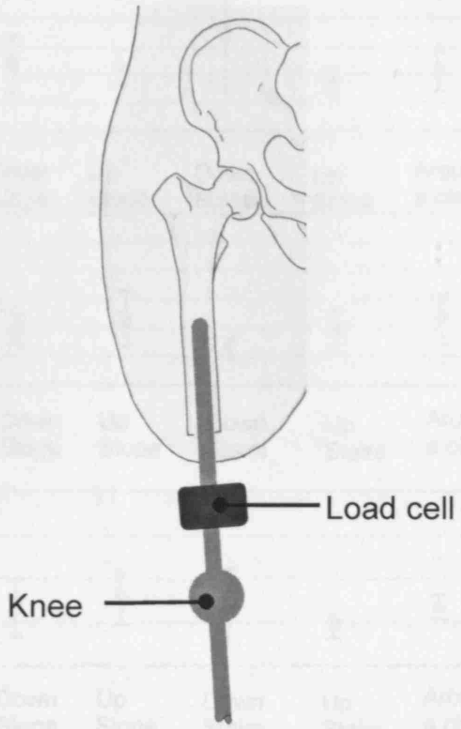

Figure 2.3 diagram of the placement of the load transducer in (Lee et al., 2007a; Lee et al., 2007b)

The first paper (Lee *et al.*, 2007b) concentrated on walking and found that a large difference was seen between amputees (twelve were tested) but that each amputee generated loads patterns that were consistent over time. In the second publication (Lee *et al.*, 2007a) tests were carried out during walking, ascending stairs and a ramp and descending stairs and a ramp and walking around a circle for nine amputees. The results are reproduced in figure 2.4. The amputees were allowed fifteen minutes to practice with the instrumented prosthesis to ensure that the alignment of the prosthesis was normal and comfortable. The load data for at least five steps were recorded for each activity.

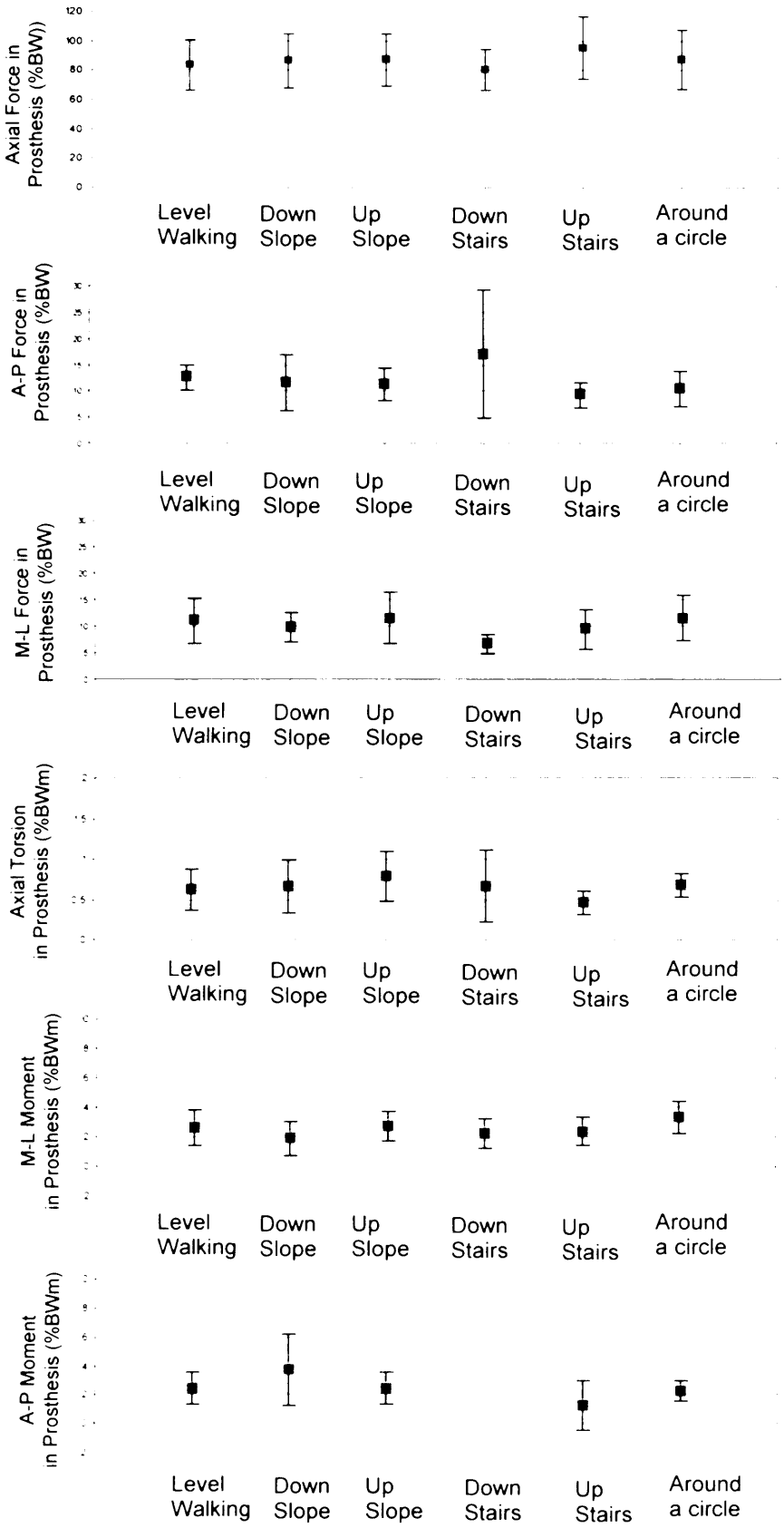

Figure 2.4 The magnitude of the load peaks measured by the load cell during different activities showing the standard deviation (Lee et al., 2007a).

There is no significant difference between the maximum forces and moments recorded for different activities. The mean axial force is less than one bodyweight. The M-L and A-P forces are both within the range of five and seventeen percent bodyweight, apart from the A-P force experienced when descending stairs where the large standard deviation may be attributed to the use of different knee mechanisms which dictate different techniques for moving down the stairs. The moments about the bone axis are below one percent bodyweight metres, and the moments about the M-L axis and the A-P axis are between one and six percent bodyweight metres. No data is recorded for the A-P moment down stairs because the researchers said no peaks were found in the data.

2.4 Other Methods of Finding the Femoral Loading

Although the methodology used in the papers mentioned above was good and the results are useful as an initial study into the loading of the skeletally-attached prosthesis, the discussion included no comparison between the loads measured and any results from other studies found using other methods of measurement. In this section other methods of calculating or measuring the femoral loading are investigated and compared with the work of Lee *et al.* to validate their work and to find values of femoral loading for activities that were not investigated such as running.

2.4.1 Measured Loads in an Instrumented Femoral Prosthesis

Telemetry is the process of obtaining measurements in one place and relaying them for recording at a distance (Oxford English Dictionary, Second Edition). A possible approximation to the loading of the femur implanted with a skeletally-attached prosthesis, such as ITAP, is a knee prosthesis or a partial-femur prosthesis used for replacing part of the femur after treatment for cancer. Figure 2.5 is a diagram of a femur implanted with a partial-femur, or 'massive', prosthesis. By equipping a distal femoral prosthesis with strain gauges

and transmitting and receiving the data by telemetry, the strain state in the femoral shaft has been measured in a number of studies (Bergmann *et al.*, 1995, Bassey *et al.*, 1997,Taylor and Walker, 2001, Taylor *et al.*, 1998).

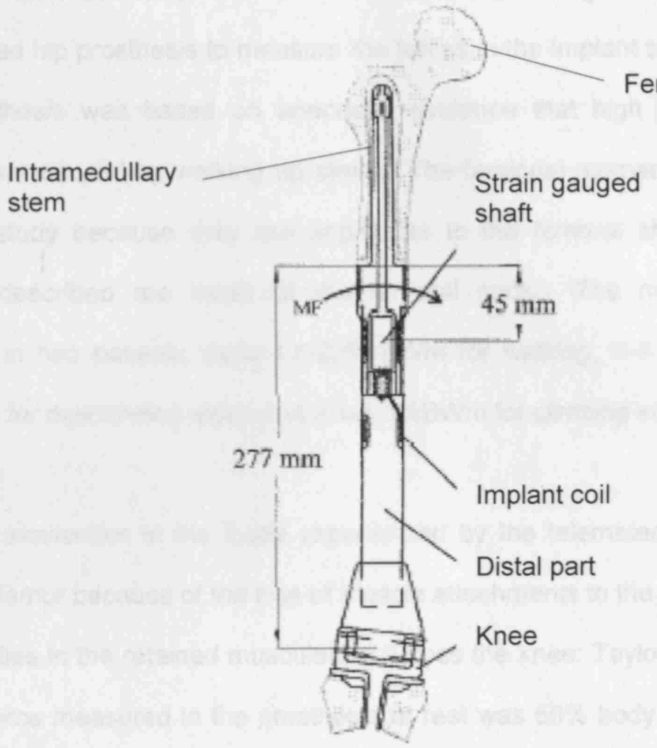

Figure 2.5. An instrumented distal femoral prosthesis. Adapted from Taylor et al. 1998.

Table 2.1 contains the maximum values recorded for forces and moments in studies using instrumented massive prostheses.

Activity		walking		down stairs	jogging		jumping
reference		Taylor 2001	Taylor 1998	Taylor 2001	Taylor 2001	Bassey 1997	Bassey 1997
number of subjects		n=2	n=1	n=2	n=1	n=1	n=1
force (%BW)	A-P		54				
	M-L						
	Axial	330	250	326	382	379	407
moment (%BWm)	About A-P	0.3		10.2	11.3		
	About M-L	5.7		3.2	7.9		
	Torsion	0.6	1	1	0.6		

Table 2.1. Forces and moment telemetered from a distal femoral prosthesis

Joint loading across the hip is not directly related to the loading throughout the shaft of the femur because of the high loads applied across the joint by the muscles (Hodge *et al.*, 1986), however studies that relate to the stem of the hip implant are relevant because the stem is lodged in the proximal part of the femoral shaft. Bergmann *et al.*, (1995) used an instrumented hip prosthesis to measure the forces in the implant stem during climbing stairs, their hypothesis was based on anecdotal evidence that high joint forces and torsional moments are caused by walking up stairs. The torsional moments are of greatest interest from this study because they are applicable to the femoral shaft whereas the bending moments described are those at the femoral neck. The median torsional moments measured in two patients were 1.6-2.5%BWm for walking, 4-4.7%BWm for jogging, 2.1-3.1%BWm for descending stairs and 3.4-4.5%BWm for climbing stairs.

There are similarities in the loads experienced by the telemetered implant and the ITAP-implanted femur because of the loss of muscle attachments to the distal femur. An important difference lies in the retained musculature across the knee: Taylor and Walker (2001) found the axial force measured in the prosthesis at rest was 50% body weight, indicating that the muscles across the knee apply a significant load to the femur. Bassey *et al.* (1997) found that the axial forces in the implant were about double the ground reaction forces and that the times at which the forces were at their highest the muscles were also acting and they conclude that the muscle activity plays an important contribution to the implant force.

2.4.2 Mathematical Calculations Based on Ground-Reaction Force of an Amputee's Gait

During the stance phase of gait, when the external forces acting on the leg are largest, the leg has been described as being approximately in static equilibrium (Burstein and Wright, 1994) which means that the sum of all of the forces acting on it is zero. By viewing the lower limb as a discrete body, and assuming static equilibrium, the forces and moments acting on it from outside can be used to estimate the forces and moments acting at a point

within it. Ground-reaction force can be measured using a force-plate set into the floor of a gait laboratory. It measures the forces in three axes.

Anticipating the development of skeletally-attached prostheses, Stephenson and Seedhom (2002) used kinematic and kinetic data from trans-femoral amputees to calculate the moments and forces that would be applied to a femoral implant. The ground-reaction forces and moments of amputees wearing socket prostheses were transferred to the proposed implantation site using the geometry of the prosthesis. Figure 2.6 shows the axes and the equations used to transfer ground-reaction forces to the femur and table 2.2 contains their results. The moment about the M-L axis (Mx) was assumed to be zero. The equations require the knee angle and the length of the leg to transfer the loads to the femur using trigonometry.

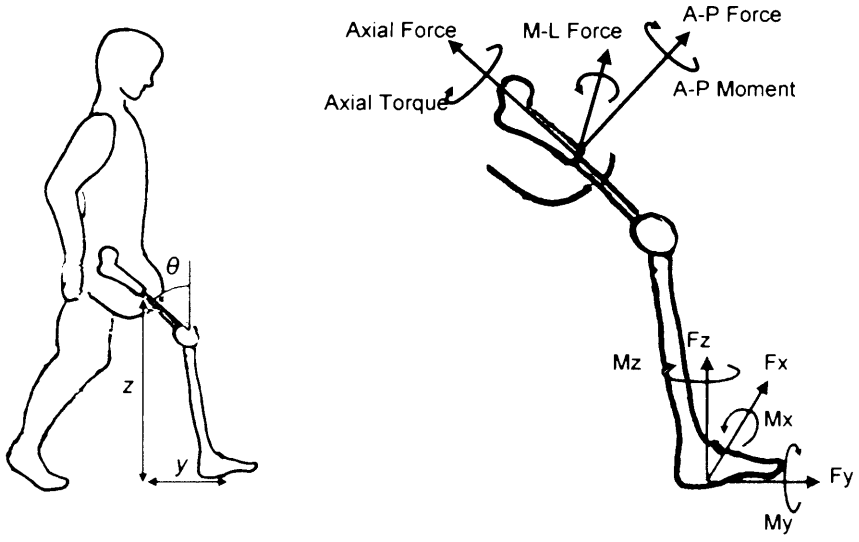

$$MLForce = Fx \qquad \text{eq. 2.1}$$

$$MLForce = Fy.\cos\theta + Fz.\sin\theta \qquad \text{eq. 2.2}$$

$$AxialForce = Fz.\cos\theta + Fy.\sin\theta \qquad \text{eq. 2.3}$$

$$APMoment = Fy.z + Fz.y \qquad \text{eq.2.4}$$

$$MLMoment = (Fx.z).\cos\theta + (Mz + Fx.y).\sin\theta \qquad \text{eq.2.5}$$

$$AxialTorque = (Mz + Fx.y).\cos\theta + (Fx.z).\sin\theta \qquad \text{eq.2.6}$$

Figure 2.6 Equations used to translate the forces and moments at the foot to the position and axis of the mid-femur derived by Stephenson and Seedhom (2002).

		Min	Max
Forces (%BW)	M-L	0	6
	A-P	-32	36
	Axial	0	100
Moments (%BWm)	About A-P	-18	14
	About M-L	-4	0
	Torsion	-2	1

Table 2.2 Walking forces and moments transferred to femur position in trans-femoral amputee (Stephenson and Seedhom, 2002)

There are a number of factors that make the calculations of Stephenson and Seedhom different from the forces and moments in the real-life situation of an amputee wearing an ITAP prosthesis. The gait of the amputees wearing socket prostheses that were studied will have had a similar gait to those wearing a skeletally-attached prosthesis but not identical (Sullivan *et al.*, 2003). There is also a difference in the alignment of the prosthetic leg. A socket fits well because it is moulded around the residual limb of each amputee. The prosthetist uses experience to attach the rest of the prosthetic limb to the socket in the correct configuration and adjusts the alignment of the components during gait observation. This results in different alignment for different patients and also differences between fittings for the same patient but allows for the changing shape of the stump. With an ITAP implant, there is no choice in the alignment of the percutaneous part of the prosthesis although components can be added to offset one component from another. There may be a need for this type of adjustability in the ITAP prosthesis because amputees have been observed, in the OPRA programme, compensating in their gait for the prosthetic knee mechanism being placed posteriorly compared with the position of the knee on a socket prosthesis (Sullivan, 2007).

2.4.3 Calculations using Mathematical Models

Finite-element analysis and other mathematical models have been used to calculate the forces and moments in the femur during daily activities. Duda et al. (1997) calculated the load state throughout the femur at different stages of gait. The maximum axial force was at

mid-stance and was 3.45 times body weight. They used a mathematical model to quantify the moments and forces in the femur during walking and found that the shear forces are close to zero in the shaft of the femur, and that torsional moments are small and constant along the bone, these findings are supported by Stephenson and Seedhom (2001) and Taylor *et al.* (1998).

Cheal *et. al.* (1992) created a finite-element model to analyse the effects of different loading conditions on the implant-bone interface of a hip prosthesis. They applied loads for normal gait and extreme loads. One of the extreme loading conditions was stair ascent and they found that a torsional moment of 5.5BWm occurred.

Finite element models of the femur are useful in determining the loads experienced by the femur in locations in which it is difficult to measure directly, for example, by applying strain gauges to the face or internal structure of the bone during gait. It is usually validated with a mechanical model or other mathematical models that can prove the results are realistic. Finite element models are usually simplified from the real-life situation because of the time required to create a perfect model using the microstructure of trabecular bone and all of the forces applied to the bone.

2.4.4 Comparison of Data from Different Sources

The load with the most information available is the axial force so this will be used to compare the data from different techniques. Figure 2.7 shows the axial load recorded for different activities as described in sections 2.31-2.33.

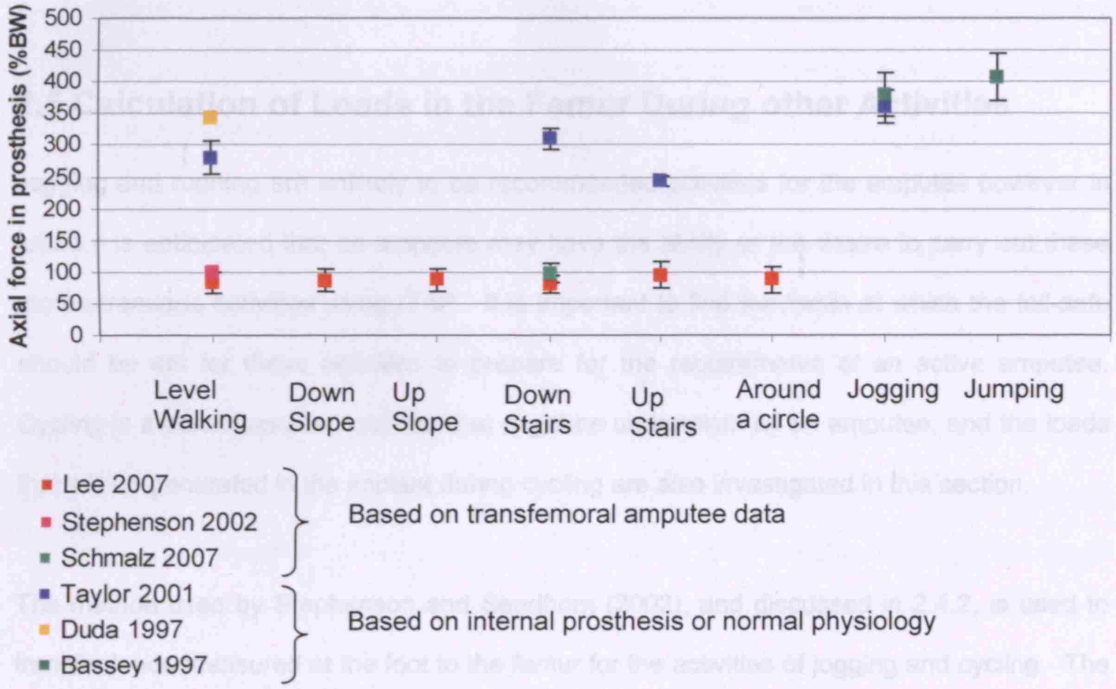

Figure 2.7 Axial force in the femur recorded using different methods for various activities showing one standard deviation where this is given in the literature.

The data in figure 2.7 can be divided into two groups: the loads measured from transfemoral amputees, and the loads from normal subjects and those with internal prostheses. The studies that used amputees give values for maximum axial force of around one bodyweight and studies based on normal femurs or those implanted with an internal prosthesis give axial force of two-and-a-half to four times bodyweight. Two of the papers cite muscle loads as the reason for the high values of axial force. A similar effect is seen in A-P and M-L loading where the forces are in the order of ten percent of bodyweight for amputee studies, but in normal subjects eighty percent for A-P force was measured and forty to sixty percent for M-L force.

Care must be taken when looking at loads from normal subjects because of the effect of muscle forces across the femur. However studies that use data from amputees by direct measurement in the prosthesis (Lee *et al.*, 2007), and by transferring the ground-reaction force (Stephenson and Seedhom, 2002) and (Schmalz *et al.* 1997) give results that are similar for axial force, as seen in figure 2.6 and also for M-L and A-P forces and moments.

2.5 Calculation of Loads in the Femur During other Activities

Jogging and running are unlikely to be recommended activities for the amputee however in future it is anticipated that an amputee may have the ability or the desire to carry out these more strenuous activities using ITAP. It is important to find the loads at which the fail-safe should be set for these activities to prepare for the requirements of an active amputee. Cycling is a cardiovascular exercise that might be undertaken by an amputee, and the loads that will be generated in the implant during cycling are also investigated in this section.

The method used by Stephenson and Seedhom (2002), and discussed in 2.4.2, is used to transfer loads measured at the foot to the femur for the activities of jogging and cycling. The free-body diagram in figure 2.8 shows the loading on the prosthetic limb.

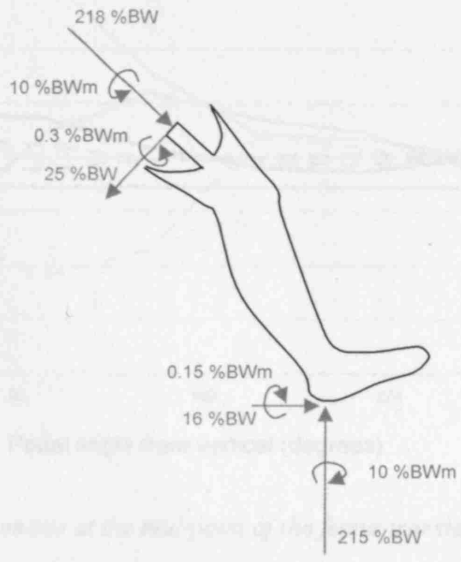

Figure 2.8 Free-body diagram of prosthetic limb during jogging showing the ground-reaction forces and moments and the moments at the implant.

Cycling is an activity that may be restored to an amputee with an ITAP prosthesis who has previously been unable because the position of the socket often creates pain and discomfort for an amputee using a standard socket prosthesis. A transfemoral amputee cycling exerts more pressure on the pedal through the sound leg than through the amputated leg and the use of the prosthetic side may be simply to stabilise the bicycle. No data are available for the loads transferred to the pedal of a bicycle for an amputee so loads measured from a normal subject are used as an approximation to estimate the loads at the level of the femur and are regarded as the maximum values that might occur. Suzuki *et al.* (1982) monitored the knee and hip angles of a cyclist as the pedal made one rotation. Davis and Hull (1981) used an instrumented bicycle pedal to measure all three forces and all moments exerted by the foot during one pedal rotation.

The loads at the pedal measured by Davis and Hull were transferred to the level the mid femur using the knee angles given by Suzuki *et al.* and equations 2.1-2.6 derived by Stephenson and Seedhom (2002). Figure 2.9 shows the loads calculated through one pedal cycle at a leisurely cycling pace of 80 wheel revolutions per minute along level ground.

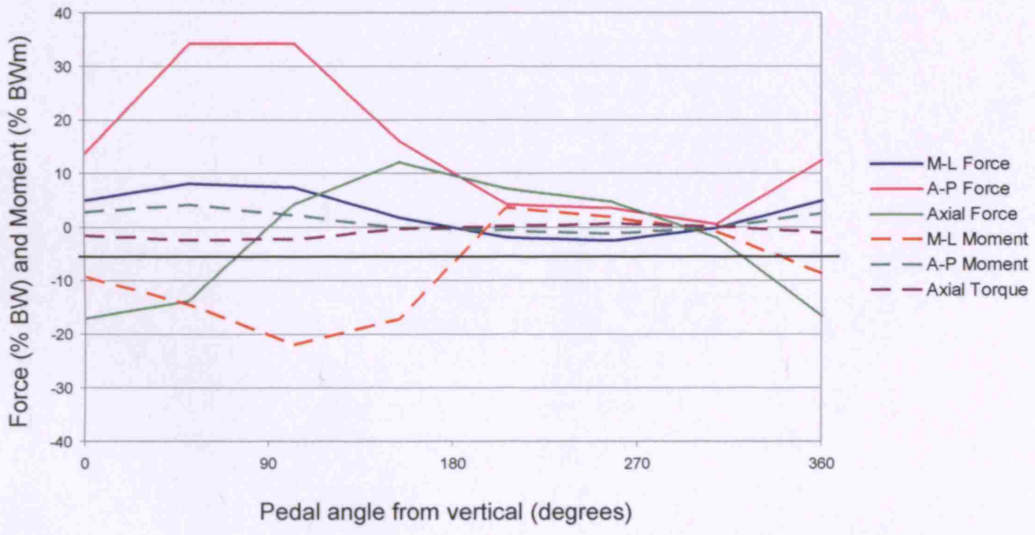

Figure 2.9 Forces and moments at the mid-point of the femur translated from pedal reaction loads.

The loads are highest between 0 degrees and 180 degrees, as this is the time when the foot is pressing down on the pedal and the highest force is experienced in the anterior direction because of the shallow angle of the knee.

No ground-reaction data are available for the transfemoral amputee running, so a study into the ground-reaction loads of able-bodied subjects is used (Keller *et al.*, 1996) as well as a study of transtibial amputees (Sanderson and Martin, 1996). The knee angle data are provided by Buckley *et al.* (2004) who recorded kinematic data for running transfemoral and transtibial amputees. The maximum loads, with those found by Lee *et al.* for walking, are in figure 2.10. The activity was defined as jogging if less than 3m/s and running over 3m/s.

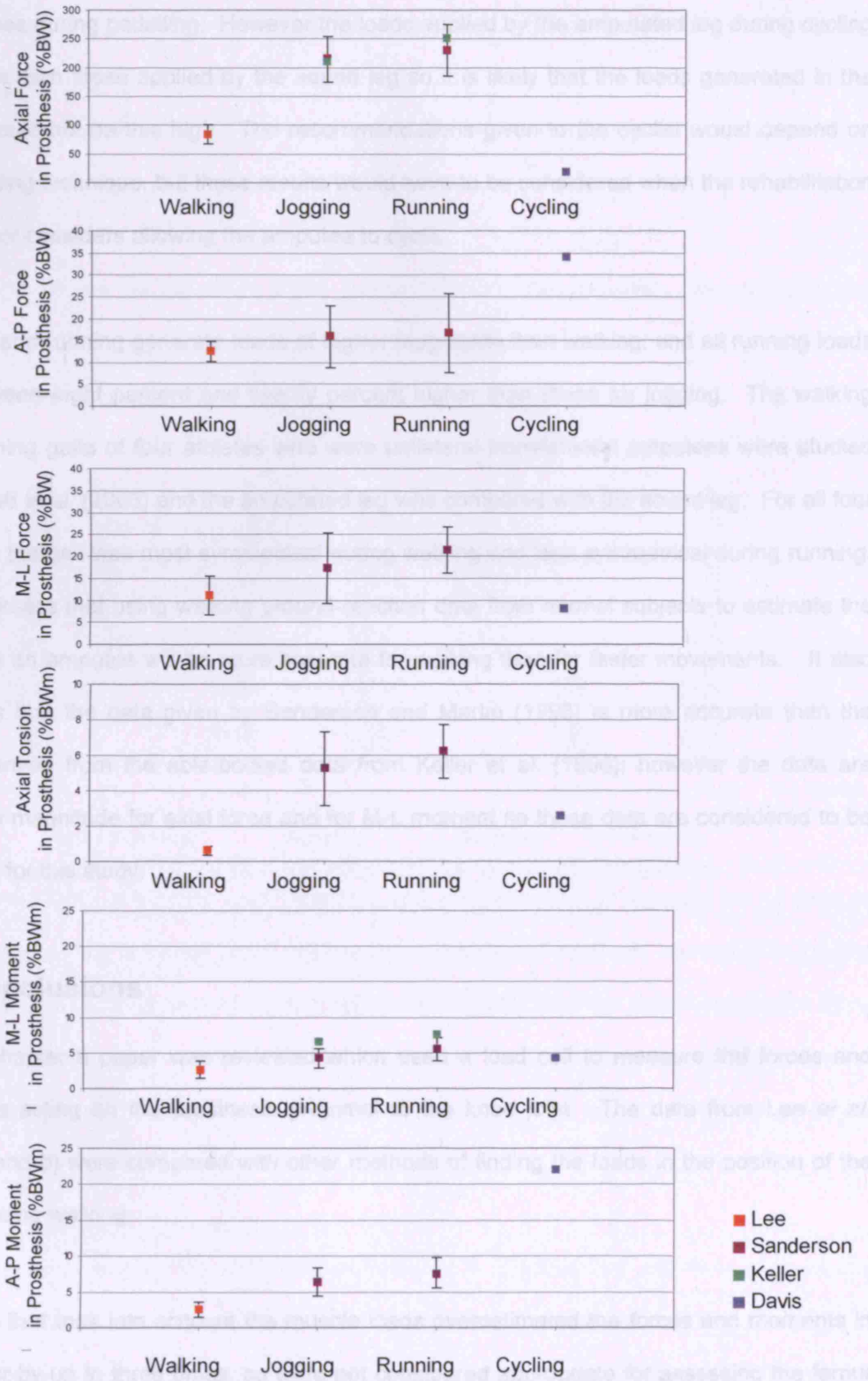

Figure 2.10 Forces and moments at the middle of the femur transferred from the reaction forces at the foot for jogging, running and cycling with direct-measured loads for walking.

The anterior-posterior force and moment are greatest for cycling because of the acute angle of the knee during pedalling. However the loads applied by the amputated leg during cycling are lower than those applied by the sound leg so it is likely that the loads generated in the femur would not be this high. The recommendations given to the cyclist would depend on their cycling technique, but these results would have to be considered when the rehabilitation supervisor considers allowing the amputee to cycle.

Jogging and running generate loads of higher magnitude than walking, and all running loads are between eight percent and twenty percent higher than those for jogging. The walking and running gaits of four athletes who were unilateral transfemoral amputees were studied by Burkett *et al.* (2003) and the amputated leg was compared with the sound leg. For all four subjects the gait was most symmetrical during walking and less symmetrical during running. This indicates that using walking ground-reaction data from normal subjects to estimate the loads for an amputee will be more accurate for walking than for faster movements. It also suggests that the data given by Sanderson and Martin (1996) is more accurate than the loads derived from the able-bodied data from Keller et al. (1996); however the data are similar in magnitude for axial force and for M-L moment so these data are considered to be accurate for this study.

2.6 Conclusions

In this chapter a paper was reviewed which used a load cell to measure the forces and moments acting on the prosthesis proximal to the knee joint. The data from Lee *et al.* (2007a and b) were compared with other methods of finding the loads in the position of the femur during walking.

Methods that took into account the muscle loads overestimated the forces and moments in the femur by up to three times, so were not considered appropriate for assessing the femur loads for a transfemoral amputee.

The trigonometric method used by Stephenson and Seedhom (1999) to transfer loads measured at the foot to the level of the mid-femur was found to match the loads measured by Lee *et al.* This method was employed to transfer forces and moments measured at the foot, for amputees and normal subjects, during jogging, running and cycling to the level of the mid-femur.

Figure 2.11 shows the maximum loads gathered for different activities. 'Normal activities' encompasses those measured by Lee *et al.*: walking, ascending and descending stairs and a ramp, and walking around a circle.

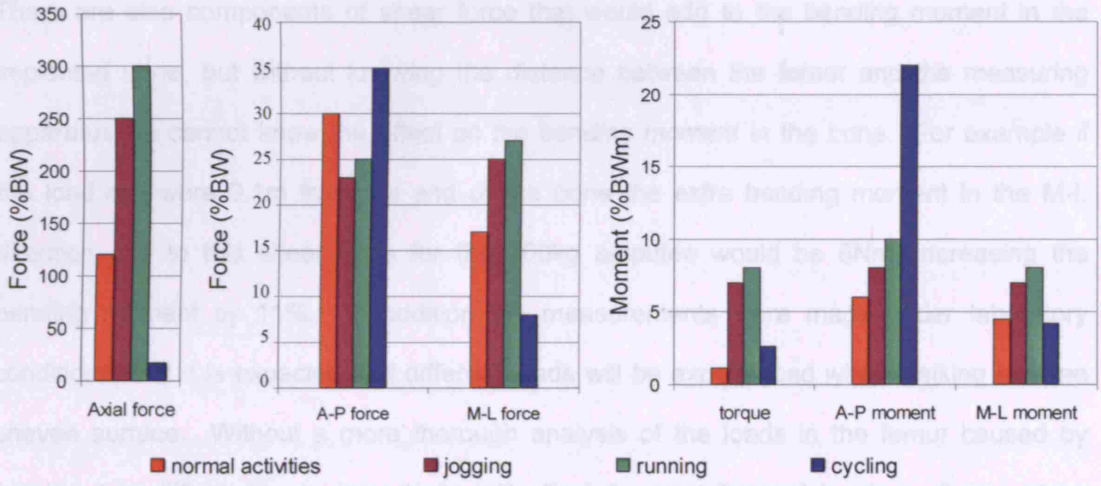

Figure 2.11 Maximum forces and moments at the mid femur during different activities.

The highest loads are in the axial direction, and are plotted on a separate set of axes to prevent diminishing the other plots. All maximum forces and moments are higher in jogging and running than while performing normal activities apart from the anterior-posterior force which is higher during normal activities because of the high loads generated by some amputees while negotiating steps. Cycling generates a high anterior force and moment because of the acute angle of the knee during pedalling.

The loads were used for the finite element analysis in chapters four and five represent the loads incident on the femur while walking, and were converted from percentage of bodyweight to forces and moments that will be experienced by an amputee of 750N. Table 2.3 contains the loads that were used.

		Load in %BW	Load for 750N amputee	Combined bending force
Lateral force	Anterior-posterior	14.0 %BW	105 N	143 N
	Medial-lateral	12.6 %BW	95 N	
Axial Force		90.0 %BW	668 N	
Torsion		1.1 %BW	8 Nm	

Table 2.3 Loads to be used in the finite-element analysis.

There are also components of shear force that would add to the bending moment in the implanted bone, but without knowing the distance between the femur and the measuring apparatus we cannot know the effect on the bending moment in the bone. For example if the load cell were 0.1m from the end of the bone the extra bending moment in the M-L direction due to this shear force for the 100kg amputee would be 8Nm, increasing the bending moment by 11%. In addition the measurements were made under laboratory conditions, and it is expected that different loads will be experienced when walking over an uneven surface. Without a more thorough analysis of the loads in the femur caused by walking it is difficult to say how these will affect the total femoral loading. It should be recognised that the loads proposed here are approximate and may need to be altered with the benefit of experience from early clinical trials.

Walking loads were applied because the fail-safe will primarily be set to allow normal activities as described by Lee *et al.* (2007) but not necessarily, for the early trials of the system, allow running or cycling. The data for these activities can be used in the future for assessing the risk to the amputee who jogs, runs and cycles and setting the fail-safe component for their requirements.

3 Material properties of the Human Femur

Introduction

Bone material properties have been studied for many different purposes but the use of computational methods for stress analysis such as finite element analysis has necessitated a more detailed knowledge of material properties throughout the bone structure. This has coincided with, and perhaps led, increased attempts to get a better understanding of bone material properties on a microscopic scale.

In explaining the material properties of any material two main features are described: the material's reaction to loads that cause failure including the type of failure experienced; and its reaction to lower loads, known as its elastic properties. In section 3.1 of this chapter the elastic properties of bone are investigated from the literature and calculated for a specific bone for use in the finite element models. In section 3.2, the variables that govern failure of bone are examined and a failure model created for analysis of the finite element model. In 3.3 the strength of the bone-implant interface is researched.

3.1 The Elastic Properties of Bone

In this section different characteristics of bone's elastic behaviour are discussed. As well as containing bone of different densities, femoral bone is also anisotropic (section 3.1.1). The Poisson's Ratio (3.1.2), the effect of the rate of loading (3.1.3) and the way in which bone changes in form due to the loads applied to it (3.1.4) are investigated. In section 3.1.5 the elastic constants (Poisson's Ratio, Young's Modulus and Shear Modulus) are defined for the cylindrical FEA model, and in section 3.1.6 the material properties for an anatomical femur model are derived from CT data.

3.1.1 Anisotropy and Heterogeneity

Bone is a composite material comprising collagen and calcium salts. The structure of bone is categorised into two types: cortical bone and trabecular, or cancellous, bone. The two different types of bone are defined by their porosity: 0-5% for cortical bone and 5-90% for trabecular bone (Reilly and Burstein, 1974) although there is a somewhat arbitrary division between the two where they meet. Trabecular bone is so called because it comprises struts, or 'trabeculae' of bone. In long bones such as the femur, the cortical bone creates a shell around the trabecular bone and forms most of the diaphysis (bone shaft).

Bone is created in a shape that is genetically predetermined (Cowin, 1984), and after this its structure and remodelling are predominantly governed by the strains it experiences (Rubin *et al.*, 1990). As a result of this so-called epigenetic effect, bone that has been lightly loaded, such as that of an amputee, has lower density and therefore strength. Long bones have trabeculae that are oriented in the principal directions of stress. Dempster and Liddicoat (1952) found the Young's Moduli in different orientations for cubes of bone. They found values in the direction of the bone axis to be over two times greater than at right-angles to it, concluding that bone is not isotropic (with uniform material properties in every direction) but orthotropic (having three perpendicular planes of symmetry at every point).

An orthotropic material whose properties are identical in two axes is called 'transversely isotropic' (Peters, 1998). The material of the shafts of long bones is often approximated to transverse isotropy because it is significantly stronger and stiffer in the axis of loading (the longitudinal axis) than perpendicular to this axis (Reilly and Burstein, 1974). As will be seen later, in table 3.1, the Young's moduli have been found to be within 12%, and Poisson's ratios within 6%, of each other in the radial and tangential directions (Ashman and Rho, 1988; Reilly and Burstein, 1974; Turner and Cowin, 1988), so transverse isotropy is often used in finite element analysis of long bones to simplify calculations.

A number of FEA studies have been carried out using isotropic material properties but more recently this has been found to be inaccurate for analyses that aim to predict failure of bony structures (Pietruszczak *et al.*, 1999) (Wirtz *et al.*, 2003). To apply orthotropic, transversely isotropic, or anisotropic material properties, the orientation of the fibres must be known, and there are different ways to apply them to a model. Many methods of describing orthotropic or anisotropic material properties have been developed and used but few have been verified by other researchers. One method (Rubin *et al.* 1993) aligned the material axis with the medial edge of the femur, which they considered to be an approximate load line through the bone. Strait *& al.* (2005) divided a skull into material regions for FEA and produced broadly realistic deformations. This method was employed in this study for the femur, dividing the bone into regions of material axis.

A mathematical algorithm of the development of trabecular architecture in the proximal femur (Miller *et al.*, 2002) predicted the structure of cancellous bone subjected to daily loading. The pattern found was compared with a drawing by Wolff (1986), and was found to be very similar.

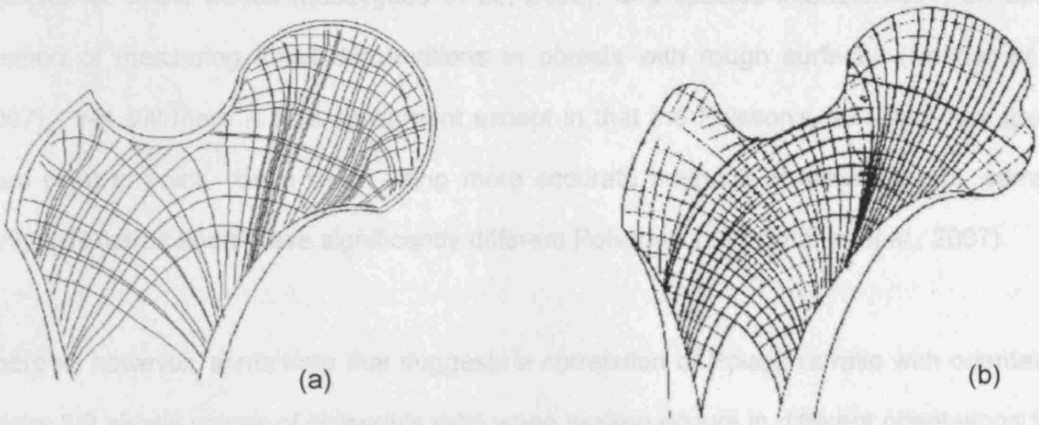

Fig. 3.1 (a) Trabecular material orientations predicted by Miller et al. (2002) and (b) the drawing by Wolff (1986) showing the orientations of trabeculae in the proximal femur. Adapted from Milller et al. (2002).

Most of the work in this project involves only the diaphysis of the femur, where the material is transversely isotropic. The orientations of the elements in the epiphysis are likely to only have significance in an FEA model representing the most proximal level of amputation.

3.1.2 Poisson's Ratio of Bone

Poisson's ratio is the strain transverse to the direction of loading divided by the strain in the normal direction (eq.3.1), and it can be anisotropic.

$$\nu = \frac{\varepsilon_z}{\varepsilon_x} \qquad eq.3.1$$

Wirtz *et al.* (2000) reported a wide variation of Poisson's ratio in the literature, between 0.20 and 0.50 for cortical bone and between 0.01 and 0.35 for cancellous bone, and state that there are no details to be found in literature about any correlation to bone density. This range spans almost all the possible values for Poisson's ratio for any material.

There is still a keen search for accurate measurements of the Poisson's ratio of bone. Due to the difficulty in measuring the Poisson's ratio accurately, modern methods are being employed such as ultrasonic measurements, calculating the acoustic velocities through

samples or whole bones (Lasaygues *et al.*, 2002), and speckle interferometry, an optical method of measuring small deformations in objects with rough surfaces (Shahar *et al.*, 2007). Yet still there is little agreement except in that the Poisson's ratio can vary greatly from point to point. Even when using more accurate methods of measurement, samples "only millimetres apart" have significantly different Poisson's ratio (Shahar *et al.*, 2007).

There is, however, some data that suggests a correlation of Poisson's ratio with orientation. Figure 3.2 shows values of Poisson's ratio when loading occurs in different orientations from a number of sources. It indicates that the Poisson's ratio found when loading the longitudinal axis is greater than when loading in the transverse plane.

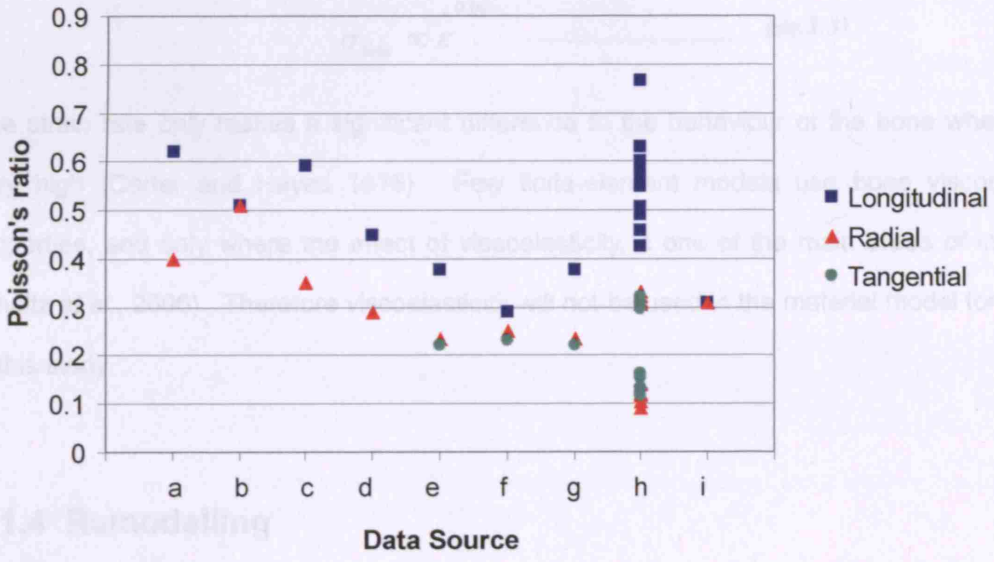

Fig 3.2 Poisson's ratios for the loading conditions longitudinal, radial and tangential in the femur and tibia. Data from a: Reilly, 1974, b: Reilly, 1975, c: Reilly, 1976, d: Reilly, 1977, e: Ashman et al., 1984, f: Turner and Cowin, 1988, g: Ashman and Rho, 1988, h: Knets et.al, 1980 and i: Wu, 1972.

In a linear finite element model with perfect contact conditions the stresses in the model will not be affected by the Poisson's ratio, because the stresses are dependent on the geometry. The values for Poisson's ratio are taken as 0.38 about the longitudinal axis and 0.235 about the transverse axes. These values have been chosen from Ashman and Rho (1988)

because they fall in the mid-range of the values in figure 3.2 and for consistency because the data from these authors is used in further ways in the model.

3.1.3 Viscoelasticity and Strain Rate

Bone is viscoelastic (Melnis and Knets, 1981; Shultz *et al.*, 2006), and this means that the rate of loading influences the material behaviour. The strain rate makes a difference to the ultimate strength and elastic modulus of bone but it is much less important than other factors such as the bone density (Carter and Hayes 1976): the strength is proportional to the density squared (equation 3.2) but is proportional to the to the strain rate to the power of 0.06 (equation 3.3)

$$\sigma_{max} \propto \rho^2 \qquad \text{(eq.3.2)}$$

$$\sigma_{max} \propto \dot{\varepsilon}^{0.06} \qquad \text{(eq.3.3)}$$

The strain rate only makes a significant difference to the behaviour of the bone when it is very high (Carter and Hayes 1976). Few finite-element models use bone viscoelastic properties, and only where the effect of viscoelasticity is one of the main areas of interest (Shultz *et al.*, 2006). Therefore viscoelasticity will not be used in the material model for bone in this study.

3.1.4 Remodelling

Bone remodels as a result of repeated loading (Wolff, 1986) resulting in fatigue behaviour that differs from engineering materials. The causes of remodelling are not understood entirely but it is thought that bone increases in density as a result of microcracks appearing in areas of high, predominantly tensile, strain (Zioupos *et al.*, 1995) and resorbs in response to low strain. Mathematical algorithms are being developed to model the magnitude and position of areas of bone development and resorption (Prendergast, 1997).

Knowledge of the remodelling characteristics are important for investigating the effects of implanting prostheses but these algorithms are beyond the scope and time-scale of this study. They may be useful in the long-term to predict bone remodelling and resorption around the ITAP implant.

3.1.5 Cortical Bone Elastic Constants for Cylinder FEA Model

In order to choose the material properties for the axisymmetric finite-element models, femoral models by other researches were investigated for their material properties. Table 3.1 shows elastic constants used by other researchers for finite element analysis models of the proximal femur. These are based on the material properties of cortical bone.

Finite-element investigation	Elastic constants			Source of material properties
(Pietruszczak *et al.*, 1999)	E_1=19.76GPa E_2=13.15GPa E_3=11.5GPa	ν_{12}=0.25 ν_{13}=0.23 ν_{23}=0.29	G_{12}=6.16GPa G_{13}=5.72GPa G_{23}=4.71GPa	(Turner and Cowin, 1988)
(Shultz *et al.*, 2006)	E_1=17GPa E_2=11.5GPa E_3=11.5GPa	ν_{13}=0.31 ν_{23}=0.31 ν_{12}=0.31	G_{12}=3.3GPa G_{23}=3.6GPa G_{31}=3.6GPa	(Reilly and Burstein, 1974)
(Stephenson, 1999)	E_1=20 GPa E_2=13.4GPa E_3=12GPa	ν_{12}=0.235 ν_{13}=0.222 ν_{23}=0.376	G_{12}=6.23GPa G_{13}=5.61GPa G_{23}=4.53GPa	(Ashman and Rho, 1988)

Table 3.1 A summary of bone material properties used in previous finite-element analysis models and the works from which the properties were taken.

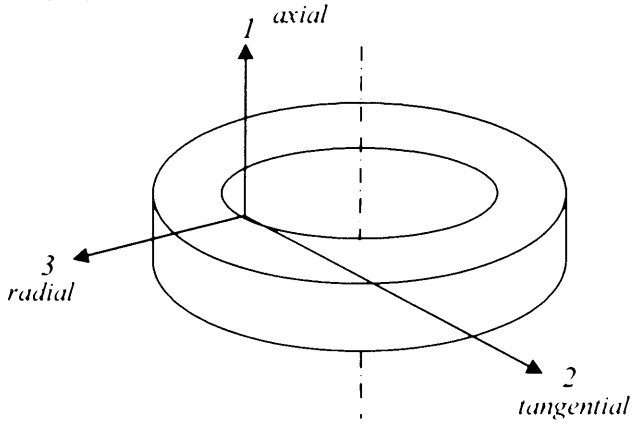

Fig. 3.3 A diagram to explain the numerical axes in table 3.1. The ring represents a coronal slice of the femur.

The cylindrical model comprises a tube of bone, representing the diaphysis of the femur, containing a cylindrical implant. This model was chosen as a geometrical simplification because the diaphysis of the femur is 'almost cylindrical' in the shaft, and comprises only cortical bone (Gray, 1898).

Since the cylindrical model contains only cortical bone, values in table 3.1 were used. A transversely isotropic material was chosen for simplicity because it is a good representation of the structure of cortical bone (Reilly and Burstein, 1974). The properties chosen are in table 3.2. All constants were taken from the same reference, (Ashman and Rho, 1988), so that they are consistent with a single model. The same reference was used to find the preliminary Poisson's ratio in section 3.1.2; again, for consistency of bone model.

	Young's Modulus	Poisson's Ratio	Shear Modulus
Longitudinal	E_1=20 GPa	v_{23}=0.376	G_{23}=4.53GPa
Transverse	E_3=12GPa	v_{12}=0.235	G_{12}=6.23GPa

Table 3.2 The material properties chosen for the cylindrical model (Ashman and Rho, 1988)

3.1.6 The Use of CT Data to find Young's Modulus

A finite element model can be created using computed tomography (CT) data of a bone, and this technique is used in chapter five to create a model of the femur. It is possible to apply material properties to such a model using the saturation of the CT images. Hounsfield Units (denoted $\overline{HU}$) are a measure of the hue of CT the plot and are approximately proportional to the porosity of the material (Rho *et al.*, 1995). A number of studies have devised relationships between the Hounsfield Unit and the Young's Modulus (E) for bone (Carter and Hayes, 1977; Rho *et al.*, 1995; Wirtz *et al.*, 2000), Young's modulus is a function of the Huonsfield Unit:

$$E = f(\overline{HU}) \text{ (Carter and Hayes, 1977)} \qquad \textit{(eq.3.4)}$$

However, it has been observed that relationships that convert $\overline{HU}$ to density and then the density to Young's Modulus appear to be more accurate than those that convert Hounsfield Unit directly to Young's Modulus (Rho, Hobatho and Ashman, 1994). This could be because the Hounsfield unit is proportional to porosity but it is *density* that is related to Young's Modulus. To prevent the inaccuracy, a method is required to find the density of the materials in the bone and then convert these densities to Young's Moduli. The following relationships can be used to find the Young's modulus from $\overline{HU}$: density is a function of Hounsfield Unit, $\rho = f(\overline{HU})$, and then Young's Modulus is a function of density, $E = f(\rho)$.

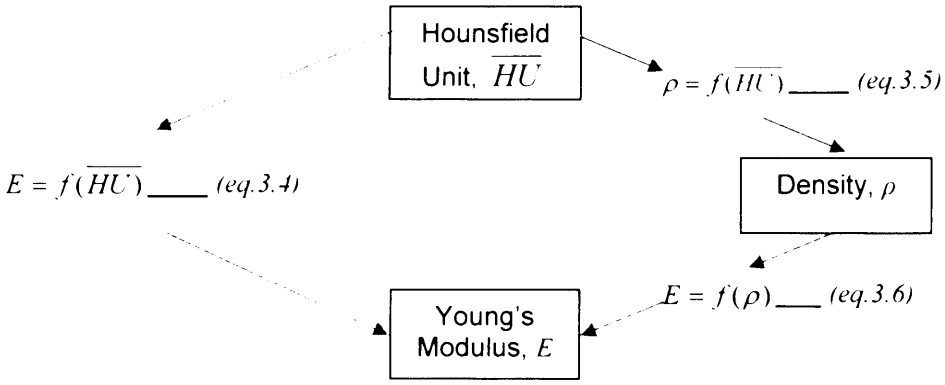

The next sections will discuss the two steps in the conversion: equation 3.5 and equation 3.6.

3.1.6.1 Conversion of Hounsfield Number to Density

An absolute relationship between Hounsfield number and density cannot be established because the value of $\overline{HU}$ depends on the strength of the radiation source in the CT scanner, and is therefore different in different machines and also variable over time in one machine. Various ways have been found to overcome this. In table 3.3, the results of three different methods are shown.

Rubin *et al.* (1993) calibrated the CT scanner by placing a 'phantom', a vial of water, in the scanner and recording the $\overline{HU}$ for water and for air. Since water and air have known densities, they were able to calibrate the values found in the bone. The relationship in table 3.3 is this calibration.

Taylor *et al.* (2002) used a relationship that had been proposed previously (Rho *et al.*, 1995) but after applying the densities of different materials in the femur, found the mass of the bone different from that of the whole bone when weighed. They varied the constant of multiplication until the calculated mss of the femur matched the reading on the scales. This method was used in this project. The whole bone was divided into five different materials, then equation 3.5b (Rho *et al.*, 1995) was used, and A was varied until the density multiplied by the volume match the mass of the bone.

Authorship	Properties used	$\rho = f(\overline{HU})$ _____ *(eq.3.5)*
Rubin & *al.* 1993	Transversely Isotropic	$\rho = 0.9811 \times \overline{HU} - 922.679$ _____ *(eq.3.5 a)*
Rho & *al.* 1995	Isotropic	$\rho = A \times \overline{HU} + 1000$_____ *(eq.3.5 b)*
Taylor & *al.* 2002	Isotropic	$\rho = 0.523 \times \overline{HU} + 1000$_____ *(eq.3.5 c)*

Table 3.3 Relationships used in previous FEA studies to convert $\overline{HU}$ to density.

Figure 3.4 Relationships between Hounsfield unit and Density from different authors from table 3.3.

3.1.6.2 Conversion of Density to Young's Modulus

Table 3.4 contains three methods that have been used to convert density to Young's Modulus.

Authorship	Properties used	$E = f(\rho)$ (eq. 3.6)
Carter and Hayes, 1977	Isotropic	$E = 2875\rho^3$ (eq. 3.6a)
Wong & *al.* 2005	Isotropic	$E = 2875\rho^3$ varies material properties by multiplying by 0.9, 0.8, 0.7 &c.
Wirtz & al. 2000	Transversely isotropic	Cortical bone axial $E = 2065\rho^{3.09}$ (eq. 3.6b) transverse $E = 2314\rho^{1.57}$ (eq. 3.6c) Cancellous bone axial $E = 1904\rho^{1.64}$ (eq. 3.6d) transverse $E = 1157\rho^{1.78}$ (eq. 3.6e)

Table 3.4 Relationships used in previous FEA studies to convert density to Young's Modulus.

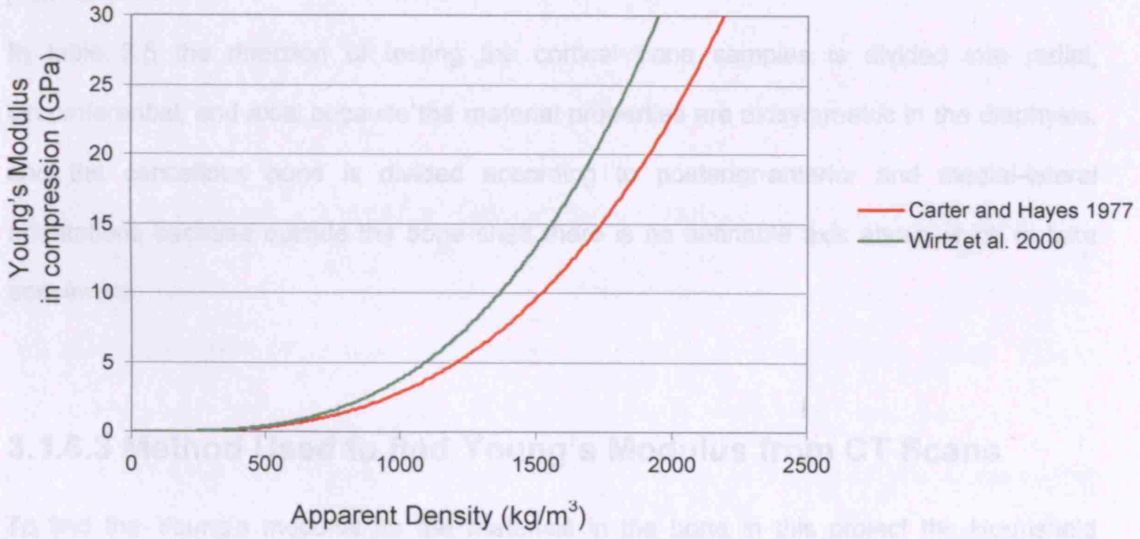

Figure 3.5 Relationships between Density and Young's modulus for cortical bone from different authors from table 3.4.

Rho, Hobatho and Ashman (1994) compared the technique of applying material properties to bone according to the density from $\overline{HU}$ with elastic properties found using an ultrasonic transmission technique, they concluded that Carter and Hayes' relationship (equation 3.6a) is only useful for predicting the material properties in cancellous bone and not in cortical bone. In 1995 they published an extensive analysis of human bone material properties and devised relationships between density and Young's modulus. The most accurate relationships they found for the proximal femur are in table 3.5.

	direction	Relationship between Young's Modulus and density
cortical bone	radial	$E = -6.087 + 0.01\rho$
	circumferential	$E = -4.007 + 0.009\rho$
	axial	$E = -6.142 + 0.014\rho$
cancellous bone	medial-lateral	$E = 0.01\rho^{1.86}$
	anterior-posterior	$E = 0.004\rho^{2.01}$
	axial	$E = 0.58\rho^{1.30}$

Table 3.5 Relationships devised by Rho et al. (1995) between density and Young's Modulus for the proximal femur.

In table 3.5 the direction of testing the cortical bone samples is divided into radial, circumferential, and axial because the material properties are axisymmetric in the diaphysis, and the cancellous bone is divided according to posterior-anterior and medial-lateral orientations because outside the bone shaft there is no definable axis about which to take specimens.

3.1.6.3 Method Used to find Young's Modulus from CT Scans

To find the Young's modulus for the materials in the bone in this project the Hounsfield numbers from the CT scans were converted to densities (using equation 3.5b in table 3.3) and verified using the volume and mass of the bone. Then the Young's modulus was found from the density. The whole range of $\overline{HU}$ numbers for the femur was divided into five

sections: two materials in the cortical range and three in the trabecular range. For each material a representative $\overline{HU}$ value was chosen. The Young's moduli calculated, using the relationships in table 3.5, for the inhomogeneous femur model are in table 3.6.

		Material number (E in Gpa)				
	Direction	1	2	3	4	5
cortical bone	radial	12.263	11.413			
	circumferential	12.508	11.743			
	axial	19.548	18.358			
Cancellous bone	medial-lateral			7.413	4.539	1.757
	anterior-posterior			8.143	5.191	0.98
	axial			12.758	5.21	0.704

Table 3.6 The Young's modulus for each orthotropic direction calculated using the relationships in table 3.5.

Although Rho *et al.* (1995) find these, their most accurate relationships between density and Young's modulus, to be less accurate for cortical bone than for cancellous bone, the values it has given (in table 3.6) for the densities in this CT scan are similar to the values found in literature and those chosen to be used in the cylindrical model (E=20MPa in the longitudinal axis, E=12MPa in the transverse axes). Therefore these values were used for the FEA because they will allow comparisons between the cylinder model and the anatomical model.

3.1.7 Conclusion – Material Properties Chosen for the FEA Models

The axisymmetric model is a simplified model of the bone shaft. It is transversely isotropic, one axis having elastic properties distinct from the transverse plane (Peters, 1998). This is regarded to be a good approximation of the bone in the shaft (Reilly and Burstein, 1974) and is often used in finite element models. The material is homogeneous because the structure of the shaft is almost completely cortical bone (Gray, 1898). These simple properties allow analytical calculations to be used in conjunction with the FEA for validation. The value for Poisson's ratio is disputed in the literature (Wirtz *et al.*, 2000) so approximate values were chosen. Table 3.7 outlines the elastic constants for the axisymmetric model.

	Young's Modulus	Poisson's Ratio	Shear Modulus
Longitudinal	E_1=20 GPa	v_{23}=0.376	G_{23}=4.53GPa
Transverse	E_3=12GPa	v_{12}=0.235	G_{12}=6.23GPa

Table 3.7 The material properties to be used in the axisymmetric model.

The anatomical model was created from scans of a whole human femur. It was inhomogeneous and the total material spectrum was divided into five different sections: two cortical 'materials', and three cancellous 'materials'. The Young's modulus for each was derived from computed tomography scans of a femur. Table 3.8 shows the young's moduli calculated. The Poisson's ratio was 0.376 in the axial direction and 0.235 in the radial and circumferential directions.

Direction		Material number (E_1 in Gpa) 1	2	3	4	5
cortical bone	radial	12.263	11.413			
	circumfererential	12.508	11.743			
	axial	19.548	18.358			
Cancellous bone	medial-lateral			7.413	4.539	1.757
	anterior-posterior			8.143	5.191	0.98
	axial			12.758	5.21	0.704

Table 3.8 Young's modulus for the five materials to be used in the three-dimensional femoral model.

3.2 Failure Model for Bone

The strength of a material is the stress it can withstand without fracture, also known as the ultimate strength, and the yield stress is the stress above which plastic deformation occurs. To tell if a loading configuration will fail an isotropic material, the maximum stress on the body is compared with a known value for strength, however the anisotropic nature of bone results in different strength characteristics in different orientations. There are many other factors to consider: bone remodels as a consequence of repeated loading (Wolff, 1986) resulting in fatigue behaviour that differs from engineering materials; bone is slightly viscoelastic so the strain rate varies the ultimate stress. As we have seen in the previous

section, the material properties are greatly affected by the density of the bone. The research into the strength of bone is still fragmentary because of the reasons above and also the methodology varies between researchers, making results difficult to compare.

This section outlines the variables that govern the strength of bone and rationale for any failure model chosen to analyse the finite element models in this project.

3.2.1 The Relationship between Bone Density and Strength

In section 3.1 differences in elastic constants were found between cortical and trabecular bone that were non-linear with density. This suggests that the cortical bone and trabecular bone must be regarded separately when considering material strength, and this approach is taken by a number of researchers (evans, 1973; gibson, 1985; Pugh *et al.*, 1973). Another approach is to regard all bone as one material with different densities (Carter and Hayes, 1977). Keller (1994) compared these two approaches and found that predictions of cortical strength based on trabecular data failed to match the strength of cortical samples and *vice versa*. Based on this finding, a method for predicting strength from density should take a different form for trabecular bone and cortical bone.

Bell et al (1967) reported that bone strength in compression is approximately proportional to the square of the density. This relationship was also found by Carter and Hayes in 1977, Benusan (1983), Ashman and Rho (1988) and Currey (1984). Keller (1994) investigated this approximate relationship and found that bone strength correlated highly with the square of the density but that different functions, between strength and density squared, were required for trabecular bone and cortical bone. This piecewise characteristic may explain the limits defined by Carter and Hayes. Results from Keller's study, where samples of human bone were measured for density and then loaded in compression to failure, give a relationship between 'ash' density and yield stress:

$$\sigma_y = 0.117\rho^{1.93\pm0.04} \quad (R^2=0.969) \text{ units of density: } kg\,m^{-3} \quad \text{(eq.3.7)}$$

To find the ash density of the bone, specimens have to be fired in a furnace and then dried, a method that is not available in this study. Although the ash density is a better predictor of strength than wet density (that measured by the CT method), Keller gives a comparison between the two, and when the values of density found using the CT scans are converted to 'ash density' results are given that fit with those from experiments in the literature. Table 3.9 shows the conversion of wet density to ash density and the yield stress that is valid for that ash density.

	Wet Density (Kgm^{-3})	'ash density' converted using graph (Keller 1994) (Kgm^{-3})	Yield Stress (MPa)
Cortical bone	1835	1290	191
	1750	1240	175
Cancellous bone	1350	960	107
	1100	780	73
	1025	730	64

Table 3.9 Yield stress for the five materials in the femur model.

The yield stress in the cortical bone and the cancellous bone were analysed separately, and for safety the lowest values for each material type were used: 175MPa for cortical bone and 64MPa for cancellous bone. The value of yield stress was chosen based on whether the high stress was found in cortical or cancellous bone.

3.2.2 The Difference in Strength between Bone in Tension and Compression

Keaveny *et al.* (1994) studied bovine tibial trabecular bone in longitudinal compression and tension. They found that the yield strength was 30% lower for tensile loading and that the strength varied linearly with Young's modulus. This is consonant with values reported by Yamada (1970) who recorded the comparisons between compressive and tensile bone strength in the human femur, shown in table 3.10.

Age range of subjects	Compressive Strength /MPa	Tensile Strength /Mpa	Percentage difference between sets of data
20-29	170	125	26%
30-39	170	122	28%
40-49	164	114	30%
50-59	158	95	39%
60-69	148	88	40%

Table 3.10 Comparisons of strength in tension and compression for different age ranges from Yamada (1970)

This table shows that the difference between the compressive strength and the tensile strength increase with age, and also that the strength decreases with age. Similar conclusions are reported by Cowin (1981) and Reilly and Burstein (1979) who find the reduction in strength in transverse loading compared with longitudinal loading of 29% and 34% respectively. The value of yield stress in tension will be taken as 32% lower than the yield strength in compression because this is the mean value of those reported by Yamada (1970).

3.2.3 The Effect of Loading Axis on the Strength of Bone

The studies by Reilly and Burstein (1975) and Cowin (1981) give values for bone strength in the longitudinal and transverse orientations. The values they find are comparable: 135 and 132 MPa in the longitudinal direction respectively and 53 and 58 MPa in the transverse plane. The strength in the transverse plane is approximately 40% of that in the longitudinal direction. This is a significant difference.

A completed finite element analysis presents a large number of results to choose from such as strain, maximum principal stress, axial stresses and von Mises stress. The following sections discuss the merits of using different types of stress in the post-processing of the finite element analysis results.

3.2.3.1 Maximum von Mises Stress

Von Mises stress is a way of combining all the components of a stress into one scalar, it is mostly used in the stress analysis of ductile materials and in fatigue analysis. Using von Mises stress to investigate the breaking of bone has been used in the past but may not be reliable because of bone's anisotropy and porosity. The strength of bone is different in compression and tension (Keaveny & al. 1994) so the direction of the stress is important. Von Mises stress gives unrealistic predictions for microcracking in the study by Zioupos *& al.* (1995), and does not take into account the structure of the material. Cezayirilioglu *et al.* (1985) found no correlation between experimental failure stresses and those predicted by the von Mises stress, it neglects the important effect of stress orientation on the bone (Natali and Pavan, 2002).

3.2.3.2 Maximum Principal Stress

A stress on a body in three-dimensions has components of shear and normal stress. At any point there exists an angle at which the shear stress is zero, where the stress-state can be described only in normal stresses. This angle is known as the principal direction and the axial stresses at this angle, the principal stresses.

There is evidence that small cracks in bone (those that may initiate remodelling) initiate perpendicular to the tensile load: the principal direction, so the maximum principal stress has been used as a predictor for remodelling (Brown & al. 1990), and was found to be effective in the short-term (up to four weeks), but not in the long term. It is thought that this is because as the small cracks grow they eventually orientate with the material axis of the anisotropic material (Zioupos *et al.*, 1995).

Although the principal stresses and von Mises stress are available in the finite element analysis results, a result that includes direction dependency is more accurate. So the

maximum principal stress or von Mises stress are not used in this project, and other failure models are outlined in the following sections.

3.2.3.3 Rigid Cellular Plastic Model

The compressive behaviour of trabecular bone has been compared to the failure of rigid cellular plastics (Carter and Hayes 1997), that is the buckling and bending of individual trabeculae. More recent research shows that the heterogeneity and anisotropy of individual trabeculae may have a significant effect on the mechanical properties of bone at a macroscopic level (Keaveny and Hayes, 1993). This research is not yet developed far enough to be used in analysing risks to bone but recent research has concluded that the breaking strains of individual trabeculae vary, in one study, by 8.8% with a standard deviation of 3.7% (Hernandez *et al.*, 2005). Further research needs to be carried out before this technique can be used to assess the risk of failure of bone, firstly the effect of microscopic failure of trabeculae will need to be related to the macroscopic effect of bone breaking.

3.2.3.4 Maximum Axial Stresses

By recording the stresses in all three axes and three planes of shear, the anisotropic nature of bone can be taken into account. Failure models have been proposed for bone that take these normal and shear stresses into account and therefore the yield properties of bone in the off-axis directions. This method of analysing the results is possible in FEA because the axial and shear stresses are readily available during finite element analysis post-processing. This method was used for analysis of the FEA and a failure criterion was chosen that can take into account the anisotropy of bone, it is discussed in section 3.2.5.

3.2.5 Failure Criterion for Bone

It is desirable to know the strength of bone in directions other than the axes because failure will not necessarily occur in these directions. Reilly and Burstein (1975) recommended Hankinson's equation, developed to predict the strength of wood, to find the ultimate stress in different orientations but this is not entirely accurate. Another option, the Hencky-von-Mises criterion gives a good approximation to experimental results (Fisher, 1967) but the ultimate stress values must be the same in tension and compression for the criterion to work which, as explained in section 3.2.2, is not the case for bone. The Tsai-Wu criterion (Tsai and Wu, 1971) for failure of composite materials was suggested by Cowin (1979) for predicting failure of bone in a study which compared bone structure with wood.

The Tsai-Wu criterion takes into account the strength in all axes of an anisotropic material. The general form of the Tsai-Wu criterion is $f(\sigma_{11}, \sigma_{22}, \sigma_{33}, \sigma^2_{12}, \sigma^2_{13}, \sigma^2_{23}) = 1$ (Tsai and Wu, 1971), This is expanded and the constants are to be found using mechanical testing of the material. The form of the equation, in two dimensions, is as follows:

$$fx.\sigma_{33} + fxx.\sigma^2_{33} + fy.\sigma_{11} + fyy.\sigma^2_{11} + fxy.\sigma_x\sigma_y + fss.\tau^2_{13} = 1 \text{ (Zioupos } et\ al.\text{, 1995)}$$

Where fx, fxx, fy and fyy are functions based on the yield stress of bone in the two directions and fs and fss are based on the maximum shear stress. σ_{33} and σ_{11} and τ_{13} are the applied stresses on the bone. When the criterion is equal to less than one, the stresses do not cause failure of the bone structure. When the criterion is equal to or more than one, bone failure occurs. Figure 3.6 shows the X- and Y-stresses that result in the Tsai-Wu criterion equal to one in two dimensions. The X-direction is the longitudinal direction of the laminae in the bone structure and the Y-direction is the transverse direction.

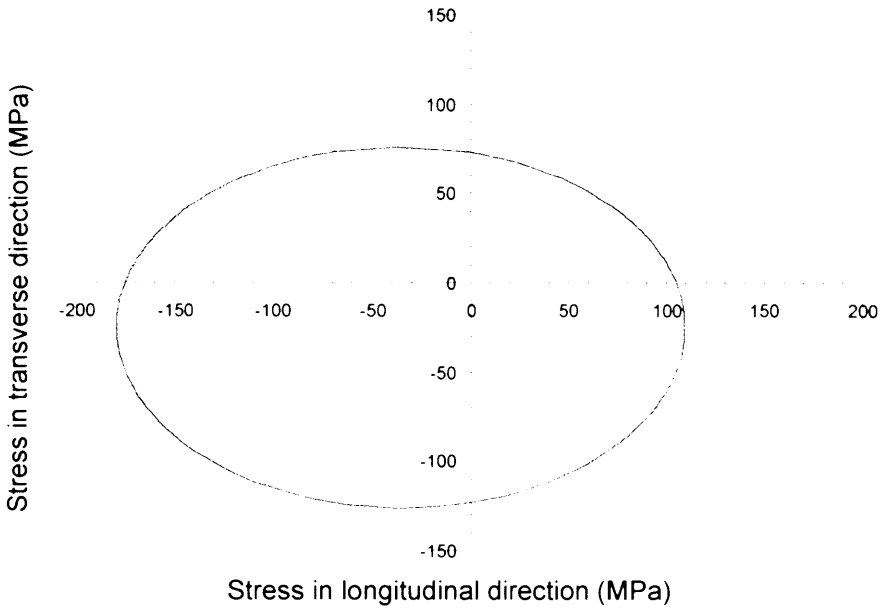

Fig. 3.6 Yield stress in combined axial and transverse loading for human femur using the Tsai-Wu criterion. Combined stresses that lie outside the loop cause fracture.

In figure 3.6 the green line represents the strength of bone under longitudinal and transverse loading according to the Tsai-Wu criterion. The Tsai-Wu criterion gave a reasonable approximation for microcracking around a circular hole in a flat plate of bone in a study in 1995 (Zioupos *et al.*, 1995). Keaveny & *al.* (Keaveny *et al.*, 1999) found it to be "only a reasonable predictor" of the multiaxial failure of bone with a mean error of ±10%, however it is still regarded as the most reliable criterion for stress in bone (Cowin, 1984; Natali and Meroi, 1989; Natali and Pavan, 2002; Pietruszczak *et al.*, 1999).

3.2.6. Bone Strength in the Amputated Femur

Sherk *et al.* (2008) used pQCT to measure bone density in transfemoral and transtibial amputees. The trans-femoral amputees had significantly lower bone density (48% ± 10% reduction in total, 39% ± 4% reduction in cortical bone) than the intact side. The cross-sectional area of the femur was the same as on the intact side but the cortical bone area was smaller, meaning that the cortical bone was thinner, with a larger intramedullary canal. No

significant correlation was made between the number of hours of prosthetic use per day to bone density and cortical cross-sectional area.

Rush et al. (1994) used Dual X-ray absorptiometry to measure the bone density of both femoral necks of sixteen unilateral above-knee amputees. The non amputated femurs had normal bone density but the amputated femurs were 32% less dense. Neither Rush *et al.* (1994) or Sherk *et al.* (2008) related time since amputation to the bone density. However both used amputees with more than three years of prosthetic use and the results had a small scatter and standard deviation, this implies that little change is made to the density of the bone after this period of amputation and prosthesis use.

Using equation 3.6, the bone densities measured by Sherk et al. (2008) were converted to elastic and ultimate material properties of bone for an amputee (table 3.11).

	Young's Modulus (GPa)	Poisson's Ratio	Yield stress in compression (MPa)	Yield stress in tension (MPa)
Longitudinal	12.2 ± 0.5	v_{23}=0.376	67.2 ± 3.1	46.7 ± 1.9
Transverse	7.3 ± 0.2	v_{12}=0.235	27.4 ± 1.0	18.0 ± 0.7

Table 3.11 Material properties of the amputated femur.

It is anticipated that the ITAP users' bone will increase in density as they load the prosthesis. Because the technique of attaching a limb to the amputated femur is a new technique further studies would need to be carried out to monitor the density of the bone in recent amputees and recent prosthetic users to measure the rate of increase in density.

3.3 Strength of the Bone-Implant Interface

In addition to fracture of the bone, another way for mechanical failure of an implanted stem is by shearing of the bone-implant interface. It was planned that the ITAP implant would be coated with hydroxyapatite over at least part of the stem. It was anticipated that the bone-implant interface would increase in strength over time.

Bone has been found to bond to titanium particularly strongly (Brånemark 1977) because of the surface properties of the metal. Hydroxyapatite encourages bone growth because it attracts and binds osteoblast cells (Porter et al., 2002). One way to measure the strength of osseointegration of an implant is to measure the load required to push it out of the bone.

Many push-out studies have been carried out using animal models where the shear strength of the interface has been measured, but the data are not necessarily relevant to human bone, and recent studies have used the non-destructive testing method of resonant frequency analysis to attempt to measure the stability of implants. Analysing the surface of implants retrieved at autopsy also gives an indication to the condition of the bone-implant interface. These methods are researched in sections 3.4.1 to 3.4.3.

3.3.1 Measurement of Interface Strength using Push-Out Tests

Svehla *et al.* (2002) implanted sheep tibiae with titanium implants of varying roughness and thickness of HA coatings. They performed push-out tests after implantation at 4, 8, 12 and 26 weeks. Failure occurred at the interface between the bone and hydroxyapatite for all time points except from at four weeks where the new bone that had grown into the drill hole fractured. In none of the cases did the HA come away from the titanium. For non-HA samples the roughest grit-blast surface gave the greatest shear strength, increasing from 3MPa at 4 weeks to approximately 30MPa at 26 weeks. 100μm of HA thickness gave an

optimum strength for the coated implants, the shear strength was 3MPa at 4 weeks and about 37MPa at 26 weeks.

A canine model was used to make a number of observations of the behaviour of HA coated titanium pegs by Cook et al. (1988). One of the experiments performed on the specimens was a push-out test to find the shear strength of the bone-implant interface at 3, 5, 6, 10 and 32 weeks. The shear strengths of bone bonded to HA-coated implants were three times the strengths of bone-implant interfaces where the implant was not coated with HA. A sharp increase in shear strength was found between weeks 3 and 5 and any variations found beyond 5 weeks were not statistically significant. The shear strength after five weeks was approximately 6MPa.

The shear strength of 6MPa found by Cook et al (1988) is much smaller that the 27MPa measured by Svelha et al (2002) and the experimental methods are similar in each study. It is possible that this is because the quality of the HA coating had improved in 2002 since 1988, so recent research was investigated to find other values for shear strength of an HA-coated implant over time. Yang and Yang (2007) found the push-out shear strength of 50μm HA-coated titanium implants in canine femurs to be 10MPa at four weeks and 14MPa at 12 weeks, and also that a thicker coating of HA (200μm) had a 20-33 percent lower shear strength. Hing *et al.* (1997) found the shear strength of the interface between rabbit bone and a porous HA implant to increase to 7MPa at 12 weeks. Aebli *et al.* (2002) measured the shear strength of rough titanium implants and HA coated implants in sheep tibiae at one, two and four weeks and found there to be no significant difference between the two. Figure 3.7 shows the change in interface shear strength found in the aforementioned studies.

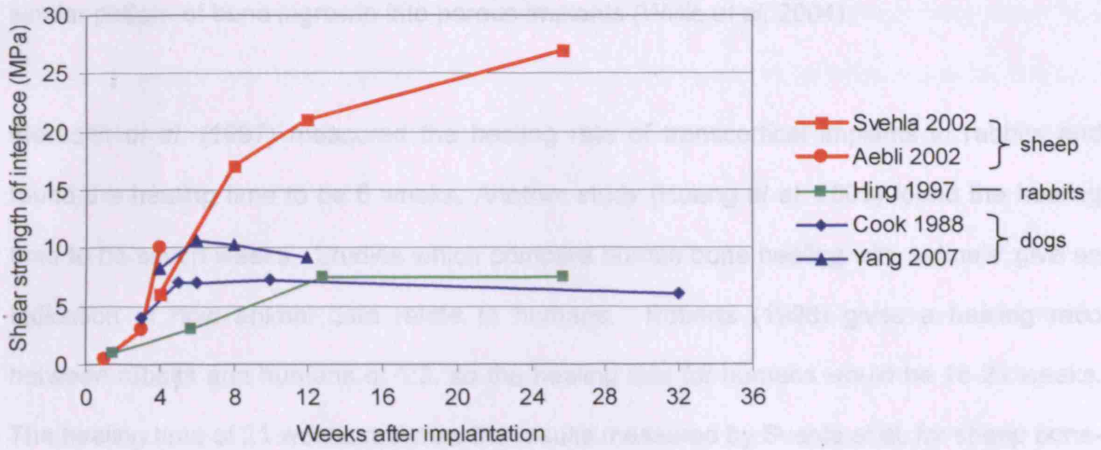

Figure 3.7 Strength of the bone-HA interface in transcortical push-out studies using HA coated titanium implants by various authors.

In figure 3.7 it is evident that the strength of the bone-implant interface increases over time, the only drop in shear stress occurs in the study by Yang *et al.* but this was found to be not statistically significant. These results can be used to estimate the general pattern of interface strengthening in the human model but cannot be used to define values for strength because human bone strength is different.

There are three drawbacks in using these studies to predict the interface strength in ITAP. Firstly, the implants are transcortical meaning that they are placed radially in the bone as opposed to longitudinally, as is the ITAP implant. Secondly the implants are not loaded and bone is known to remodel as a result of load bearing (Ducheyne *et al.* 1977). The third drawback is that the bone on which the tests have been carried out is not human, and therefore has different mechanical properties.

Aerssens *et al.* (1998) studied the construction of bones from different species and found that canine bone was most similar to human but that it is stronger. This finding is backed-up by another group (Wong *et al.* 1998) who found that canine bone has significantly greater mineral density than human bone. Ovine models are often used for studies into bone

remodelling, because sheep display similar healing rates and have been found to develop a similar pattern of bone ingrowth into porous implants (Willie *et al.* 2004)

Meredith *et al.* (1997) measured the healing rate of transcortical implants in rabbits and found the healing time to be 6 weeks. Another study (Huang *et al.* 2003) found the healing time to be seven weeks. Studies which compare human bone healing with animals' give an indication of how animal data relate to humans. Roberts (1998) gives a healing ratio between rabbits and humans of 1:3, so the healing rate for humans would be 18-21 weeks. The healing time of 21 weeks matches the results measured by Svehla et al. for sheep bone-implant healing, as seen in figure 3.25, and because sheep models are regarded as the best for predicting human bone growth, this healing period was used in this project to represent healing time for the ITAP amputees.

According to Helgason *et al.* (2008), although numerous push-out tests have been published, researchers are 'still some way off' in developing accurate numerical models to simulate implant stability. Therefore other methods should be pursued to investigate the strength of the bone implant interface.

One of the drawbacks to the push-out tests reported above was that the bone of different species' have different material properties. There are two methods of measuring the interface strength directly in humans that might be possible: retrieval of implants post-mortem or measurement of the torque required to remove a temporary bone screw such as for fracture fixation. The shear strength of the interface has not been measured in post-mortem retrievals, but studies of screw removal torque can be used to calculate the shear strength of the interface.

To calculate the strength of the bone-implant interface, studies of temporary implant removal were chosen that include implantation into cortical bone. All implants were transcortical and had a coating of hydroxyapatite. The implants included screws for leg lengthening fixtures

(Placzek et al. 2006) and two studies of external fixation pins (Magyar et al. 1997), (Moroni et al. 1998). In all three papers the pins were removed using a torque wrench. The measured torque was used to calculate the force acting on the bone adjacent to the implant and this force was divided by the area of bone-implant contact to find the shear strength of the bone-implant interface. The results were all given as mean values with the range of all values. The papers reporting removal torque of external fixation screws had removal torques of 22MPa (maximum 28MPa, minimum 11MPa) and 20MPa (maximum 38MPa, minimum 10MPa) and the paper with the leg lengthening fixture screws gave shear strength of 18MPa (maximum 26MPa, minimum 6MPa). Based on these results, 20MPa was chosen to represent the shear strength of the bone-implant interface because it is the mean of the values obtained from the literature. It should be noted, however, that bone surrounding transcortical screws differs from the bone surrounding the intramedullary canal due to bone anisotropy, so the value might not be precise.

3.3.2 Measurement of the Interface using Resonant Frequency Analysis

Another option of analysing the bone-implant interface is the non-destructive technique of resonant frequency analysis (RFA). RFA is being developed for studying dental implant integration and can be used to measure the development of bone-implant healing over time in percutaneous implants. The external part of a percutaneous implant is struck and allowed to vibrate and a transducer measures the resonant frequency (the frequency at which it oscillates with the highest amplitude). It has been found in the studies of tooth implants that the resonant frequency increases with time and that a higher frequency relates to better bone integration. Zhou *et al.* (2007) found that resonant frequency analysis compared well with the amount of bone attached to the implant, and proposed it as a reliable technique to measure the osseointegration of an implant.

The OPRA implant was tested using resonant frequency analysis (Shao *et al.*, 2007). The tests were carried out just before the amputee began weight bearing on the prosthesis and then each day for three days followed by once a fortnight (figure 3.8 (a)). The results are not directly relevant to the prediction of remodelling at the bone-implant interface during the time after implantation because the measurements were taken 8 months after the implant was inserted into the femur.

In a clinical study, Crismani et al. (2006) measured the resonance of dental plates weekly for 12 weeks after implantation (figure 3.8(b)). They found that the resonant frequency did not plateau, but continued to increase up to the end of the study. Similar results were found by another study (Huwiler *et al.* 2007) in a clinical study of dental implants: the resonant frequency continued to increase over a 12 week study. This could be confirmation that time for the bone-implant interface to heal is more than twelve weeks.

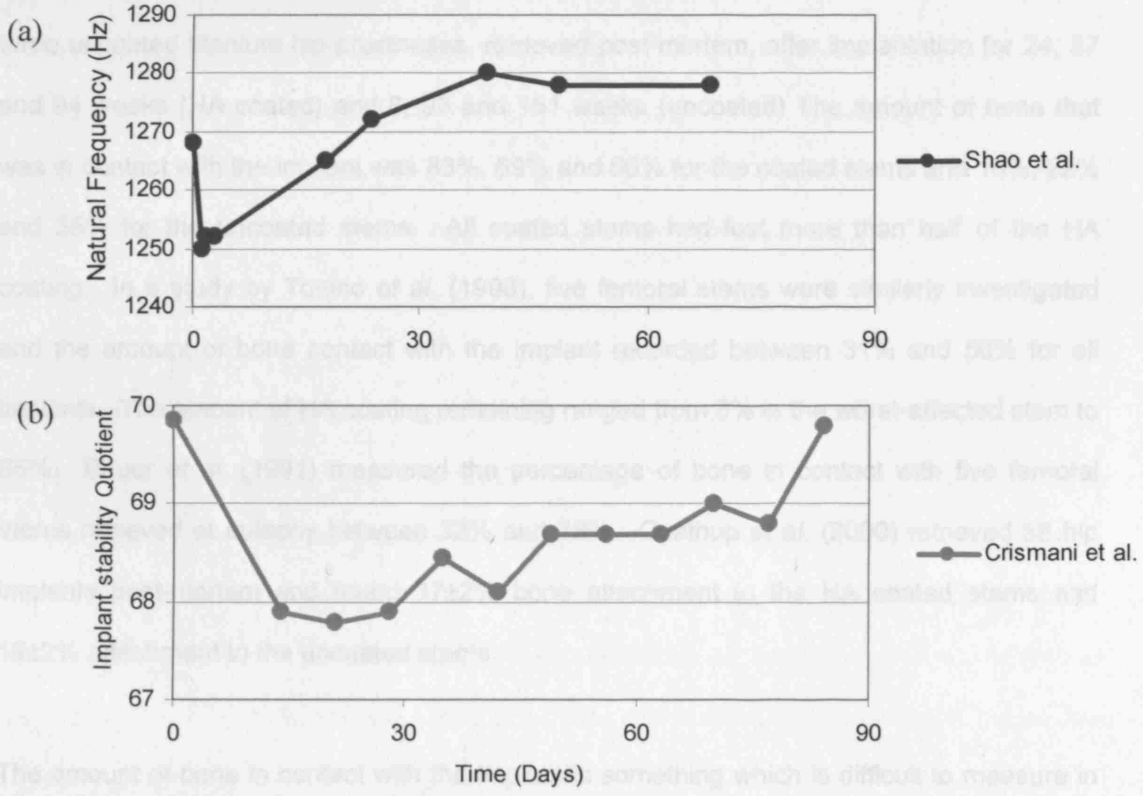

Figure 3.8 Results of two resonant frequency analyses of implants. (a) OPRA implant for femoral prosthesis attachment (Shao et al. 2007) and (b) dental bridge implant (Crismani et al. 2006)

Figure 3.8 (a) shows that the resonant frequency reduced after the first load bearing exercise and then increased. Figure 3.8 (b) shows a similar pattern in the 'implant stability quotient', which is a dimensionless indicator of the level of osseointegration derived from the resonant frequency, in a dental bridge that was immediately loaded after implantation. These results indicate that the stability of the implant might reduce after the first loading and then increase again. Further research using this technique might be beneficial in increasing knowledge of the development of the bone-implant interface and it would be useful to understand the significance of the dip in natural frequency after implant loading. This data should be used with caution because the change in implant stability shown in figure 3.8 might be insignificant and it is difficult to know what is meant by readings of RFA in general.

3.3.3 Bone Attachment to Implant

Porter *et al.* (2003) analysed the amount of bone attached to three HA coated titanium and three uncoated titanium hip prostheses, retrieved post-mortem, after implantation for 24, 37 and 94 weeks (HA coated) and 6, 93 and 151 weeks (uncoated) The amount of bone that was in contact with the implant was 83%, 69% and 66% for the coated stems and 18%, 22% and 35% for the uncoated stems. All coated stems had lost more than half of the HA coating. In a study by Tonino *et al.* (1998), five femoral stems were similarly investigated and the amount of bone contact with the implant recorded between 31% and 56% for all implants. The amount of HA coating remaining ranged from 5% in the worst-affected stem to 65%. Bauer *et al.* (1991) measured the percentage of bone in contact with five femoral stems retrieved at autopsy between 32% and 78%. Coathup *et al.* (2000) retrieved 58 hip implants post-mortem and found 37±2% bone attachment to the HA coated stems and 19±2% attachment to the uncoated stems.

The amount of bone in contact with the implant is something which is difficult to measure in patients and would not be measured as part of the normal rehabilitation programme, so to

safely model the bone-implant interface a low percentage of bone attachment should be used. 25% microscopic bone attachment is two-thirds of the amount of bone attachment to an HA coated stem measured by Coathup *et al.* (2000) and will be used for safety.

3.4 Conclusions

In this chapter investigations have been made into the factors that influence the elastic constants and failure of bone. In part 3.1, the material properties for the FEA models were selected from previous research and in part 3.2, the different approaches to analysing the stresses apparent in bone models were discussed and an a failure criterion that takes into account the anisotropy of bone was chosen.

The elastic constants were found using published literature on the properties of the human femur. For the cylindrical model of the bone shaft, a transversely isotropic material was chosen because it is regarded to be a good approximation of the bone in the shaft and is often used in finite element models (Reilly and Burstein, 1974). The material is also homogeneous so that validation can be carried out using analytical calculations. There are many different values for Poisson's ratio in the literature (Wirtz *et al.*, 2000) so approximate values were chosen.

In order to create an anatomical femur model for FEA, a method was discussed for finding inhomogeneous material properties throughout a bone from computed tomography scans. A human femur was scanned and the Young's modulus calculated for regions of different densities using formulae devised by Rho *et al.* (1995) and developed by Taylor *et al.* (2002). Again, approximate values were used for Poisson's ratio because there is little agreement in the literature. The Poisson's ratio is 0.376 in the longitudinal direction and 0.235 in the transverse direction.

In section 3.2, factors that influence the ultimate strength and yield stress of bone were studied. The yield stresses of the five 'materials' in the anatomical FEA model were calculated from Keller (1994), who brought together a number of different approaches to converting density to strength for bone. The yield stress in tension was found to be 32% lower than that the yield stress in compression based on results by Keaveny *et al.* (1994), Yamada (1970), Cowin (1981) and Reilly and Burstein (1979). When combined loads are applied to bone, the fracture risk can be assessed using a criterion of the form $f(\sigma_{11}, \sigma_{22}, \sigma_{33}, \sigma^2_{12}, \sigma^2_{13}, \sigma^2_{23}) = 1$ (Wu, 1972), created by Tsai and Wu for analysing composite materials. The Tsai-Wu criterion was used to investigate the combined effects of axial and transverse stresses occurring at a point (Pietruszczak *et al.*, 1999). Density measurements for the femurs of trans femoral amputees were used to calculate the strength of bone for a trans femoral amputee.

In section 3.3 the shear strength of the bone-implant interface was studied from published research using in vivo tests that record push-out load of implants, clinical removal torque studies of temporary implants and resonant frequency analysis. The amount of bone in contact with the implant in retrieval studies was considered.

Tables 3.12, 3.13, 3.14 and 3.15 summarise the material properties for the different FEA models.

	Young's Modulus/ GPa	Poisson's Ratio	Shear Modulus/ MPa	Yield stress in compression/ MPa	Yield stress in tension/ MPa
Longitudinal	E_1=20	v_{23}=0.376	G_{23}=4530	175	123
Transverse	E_3=12	v_{12}=0.235	G_{12}=6230	105	73

Table 3.12 The material properties to be used in the cylinder model.

	Young's Modulus	Poisson's Ratio	Shear Modulus/ GPa	Yield stress in compression/ MPa	Yield stress in tension/ MPa
Longitudinal	See table 3.14	v_{23}=0.376	G_{23}=4530	Cortical 175	Cortical 123
				Cancellous 64	Cancellous 45
Transverse		v_{12}=0.235	G_{12}=6230	Cortical 105	Cortical 73
				Cancellous 38	Cancellous 27

Table 3.13 Material properties for cortical and cancellous bone for the three-dimensional model.

	Direction	Material number (E_1 in Gpa) 1	2	3	4	5
cortical bone	radial	12.263	11.413			
	circumfererential	12.508	11.743			
	axial	19.548	18.358			
Cancellous bone	medial-lateral			7.413	4.539	1.757
	anterior-posterior			8.143	5.191	0.98
	axial			12.758	5.21	0.704

Table 3.14 Young's modulus in compression for the five materials to be used in the three-dimensional femoral model.

Strength of bone-implant interface at implantation	Strength of bone-implant interface after healing	Time to heal bone – implant interface	amount of bone attached to implant
6MPa	20MPa	21 weeks	25%

Table 3.15 Properties of the bone-implant interface

4 The Effect of Geometric and Material Variables on the Stress Transferred to the Femur

4.1 Introduction

Finite element analysis was used to investigate the way in which the load is transferred from the implant to the bone and the effect on the pattern of stress transfer of altering the geometry of the implant, the geometry or material properties of the bone or the nature of the interface between the bone and the implant.

In this chapter these variables were modelled: the diameter of the bone and the amount of the implant in contact with cortical bone (to investigate the differences between amputees); and the length and diameter of the implant and the effect of including a collar on the implant at the end of the bone (to inform the design of the implant). The imposed stresses in these models were studied in bending, torsional loading and axial loading.

4.2 Method

To create a finite element model for stress analysis the geometry, material properties and boundary conditions were defined. The type of mesh was chosen and the size of the mesh was selected to give accurate results.

4.2.1 Femur Geometry

The femur is a long, slender, bone with extremities that make the articulating surfaces at the hip and knee joints. It is almost cylindrical along most of its length apart from a prominent posterior ridge, the *linea aspera* (Gray, 1858b), see figure 4.1b), giving it an ovular appearance in cross-section. It is curved in the saggital plane (front-to-back) with the convex side facing forwards (Gray, 1858b) see figure 4.1c).

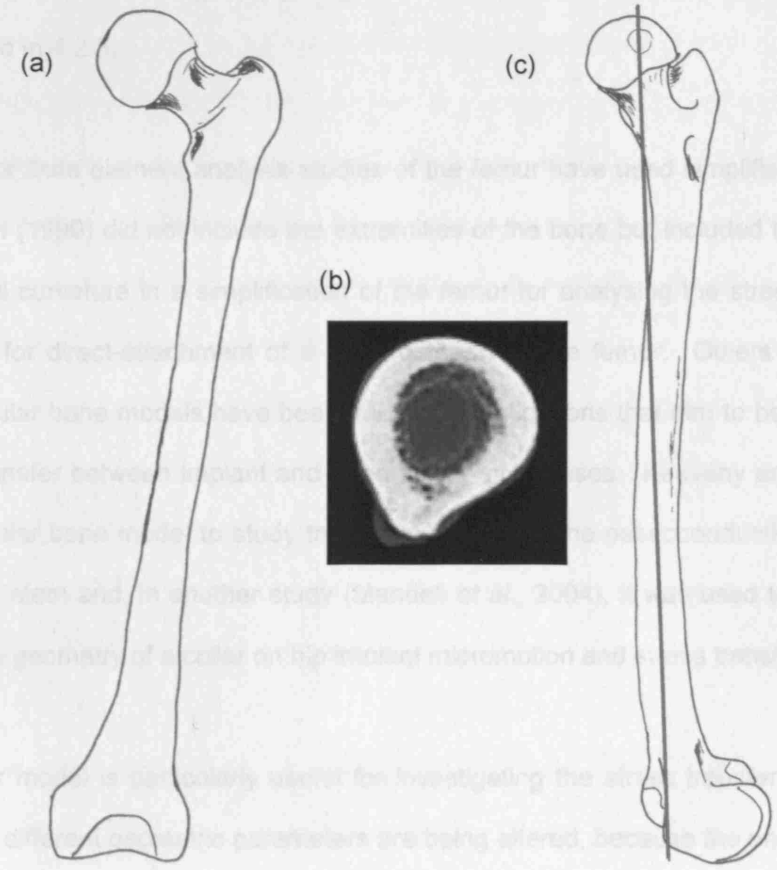

Figure 4.1 The anatomy of the femur; a) in the frontal plane, b) the cross-section in the mid-shaft, c) in the saggital plane. (a) and (c) adapted from Palastanga, Field and Soames (1998), (b) CT scan taken for use in this project.

In the past there have been three main reasons for simplifying the geometry of the femur for finite element analysis: the first has been because of software limitations in speed and complexity; the second reason is to reduce the cost because the creation and analysis of a complicated model is time-consuming; the third reason is to remove the confounding effects of bone geometry on the analysis of conditions at the implant-bone interface (Keaveny and Bartel, 1994) if these are of interest. As finite element analysis software improves and hardware becomes faster at processing data, the limitations caused by them are reduced. In this piece of work the software available is adequate to handle the demands of an anatomical model of bone and the execution of such a model is not prohibitively time consuming. However the third reason, given above, is of relevance here and a cylindrical model was considered to be appropriate for this investigation. The model was carefully adjusted to prevent it taking a very long time to run, without affecting the accuracy, this is documented in 4.2.5.

A number of finite element analysis studies of the femur have used simplified bone models. Stephenson (1999) did not include the extremities of the bone but included the *linea aspera* and femoral curvature in a simplification of the femur for analysing the stress transfer from an implant for direct-attachment of a leg prosthesis to the femur. Others have simplified further; tubular bone models have been used in investigations that aim to better understand the load transfer between implant and bone for hip prostheses. Keaveny and Bartel (1994) used a tubular bone model to study the effect of varying the osseoconductive coating on a cementless stem and, in another study (Mandell *et al.*, 2004), it was used to determine the effect of the geometry of a collar on hip implant micromotion and stress transfer.

The tubular model is particularly useful for investigating the stress transfer throughout the bone when different geometric parameters are being altered, because the only variables that influence the stress in the model are the boundary conditions (the loads applied and the way in which the model's movement is constrained) and the particular geometry used in each manipulation of the model. This was the format used in this chapter: a cylindrical implant

contained within a tubular bone in which the dimensions of the tube and cylinder are altered for investigating geometric variables.

Much of the work in this chapter could have been carried out using analytical calculations that take into account stress concentrations, material properties and geometry of the structure. However the FEA models created form the basis of further work, and provide validation for the anatomical model created in chapter five.

4.2.2 Basic Model Geometry

A radiograph of a femur was measured to find the place where the minimum outer diameter coincided with the maximum intramedullary diameter to give the dimension of the section of bone that is at the highest risk of breaking because it has a small second moment of area. The dimensions were confirmed from literature (Stephenson and Seedhom, 1999) where a femur was sectioned at ten millimetre intervals and each cross-sectional area measured. In both cases the maximum inner diameter of cortical bone in the mid-third of the femur is twelve millimetres and the minimum outer diameter is twenty millimetres. The standard FEA bone model created was a tube of twenty millimetres diameter with an inner diameter of twelve millimetres. Although the distance from the central axis of the model to the outer surface was the same as the distance measured from the x-ray and found in Stephenson (1999), the second moment of area and the polar moment of area are smaller in a tube than in the femur because of the *linea aspera*, this means that stresses in the tubular model were calculated to be higher than they would be in a model of accurate bone geometry. In this way a margin of safety was included in the model.

In order to investigate the effect of geometric variables on a structure, a basic model must be described which is to be varied. The basic model was a tube of bone containing a cylinder of titanium implant. Figure 4.2 shows how this was created using the finite element modelling software. The elements in this figure were 'expanded' around the centre line to give a solid. Figure 4.2(b) shows the entire model, revolved around the centre line. The basic implant

was 150mm long, with 100mm within the bone medulla. This is consistent with a standard implant length for a patient with enough residual bone.

The basic model was linear because the implant and bone had perfect boundary conditions (they were 'glued' together). The applied transverse load produced an increasing bending moment along the model (and a constant shear force) and the axial and torsional loads gave a constant load along the model. For one part of this study the length of bone contact with the implant was varied and this model was nonlinear because of friction between the implant and the non-bonded bone.

The proximal end of the model implant was flat but the actual implants are likely to have a rounded end to prevent damage to the bone during insertion. It was found that, due to the perfect boundary conditions, there was no difference in the stress distribution in the bone from the flat-ended implant and the rounded implant, so a flat implant was used for the model with perfect contact.

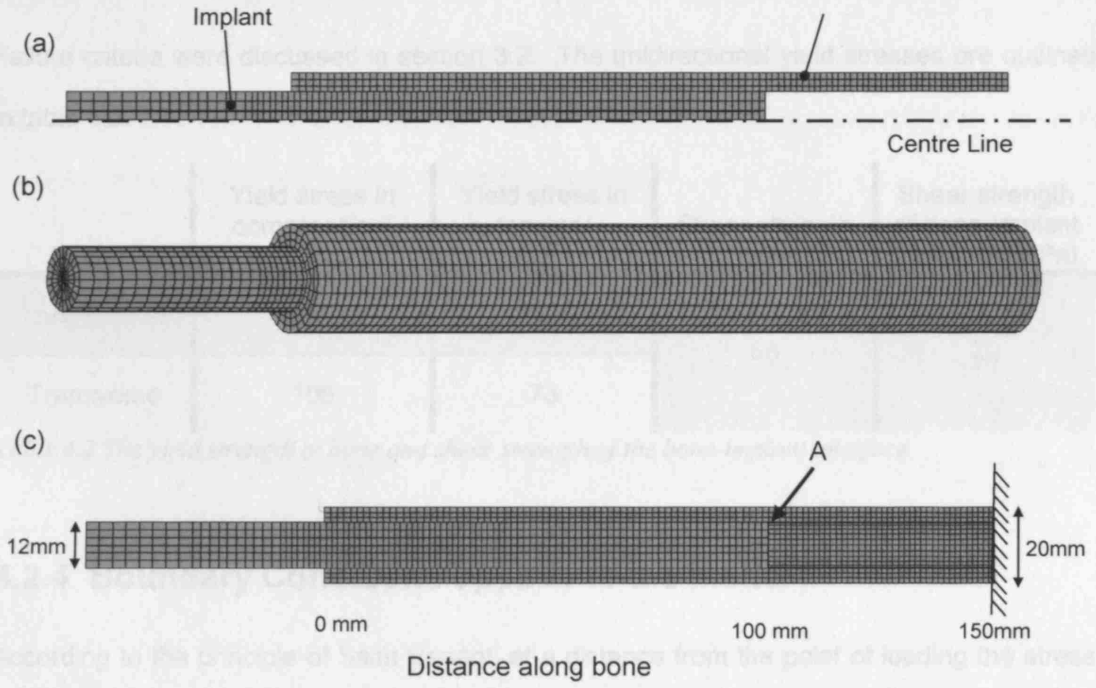

Figure 4.2 The geometry of the bone model; (a) section before revolving the elements (b) the solid model created from revolving the elements (c) a cross-sectional view of the model showing the geometry.

4.2.3 Material Properties

The material properties found in chapter three were used in the finite element analysis. The model was transversely isotropic, the bone axis having elastic properties distinct from the normal plane (Peters, 1998). This is regarded to be a good approximation of the bone in the shaft and is often used in finite element models (Reilly and Burstein, 1974). The material is homogeneous because the structure of the shaft is almost completely cortical bone (Gray, 1898). These simple properties allow analytical calculations to be used in conjunction with the FEA for an initial validation of the model. The value for Poisson's ratio is disputed in the literature (Wirtz *et al.*, 2000) so approximate values were chosen. Table 4.1 outlines the elastic constants for the axisymmetric model.

	Young's Modulus (GPa)	Poisson's Ratio	Shear Modulus/ (MPa)
Longitudinal	E_1=20	v_{23}=0.376	G_{23}=4530
Transverse	E_3=12	v_{12}=0.235 v_{31}=0.235	G_{12}=6230 G_{31}=6230

Table 4.1 The material properties to be used in the axisymmetric model

Failure criteria were discussed in section 3.2. The unidirectional yield stresses are outlined in table 4.2.

	Yield stress in compression/ MPa	Yield stress in tension/ MPa	Shear strength (MPa)	Shear strength of bone-implant interface (MPa)
Longitudinal	175	123	68	20
Transverse	105	73		

Table 4.2 The yield strength of bone and shear strength of the bone-implant interface

4.2.4 Boundary Conditions applied to the Model

According to the principle of Saint Venant, at a distance from the point of loading the stress distribution is independent of the mode of load application. This principle was utilised in these models by applying the boundary conditions at a distance from the areas that were being investigated. The bone was held as a cantilever with the loads applied to the implant.

The stresses at the point of holding were high but they died away very quickly as the distance from the end of the bone increased. As long as the implant is situated far enough away from the held end of the bone the high stresses caused by the cantilever constraint do not affect the stresses in the bone adjacent to the implant.

The loads applied to the implant were taken from research in chapter two. To summarise, the loads chosen were those to be found during normal activities. The loads were applied from the position of the knee, a distance from the knee to the femur of 170mm was chosen to represent a fairly short residual limb.

The loads were obtained from a study in which a load-cell was incorporated into twelve osseointegrated prostheses (from the OPRA system) to measure the forces and moments during walking in the implant of twelve amputees (Lee *et al.*, 2007a). The loads are the maximum experienced during normal activities. The data were given in percentage of bodyweight and were converted to be relevant for a patient of 750N with a femur resected half-way along. The loads were consistent with other, comparable, studies (Stephenson and Seedhom, 2002b; Taylor and Walker, 2001b). The loads used were 143N bending force applied 170mm from end of stump (the position of the knee) to generate shear forces and bending moments, 664N axial load and 8Nm axial torque.

4.2.5 Mesh Details

MARC (Msc Software Inc. USA), with the MENTAT pre-and post-processor (Msc Software Inc. USA), was used for the finite element analysis. This combination was chosen for the ease with which the contact conditions can be altered.

The model was created using hexahedral elements. There are different benefits to using tetrahedral or hexahedral elements: tetrahedral elements use less computing time (Viceconti et al. 1998) but results from models with hexahedral elements have been found to be less influenced by the size of the elements (Ramos et al. 2006). Hexahedral elements are also

easier to generate for a cylindrical model. Hexahedral elements were used in this model with a core of tetrahedral elements through the centre of the implant.

A convergence study was carried-out to find the appropriate mesh size to use. Finite element analysis gives an approximate solution to a problem, the smaller the elements the more accurate the solution. However, computing a very fine mesh is time-consuming and a trade-off has to be made between accuracy and time taken to compute the results. The same geometry and boundary conditions were used to assess the maximum stress recorded and a permissible relative error of five percent was used to choose the mesh (Cook, 1994). Figure 4.4(a) shows the increase in accuracy found for meshes that contain smaller elements. Figure 4.4(b) shows the time taken to compute the analyses in figure 4.4(a). The model chosen contained 20026 8-node hexahedral elements that had an edge length of 1mm in the axial and radial directions. The edge length varied tangentially with the radius but was 1mm at the implant-bone interface, around the inner surface of the bone and outer surface of the implant.

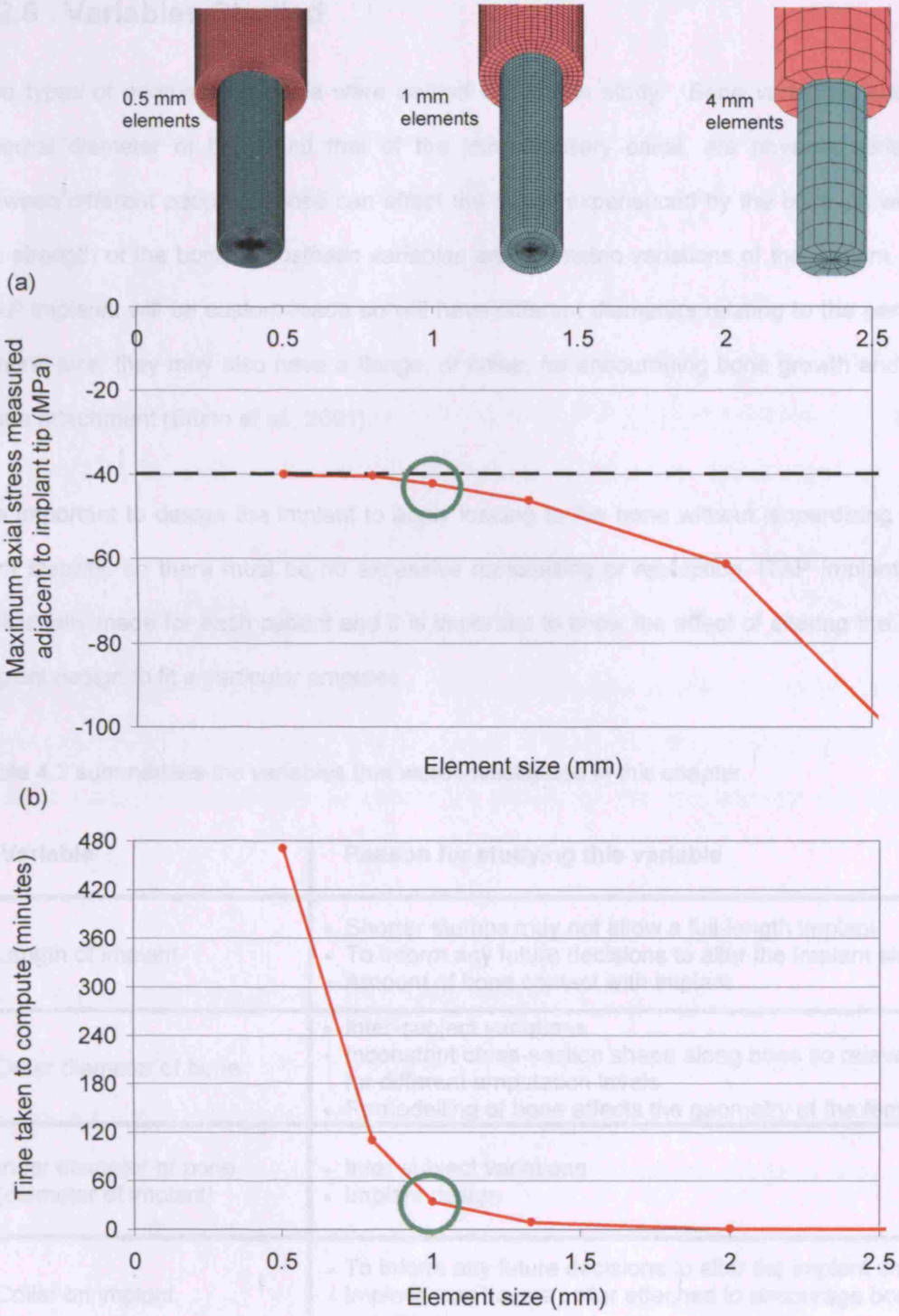

Figure 4.3 (a) Convergence study for the cylindrical model in MARC with stress at point A marked in figure 4.2(c). (b) The time taken to solve the analysis using the same geometry and loading conditions with different element sizes. In (a) and (b) the green ring indicates the mesh chosen for this study.

4.2.6 Variables Studied

Two types of geometric variable were carried out in this study. *Bone variables*, such as external diameter of bone and that of the intramedullary canal, are physical variations between different people. These can affect the stress experienced by the bone as well as the strength of the bone. *Prosthetic variables* are geometric variations of the implant. The ITAP implants will be custom-made so will have different diameters relating to the person's femoral size; they may also have a flange, or collar, for encouraging bone growth and soft-tissue attachment (Blunn *et al.*, 2001).

It is important to design the implant to apply loading to the bone without jeopardising long-term stability, so there must be no excessive remodelling or resorption. ITAP implants are individually made for each patient and it is important to know the effect of altering the basic implant design to fit a particular amputee.

Table 4.3 summarises the variables that were investigated in this chapter.

Variable	Reason for studying this variable
Length of implant	• Shorter stumps may not allow a full-length implant • To inform any future decisions to alter the implant shape • Amount of bone contact with implant
Outer diameter of bone	• Inter-subject variations • Inconstant cross-section shape along bone so relevant for different amputation levels • Remodelling of bone affects the geometry of the femur
Inner diameter of bone (diameter of implant)	• Inter-subject variations • Implant design
Collar on implant	• To inform any future decisions to alter the implant shape • Implant may have a collar attached to encourage bone growth
Bone material properties	• Loading of implant in early stages after implantation
Amount of bone attached to implant	• Remodelling • Proximal amputation with diverging cortex • Implant partially coated with HA

Table 4.3 Variables investigated with the tubular finite-element model

4.2.7 Plan of Work

The model geometry described in 4.2.2 was loaded with a number of different values of force and moment to prove that the model behaves linearly. The stress distributions in the bone were investigated and validated by comparing them with analytical calculations (subchapter 4.3).

Each geometric variable was studied by creating a separate model for each variation and loading the model with the axial force, bending force and torsional moment described in 4.2.4. This is documented in subchapter 4.4.

4.3 Validation of Basic Model Results

In order to analyse the variables listed in 4.2.6 the basic model to which the variations will be made must be fully understood. The behaviour of the basic bone-implant model under different loading was explored to inform the effects of the variables on the stresses experienced by the bone.

4.3.1 Validation by Analytical Calculations

The mesh chosen in 4.2.5 was loaded separately in torsion, bending and axial loading. The stresses in the bone were investigated to find out which locations and which stresses should be measured. The basic model was linear and the contact between the bone and implant was assumed to be perfect.

The linear nature of the model allowed for an analytical mathematical validation. Figures 4.4 -4.6 show the basic model loaded in bending, torsion and axially. The loads were applied at the distal end of the implant and the bone was constrained to be fixed at the proximal end. The calculations beneath each figure are analytical calculations of the stresses at various points in the models using beam theory.

4.3.1.1 Transverse Load

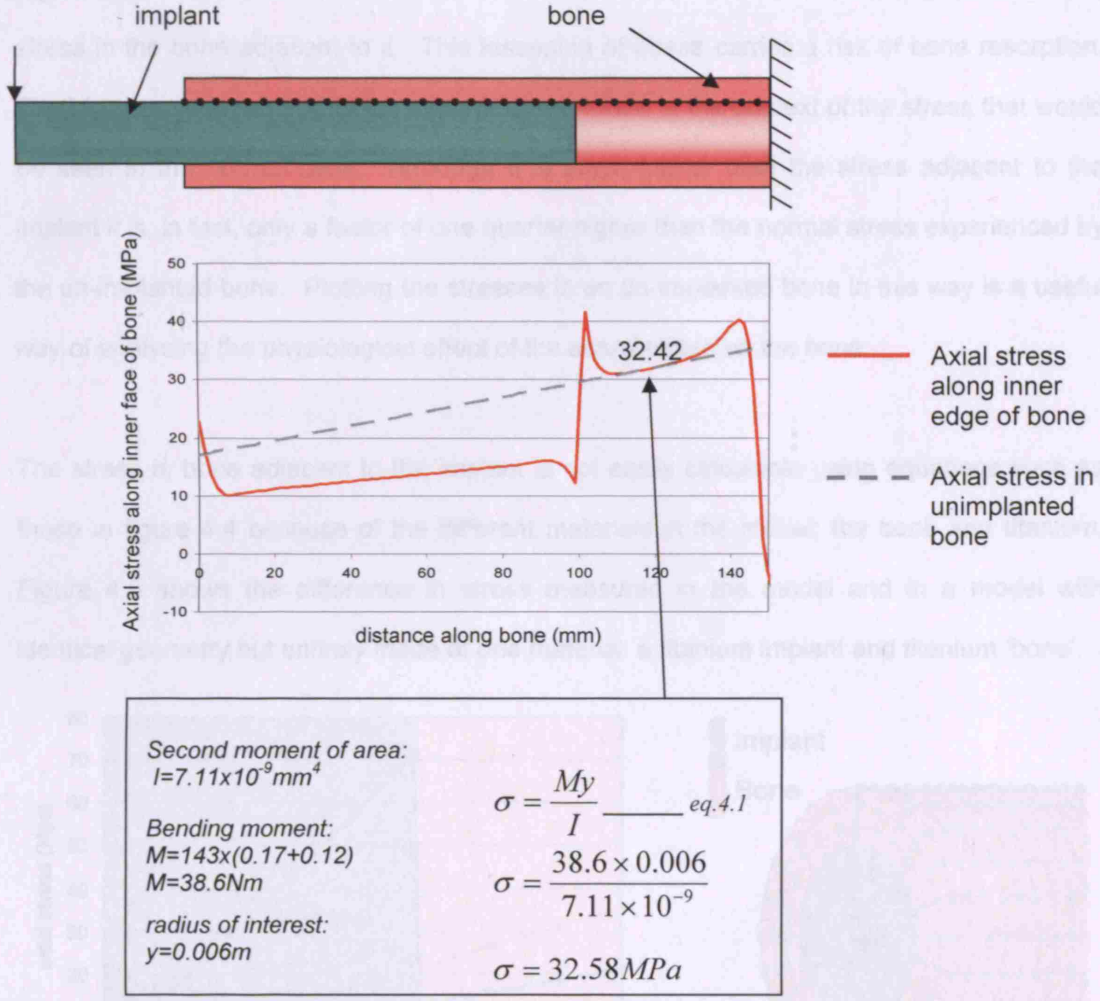

Figure 4.4 Validation of model under a transverse force, using beam-theory equations.

A force applied transversely to the free end of a cantilever induces a bending moment in the beam that has a value of zero at the free end and a maximum value at the fixed end and increases linearly along the beam. This is why the stress increases linearly along the bone under a transverse loading shown in figure 4.4. The second moment of area, which is a structure's ability to resist bending, is different for the implanted bone and the bone proximal to the implant so the linear stress increase is a different gradient for each section.

The dashed line in figure 4.4 shows the stress that would be experienced by the bone if there were no implant. The line matches that found using finite-element analysis for the region of no implant attachment and it shows how the presence of the implant reduces the stress in the bone adjacent to it. This lessening of stress carries a risk of bone resorption. The high stress at the end of the implant is seen here in the context of the stress that would be seen in the normal bone. Although it is much higher than the stress adjacent to the implant it is, in fact, only a factor of one quarter higher than the normal stress experienced by the un-implanted bone. Plotting the stresses in an un-implanted bone in this way is a useful way of analysing the physiological effect of the actual stress on the bone.

The stress in bone adjacent to the implant is not easily calculable using equations such as those in figure 4.4 because of the different materials in the model: the bone and titanium. Figure 4.5 shows the difference in stress measured in the model and in a model with identical geometry but entirely made of one material: a titanium implant and titanium 'bone'.

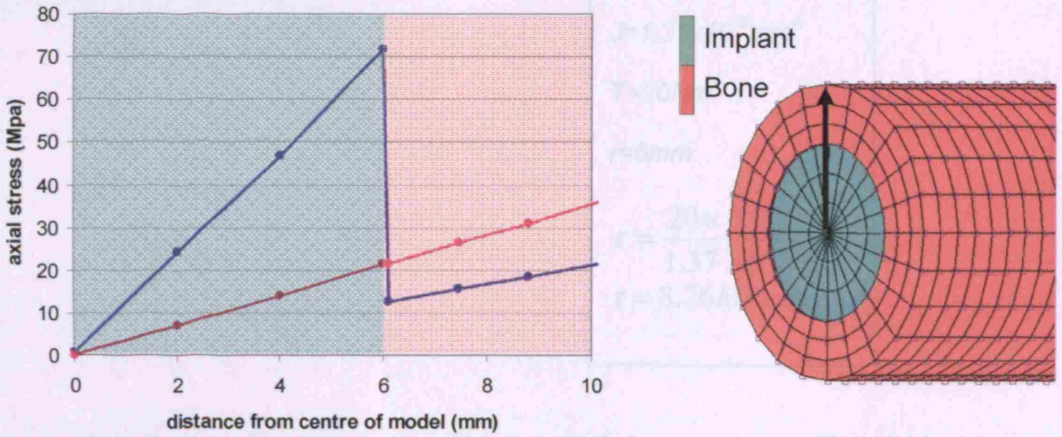

Figure 4.5 The axial stress measured at 40mm along the bone under transverse loading with bone and titanium (blue) and homogeneous (pink). The node path taken is radial from the centre of the implant to the outer surface of the bone.

There are concentrations of stress at the ends of the bone and at the proximal end of the implant, which are due to the geometric discontinuities, and they will be discussed in 4.3.2.

4.3.1.2 Torsional Load

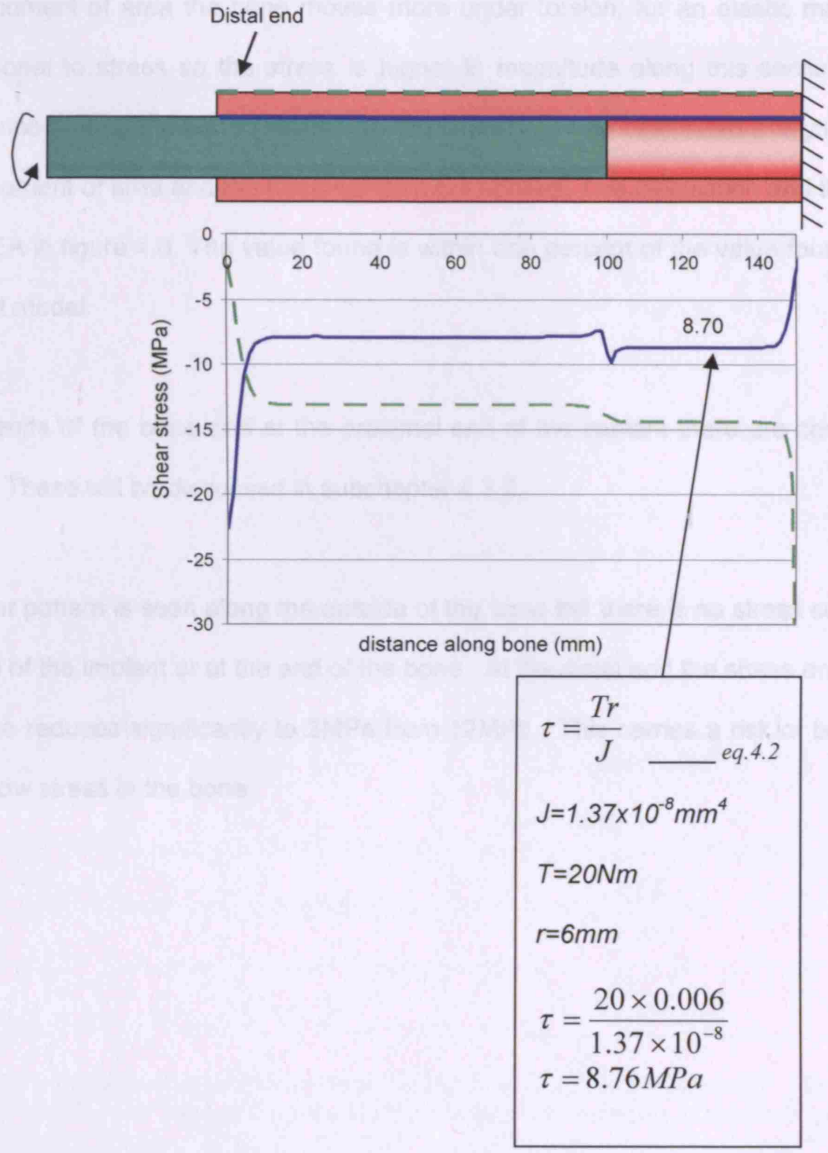

Figure 4.6 Validation of model in torsional loading, shaft-theory equations. The solid line shows the stress on the inner edge of the bone and the dashed line shows the stress on the outer edge of the bone.

Torsional moment applied to the free end of a cantilever with constant cross-section results in a constant torsion along the beam, therefore the shear stress experienced at the interface of the bone and implant is constant all the way along apart from at discontinuities in the geometry, this can be seen in figure 4.6. The stress along the bone proximal to the implant is also constant but of a different value because the polar moment of area, which quantifies a

structure's ability to resist torsion, is smaller without the implant in place. With this lower polar moment of area the bone moves more under torsion; for an elastic material strain is proportional to stress so the stress is higher in magnitude along this section. The stress experienced along the bone proximal to the implant can be calculated analytically using the polar moment of area and the torsional moment applied. This calculation and the value found from FEA in figure 4.6. The value found is within one percent of the value found in the finite-element model.

At the ends of the bone and at the proximal end of the implant there are concentrations of stress. These will be discussed in subchapter 4.3.2.

A similar pattern is seen along the outside of the bone but there is no stress concentration at the end of the implant or at the end of the bone. At the distal end the stress on the outside of the bone reduces significantly to 2MPa from 12MPa. This carries a risk of bone resorption due to low stress in the bone.

4.3.1.3 Axial Load

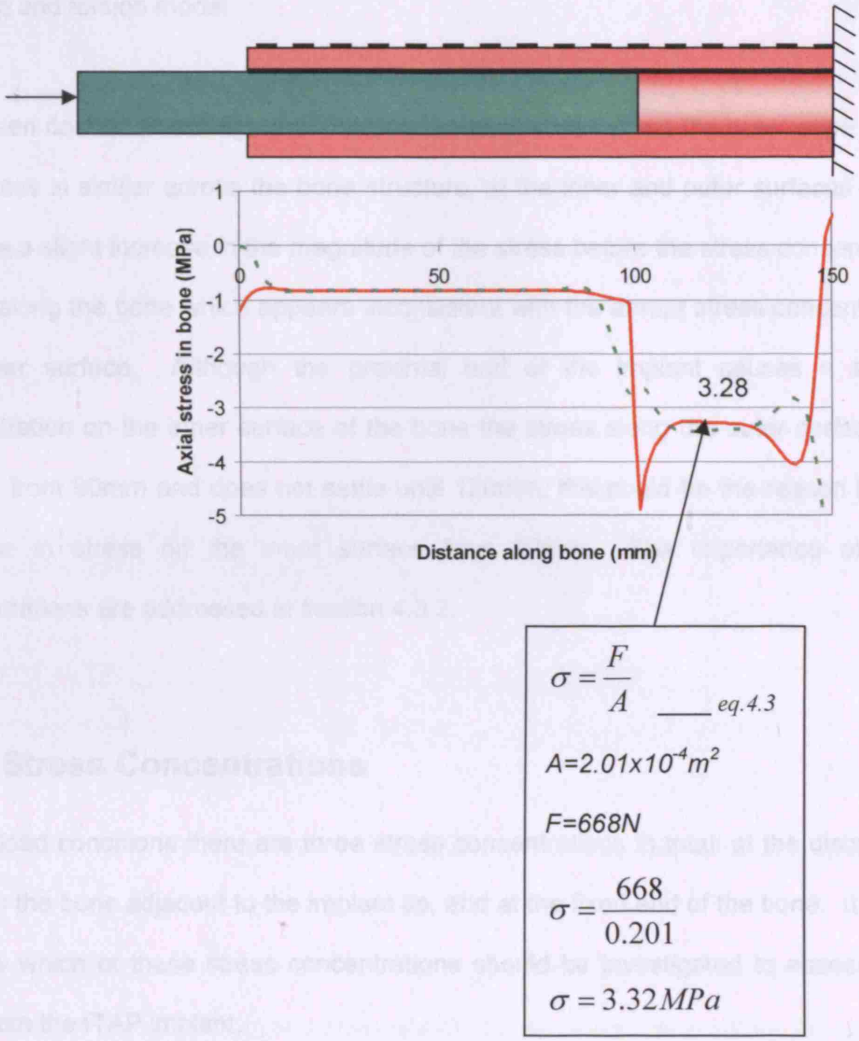

Figure 4.7 Validation of model under axial loading using shaft-theory equations. The solid line shows the stress on the inner edge of the bone and the dashed line shows the stress on the outer edge of the bone.

In axial loading the stress in the bone proximal to the implant can be calculated by dividing the force by the cross-sectional area of bone. The value calculated is less than two percent different from the value calculated with finite element analysis. The stress caused by an applied force remains constant along the beam as long as the structure is homogeneous in geometry and material therefore the stress distribution is constant apart from at points where the homogeneity is interrupted. The stress along the bone-implant interface cannot be simply

calculated because of the inhomogeneous material properties in the model, as for the bending and torsion model.

The green dashed line in figure 4.7 shows the axial stress along the outer edge of the bone. The stress is similar across the bone structure, at the inner and outer surfaces of the bone. There is a slight increase in the magnitude of the stress before the stress concentration, from 90mm along the bone which appears inconsistent with the abrupt stress concentration along the inner surface. Although the proximal end of the implant causes a sharp stress concentration on the inner surface of the bone the stress along the outer surface increases sharply from 90mm and does not settle until 120mm, this could be the reason for the small increase in stress on the inner surface from 90mm. The importance of the stress concentrations are addressed in section 4.3.2.

4.3.2 Stress Concentrations

For all load conditions there are three stress concentrations in total: at the distal end of the bone, in the bone adjacent to the implant tip, and at the fixed end of the bone. It is important to know which of these stress concentrations should be investigated to assess the risk to bone from the ITAP implant.

The stresses normally experienced by the bone are normally withstood by the femur so the finite element model was analysed with an unimplanted femur to show the stresses that would be experienced by the bone if it did not have an implant inside. Figure 4.8 shows the axial stress along the inner surface of the bone with and without an implant under a lateral load. In this figure the stress concentrations can be compared with the stress normally experienced by the femur.

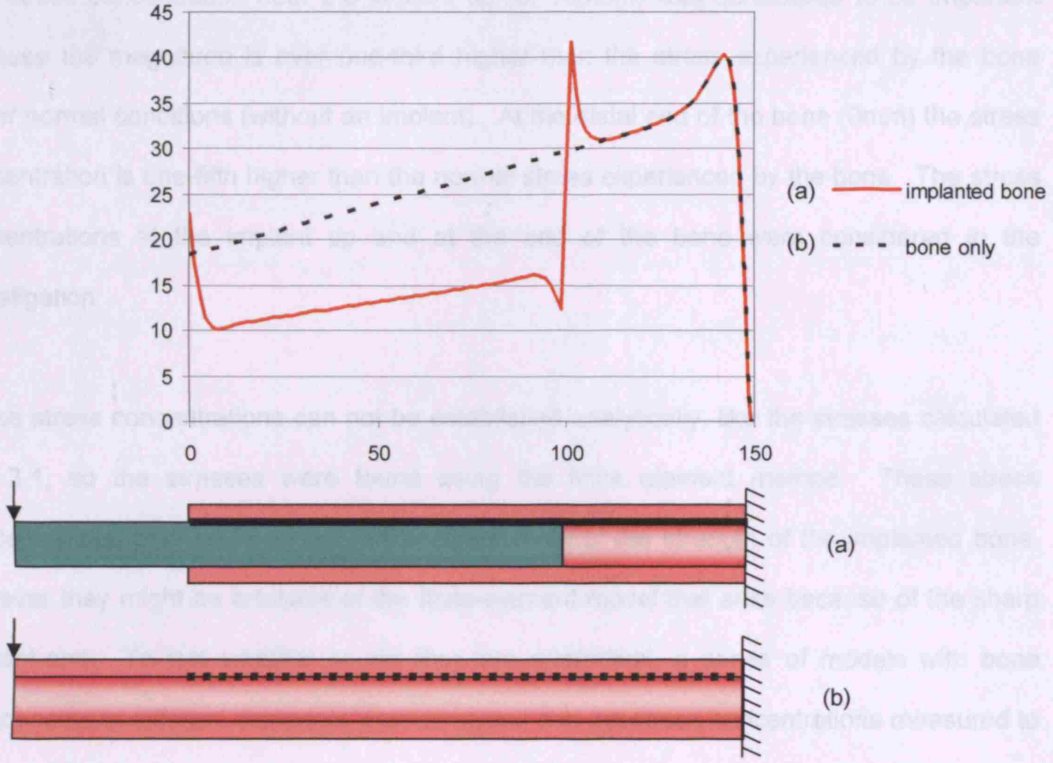

Figure 4.8 Axial stress along the inner surface of the bone for (a) an implanted bone, and (b) for bone without an implant.

The stress concentrations in the implanted model are higher than the stress normally experienced by the bone and the values are the same in the region where the bone is not in contact with the implant (proximal to 115mm).

The fixed end of the bone was not considered in the investigation of the stress concentrations because it is an artificial boundary condition. In the femur the 'fixed' points of the model are at the hip joint and at the muscle attachment points. The increased stress near the fixed end is too close to the boundary condition to be covered by the principle of Saint Venant, and can not be considered to be of realistic magnitude. From this point onwards, the twenty millimetres nearest the fixed end was no longer considered and will not be shown on any graphs.

The stress concentration near the implant tip (at 100mm) was considered to be important because the magnitude is over one-third higher than the stress experienced by the bone under normal conditions (without an implant). At the distal end of the bone (0mm) the stress concentration is one-fifth higher than the normal stress experienced by the bone. The stress concentrations at the implant tip and at the end of the bone were considered in the investigation.

These stress concentrations can not be established analytically, like the stresses calculated in 4.3.1, so the stresses were found using the finite element method. These stress concentrations may be important in the assessment of the strength of the implanted bone, however they might be artefacts of the finite-element model that arise because of the sharp implant-end. To test whether or not they are artefactual, a series of models with bone components of different diameters were analysed and the stress concentrations measured to find out whether the stress concentrations varied with the geometry or not. Figure 4.9 shows the axial stress along the inner bone surface for the models used for this test and table 4.4 shows the magnitude of the stress concentration at the stem tip.

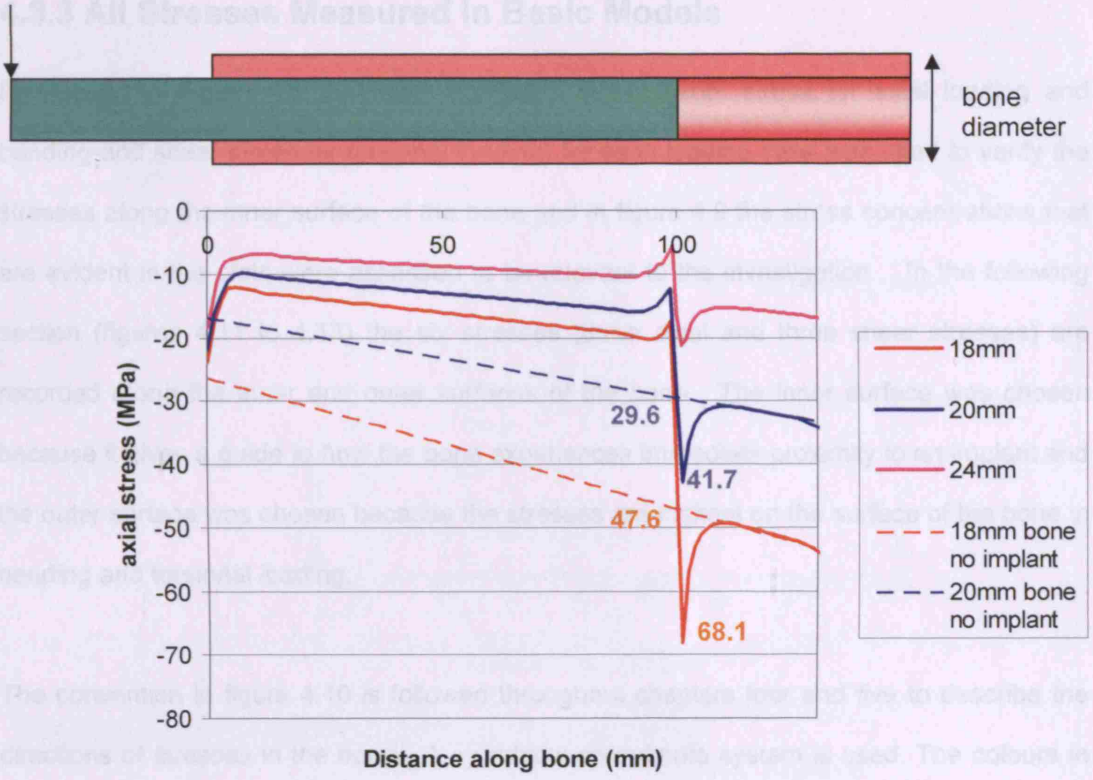

Figure 4.9 Chart indicating the axial stress concentrations and stress in a bone-only mode at 100mm along the bone for femora of different diameters.

Bone diameter	Axial stress in bone-only model at 100mm (A)	Stress concentration at stem tip (C)	$\frac{C}{A}$
24mm	14.8 MPa	21.3 MPa	1.40
20mm	29.6 MPa	41.7 MPa	1.40
18mm	47.6 MPa	68.1 MPa	1.40

Table 4.4 The stress concentration at the stem tip compared with the stress at the same distance along a bone without an implant.

The ratio of stress concentration to the stress experienced by the bone without an implant is 1.40 and is the same for each model. This indicates that the stress concentration is related to the geometry of the model and is therefore a credible stress value to study and not an artefact of the finite element analysis; it must be taken into account when analysing the results of the models.

4.3.3 All Stresses Measured in Basic Models

Previously, in Figure 4.5 the most significant stress (axial stress for axial loading and bending and shear stress for torsional loading) for each loading case was used to verify the stresses along the inner surface of the bone and in figure 4.9 the stress concentrations that are evident in the plots were assessed to be relevant to the investigation. In the following section (figures 4.11 to 4.13) the six stresses (three axial and three shear stresses) are recorded along the inner and outer surfaces of the bone. The inner surface was chosen because it gives a guide to how the bone experiences immediate proximity to an implant and the outer surface was chosen because the stresses are highest on the surface of the bone in bending and torsional loading.

The convention in figure 4.10 is followed throughout chapters four and five to describe the directions of stresses in the bone. A cylindrical co-ordinate system is used. The colours in 4.10(b) are used to distinguish between the normal and shear stresses on graphs.

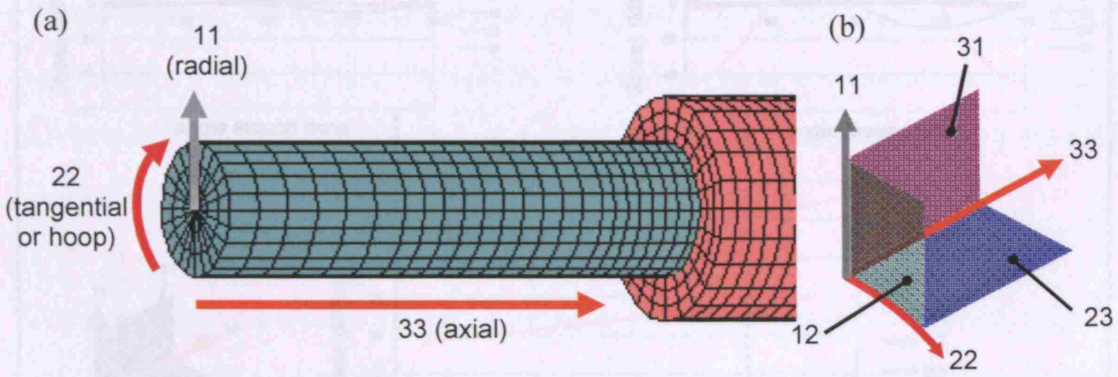

Figure 4.10 (a) Standard for describing normal stress components (b) colour convention for normal and shear stresses.

4.3.3.1 Bending

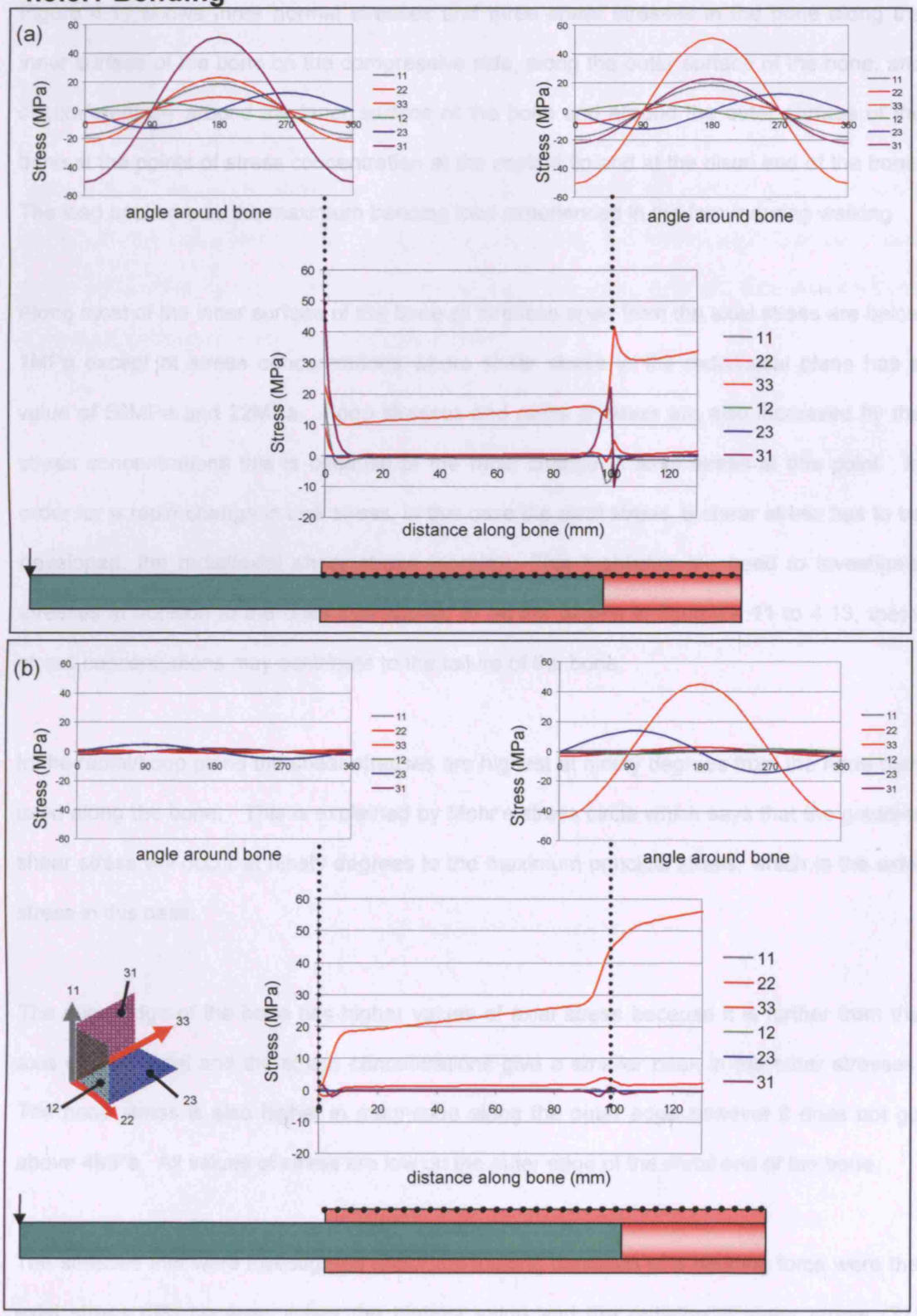

Figure 4.11 Normal and shear stresses in the basic model under transverse loading (a) along the inner surface of the bone and (b) along the outer surface of the bone. The graphs at the top of the two sections are stresses that are found around the bone at the distal end and adjacent to the implant tip.

Figure 4.11 shows three normal stresses and three shear stresses in the bone along the inner surface of the bone on the compressive side, along the outer surface of the bone, and circumferentially around the inner surface of the bone and around the outer surface of the bone at the points of stress concentration at the implant tip and at the distal end of the bone. The load applied was the maximum bending load experienced in the femur during walking.

Along most of the inner surface of the bone all stresses apart from the axial stress are below 1MPa except at stress concentrations where shear stress in the radial/axial plane has a value of 50MPa and 22MPa. Hoop stresses and radial stresses are also increased by the stress concentrations this is because of the rapid change in axial stress at this point. In order for a rapid change in one stress, in this case the axial stress, a shear stress has to be developed, the radial/axial shear stress (purple). This highlights the need to investigate stresses in addition to the ones that appear to be the largest in figures 4.11 to 4.13; these stress concentrations may contribute to the failure of the bone.

In the radial/hoop plane the shear stresses are highest at ninety degrees from the node path used along the bone. This is explained by Mohr's stress circle which says that the greatest shear stress will occur at ninety degrees to the maximum principal stress, which is the axial stress in this case.

The outer edge of the bone has higher values of axial stress because it is further from the axis of the model and the stress concentrations give a smaller peak in the other stresses. The hoop stress is also higher in magnitude along the outer edge however it does not go above 4MPa. All values of stress are low on the outer edge of the distal end of the bone.

The stresses that were investigated under the loading condition of a bending force were the axial stress (33) because it has the highest value and the radial/axial shear stress (31) because it has the largest stress concentration. The axial stress along the outer edge of the

bone has the highest magnitude of all but there are no stress concentration peaks and the stresses do not go above those that would be found in a bone without an implant. However while studying variables that affect the diameter of the bone or implant the axial stress on the outer edge of the bone might be increased to a level that is too high. The lesser stress concentrations in the radial and tangential directions highlight the need to look at stresses apart from the ones that appear to be the largest during this investigation because these stress concentrations may contribute to the failure of the bone. They will be considered, if it is deemed necessary, during the parametric study.

4.3.3.2 Torsion

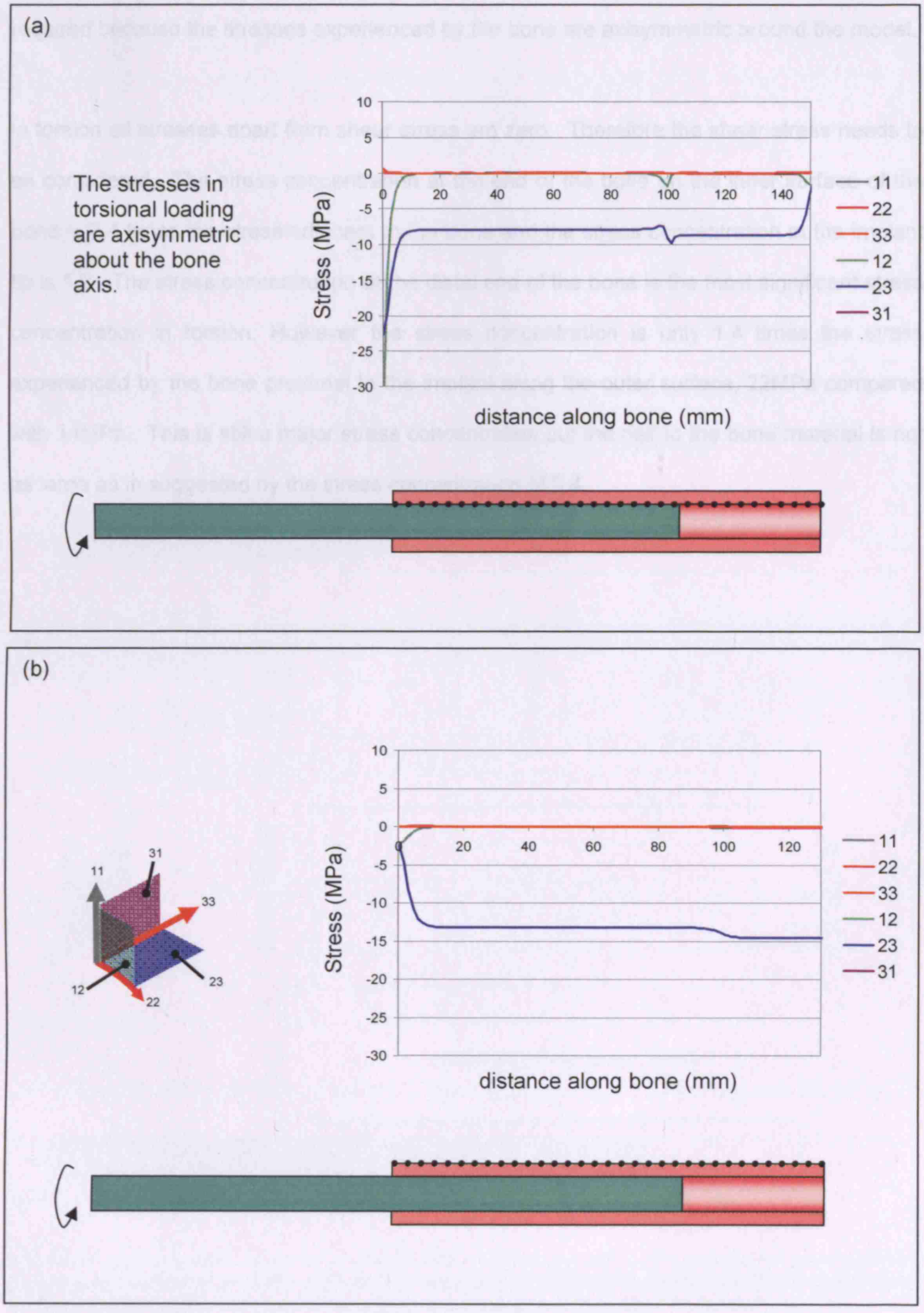

Figure 4.12 Stresses in the three axes and shear stresses in the basic model in torsion; (a) along the inner surface of the bone and (b) along the outer surface of the bone

In axial and torsional loading, the circumferential node paths around the bone are not required because the stresses experienced by the bone are axisymmetric around the model.

In torsion all stresses apart from shear stress are zero. Therefore the shear stress needs to be considered. The stress concentration at the end of the bone on the inner surface of the bone is 3.4 times the stress adjacent to the bone and the stress concentration at the implant tip is 1.2. The stress concentration at the distal end of the bone is the most significant stress concentration in torsion. However the stress concentration is only 1.4 times the stress experienced by the bone proximal to the implant along the outer surface, 22MPa compared with 14MPa. This is still a major stress concentration but the risk to the bone material is not as large as is suggested by the stress concentration of 3.4.

4.3.3.3 Axial Loading

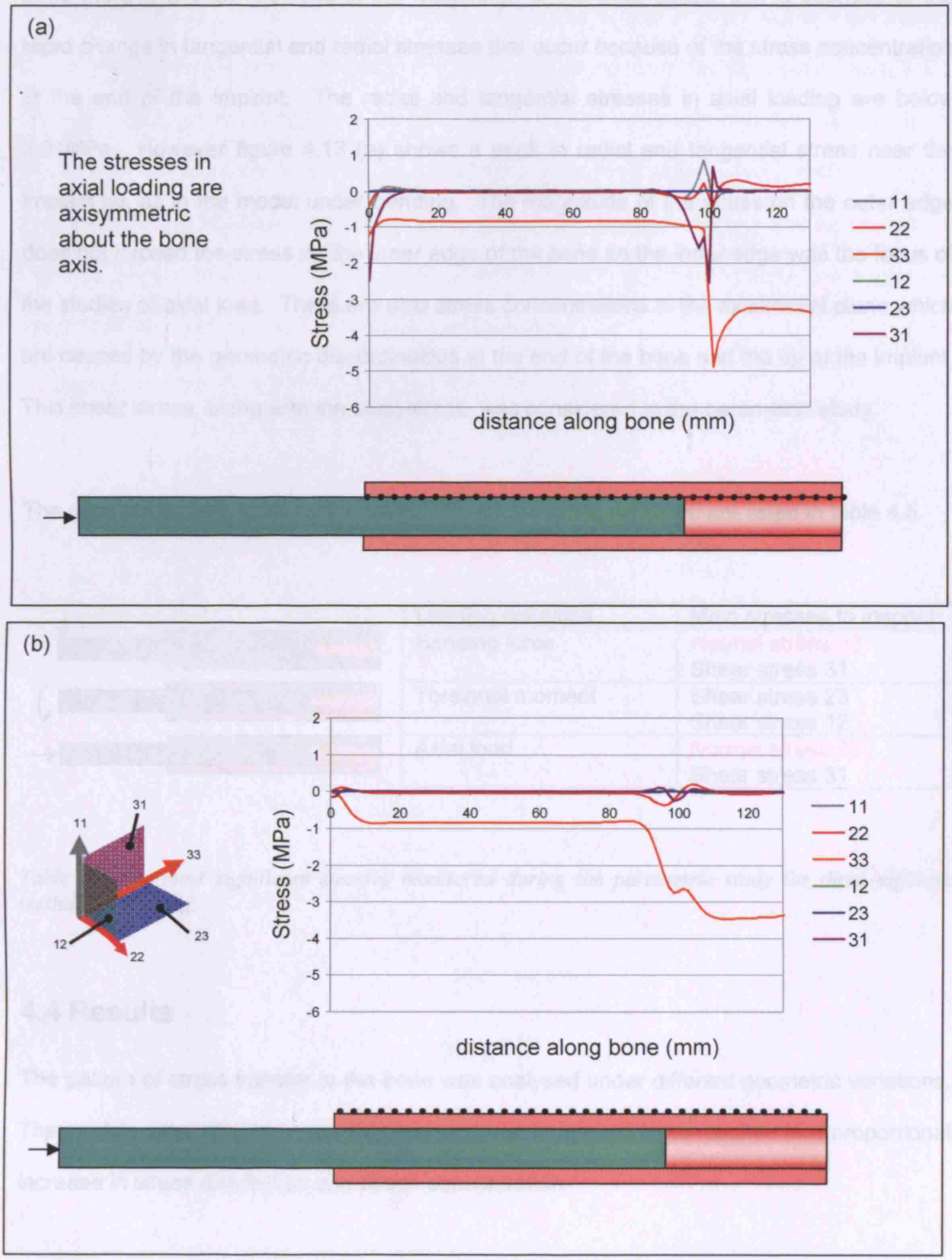

Figure 4.13 Stresses in the three axes and shear stresses in the basic model in axial loading; (a) along the inner surface of the bone and (b) along the outer surface of the bone.

Under axial loading the axial stress has the greatest magnitude. At about 90mm along the bone there is a slight increase in the magnitude of the axial stress, this is because of the rapid change in tangential and radial stresses that occur because of the stress concentration at the end of the implant. The radial and tangential stresses in axial loading are below 0.01MPa. However figure 4.13 (a) shows a peak in radial and tangential stress near the implant tip, as in the model under bending. The magnitude of the stress on the outer edge does not exceed the stress on the inner edge of the bone so the inner edge was the focus of the studies of axial load. There are also stress concentrations in the axial/radial plane which are caused by the geometric discontinuities at the end of the bone and the tip of the implant. This shear stress, along with the axial stress, was considered in the parametric study.

The main stresses that will be considered for each loading condition are listed in table 4.5.

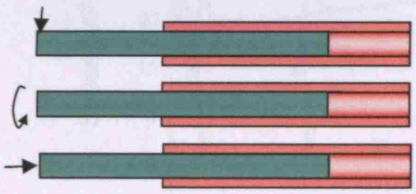

Loading condition	Main stresses to inspect
Bending force	Normal stress 33 Shear stress 31
Torsional moment	Shear stress 23 Shear stress 12
Axial load	Normal stress 33 Shear stress 31

Table 4.5 The most significant stresses monitored during the parametric study for three different methods of loading.

4.4 Results

The pattern of stress transfer to the bone was analysed under different geometric variations. The models were linear in nature so any increase in applied force resulted in a proportional increase in stress distribution and stress concentration.

4.4.1 Implant Length

There are two reasons why the implant can be 'shorter' in mechanical terms: if the patient has a short residual femur they may be fitted with an implant that is smaller, also if the implant is only in contact with bone for a small part of its length due to diverging bone geometry it transfers the stress to the bone in the same way as if it were a shorter implant. Figures 4.14 to 4.16 show the effect of altering the implant length on the stress in the bone in bending, torsion and axial loading. The stresses chosen for these graphs are those that were deemed to be the most significant in subchapter 4.3.

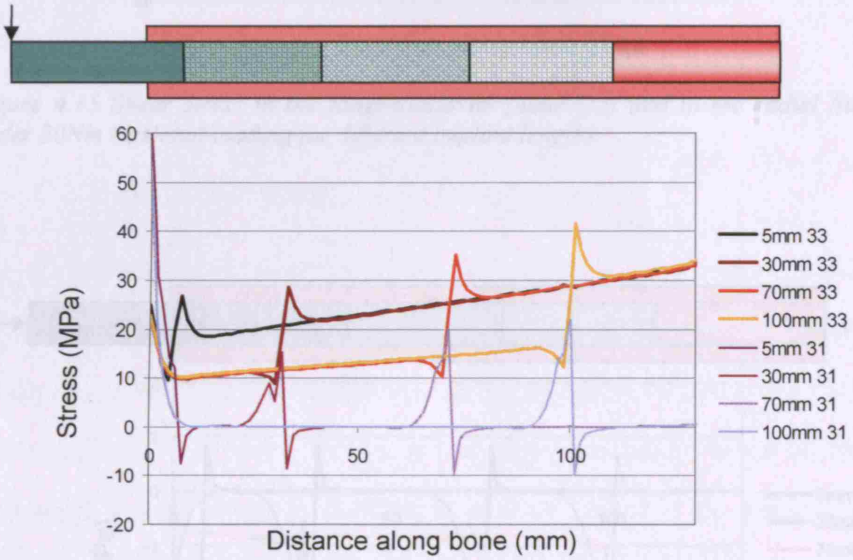

Figure 4.14 axial stress (33) and shear stressing the radial/axial plane (31) in bending for implants of length 100mm, 70mm, 30mm and 4mm.

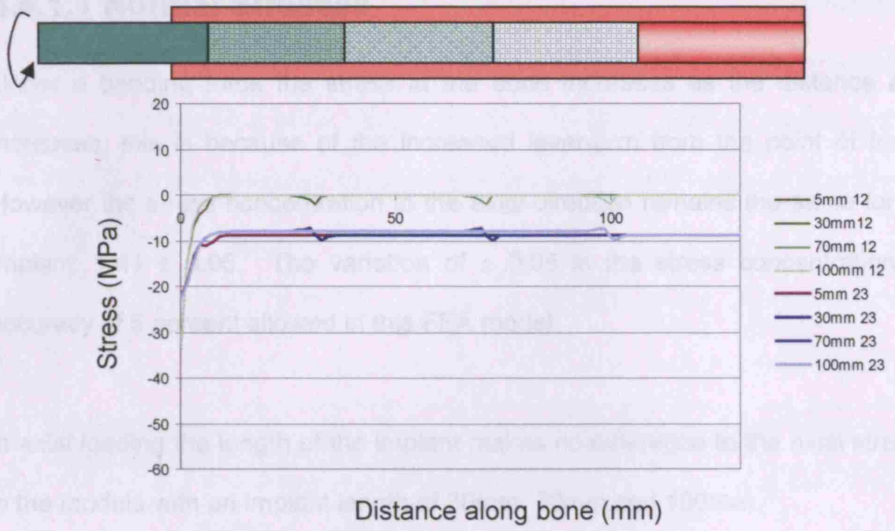

Figure 4.15 Shear stress in the tangential/axial plane (23) and in the radial /tangential(12) plane under 20Nm torsional loading for different implant lengths

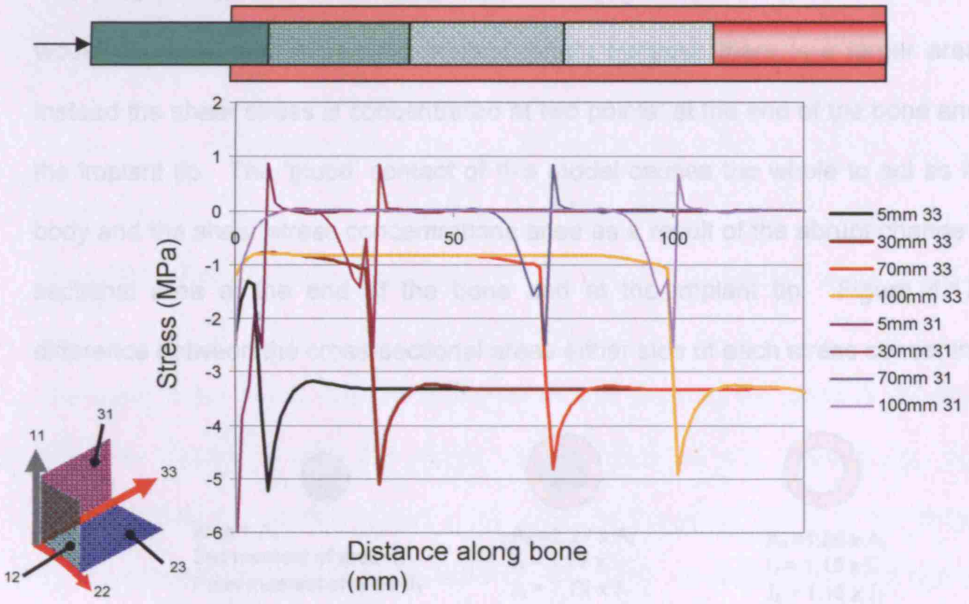

Figure 4.16 Axial stress (33) and radial/axial shear stress (31) under 668N axial loading for different implant lengths

4.4.1.1 Normal Stresses

Under a bending force the stress in the bone increases as the distance along the bone increases, this is because of the increased lever-arm from the point of force application. However the stress concentration in the axial direction remains the same for each length of implant: 1.41 ± 0.05. The variation of ± 0.05 in the stress concentrations is within the accuracy of 5 percent allowed in this FEA model.

In axial loading the length of the implant makes no difference to the axial stress experienced in the models with an implant length of 30mm, 70mm and 100mm.

4.4.1.2 Shear Stresses

The shear stress is not distributed uniformly along the bone implant interface. If it were, it would decrease with increasing implant length because there is a larger area of contact. Instead the shear stress is concentrated at two points: at the end of the bone and adjacent to the implant tip. The 'glued' contact of this model causes the whole to act as if it were one body and the shear stress concentrations arise as a result of the abrupt change in the cross-sectional area at the end of the bone and at the implant tip. Figure 4.17 shows the difference between the cross-sectional areas either side of each stress concentration.

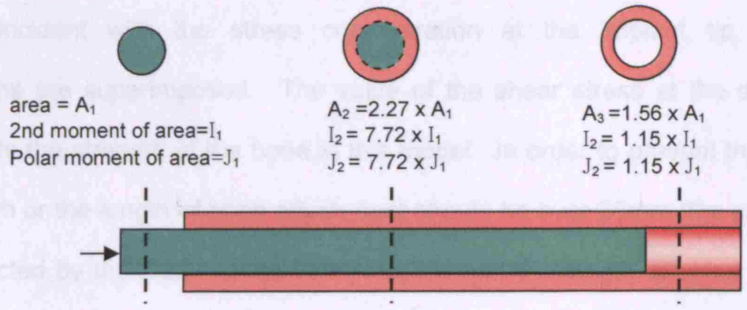

Figure 4.17 Difference in cross-sectional area, second moment of area and polar moment of area at each side of the stress concentrations at the bone-end and the implant-tip.

The five millimetre implant is a special case here and needs further explanation. An implant 5mm in length would not be provided in the ITAP system but this parameter was used to explore the effect of a bone having only a very small area of contact with cortical bone. Figure 4.18 shows the shear stress in axial loading for the five millimetre implant and for the hundred millimetre implant.

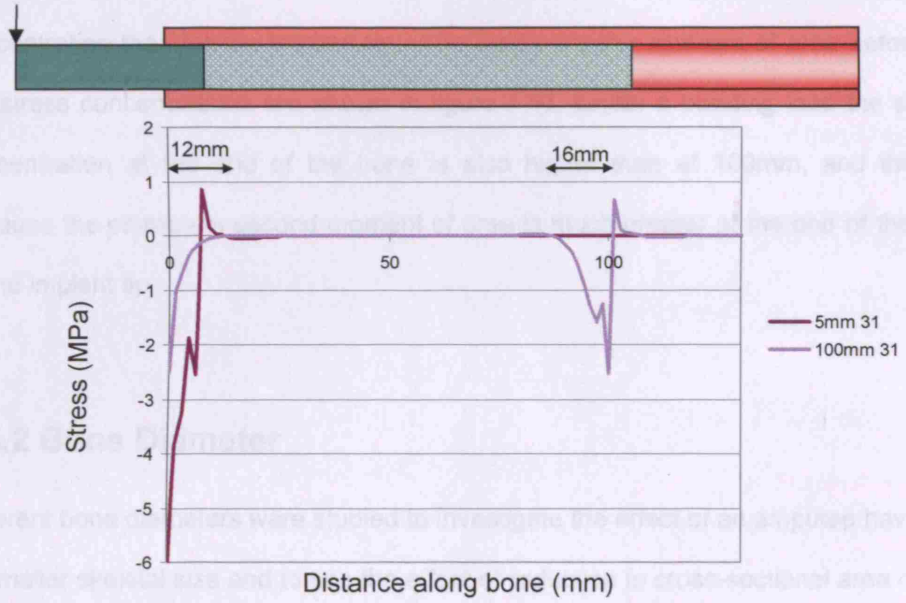

Figure 4.18 The axial/radial shear stress in the bone for an implant of 5mm and an implant of 100mm.

The shear stress is very high for the 5mm implant because the effect of the distal end of the bone is coincident with the stress concentration at the implant tip, so the stress concentrations are superimposed. The value of the shear stress at the distal end of the bone exceeds the strength of the bone in this model. In order to prevent this occurring, the implant length or the length of bone attachment should be over 28mm (the sum of the length of bone affected by the distal stress concentration and the length affected by the proximal concentration) to avoid the stress concentrations overlapping in this way.

Implants of 30mm and above have the same stress concentrations in all modes of loading so, in this model with perfect boundary conditions, no benefit is gained from using a longer implant.

Under torsional loading the shear stress concentration at the end of the bone is ten times higher than the stress concentration at the implant tip. This may be explained by the change in polar moment of area at each point which is much greater for the distal stress concentration than for the implant tip. The ratios of polar moment of area before and after the stress concentrations are shown in figure 4.17. Under a bending load the shear stress concentration at the end of the bone is also higher than at 100mm, and this could be because the change in second moment of area is much greater at the end of the bone than at the implant tip.

4.4.2 Bone Diameter

Different bone diameters were studied to investigate the effect of an amputee having a larger or smaller skeletal size and to see the effect of reduction in cross-sectional area due to bone resorption on the risk to the bone of fracture. Figures 4.19-4.20 show the axial and shear stresses in bending and in torsional loading.

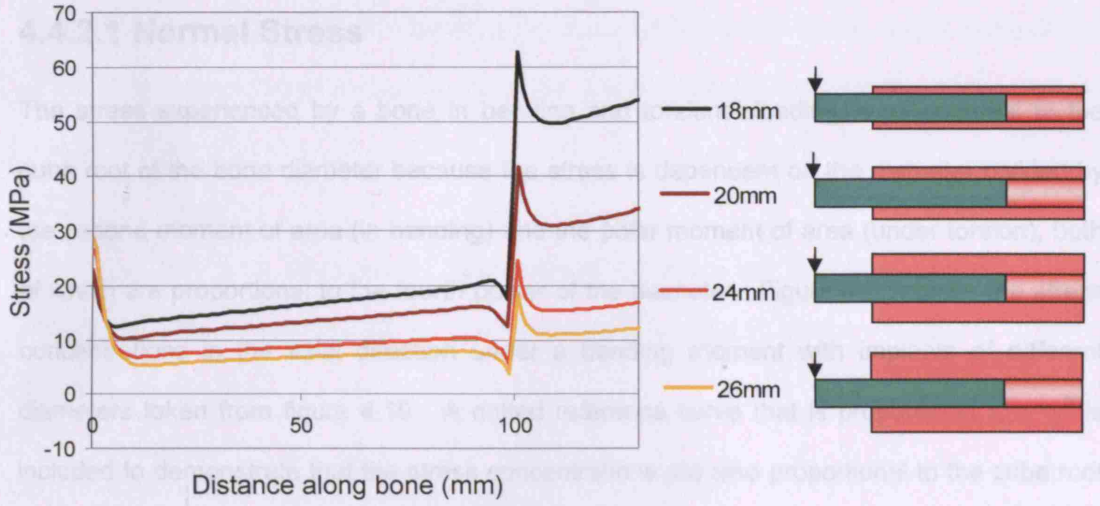

Figure 4.19 Axial stress in bones of diameter 18mm, 20mm, 24mm and 26mm under a bending load.

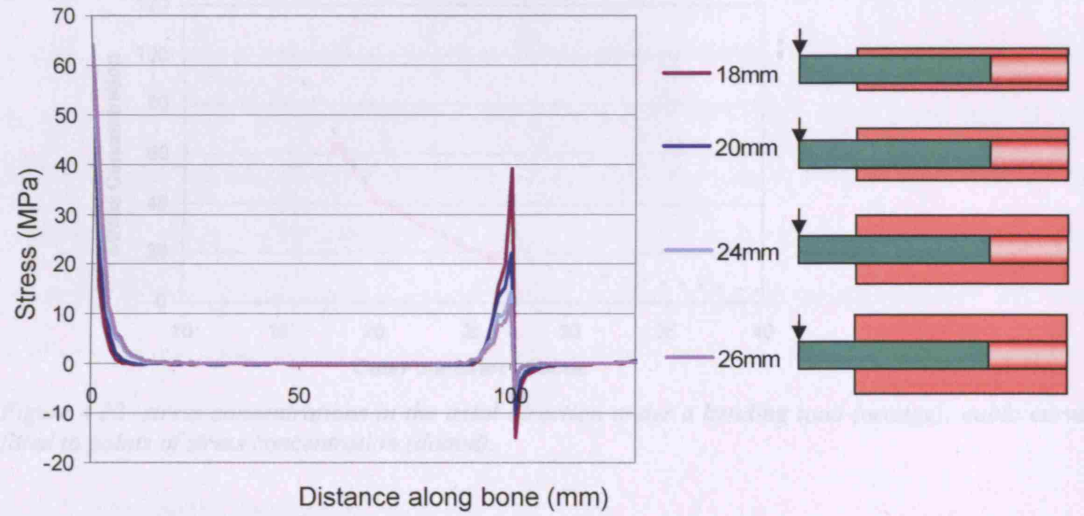

Figure 4.20 Radial/axial shear stress in bones of diameter 18mm, 20mm, 24mm and 26mm in bending

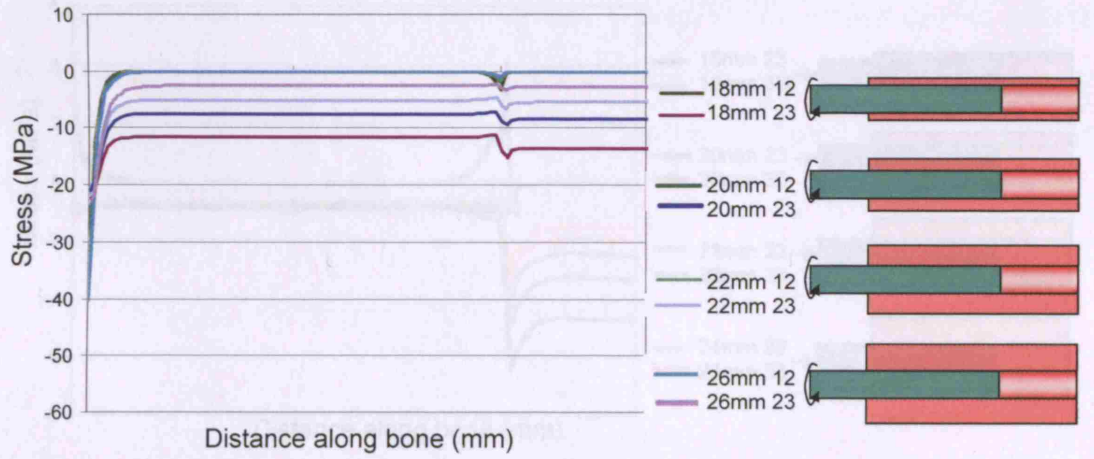

Figure 4.21 Shear stress in torsional loading in bones of outer diameters18mm, 20mm, 24mm and 26mm

4.4.2.1 Normal Stress

The stress experienced by a bone in bending and torsional loading is proportional to the cube root of the bone diameter because the stress is dependent on the diameter divided by the second moment of area (in bending) and the polar moment of area (under torsion), both of which are proportional to the fourth power of the diameter. Figure 4.22 shows the stress concentrations in the axial direction under a bending moment with implants of different diameters taken from figure 4.19. A dotted reference curve that is proportional to $x=y^3$ is included to demonstrate that the stress concentrations are also proportional to the cube root of the diameter and, therefore, the rest of the stresses in the bone.

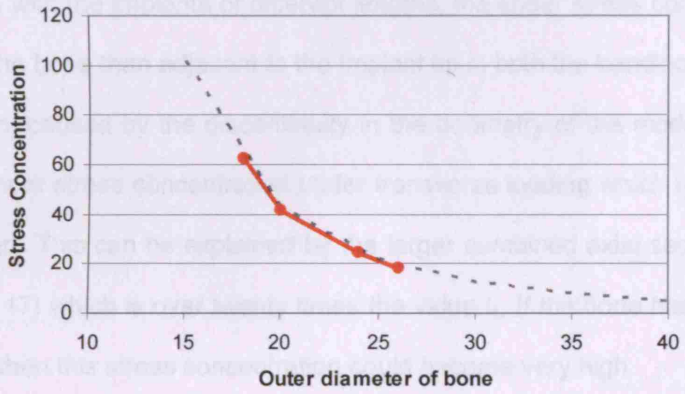

Figure 4.22 stress concentrations in the axial direction under a bending load (orange); cubic curve fitted to points of stress concentration (dotted).

Figure 4.23 shows the axial and shear stresses in the bone under axial loading.

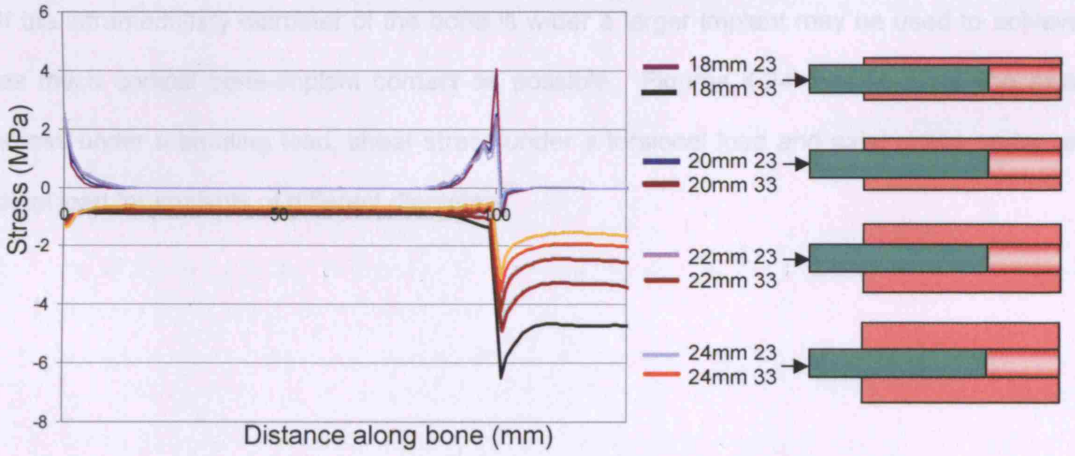

Figure 4.23 Axial and shear stresses in the bone due to an axial load with bones of different diameters

Under axial loading the stress concentration is also proportional to the stress in the bone, which itself is proportional to the square of the diameter (as opposed to diameter cubed, as in figure 5.)

The cube root and square root relationships between the diameter and the stress concentration show that a small decrease in diameter results in a large increase in stress in the bone.

4.4.2.2 Shear Stress

As seen with the implants of different lengths, the shear stress concentration is higher at the end of the bone than adjacent to the implant tip in both the bending and torsion models. This is, again, caused by the discontinuity in the geometry of the model. Of interest here is the distal shear stress concentration under transverse loading which is greater for a larger bone diameter. This can be explained by the larger combined axial second moment of area (I_2 in figure 4.17) which is over twenty times the value I_1 If the bone has good integration with the implant then this stress concentration could become very high.

4.4.3 Implant Diameter

If the intramedullary diameter of the bone is wider a larger implant may be used to achieve as much cortical bone-implant contact as possible. Figures 4.24 to 4.26 show the axial stress under a bending load, shear stress under a torsional load and axial stress under an axial load for implants of different diameters.

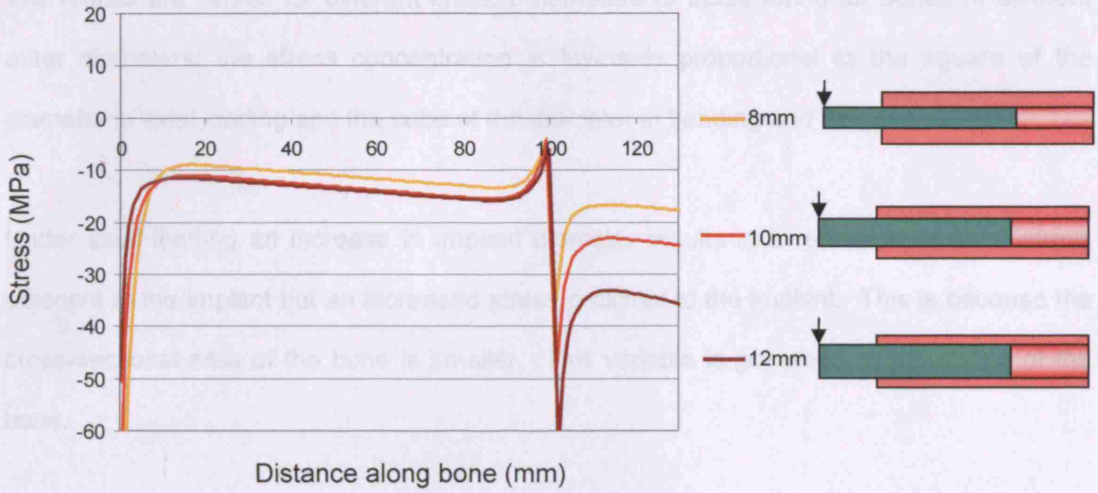

Figure 4.24 Axial stress in the bone due to a bending moment with implants of different diameters

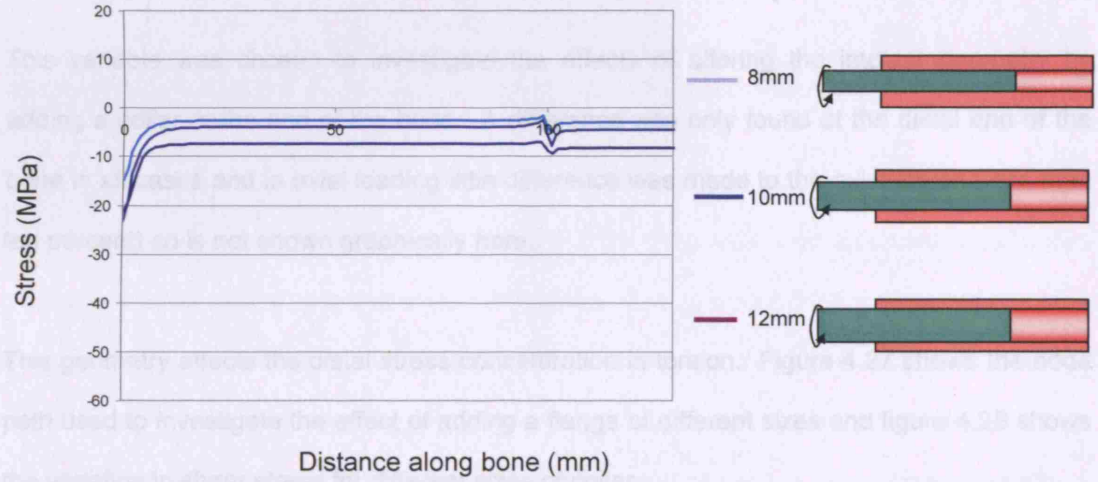

Figure 4.25 Shear stress in the bone under torsional loading for implants with different diameters

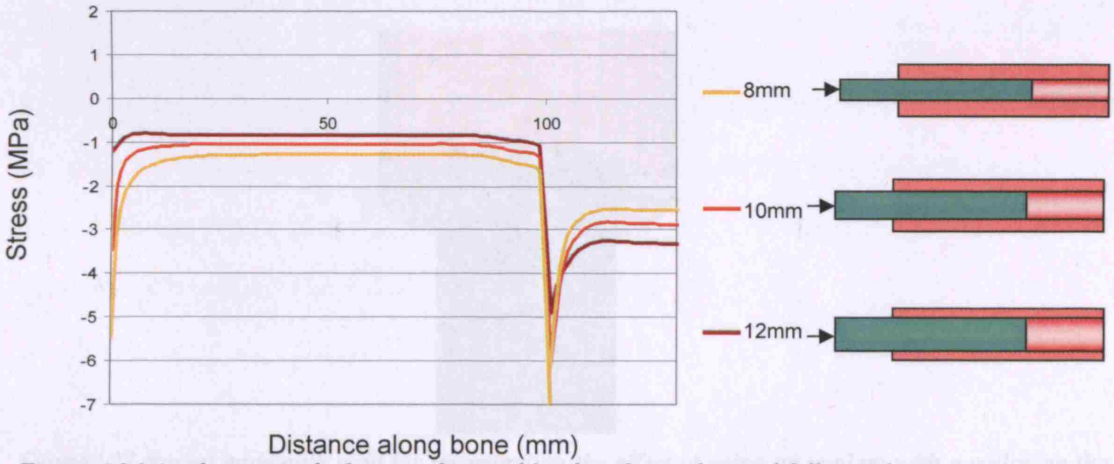

Figure 4.26 Axial stress in the bone under axial loading for implants of different diameters

The results are similar for different implant diameters to those found for bones of different outer diameters: the stress concentration is inversely proportional to the square of the diameter in axial loading and the cube of the diameter in bending and torsion.

Under axial loading an increase in implant diameter results in a reduction of bone stress adjacent to the implant but an increased stress proximal to the implant. This is because the cross-sectional area of the bone is smaller. This variable is governed by the shape of the bone.

4.4.4 Collar

This variable was chosen to investigate the effects of altering the implant geometry by adding a collar at the end of the bone. A difference was only found at the distal end of the bone in all cases and in axial loading little difference was made to the axial stress (less than ten percent) so is not shown graphically here.

This geometry affects the distal stress concentration in torsion. Figure 4.27 shows the node path used to investigate the effect of adding a flange of different sizes and figure 4.28 shows the variation in shear stress for different sizes of collar.

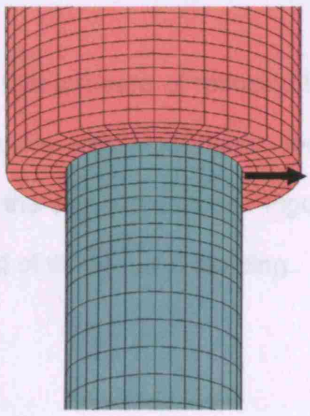

Figure4.27 Radial node path used for investigating the effect of using an implant with a collar on the stresses at the end of the bone

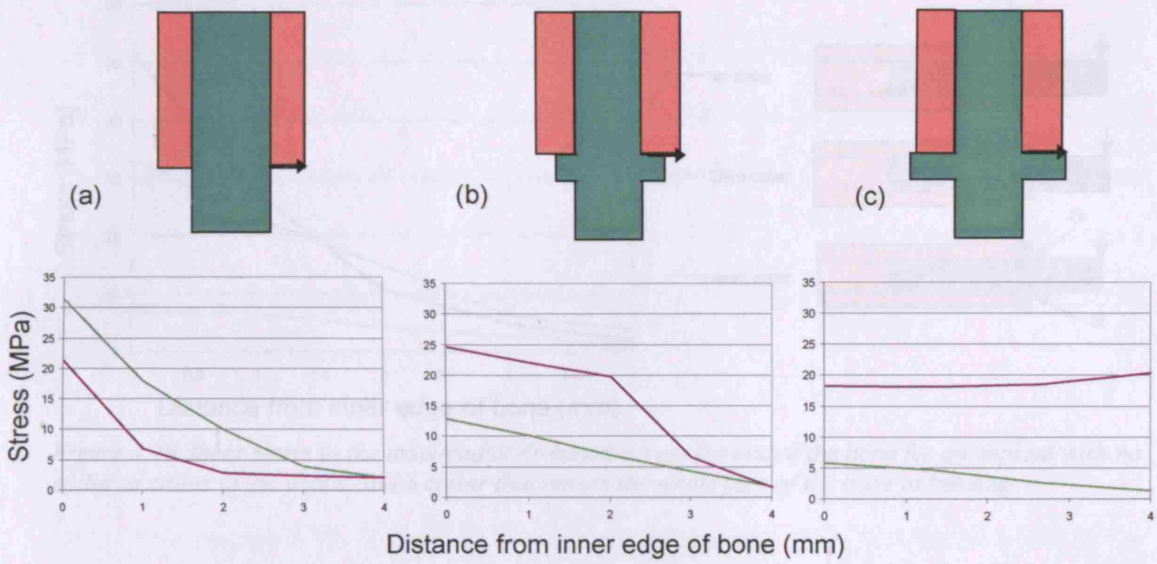

Figure 4.28 shear stress in the radial/tangential (green) and the axial/tangential(purple) planes for implants with (a), no collar (b) a collar 2mm in width and (c) a collar 4mm in width.

Image (a) in figure 4.28 shows the distribution of shear stress across the end of the bone with no collar, (b) shows the effect of including a 2mm deep collar and (c) shows a collar that covers the whole of the resected end of the bone. The greatest difference is found in the shear stress in the radial/tangential plane at the inner edge of the bone, which is reduced to one-sixth of its maximum value by the addition of a full-size collar. The stress concentration in the axial/tangential plane is also reduced but is eighty percent of its original value with a full-size collar and is higher with a smaller collar.

In part 4.4.2 it was mentioned that a means of reducing the distal stress concentration would be of particular benefit to amputees with larger bones because this stress is increased by the abrupt change in geometry at the end of the bone. Figure 4.29 shows the change made to the stress across the distal end of the femur in bending.

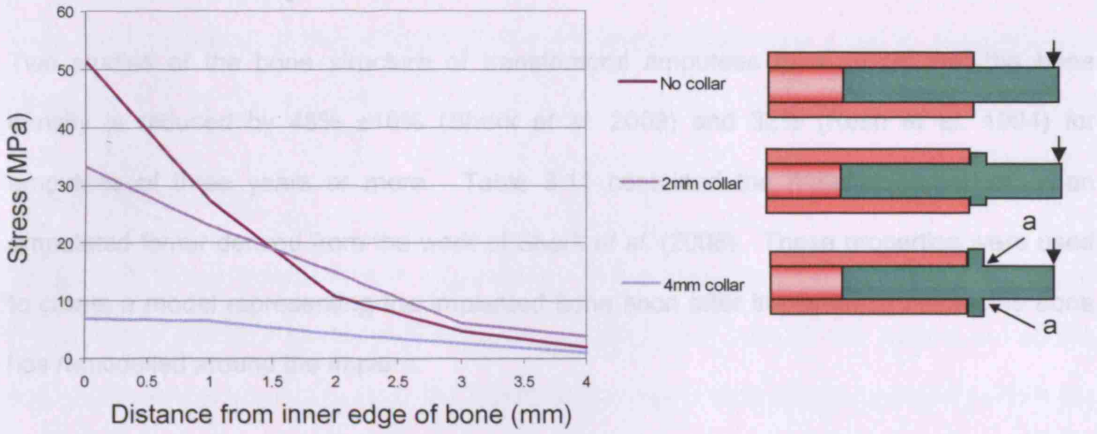

Figure 4.29 Shear stress in the axial/radial direction across the end of the bone for an implant with no collar, a collar of 2m width, and a collar that covers the whole face of the bone in bending.

There is a stress concentration at point 'a' in figure 4.29, as this is where the abrupt geometry change occurs, so the strain is evenly distributed at the distal end of the bone. In this model the collar reduces the stress concentration (at point 0mm in figure 4.29) so the addition of a collar would be of benefit in reducing the risk of fracture.

Including a collar on the implant can have mechano-biological effects. For example a collar has been shown to induce bone growth in distal femoral prostheses and reduce implant loosening in distal femoral prosthetic replacement (Maruthainar *et al.*, 2006). There appears to be a stress shielding effect on the outer surface of the distal femur without a collar. From figure 4.28(c) it can be hypothesised that the bone is encouraged to remodel and not resorb because the shear stress is retained over the distal end of the bone.

4.4.5 Bone Quality

Two studies of the bone structure of transfemoral amputees have found that the bone density is reduced by 48% ±10% (Sherk *et al.* 2008) and 32% (Rush *et al.* 1994) for amputees of three years or more. Table 3.11 contained the material properties of an amputated femur derived from the work of Sherk *et al.* (2008). These properties were used to create a model representing the implanted bone soon after implantation before the bone has remodelled around the implant.

The stress transfer patterns were almost identical to those in the bone of 'normal strength' as recorded in figures 4.11, 4.12 and 4.13. The consequences of the reduced strength of the bone are discussed in subchapter 6.4.3.

4.4.6 Amount of Cortical bone Contact with Implant

There were two reasons for investigating the amount of cortical bone attached to the implant. There was a possibility that the implant would only be coated with HA for part of its length, to reduce the amount of bone undergoing stress shielding, in order to prevent excessive resorption (Blunn *et al.*, 2001). Secondly, the bone might not make an intimate connection with the implant along its length leaving parts of the implant abutting, but not connected to, the bone.

The part of the bone connected to the implant was modelled with perfect contact, and the unattached bone was modelled with friction. With a partially-coated implant, the purpose of limiting the HA coating is to prevent bone attachment to the uncoated part, so the remaining implant is polished. In the case of incomplete bone ingrowth, the part of the implant not attached to cortical bone could have a rough surface, and possibly a coating of HA. The coefficient of friction between bone and a porous implant surface has been measured to be 0.58, and 0.15-0.3 for a smooth implant (Shirazi *et al.* 1993). When the model was run with

coefficients of friction of 0.58 and 0.2 to represent rough and smooth implants, the results were almost identical so the polished stem coefficient of friction was used to represent both situations.

4.4.6.1 Bending

Figure 4.30 shows the stresses in all directions on the compressive and tensile inner edges of the model with 25% bone integration. Stresses on both sides of the implant are shown because the model is nonlinear (in the previous models the stresses on the tensile side were the same magnitude as the stresses on the compressive side).

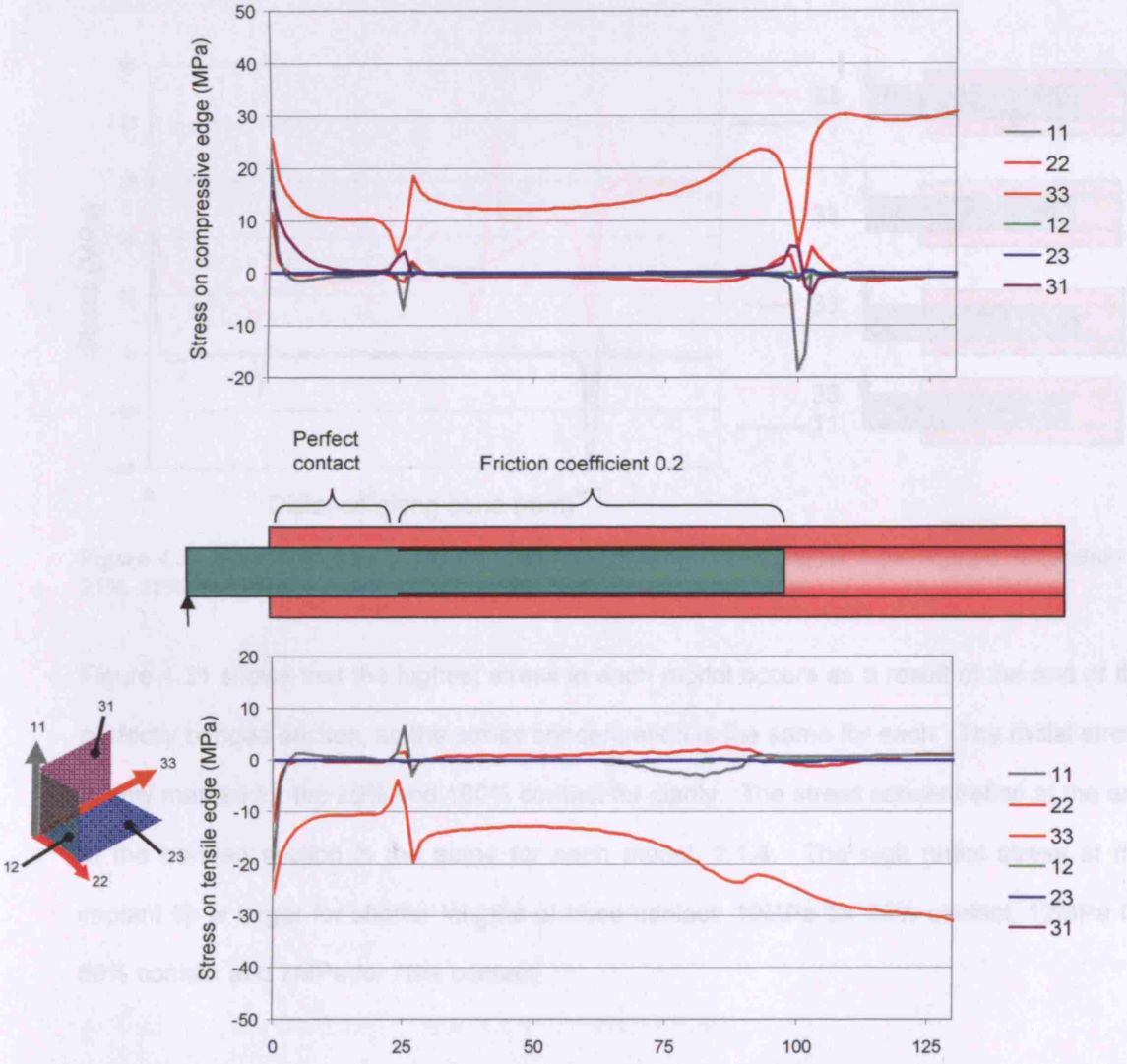

Figure 4.30 Stresses on inner edge of bone in bending with 25% bone-implant contact

In bending, the part of the bone integrated with the implant experiences stresses that are the same as those with a short implant. The part of the bone that is not in contact with the implant has a higher axial stress which varies nonlinearly but does not exceed the stress proximal to the implant. All other stresses are low in magnitude apart from the radial stress (grey) which has two peaks, one at the cessation of bone contact and one near the tip of the implant.

Figure 4.31 shows the axial and radial stress in bending for bone contact of 25%, 50%, 75% and 100%.

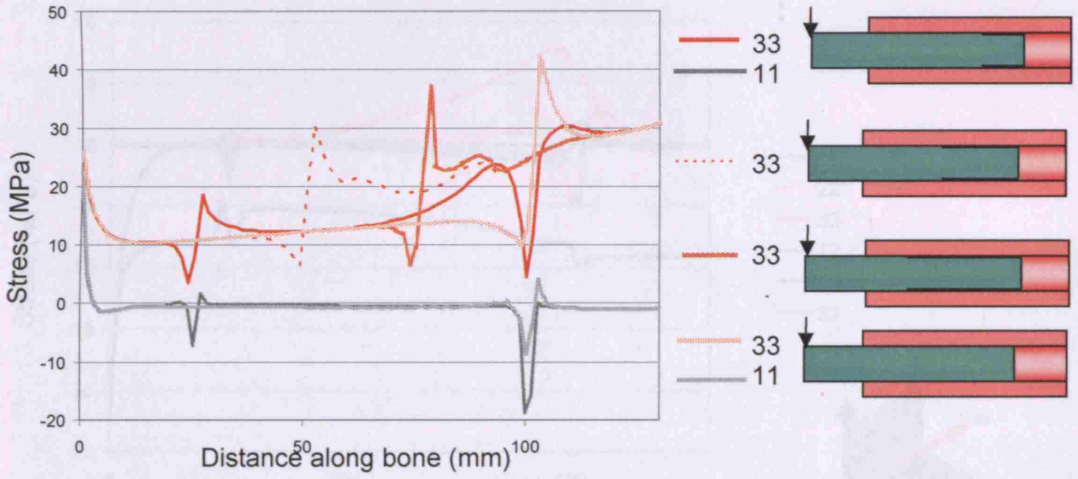

Figure 4.31 Axial and radial stress on inner edge of bone in bending for bone-implant integration of 25%, 50% and 75%

Figure 4.31 shows that the highest stress in each model occurs as a result of the end of the perfectly bonded section, so the stress concentration is the same for each. The radial stress is only marked for the 25% and 100% contact for clarity. The stress concentration at the end of the bonded section is the same for each model, 1:1.4. The high radial stress at the implant tip is larger for shorter lengths of bone contact: 19MPa for 25% contact, 12MPa for 50% contact and 7MPa for 75% contact.

4.4.6.2 Torsional Load

With perfect contact between the bone and implant, the only stress at the inner edge of the bone in torsion was the tangential/axial shear stress, and there was a small region of radial-tangential shear stress at the end of the bone and adjacent to the implant tip (figure 4.12). Figure 4.32 shows the stresses in the model with 25% of the implant in perfect contact and the remaining with frictional contact. The stresses are axisymmetric in torsional loading so only one node path was recorded.

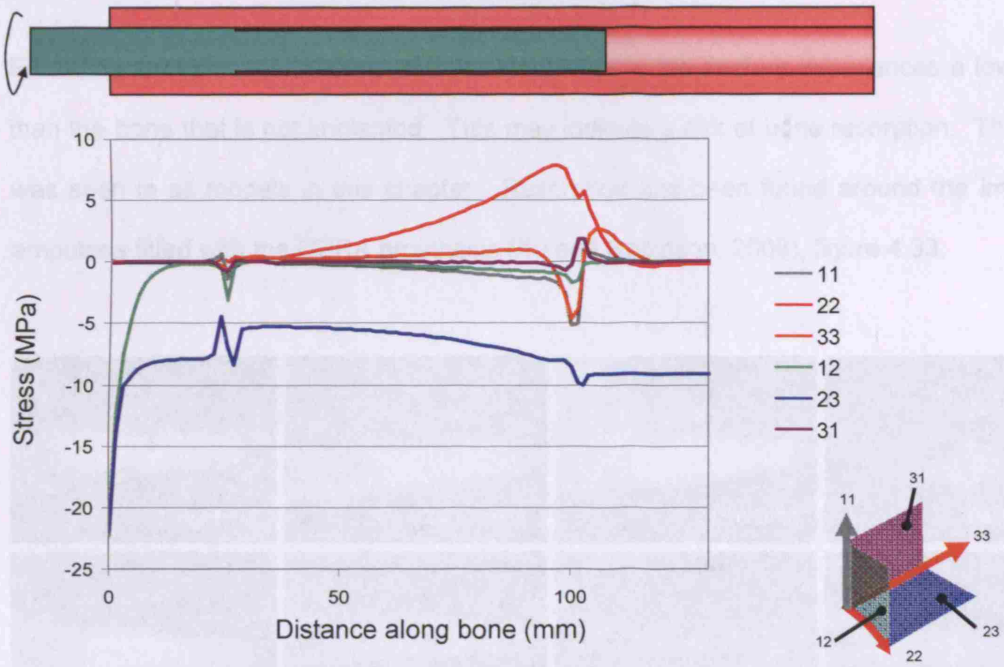

Figure 4.32 Stresses on inner edge of bone in torsion with 25% bone-implant integration.

The stress in the bone increases along the region of frictional contact. This is because there is a stress gradient between the bone and implant.

The stress of the highest magnitude is the shear stress (23). However the tangential stress (22) is almost as high in value at the implant tip. If the part of the implant in frictional contact were longer, the tangential stress might exceed the shear stress.

4.4.6.3 Axial Load

The stresses in the implanted bone under axial loading are the same for all amounts of bone integration and match the results, in figure 4.16, for different lengths of implant. There is no stress transfer between the bone and implant where there is no bone integration because there is no stress gradient between the bone and implant.

4.5 Discussion

Excluding stress concentrations, the bone adjacent to the implant experiences a lower load than the bone that is not implanted. This may indicate a risk of bone resorption. This effect was seen in all models in this chapter. Resorption has been found around the implant in amputees fitted with the OPRA prosthesis (Xu and Robinson, 2008), figure 4.33.

Figure 4.33 Radiographs of a femur implanted with the OPRA implant over seven years adapted from Xu and Robinson, 2008.

In figure 4.33, radiographs taken over seven years show resorption of bone at the distal end and bone remodelling at the proximal end of the implant. The first image was taken before load-bearing commenced. It appears that at seven years, resorption and remodelling have ceased to alter the shape of the bone, because the last image appears to have similar bone geometry the one two before it, marked *14/08/2003*. However it is possible that this remodelling continues, and this subject requires further study.

The perfect contact of the bodies created stress concentrations at the end of the bone and at the implant tip due to the geometric discontinuity. If an implant is well integrated into the bone these stress concentrations may increase the risk of bone fracture. Bone fractures have occurred at the tip of the intramedullary stem of total knee prostheses. Figure 3.34 shows a fracture at the tip of an intramedullary implant that occurred during a traffic accident.

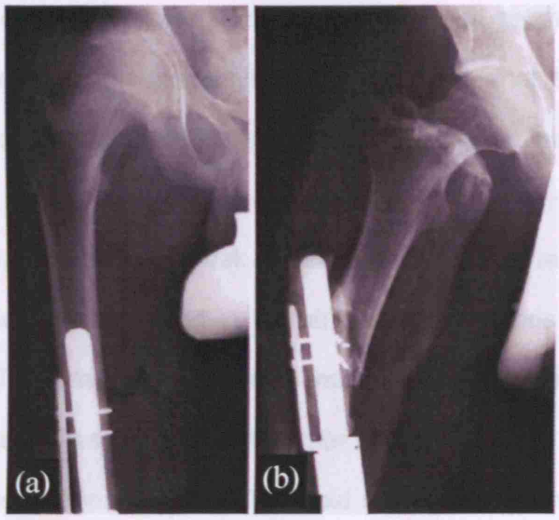

Figure 4.34 (a) Distal femoral prosthesis. (b) Periprosthetic fracture of femur at the tip of intramedullary rod. Adapted from Orlic et al. *(2006).*

The stress concentration at the implant tip is of special concern when a patient has both a hip and knee prosthesis in the same femur because the stress concentrations at the tips of both implants can overlap to cause a very high stress. It is possible that an ITAP amputee might sustain an injury that requires intramedullary fixation (one of the amputees in the OPRA programme has suffered a broken hip on his amputated side (Ax, 2004)). The implant would need to be chosen to prevent fracture at a combined stress concentration.

In all models the stresses caused by walking values of axial loading were much lower than the stresses caused by walking values of bending or torsion. The axial stress is in the order of 10% of the axial stress in bending and the shear stress is in the order of 5% of the shear stress measured in torsion.

Xu et al. (2006) used FEA to analyse an intramedullary femoral implant for attachment of a prosthetic limb and found the maximum von Mises stress in the bone near the implant tip to be 38.2MPa and 41.3MPa for implants of 21.5mm and 22mm diameter. These values are close to the 42MPa axial stress found in this study. The von Mises stress at the distal end of the bone was 18.4MPa and 13.9MPa, and in this study it was 22MPa for the basic model. These results are not directly comparable because the implant geometries are different (for example theirs is threaded) but the similar values indicate that the two techniques of prosthetic attachment can be compared in terms of the stress state in the bone.

The implant length was varied to model the effects of a small amount of bone-implant contact. No difference was measured in the stress concentrations for implants of length 30mm and longer. The 5mm implant experienced a much higher stress concentration because the two stress-raisers were close together, and their effects were superimposed to create one large concentration of stress. To avoid this effect the implant must be at least 30mm long and have more than 30mm of bone-implant contact. Xu et al. (2000) when carrying out a finite element analysis of the OPRA implant found that a longer implant generated no higher strains in the bone, although they only used two lengths of 60mm and 90mm.

The diameter of the bone was varied to reproduce the effect of a patient having a larger bone, or resorption that reduces the diameter. Higher stresses were experienced in bone with a smaller diameter in bending and axial loading. In torsion the shear stress on the outer edge of the bone was higher for a larger bone. In torsion there was also a higher shear stress concentration at the distal end of the bone because the larger second moment of area exacerbated the effects of the geometric discontinuity. This variable is of importance to the ITAP implant because of the variation in bone size of the amputees when the implant is first inserted, and also because of the possibility of bone remodelling due to stress shielding around the bone.

The next variable studied was the implant diameter which would be altered, if the amputee's intramedullary canal is of a different size or if the canal is not circular, to make sure that as much bone is in contact with the implant as possible. In axial loading a larger implant caused a reduction in the axial stress in bone adjacent to it, but a higher stress in the bone proximal to the implant. The relationship between outer diameter and stress concentration at the implant tip was proportional to the cube of the bone diameter, this resulted in a threefold increase in distal stress concentration with a diametral reduction from 24mm to 18mm. In torsional and transverse loading the shear stress and normal stress were smaller for a smaller implant. The reduction in stress concentration matches the values found by Xu et al. (2000) who reported a 40% reduction in stress when the implant diameter was reduced from 22mm to 26mm. The maximum stress in this study was 30MPa for an implant of 22mm and 18MPa for an implant of 26mm, this is a reduction of 40%. Figure 4.33 showed the reduction in bone diameter that is possible with remodelling around an intramedullary implant. Keeping in mind the changes made to the stress in bone as a result of smaller bone diameter, the bone diameter should be regarded as an important factor in choosing the settings for the fail-safe device.

A collar may be added to the implant to encourage bone growth, and two collar geometries were studied: a collar that covers the whole of the end of the bone and a collar that is 2mm larger in diameter than the implant shaft. A very small difference was made to the stress in bone due to axial loading. In torsion the shear stress in the tangential/axial plane became more evenly spread across the end of the bone with a collar, reducing the stress concentration on the inner edge to one fifth of its value with no collar. The stress in the radial/tangential plane was also more even across the end of the bone with a collar, possibly preventing resorption on the outer edge of the bone by increasing the shear stress here. An illustration of this from clinical practice is shown in figure 1.5 where there is no bone resorption at the outer edge of the bone at the distal end and the collar has encouraged bone remodelling, increasing the stability of the implant.

The bone of an amputee is weaker and has a lower Young's modulus than healthy bone (Sherk et al. 2008), (Rush et al. 1994). Both studies by Xu *et al.* (2000) and (2006) used the material properties of normal bone. The femur is expected to increase in strength and stiffness with time, so this is correct for normal use of the prosthesis. The rehabilitation process for ITAP is much shorter than that of the implant studied by Xu *et al.* and so, to protect the developing bone, it was necessary to study the implanted femur with poorer bone quality as well as with 'normal' bone quality. There was little difference between the pattern of stress transfer in the lower stiffness bone of an amputee who uses a socket prosthesis and the bone of normal strength. The lower stiffness bone is also less strong (Rho et al., 1995) and therefore the same stresses are more likely to cause fracture.

An implant with partial osseointegration was modelled using perfect contact for the osseointegrated part and frictional contact for the non-osseointegrated surface. The stress transfer patterns were similar for models with the frictional characteristics of a polished implant and for a rough implant. In axial loading the stresses were the same for all amounts of osseointegration, but in bending and torsion there was a gradual transfer of stress to the bone along the non-osseointegrated part although the maximum stress recorded did not exceed that of the model with total osseointegration. In torsion the tangential stress had a high value towards the tip of the implant. It is possible that the ITAP implant will be partially coated with HA because this preserves the length of the implant to transmit bending loads but reduces the amount of bone at risk of resorption due to stress shielding (Blunn et al. 2000).

4.6 Conclusions

A tubular model of the femur implanted with a cylindrical bone was investigated and parameters were varied to study their influence on the stress in the bone. The variables were chosen to represent anatomical features of different amputees and possible changes to the implant geometry and surface finish.

In chapter six recommendations will be made for setting the fail-safe device and the most important variables from this chapter will be considered. The bone diameter will be used because it has been found in this chapter to make a great difference to the stress at the bone-implant interface. The bone quality will be used because the bone of amputees is known to be significantly weaker than normal bone so the amputee is at greater risk during the early loading of the implant. The length of bone contact will be used because there are a number of reasons for the implant being in contact for only part of its length: due to divergent bone geometry, regions of poor osseointegration, and partial HA coating.

5 Effect of Amputation Level on the Stress Transferred to the Femur

Introduction

In the previous chapter a cylindrical model was used to represent the shaft of the femur. The level at which an amputation is carried out dictates whether or not this simplification is valid because the femur is not cylindrical at its extremities. The finite element analysis model in this chapter is a much more detailed representation of a femur to assess the effects of different levels of amputation on the stresses in the bone. The femur shape was taken from a CT scan and the varying density in the bone, calculated from the CT images, was used to model the material properties throughout the model. Three different resection levels were modelled and implants designed for each resection level in the way they would be designed for an amputee.

5.1 Method

A human femur was scanned using computed tomography. MIMICS 9.1 (Materialise, Belgium) was used to convert the CT data into geometry and material property information to create a three-dimensional model of a femur. The model was imported into the FEA software (MARC/MENTAT) and analysed. Figure 5.1 contains a guide to the steps taken to create the model.

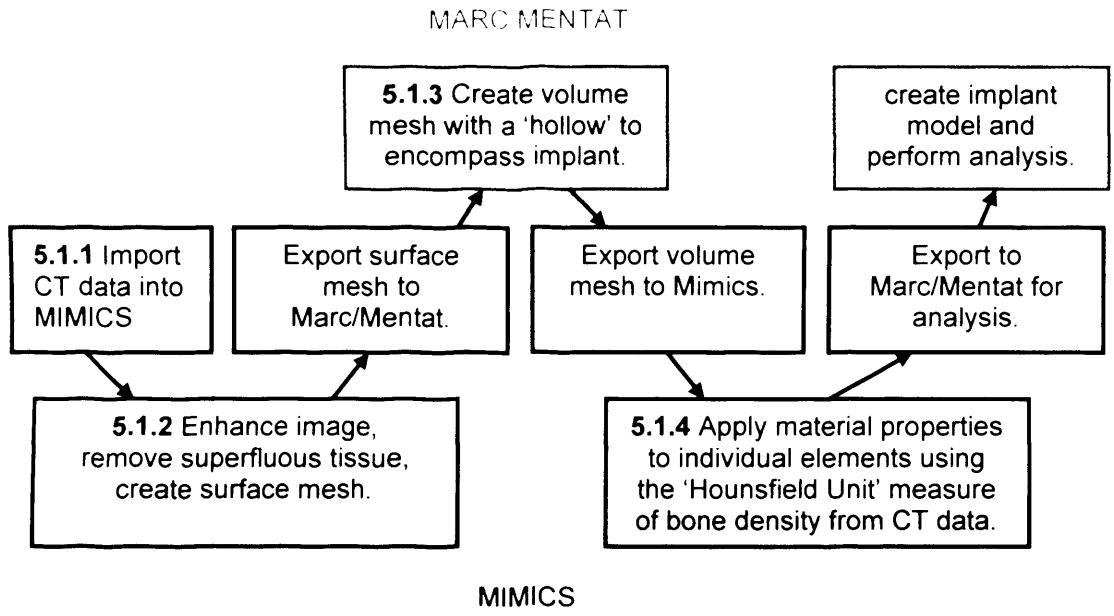

Figure 5.1 Steps taken to create an anatomical model of the femur for finite element analysis including the subchapter in which each stage is documented.

5.1.1 Gathering CT Data

A femur that had been preserved by freezing was scanned every two millimetres from the femoral head to the lesser trochanter and then at five millimetre intervals through the rest of the bone. Figure 5.2 shows examples of the CT images gathered.

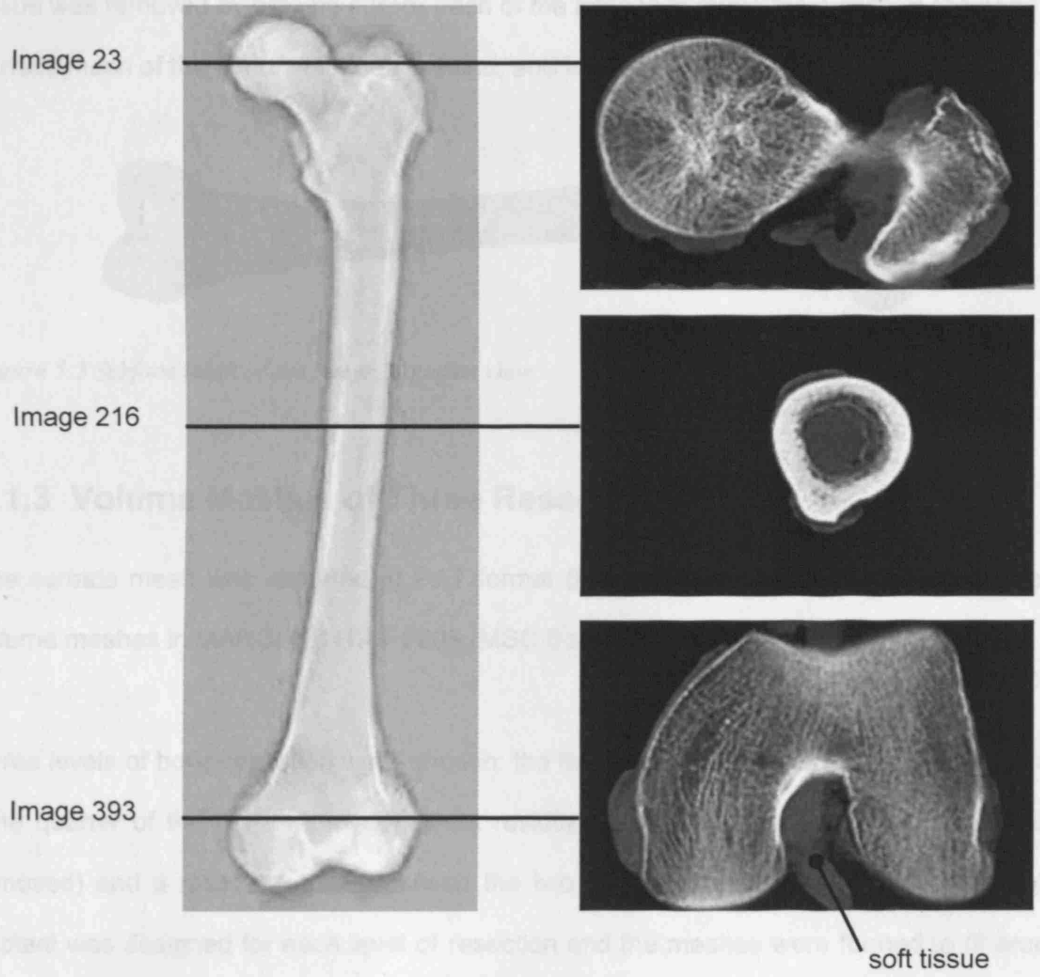

Figure 5.2 Examples of the CT scans taken at different levels of the femur.

5.1.2 Creating a Surface Mesh

The images were saved in JPEG format and imported into MIMICS 9.1 (Materialise, Belgium) and the information that defined their positions was used to create a three-dimensional image of the bone, including any soft tissue that was attached. Superfluous soft tissue was removed by erasing it from each of the images to leave the outline of the bone. A surface mesh of the femur was then created, and is shown in figure 5.3.

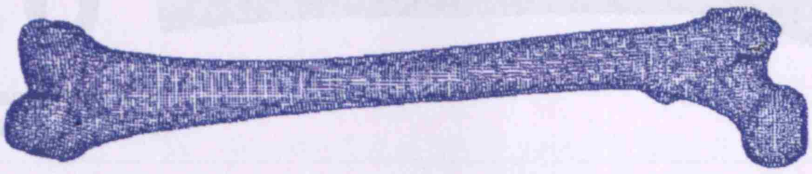

Figure 5.3 Surface mesh of the femur, anterior view.

5.1.3 Volume Meshes of Three Resection Levels

The surface mesh was exported in PAT format (MSC Software, USA) and used to create volume meshes in MARC/MENTAT 2005 (MSC Software, USA).

Three levels of bone resection were chosen: the three models represent a long residual limb (one quarter of the bone removed), short residual limb (three-quarters of the bone length removed) and a resection level between the two (half of the bone removed). A different implant was designed for each level of resection and the meshes were formed to fit around an implant, with a hollow to match the shape of the implant. The elements used were tetrahedral in form, which are more accurate than hexahedral for describing irregular three-dimensional shapes and use less computing time (Viceconti et al. 1998).

Figure 5.4 shows cross-sectional images of the three models showing the cavities left for the implants. The implant for the femur with three-quarters of the bone removed is the shortest because there is no space for a larger implant but the implants for the other models are similar in length. The implants were shaped to be congruous with the intramedullary canal of

the femur and to be in contact with as much cortical bone as possible without removing too much bone. For two of the models this meant being straight but the femur with half the bone resected is curved 5 degrees distally in the anterior direction because of the large amount of femoral curvature in the bone used.

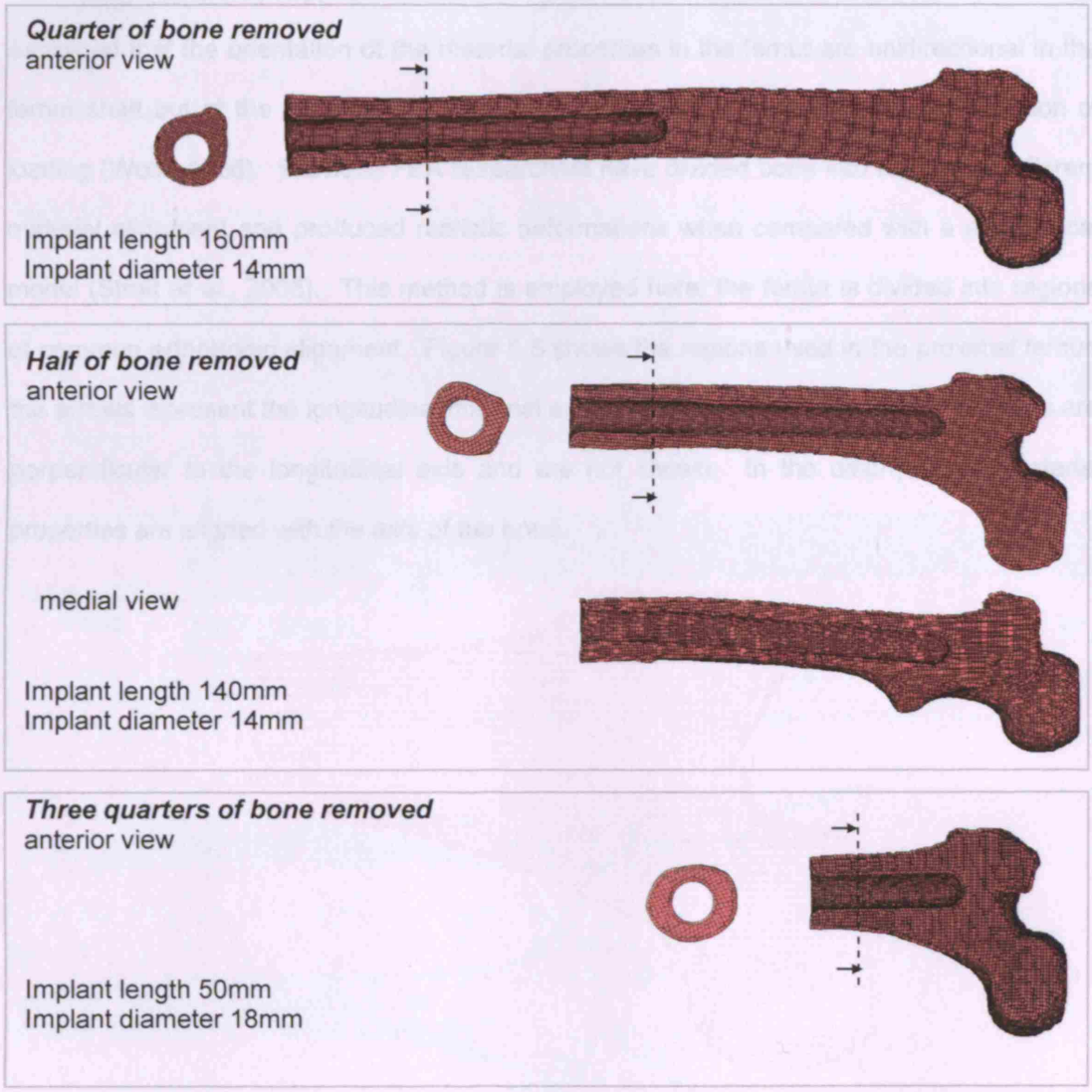

Figure 5.4 Cross-sectional images of the three femur models showing the cavity to fit the implants.

5.1.4 Assignment of Material Properties

The models were exported back to MIMICS for the material properties to be allocated. This task was carried out by comparing the position of each element with the average density in

that volume. In a CT scan the density is described by the depth of colour, also known as the 'grey value', and is quantified using the Hounsfield Unit. The greyvalues were converted into five material types using the technique described in chapter three, section 3.1.6.

The material properties applied were inhomogeneous and orthotropic. In section 3.11 it was explained that the orientation of the material properties in the femur are unidirectional in the femur shaft but at the ends of the bone they are aligned in approximately the direction of loading (Wolff, 1986). Previous FEA researchers have divided bone into regions of different material alignment and produced realistic deformations when compared with a mechanical model (Strait *et al.*, 2005). This method is employed here: the femur is divided into regions of common orthotropic alignment. Figure 5.5 shows the regions used in the proximal femur, the arrows represent the longitudinal material axis of each element. The transverse axes are perpendicular to the longitudinal axis and are not shown. In the diaphysis the material properties are aligned with the axis of the bone.

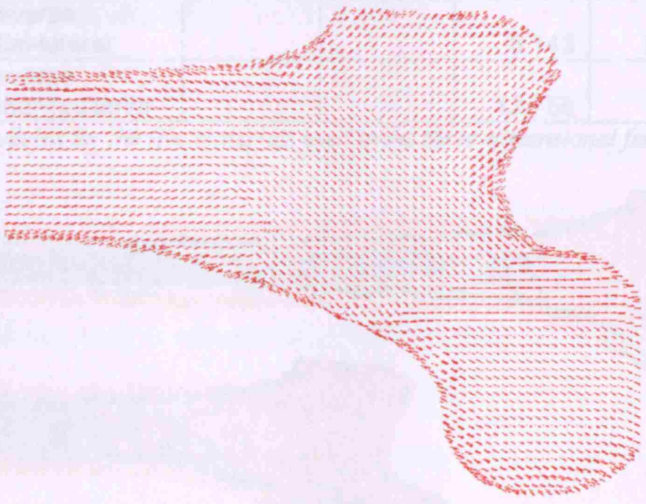

Figure 5.5 A cross-sectional image of the proximal part of the finite-element model of the femur showing the principal material axis of the elements as red arrows.

The total material spectrum was divided into five different sections: two cortical 'materials', and three cancellous 'materials' tables 5.1 and 5.2 specify the material properties used and

are based on values calculated in chapter three. Figure 5.6 shows the distribution of the material properties in the models.

	Young's Modulus/ MPa	Poisson's Ratio	Shear Modulus/ GPa	Yield stress in compression/ MPa	Yield stress in tension/ MPa
Axial	See table 5.2	v_{23}=0.376	G_{23}=4530	Cortical 175	Cortical 123
				Cancellous 64	Cancellous 45
Transverse		v_{12}=0.235	G_{12}=6230	Cortical 105	Cortical 73
				Cancellous 38	Cancellous 27

Table 5.1 Material properties for cortical and cancellous bone for the three-dimensional model.

Direction		Material number (E_1 in Gpa) 1	2	3	4	5
cortical bone	axial	12.263	11.413			
	transverse radial	12.508	11.743			
	transverse circumfererential	19.548	18.358			
Cancellous bone	axial			7.413	4.539	1.757
	transverse medial-lateral			8.143	5.191	0.98
	transverse anterior-posterior			12.758	5.21	0.704

Table 5.2 Young's modulus for the five materials used in the three-dimensional femoral model.

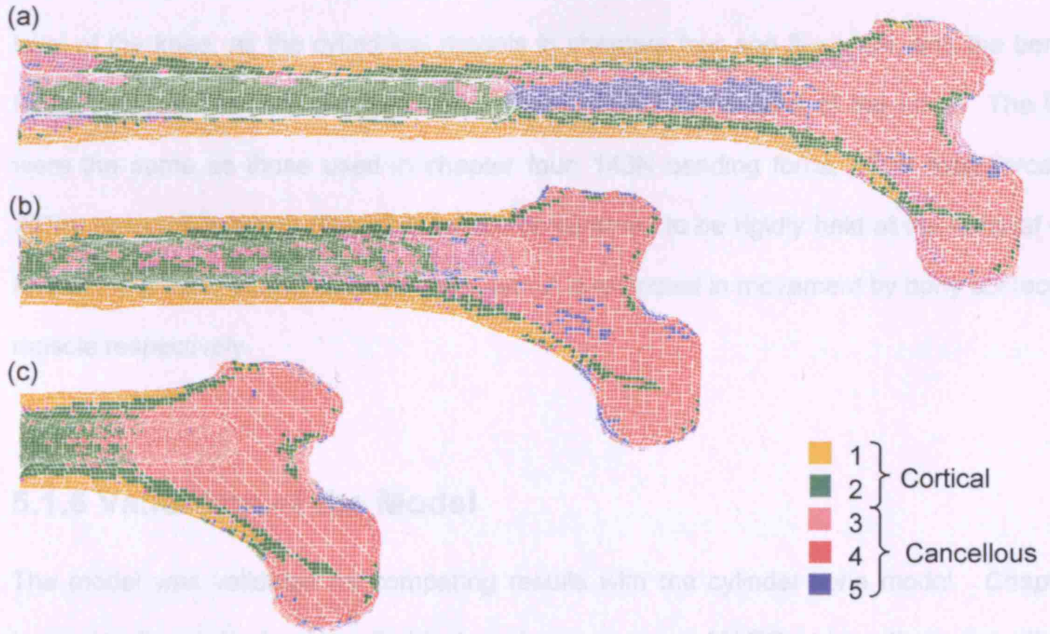

Figure 5.6 Cross-section views of the femur models showing the distribution of materials.

In figure 5.6, the gold and green represent cortical bone and the other colours represent cancellous bone of different densities. In figure 5.6(a) the cavity for the implant has green adjacent to most of its length, showing contact with the cortical bone. At the distal end of the bone, there is little cortical bone contact because the cortical bone diverges towards the knee. 5.6(b) shows the femur with half resected and there is patchy contact with the cortical bone along most of the length of the implant which reduces near the proximal end. The implant is in an area of cancellous bone at the proximal end. 5.6(c) shows the femur with three-quarters resected, where the implant is only partly in contact with cortical bone.

The implant model is composed of titanium alloy (Ti6Al4V) and has a Young's modulus of 110GPa and Poisson's Ratio of 0.3. The material properties of titanium were discussed in chapter one.

5.1.5 Analysis of the Models

After exporting back into MARC/MENTAT, and coupling with implant meshes, the models had boundary conditions applied and were analysed. The implants were extended to the level of the knee, as the cylindrical models in chapters four and five were, and the bending force, torsional moment and axial force were applied at the level of the knee. The loads were the same as those used in chapter four: 143N bending force, 668N axial force and 20Nm torsional moment. The bones were constrained to be rigidly held at the femoral head and at the greater trochanter, where the femur is restricted in movement by bony contact and muscle respectively.

5.1.6 Validation of the Model

The model was validated by comparing results with the cylinder-bone model. Chapter 4 presented the analysis of a cylindrical model produced in MARC to investigate the effect of

changing the geometry of implant and bone. A cylinder model, with appropriate geometry and perfect contact between the bone and implant, was chosen and compared with an anatomical model of the bone and implant that were also in perfect contact. The 'quarter-resected' bone was chosen for this because it is the most cylindrical in nature and so more comparable to the cylindrical model.

The bone is dissimilar from the tube model in that it is not axisymmetric so appropriate implant and bone diameters needed to be decided. The implant diameter used was 14mm, the same as for the anatomical model. Analytical equations were used to calculate the outer diameter that would be required for the tubular bone analogue to generate the same stress as the anatomical model. The calculation of the outer diameters required to compare with the anatomical model for each type of loading are shown in the following equations.

Bending Force	Axial Force	Torsion
Governing equations		
$\sigma = \frac{My}{I}$ _____(eq. 5.1)	$\sigma = \frac{F}{A}$ _____(eq. 5.2)	$\tau = \frac{Tr}{J}$ _____(eq.5.3)
$I = \frac{\pi(D^4 - d^4)}{64}$	$A = \pi(\frac{D^2}{2} - \frac{d^2}{2})$	$J = \frac{\pi(D^4 - d^4)}{32}$
Rearrange for outer diameter		
$D = \sqrt[4]{\frac{64My}{\pi\sigma} + d^4}$	$D = 2\sqrt{\frac{F}{\pi\sigma} + \left(\frac{d}{2}\right)^2}$	$D = \sqrt[4]{\frac{32Ty}{\pi\tau} + d^4}$
$M = 16.2Nm$ $y = 6.0mm$ $\sigma = 12.2MPa$ $d = 14.0mm$	$F = 668N$ $d = 14.0mm$ $\sigma = 1.85MPa$	$T = 20.0Nm$ $y = 6.0mm$ $\tau = 2.5MPa$ $d = 14.0mm$
Outer diameter		
$D = 25.5mm$	$D = 25.6mm$	$D = 26.7mm$

These calculations show that the stresses on the inner edge of a tubular bone model with an inner diameter of 14mm are similar to the stresses found in an anatomical model of the femur with one quarter removed if the bone diameter is 25.5mm (when subjected to a lateral force), 25.6mm (under an axial force) or 26.7mm (with a torsional moment applied). A diameter of 26mm was chosen because it is approximately the mean value of these three (25.7mm).

A cylindrical model of the bone with outer diameter 26mm, implant diameter of 12mm and implant length of 160mm was created and loaded in bending. Figure 5.8 shows the axial stress recorded along the inner surface of the bone for both the cylindrical model and the

anatomical model under the same load. The solid line shows the data for the anatomical model and the dashed line for the cylinder model.

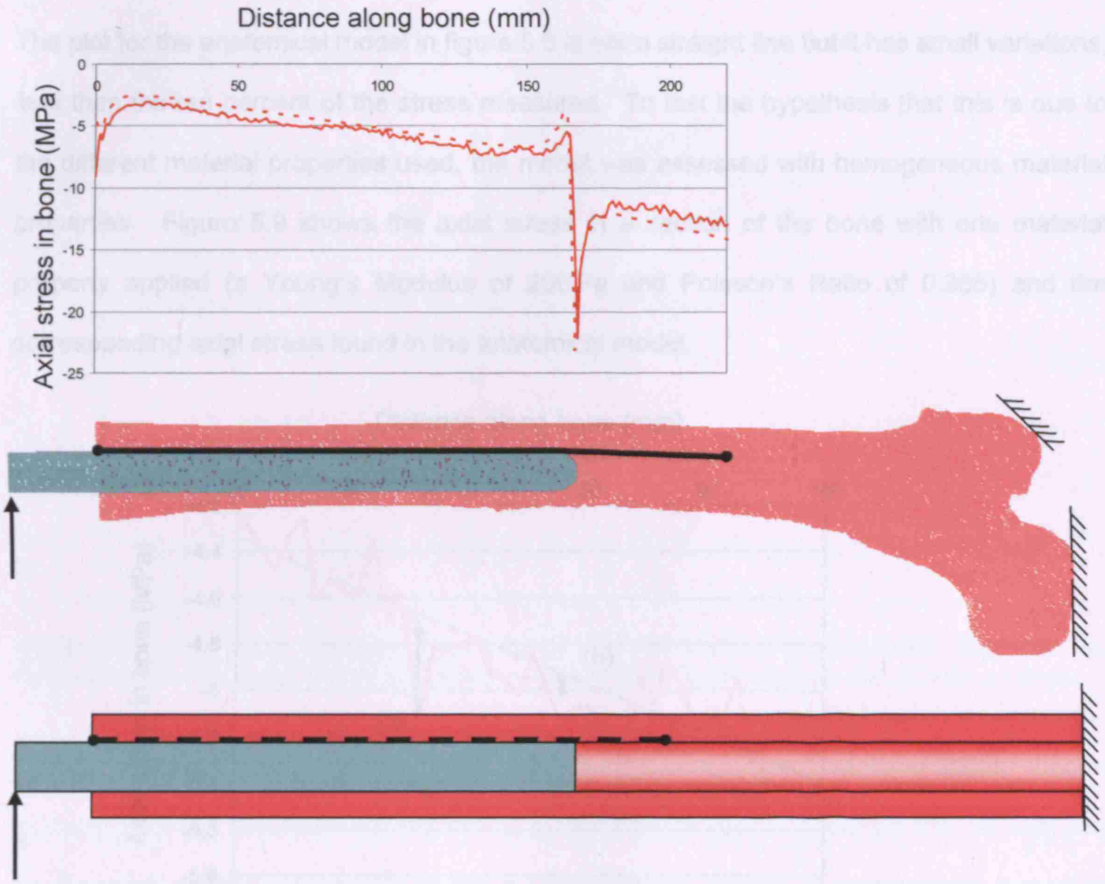

Figure 5.8 The axial stress along the inner edge of the bone for the anatomical model and a cylindrical model under a bending force.

The axial stresses in the models match each other, however there are small variations in the stress in the anatomical model. The maximum difference between the stress adjacent to the implant is twenty percent, this occurs at 52mm from the end of the bone, and the stresses are most similar between 85 and 100mm from the end of the bone. The variations are due to the geometry of the anatomical model. The stress concentration at the end of the implant is five percent higher for the cylinder model than for the anatomical model. Proximal to the implant, the stress in the cylinder model is eight percent higher than that in the bone. This lower stress can be explained by the sudden increase in the second moment of area because the bone model is not hollow, whereas the cylindrical model is hollow. The material

properties in the centre of the anatomical model have low stiffness (Young's Modulus of 4MPa), however they contribute to the rigidity of the whole bone.

The plot for the anatomical model in figure 5.8 is not a straight line but it has small variations, less than the ten percent of the stress measured. To test the hypothesis that this is due to the different material properties used, the model was assessed with homogeneous material properties. Figure 5.9 shows the axial stress in a section of the bone with one material property applied (a Young's Modulus of 20GPa and Poisson's Ratio of 0.365) and the corresponding axial stress found in the anatomical model.

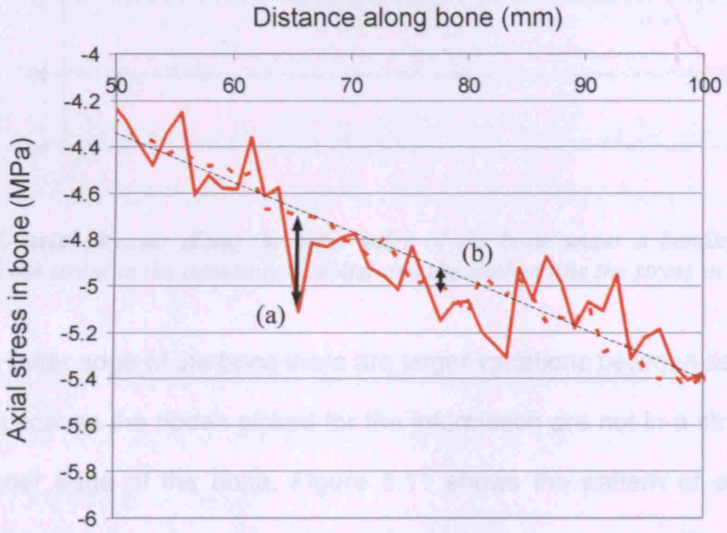

Figure 5.9. Axial stress in a section of the bone with homogeneous material properties (dotted line) and with anatomical material properties (solid line)

There is a smoother plot in the value of axial stress for a bone made of one material property (a variation of approximately three percent (b) as opposed to a variation of just under ten percent (a)). The variation found in the anisotropic model is one drawback of the allocation of a number of different material properties, and may be improved by increasing the number of different materials used so that the difference between adjacent elements is smaller; five materials were chosen because of computational time constraints. The node-to-node variation in the inhomogeneous model is less than ten percent and is a more accurate representation of the femur, and it was deemed suitable for this study.

Figure 5.10 shows the axial stress along the outer edge of the bone to further investigate how well the anatomical model matches the cylindrical model. The solid line represents the stress in the anatomical model and the dashed line the stress measured in the cylinder model.

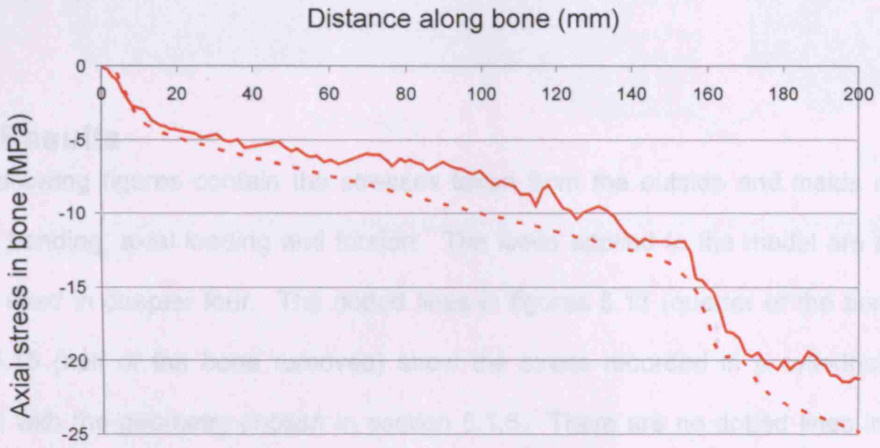

Figure5.10 axial stresses along the outer edge of the bone under a bending load. The solid line represents the stress in the anatomical model and the dashed line the stress in the cylinder analogue.

Along the outer edge of the bone there are larger variations between adjacent nodes. This is probably because the nodes picked for the information are not in a straight line, as they are for the inner edge of the bone. Figure 5.11 shows the pattern of elements on the inner surface of the bone and on the outer surface of the bone. In addition, the inner surface of the bone is created by using a reamer that gives an edge congruent with the implant which is smooth but the outside of the bone is not regular in shape.

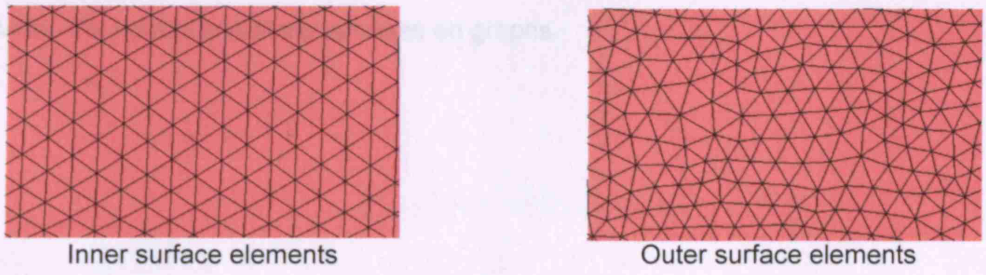

Figure 5.11 Pattern of elements on the inner and outer surfaces of the bone.

In this section the anatomical model has been compared with a cylinder model of similar geometry, and the stresses caused by loading in bending have been found to be similar for both, apart from variations caused by the geometry and material properties used in the anatomical model. The model is therefore acceptable for studying the stresses in the bone under implant loading.

5.2 Results

The following figures contain the stresses taken from the outside and inside of the femur under bending, axial loading and torsion. The loads applied to the model are the same as those used in chapter four. The dotted lines in figures 5.13 (quarter of the bone removed) and 5.15 (half of the bone removed) show the stress recorded in a cylindrical cantilever model with the geometry chosen in section 5.1.6. There are no dotted lines in figure 5.16 because the geometry can no longer be described as a cantilever in the model with three-quarters removed due to the geometry.

The models were checked throughout to find the highest stresses, and the node paths that are recorded here include the highest stresses in the bone apart from the artefactual stresses at the points of holding.

A cylindrical co-ordinate system was used and the convention in figure 5.12 is followed to describe the directions of stresses in the bone. The colours in 5.12(b) are used to distinguish between the normal and shear stresses on graphs.

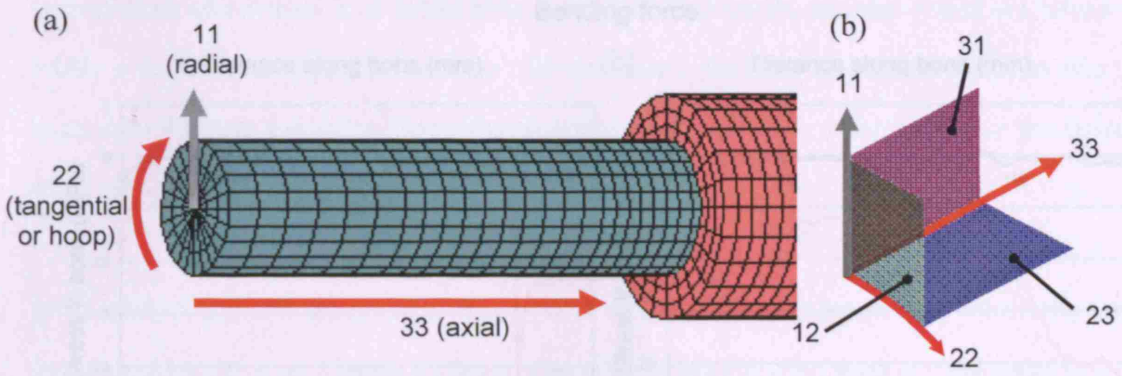

Figure 5.12(a) Standard for describing normal stress components (b) colour convention for normal and shear stresses.

5.2.1 Quarter of the Femur Removed

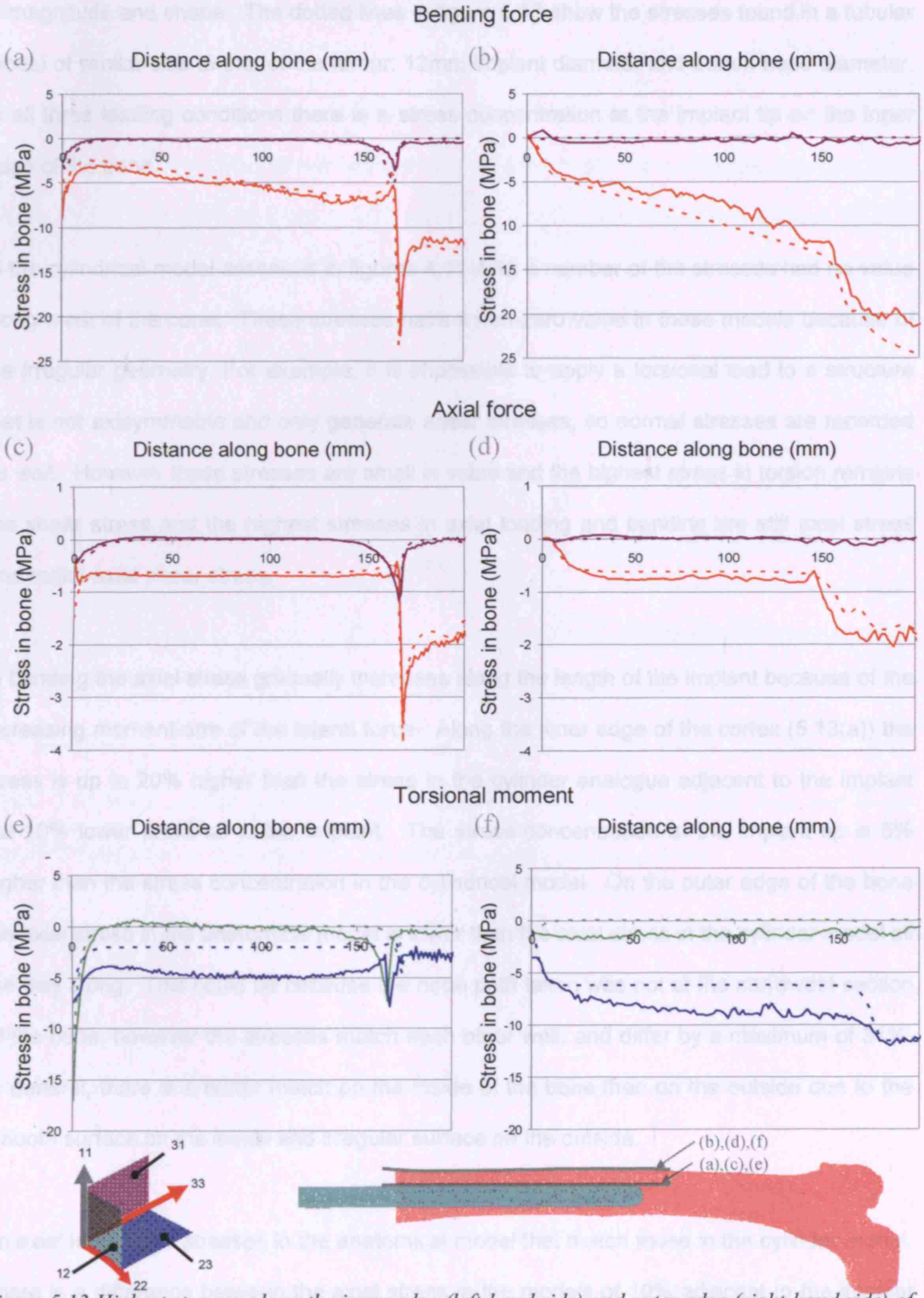

Figure 5.13 Highest stresses along the inner edge (left-hand side) and outer edge (right-hand side) of the bone under bending, axial and torsional loading for a femur with one-quarter resected. Dotted lines show the maximum stresses in cylindrical models with similar geometry.

The stresses recorded in figure 5.13, when compared with the cylindrical model, are similar in magnitude and shape. The dotted lines in figure 5.13 show the stresses found in a tubular model of similar size to that of the femur: 12mm implant diameter and 26mm bone diameter. In all three loading conditions there is a stress concentration at the implant tip on the inner edge of the bone.

In the cylindrical model assessed in figures 4.11-4.13 a number of the stresses had no value along most of the bone. These stresses have a non-zero value in these models because of the irregular geometry. For example, it is impossible to apply a torsional load to a structure that is not axisymmetric and only generate shear stresses, so normal stresses are recorded as well. However these stresses are small in value and the highest stress in torsion remains the shear stress and the highest stresses in axial loading and bending are still axial stress and radial-axial shear stress.

In bending the axial stress gradually increases along the length of the implant because of the increasing moment-arm of the lateral force. Along the inner edge of the cortex (5.13(a)) the stress is up to 20% higher than the stress in the cylinder analogue adjacent to the implant but 10% lower proximal to the implant. The stress concentration at the implant tip is 5% higher than the stress concentration in the cylindrical model. On the outer edge of the bone the axial stress in the anatomical model is lower than the axial stress in the cylinder model all the way along. This could be because the node path taken was not at the narrowest section of the bone, however the stresses match each other well, and differ by a maximum of 31%. In general, there is a better match on the inside of the bone than on the outside due to the smooth surface on the inside and irregular surface on the outside.

An axial load elicits stresses in the anatomical model that match those in the cylinder model. There is a difference between the axial stress in the models of 10% adjacent to the implant

and also at the stress concentration. As the model is linear, the discrepancy could be removed by using a cylinder of a slightly smaller diameter.

The cylindrical model geometry was chosen to match the stress proximal to the implant (see 5.13(e)) however this model poorly represents the stress in the bone adjacent to the implant, where the bone-implant structure is believed to be most at-risk from overloading in torsion, especially during the period of bone healing after implantation. A further cylindrical model in torsion model was created to match the stresses in the bone next to the implant. The geometry chosen has an outer diameter or 23mm. Figure 5.14 shows the shear stresses recorded in this narrower cylinder model.

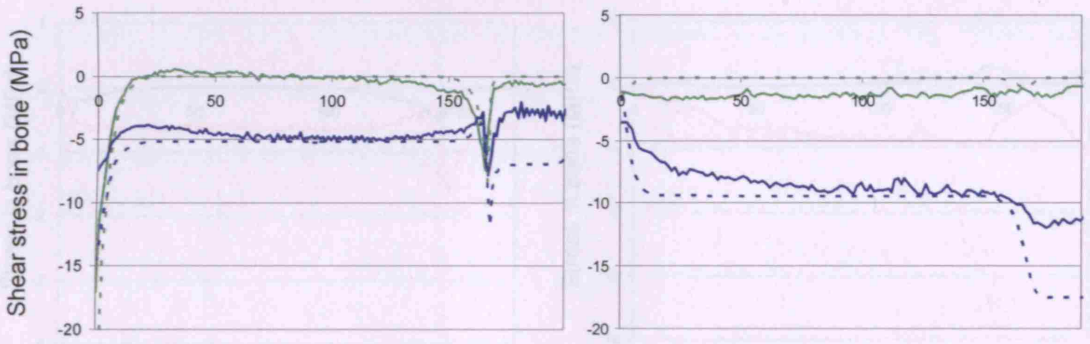

Figure 5.14 Shear stresses recorded in the anatomical model in torsion (solid line) and in the cylindrical model with an outer diameter or 23mm (dotted line). The blue lines represent the tangential/axial stress and the green line represents the radial/ tangential stress.

The shear stress proximal to the implant is double that in the anatomical model. The stress concentration at the implant tip is 41% higher than in the anatomical model. This approximation to the stress in the bone, with a diameter of 23mm, is a safer one to use than the model with a diameter of 28mm because it consistently overestimates the stress in the bone.

5.2.2 Half of the Bone Removed

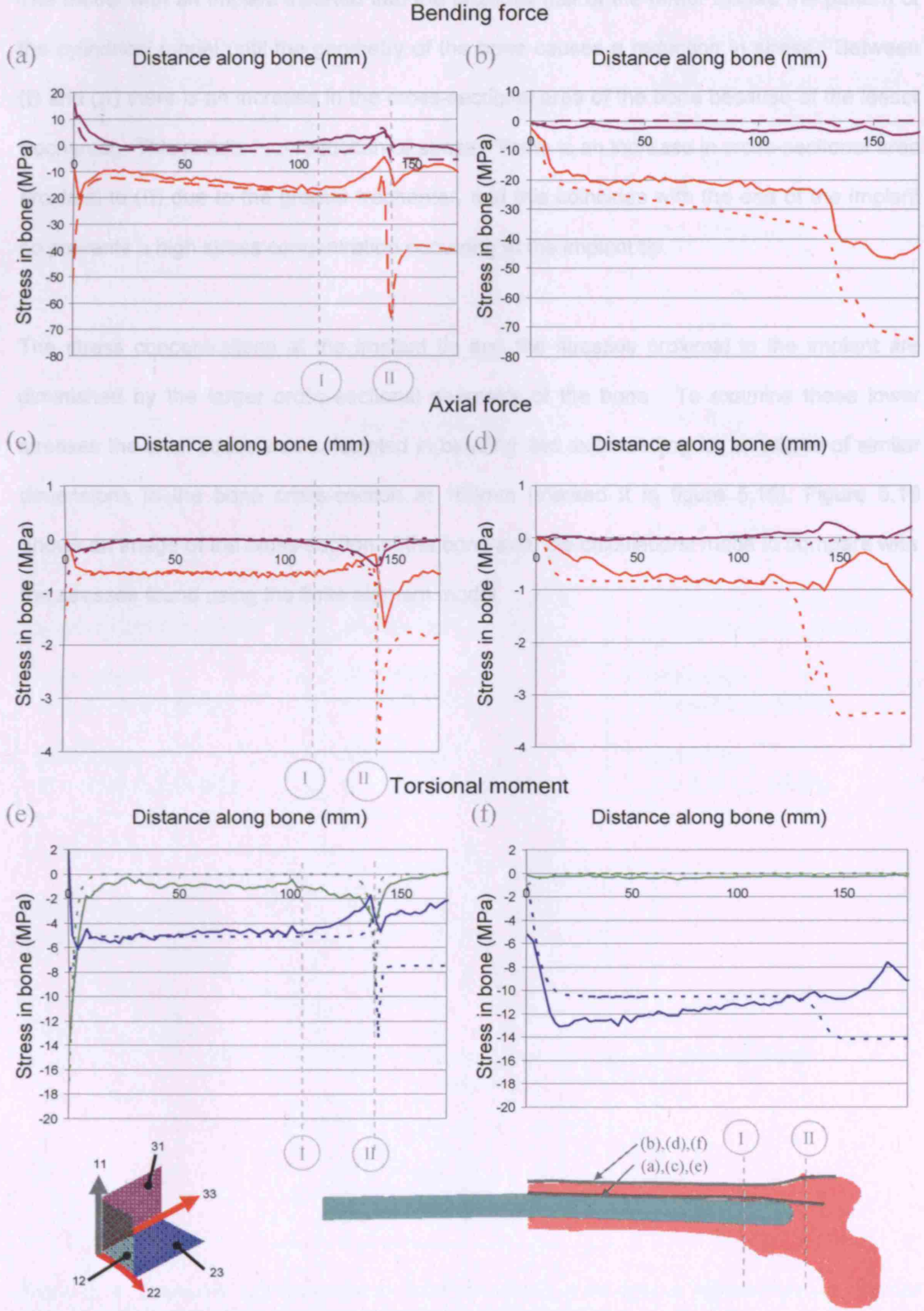

Figure 5.15 Highest stresses along the inner edge (left-hand side) and outer edge (right-hand side) of the bone under bending, axial and torsional loading for a femur with one-half resected.

The model with an implant inserted into the proximal half of the femur follows the pattern of the cylindrical model until the geometry of the bone causes a reduction in stress. Between (I) and (II) there is an increase in the cross-sectional area of the bone because of the lesser trochanter. This results in a reduction of stress. There is an increase in cross-sectional area proximal to (II) due to the greater trochanter, and this coincides with the end of the implant so prevents a high stress concentration occurring at the implant tip.

The stress concentrations at the implant tip and the stresses proximal to the implant are diminished by the larger cross-sectional geometry of the bone. To examine these lower stresses the axial stress was calculated in bending and axial loading for an ellipse of similar dimensions to the bone cross-section at 160mm (marked II in figure 5.15). Figure 5,16 shows an image of the cross-section of the bone and the calculations made to compare with the stresses found using the finite element model.

Bending	Axial force	Torsion
$M = 143x(340+160)$ $M = 16200Nmm$ $y(innersurface) = 7mm$ $y(outersurface) = 25mm$ $I = \frac{\pi x 25 x 15^3}{4}$ $I = 66268mm^4$ $\sigma = \frac{My}{I}$ _____(eq.5.1) inner edge $\sigma = 7.5MPa$ outer edge $\sigma = 37.0MPa$	$F = 688N$ $A = \pi x 15 x 25$ $A = 1178mm^2$ $\sigma = \frac{F}{A}$ _____(eq.5.2) over whole cross section $\sigma = 0.6MPa$	$M = 20{,}000Nmm$ $y(innersurface) = 7mm$ $y(outersurface) = 25mm$ $J = \frac{\pi x 25^2 x 15^2}{16}$ $J = 27612mm^4$ $\tau = \frac{My}{J}$ _____(eq.5.3) inner edge $\tau = 2.6MPa$ outer edge $\tau = 9.1MPa$
Approximate value from anatomical FEA model inner edge $\sigma = 8.0 \pm 1.0MPa$ outer edge $\sigma = 43.0 \pm 3.0MPa$	Approximate value from anatomical FEA model inner edge $\sigma = 0.6 \pm 0.2MPa$ outer edge $\sigma = 0.4 \pm 0.2MPa$	Approximate value from anatomical FEA model inner edge $\tau = 3.0 \pm 2.0MPa$ outer edge $\tau = 8.6 \pm 2.0MPa$

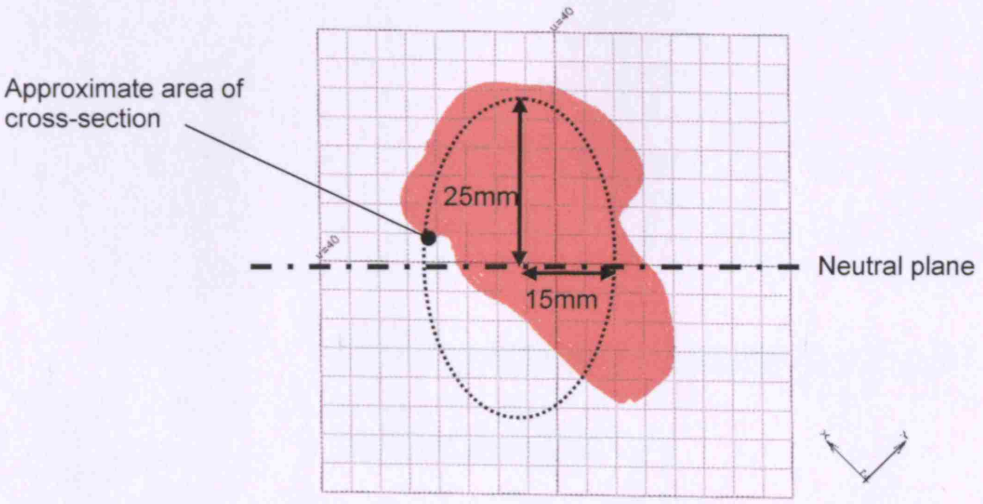

Figure 5.16 Geometric approximation to the cross-section of the bone at 160mm from the resected end and approximate values for stress in bending and axial loading.

The values of stress calculated for the ellipse approximation to the cross-section of the bone correlate with the results found in the anatomical model. It can be drawn from this that the stresses measured on the inner edge of the cylinder and bone models (5.15 (a), (c) and (e)) for all three loading conditions are realistic. The stresses on the outside of the bone are diminished to the same extent as the stress on the inside of the bone by the geometry of the proximal femur in all three loading conditions and match the predictions made using the ellipse approximation. The correlation of the stresses along the bone-implant interface with the ellipse calculations shows that the stress concentration in the FEA model is representative of the stress found at the implant tip for a femur of this geometry.

5.2.3 Three Quarters of the Bone Removed

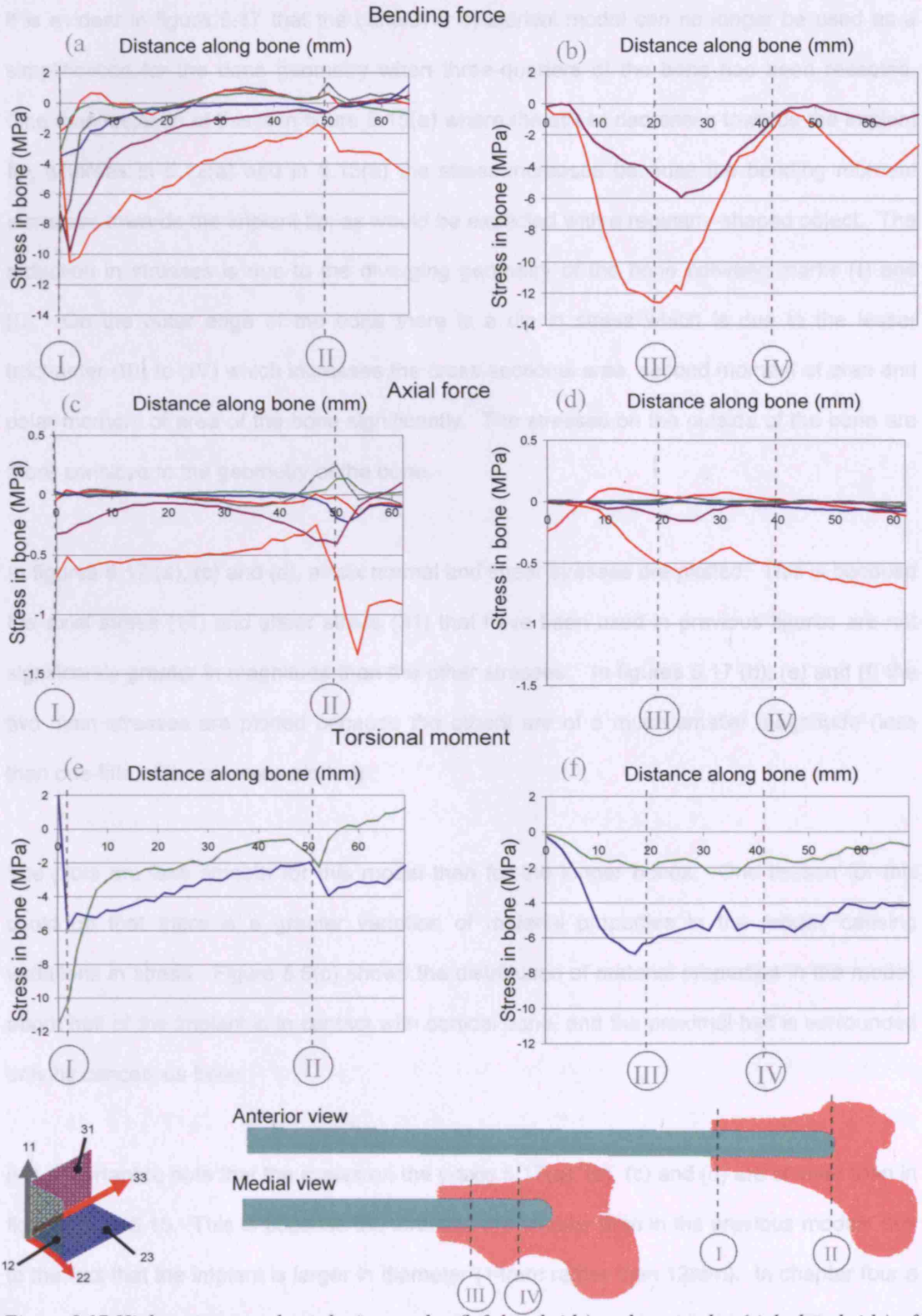

Figure 5.17 Highest stresses along the inner edge (left-hand side) and outer edge (right-hand side) of the bone under bending, axial and torsional loading for a femur with three-quarters resected.

It is evident in figure 5.17 that the cantilever cylindrical model can no longer be used as a simplification for the bone geometry when three-quarters of the bone has been resected. One manifestation of this is in figure 5.15(a) where the stress decreases towards the implant tip, whereas in 5.12(a) and in 5.13(a) the stress increases because the bending moment increases towards the implant tip, as would be expected with a regularly-shaped object. The reduction in stresses is due to the diverging geometry of the bone between marks (I) and (II). On the outer edge of the bone there is a dip in stress which is due to the lesser trochanter (III) to (IV) which increases the cross-sectional area, second moment of area and polar moment of area of the bone significantly. The stresses on the outside of the bone are more sensitive to the geometry of the bone.

In figures 5.17 (a), (c) and (d), all six normal and shear stresses are plotted. This is because the axial stress (11) and shear stress (31) that have been used in previous figures are not significantly greater in magnitude than the other stresses. In figures 5.17 (b), (e) and (f) the two main stresses are plotted because the others are of a much smaller magnitude (less than one-fifth of the stresses plotted).

The plots are less smooth for this model than for the longer bones. One reason for this could be that there is a greater variation of material properties in the model, causing variations in stress. Figure 5.6(c) shows the distribution of material properties in the model: about half of the implant is in contact with cortical bone, and the proximal half is surrounded only by cancellous bone.

It is important to note that the scales on the y-axis 5.17(a), (b), (c) and (d) are smaller than in figures 5.13-5.15. This is because the stresses are smaller than in the previous models due to the fact that the implant is larger in diameter (14mm rather than 12mm). In chapter four a larger implant was found to 'shield' the bone from stress because of its higher stiffness, and

this is evident in axial loading and bending. The implant diameter has the opposite effect on the shear stress adjacent to the bone in torsion because the distance from the centre of rotation is greater, making the shear stress larger. The larger polar moment of area of the bone would cause a reduction in shear stress compared with the other models if the implant were the same diameter. In this case, however, the effects of the larger implant and larger bone are combined so that the stress is one-fifth of the stress in the previous models at the distal end and reduces along the length of the implant because of the diverging geometry of the bone.

5.3 Discussion

In chapter four it was noted that a shorter femur would result in a higher stress concentration adjacent to the implant tip, because the lever arm for any loads applied at the knee or the foot would be longer. This is not apparent in this chapter because the implants in the shorter femoral models encounter a larger second moment of area at the implant tip. As a result, the stress concentration is actually lower for the shorter femurs: 22MPa for the model with quarter removed, 14MPa for the femur with half removed and 10MPa for the shortest model. An immediate conclusion might be that an implant that terminates in the epiphysis of the femur is preferable to one that is situated only in the shaft because the stress concentration is lower. This is not necessarily the case, however, because the bone adjacent to the implant in the epiphysis is cancellous bone which is about one-third weaker than the cortical bone found in the shaft so requires a lower stress to fracture. In the femur with three quarters removed the maximum tensile stress in the transverse direction is 10MPa (figure 5.17(a)). The strength of cancellous bone is 27MPa (see table 5.2) which only gives a safety factor of 2.7. In the longest femur model the maximum stress is 23MPa, but the strength is 73MPa, giving a safety factor of 3.2. Therefore the risk of fracture is actually greater in the shorter femur.

The cylinder model gives a good approximation to the stresses found in the model with one-quarter removed (figure 5.13). This indicates that the cylinder model could be employed for assessment of the stresses occurring in the femur of an amputee with a long residual limb using ITAP. The stress concentration at the implant tip is overestimated by 5% by the cylinder model because it is hollow. However, it may be safe to use the cylinder model as an approximation because this overestimation gives a 5% safety factor.

There are a number of ways to choose the outer diameter for a tubular representation of the bone shaft. Three are considered here: (a) by matching the cross-sectional area of the bone, (b) by matching the broadest or narrowest part of the bone cross-section or (c) by measuring the bone thickness in the A-P plane and the M-L plane and using the most appropriate of these measurements. Table 5.3 shows the cylinder bone diameters calculated from each of the three methods for the femur scanned for use in this chapter. The cross-section of the femur used is half-way along the implant length.

	Anatomical Model	Cylinder Model
(a) Cross-sectional area	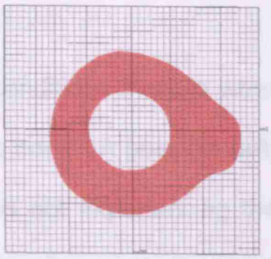 area = 440mm^2	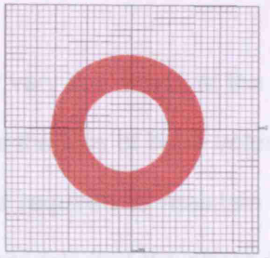 area = 440mm^2 gives outer diameter = 28.0 mm
(b) Minimum and maximum bone radius	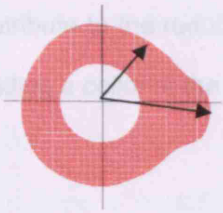 Minimum radius = 13.2 mm Maximum radius = 18.0 mm	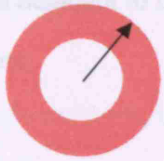 diameter = 13.2 x 2 = 26.4 mm or diameter = 18.0 x 2 = 36.0 mm
(c) A-P and M-L Measurement	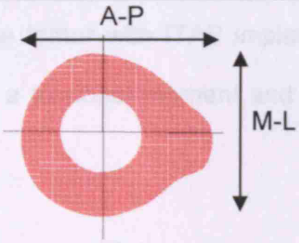 A-P thickness = 32.0 mm M-L thickness = 26.0 mm	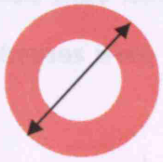 diameter = 32.0 mm or diameter = 26.0 mm

Table 5.3 calculations of cylinder bone diameter using three different measurements of the anatomical model.

The diameters calculated in table 5.3 are in the range 26-36mm, and the model that was found to correlate with the anatomical model in section 5.1.6 was 26mm. 'Minimum radius' and 'M-L thickness' measurements give cylinder diameters of 26.0 and 26.4mm respectively, so are appropriate for selecting the cylinder diameter. It is only possible to measure the minimum radius of the bone if a CT scan is available for the amputee, but only a radiograph taken in the correct orientation is required for measuring the M-L thickness of the bone. It is,

therefore, proposed that this method be used to choose the diameter for a simple representation of the bone.

In all models in all loading conditions there is either no stress or very low stress at the outer edge of the distal end of the bone. A possible outcome of this is the loss of bone volume or density because the bone is not experiencing the strain that is required to maintain bone mass. It is also noticeable, particularly in the two longest bone models that the stress in the bone is lower adjacent to the implant than proximal to the implant. As discussed in chapter four, this lower stress can contribute to the reduction in bone volume adjacent to the implant and can be prevented by including a collar at the distal end of the bone.

5.4 Conclusions

A femur was scanned and finite element models created of amputations of one quarter, one half and three quarters of the femur with ITAP implants. The models were loaded with a lateral force, axial force and a torsional moment and the highest stresses were plotted for each loading condition.

The stresses in the model with one quarter of the femur removed matched those predicted with a cylinder model.

The stresses in the model with half removed matched the stresses in the cylinder model up to the point where the bone geometry diverged and the stresses decreased. As a result of the geometry the stress concentration was much smaller than for the model with one quarter removed despite the bending moment being larger from the lateral loading.

The model with three quarters of the bone removed was not compared with a cylinder model because its geometry is different from that of a cylinder. The stresses recorded on the inner

edge of the bone were explainable by the almost conical shape of the bone. The stresses on the outer edge of the bone were more sensitive to other bony structures on the edge of the bone, in particular the greater and lesser trochanters.

The femur of an amputee with an ITAP implant that does not extend proximal to the diaphysis can be modelled for stress distribution using a tubular bone containing a cylindrical implant. The implant diameter for the model is the diameter of the implant designed for the amputee and the outer diameter of the bone is the thickness of the bone in the medial-lateral direction, as measured from a radiograph or CT scan.

Although the stress concentration at the implant tip is lower for the models where the implant extends into the epiphysis, the bone is weaker here and is at higher risk of fracture as a result. Further analysis of the fracture risk is considered in the following chapter.

6 Recommendations for Setting the Fail-Safe

6.1 Introduction

In this chapter the expected failure loads are calculated and used as a basis for recommending settings for the fail-safe mechanism. A number of factors were identified in chapters four and five which might be expected to affect the failure load: the level of amputation, the bone diameter, bone-implant contact length and the quality of the bone. The settings for the fail-safe mechanism reflect the increased risk associated with each of the variables studied.

6.2 Failure Criteria for Bone and the Bone-Implant Interface

There are three predictors of bone failure, and they are summarised in table 6.1. Locations of failure are shown in figure 6.1.

Mode of failure and reason for using	Governing stresses	Method of calculating failure load
1. Shear failure of interface. Reason: Bone-implant interface is weaker than the surrounding bone for shear/torsional loading	Shear strength of interface (axial/tangential shear stress and radial/tangential shear stress)	Shear strength of HA-implant interface is 35MPa Shear strength of HA-bone interface is 20MPa after 21 weeks implantation but MAY reduce after first loading exercises (Shao *et al.*, 2007). Therefore strength of bone-HA interface governs failure.
2. Material failure of bone due to stress concentration near the end of the bone and implant tip. Reason: High stress at ends were recorded in chapter 4.	Composite material failure criterion taking into account stresses in all directions	Criterion used is Tsai-Wu for composite materials Bone strength exceeded when criterion = 1
3. Material failure of bone in the rest of the femur. Reason: Loads experienced by femur are unlike those in normal femur, as found in chapter 2.	Composite material failure criterion taking into account stresses in all directions	Criterion used is Tsai-Wu for composite materials Bone strength exceeded when criterion = 1

Table 6.1 Modes of possible bone failure due to loading of intramedullary implant in femur and methods of calculating the failure load.

6.3 Failure Analysis of the Anatomical FEA Models

The anatomical FEA models were designed to give a prediction for the stress in the implanted bone at different levels of amputation. The stresses in the three possible failure modes described in table 6.1 were examined and the failure load was extrapolated. In chapter five, the models were assumed to be linear, meaning that an increase in load results in a proportionate increase in stress.

Figure 6.1 gives a graphical representation of the failure criteria and locations outlined in table 6.1 for each of the three levels of amputation. The dotted line (in torsion only) shows the shear strength of the bone-implant interface, which is equal to the strength of the bone-implant interface divided by the area of contact. This is not shown in the bending graphs because the shear stress at the interface is relatively small in pure bending. The green and red lines show the value of the Tsai-Wu criterion at the point of maximum stress in the bone at the end of the bone ('distal') and adjacent to the tip of the implant ('proximal'). The blue line indicates the Tsai-Wu criterion for the maximum stress experienced by the bone proximal to the implant. Where the Tsai-Wu criterion lines cross the level '1' the strength of the bone is exceeded and it is predicted to fail.

Over the duration of this project the proposed implant design was changed a number of times with regard to whether or not it would include a collar at the end of the bone. The inclusion of a collar was investigated in section 4.4.4 to calculate the effect of using a collar of different sizes. A collar the diameter of the bone removed the stress concentration at the distal end of the bone completely. It has now been decided by the implant designers that the implants will include a collar so the high stress seen at the end of the bone will not be present, and this should be taken into account when studying the 'distal' failure mode.

In bending, failure is predicted to occur at different places in each of the three models, and there are a number of reasons for this due to the material and geometric properties of the bone. The longest bone is predicted to fail near the tip of the implant, due to the small bone cross-sectional area at this point. With half of the bone resected the femur is predicted to fail proximal to the implant or adjacent to the implant tip because the tip is in a region of reduced bone strength. The shortest model displays a very high stress concentration at the end of the bone because the lever arm of the bending moment is greatest in this model.

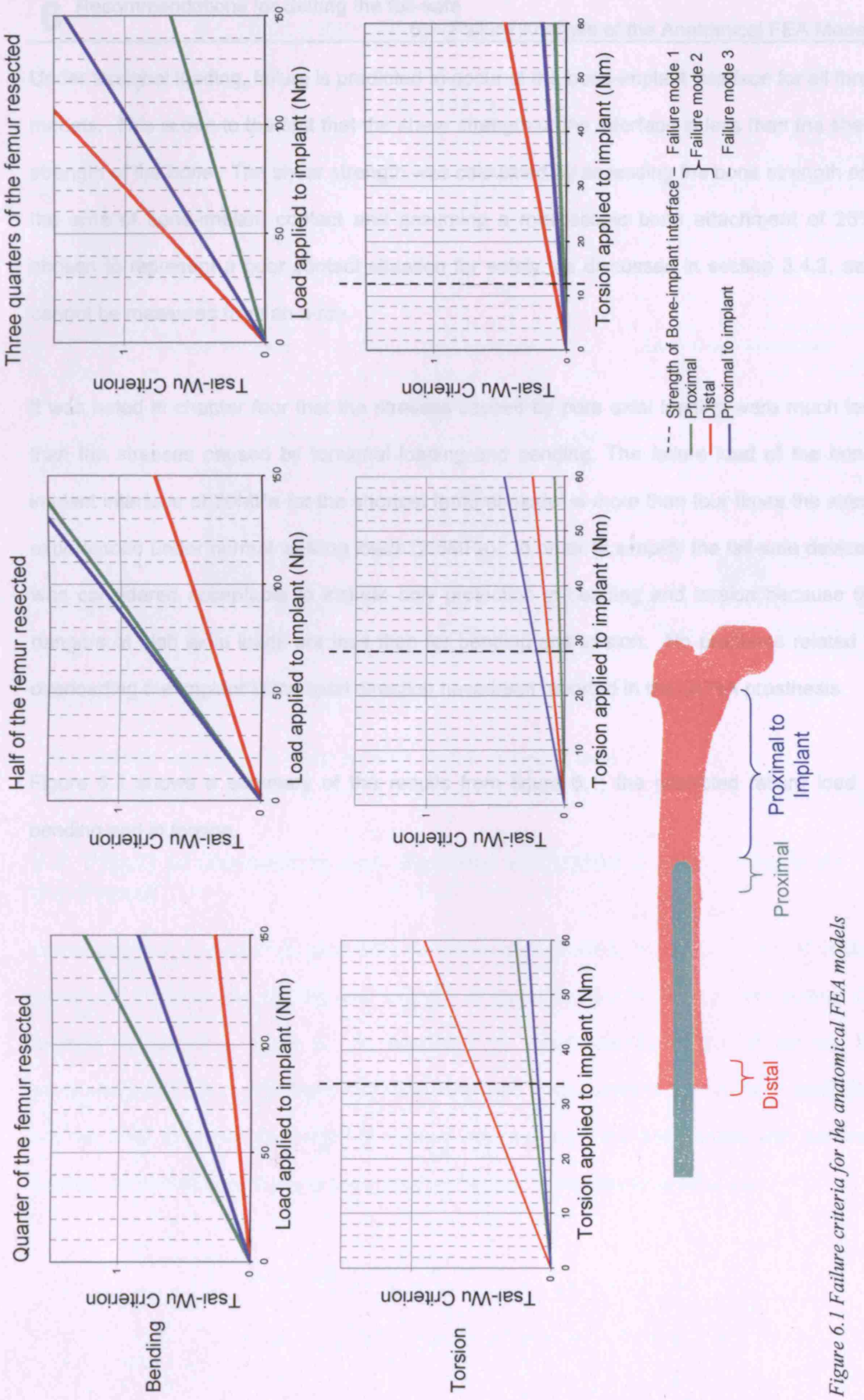

Figure 6.1 Failure criteria for the anatomical FEA models

Under torsional loading, failure is predicted to occur at the bone-implant interface for all three models. This is due to the fact that the shear strength of the interface is less than the shear strength of the bone. The shear strength was calculated by assessing the bone strength and the area of bone-implant contact and assuming a microscopic bone attachment of 25%, chosen to represent a poor contact situation for safety, as discussed in section 3.4.2, as it cannot be measured from an x-ray.

It was noted in chapter four that the stresses caused by pure axial loading were much less than the stresses caused by torsional loading and bending. The failure load of the bone-implant interface of 20MPa for the shortest femoral model is more than four times the stress experienced under normal walking loads (2.5MPa). In order to simplify the fail-safe device it was considered acceptable to include only protection in bending and torsion because the dangers of high axial loads are less than for bending and torsion. No problems related to overloading the implant in the axial direction have been reported in the OPRA prosthesis.

Figure 6.2 shows a summary of the results from figure 6.1; the predicted failure load in bending and in torsion.

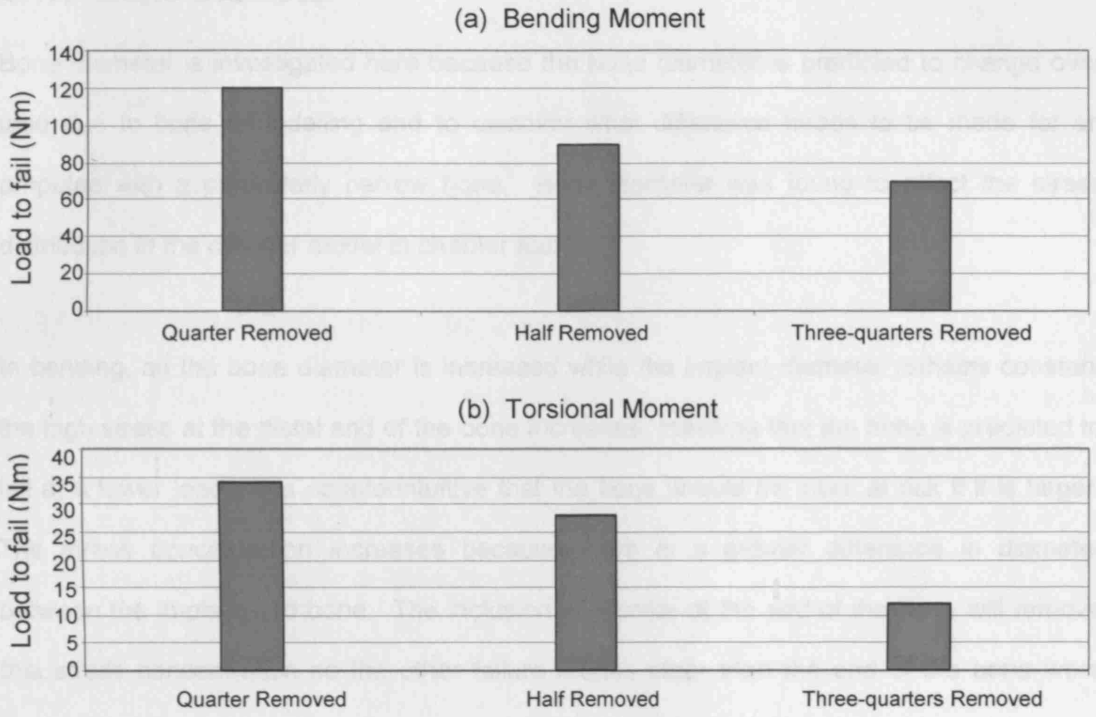

Figure 6.2 Failure loads in bending and torsion for the three levels of bone resection.

The predicted load to fail is lower for each higher resection level.

6.4 Effect of Geometric and Material Variables on the Failure of the Femur

In chapter four a number of geometric variables were studied, but they do not all have a significant effect on the loading and strength of the implanted femur. In this section the method described in figure 6.1 is employed to investigate the effect of varying the parameters that are considered to be most important. The variables that will be investigated are the bone diameter, the length of contact between the bone and implant and the bone quality. All of these calculations are based on the tubular models in chapter four.

6.4.1 Bone Diameter

Bone diameter is investigated here because the bone diameter is predicted to change over time due to bone remodelling and to discover what difference needs to be made for an amputee with a particularly narrow bone. Bone diameter was found to affect the stress distribution in the cylinder model in chapter four.

In bending, as the bone diameter is increased while the implant diameter remains constant the high stress at the distal end of the bone increases, meaning that the bone is predicted to fail at a lower load. It is counterintuitive that the bone should be more at risk if it is larger. The stress concentration increases because there is a greater difference in diameter between the implant and bone. The inclusion of a collar at the end of the bone will remove this stress concentration so the other failure modes other than the end of the bone were considered. The position that governs the failure in bending is the stress concentration at the implant tip. The bending moment predicted to cause failure is displayed in figure 6.3(a).

A similar situation is seen in torsion, where a larger cross sectional area results in a larger stress concentration at the implant tip. The shear strength at the bone-implant interface is used to asses the strength in torsion, which isn't affected by the bone diameter.

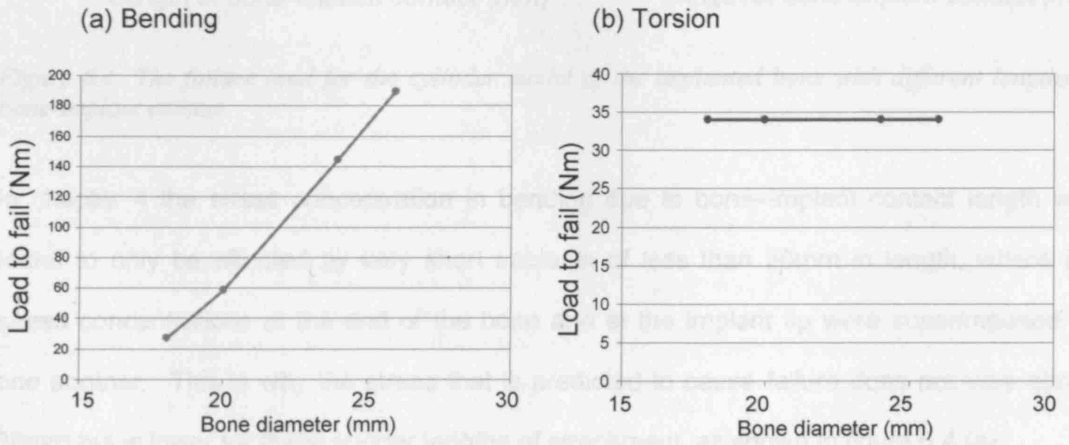

Figure 6.3 Maximum load in the cylinder FEA model with different bone outer diameters (a) in bending, and (b) in torsion

The bone diameter has a great effect on the stress near the implant tip, figure 6.3 (a), the strength of the bone halves with a decrease in diameter of 4mm. The shear stress at the bone-implant interface is not affected by the increase in bone diameter because it is dependent on the implant diameter and length, neither of which is altered here.

6.4.2 Length of Cortical Bone-Prosthesis Attachment

The length of bone attachment to the implant is regarded as an important variable to study because it directly affects the stress at the bone-implant interface and because it is likely to vary between amputees with different resection levels by nature of the bone geometry; it may also inform the choice of implant length.

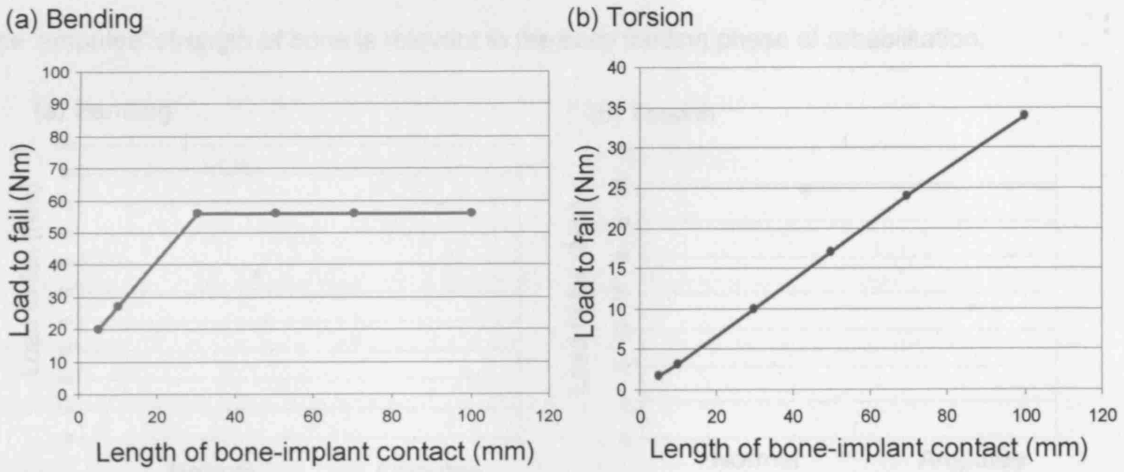

Figure 6.4 The failure load for the cylinder model of the implanted bone with different lengths of bone-implant contact

In chapter 4 the stress concentration in bending due to bone–implant contact length was found to only be affected by very short implants of less than 30mm in length, where the stress concentrations at the end of the bone and at the implant tip were superimposed on one another. This is why the stress that is predicted to cause failure does not vary above 30mm but is lower for these shorter lengths of attachment, as shown in figure 6.4 (a).

The shear stress at the bone implant interface is directly proportional to the area of contact so there is a linear relationship between the failure torsional load and the length of bone-implant contact (figure 6.4(b)).

6.4.3 Bone Quality

Transfemoral amputees who use socket prostheses have lower bone density (Sherk *et al.* 2008) and therefore lower bone strength than non-amputees because the bone is loaded less than normal. In section 4.4.5 this variable was investigated and the results are reproduced in figure 6.5. To produce these results the density of the femur measured in an amputee was converted to Young's Modulus and yield strength using equation 3.5. The cylinder model was run using the 'amputee' bone quality. It is expected that the bone density will increase in an amputee fitted with ITAP due to the loading of the prosthesis so the 'amputee' strength of bone is relevant to the early loading phase of rehabilitation.

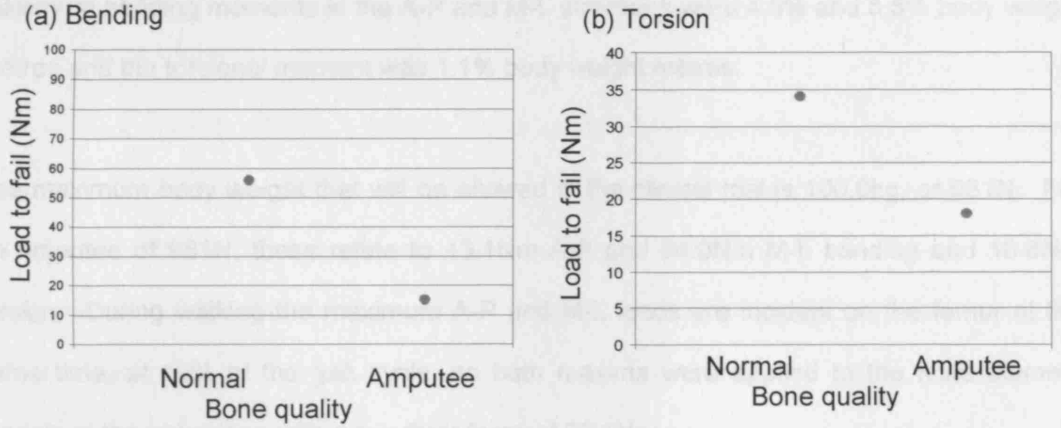

Figure 6.5 Effect of applying osteoporotic bone properties to the bone-implant FEA model

The maximum bending moment allowable for an amputee who has used a socket prosthesis is 28% of the bending moment allowable for the bone of normal strength (figure 6.5(a)). This is governed by failure mode 2, the stress concentration at the implant tip. It is anticipated that the ITAP amputee will develop bone strength similar to that of a normal person through the use of their prosthesis, so in the early loading regime care must be taken not to exceed the maximum moment.

The maximum torsional moment for an osteoporotic amputee is 53% of the maximum load allowable for normal bone. The maximum allowable torque is governed by the shear strength of the bone-implant interface with the model of normal bone strength, but failure of the lower density model is dependent on failure mode 2 because the stress concentrations exceeded the failure criterion in the weaker bone (figure 6.5(b)).

6.5 Normal Loading Expected in the Femur

The normal loading expected was assessed in chapter two and typical daily loads were used as boundary conditions in the finite element models. Lee *et al.* (2007(a) and(b)) used a load cell in series with the OPRA prosthesis to measure the forces and moments. For an amputee carrying out normal activities, including walking and negotiating stairs, the maximum bending moments in the A-P and M-L directions were 4.0% and 5.5% body weight metres and the torsional moment was 1.1% body weight metres.

The maximum body weight that will be allowed in the clinical trial is 100.0kg, or 981N. For an amputee of 981N, these relate to 43.1Nm A-P and 54.0Nm M-L bending and 10.8Nm torsion. During walking the maximum A-P and M-L loads are incident on the femur at the same time, at 10% of the gait cycle, so both maxima were applied to the finite element models at the same time with a resultant force of 69.1Nm.

The average mass of an adult in the United Kingdom is 73.8kg, measured for a Europe-wide study (Haftenberger *et al.*, 2002). The maximum loads in the femur during walking for someone of average mass would be 51.0Nm bending moment and 8.1Nm torsional moment.

Figure 6.6 can be used to find the walking loads for amputees of different mass.

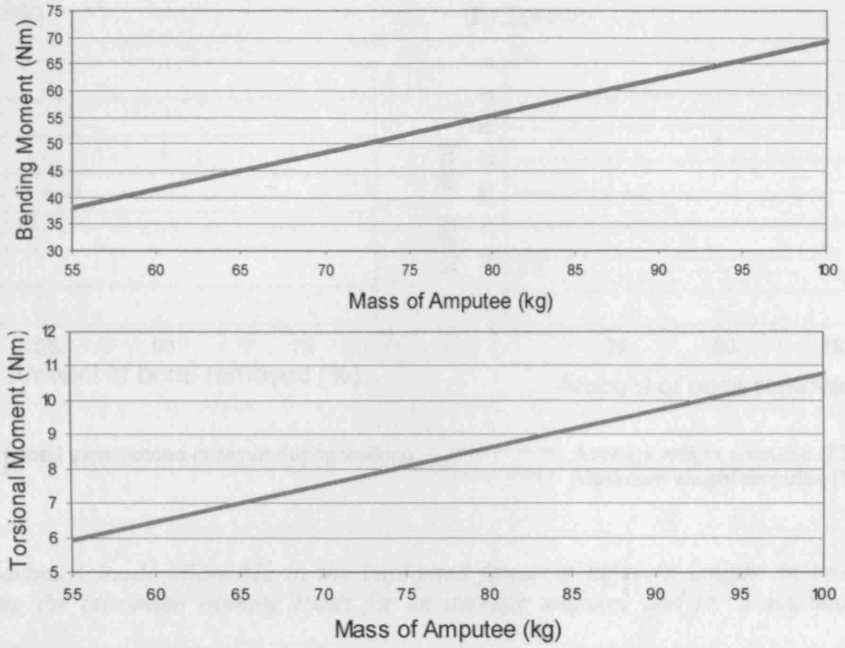

Figure 6.6 maximum bending moment and maximum torsional moment during walking for amputees of 55kg to 100kg data from Lee et al. (2007).

6.6 Discussion

An ideal situation would be to allow for a safety factor of three between the fail-safe activation load and the strength of the bone. This is not possible because the predicted loads from daily use of the prosthesis are relatively high. In this section the failure loads are compared with the normal loading data to give appropriate settings for the fail-safe under different conditions.

6.6.1 Settings for the Fail-Safe for Different Levels of Amputation

In figure 6.7 the values of maximum bending moment and maximum torsion (from figure 6.2) are plotted with the maximum likely load during daily activities (from section 6.5).

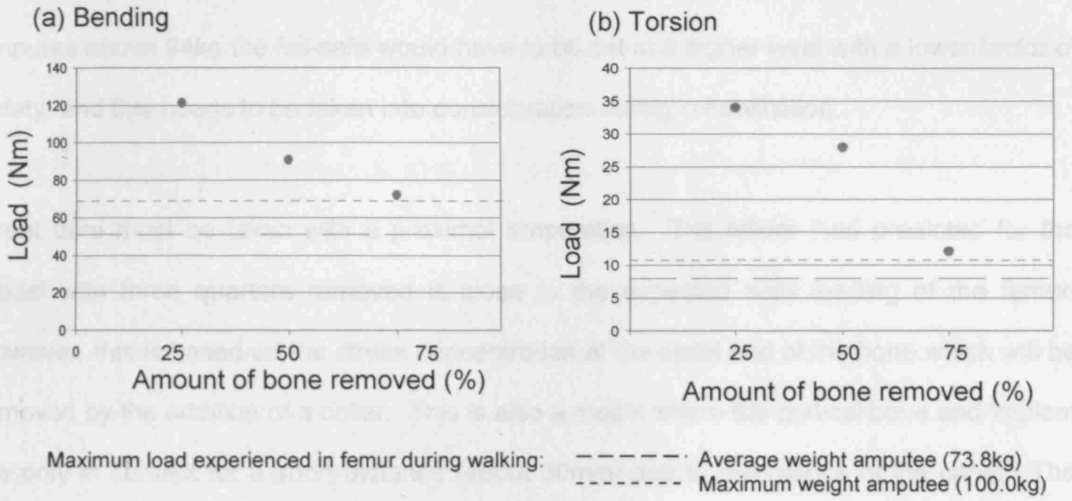

Figure 6.7 Maximum loads allowable in the implanted femur of different lengths in bending and torsion showing the maximum walking loads for an average amputee and for a maximum weight amputee.

The amputees in the OPRA project were given a choice whether or not to have a device to protect the femur in bending and torsion. All of the amputees in the British study decided not to use it because it was set to disengage the prosthesis with a low load and activated readily during exercise. This made them feel unsafe because they did not trust the prosthesis to hold their weight, and they elected to use the prosthesis without the safety device (Sullivan, 2007). With this in mind, the fail-safe should not be set at a level which could make the amputee feel that they cannot trust the prosthesis. However in figure 6.7 the ideal situation of a safety factor of 3 is not achievable because the fail-safe would activate under normal loading, and a safety factor of 2 is only possible for the femur model with one-quarter removed. A safety factor of 1.5 is possible for the bone with one quarter removed and one half removed for an amputee of normal weight. With this safety factor, the fail-safe can be set to 80Nm and 65Nm in bending and 25Nm and 15Nm torsion for a femur with quarter and half removed respectively.

With a heavy amputee the failure load is nearer the expected walking load, and a safety factor of 1.5 is not possible in bending. It can be seen in figure 6.6 that an amputee of over 94kg is likely to generate bending moments of 65Nm during walking. It is appropriate for a

heavier amputee with half of the femur resected to be fitted with an ITAP implant but for an amputee above 94kg the fail-safe would have to be set at a higher level with a lower factor of safety, and this needs to be taken into consideration during rehabilitation.

Great care must be taken with a proximal amputation. The failure load predicted for the model with three quarters removed is close to the expected daily loading of the femur. However, this is based on the stress concentration at the distal end of the bone which will be removed by the addition of a collar. This is also a model where the cortical bone and implant are only in contact for a short distance (about 30mm) due to divergence of the canal. The closeness of the bone strength to the daily loading for this model shows how care must be taken in the choice of implant for proximal amputations. A femur with three quarters removed might be fitted with a different implant, similar to the 'gamma nail' fixation device for fracture distal to the lesser trochanter (shown in figure 6.8) because of the small amount of cortical bone available for fixation and to allow greater torsion. For the reasons mentioned here and also because the cylinder model does not represent the stresses in the highest level of amputation, the geometric and material variables will not be related to the three-quarter level of resection.

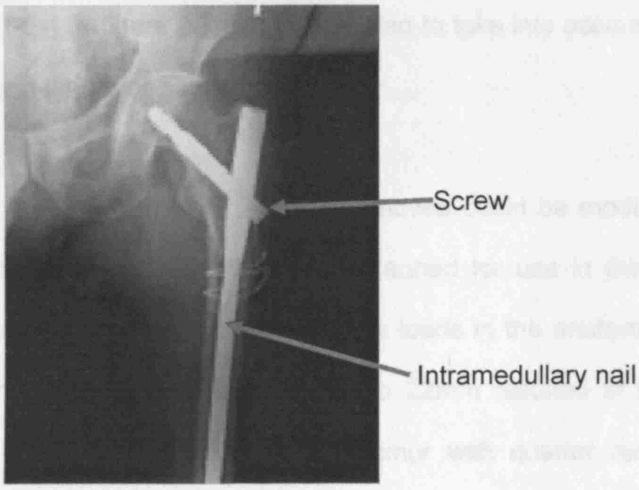

Figure 6.8 'Gamma nail' fixation of subtrochanteric fracture. Adapted from Jiang et al. 2007.

It is recommended that an amputee with an amputation at or above the three-quarters level of resection not be supplied with a straight implant as modelled in this study, but a fixation device such as that pictured in figure 6.8 could be considered to allow the torsion and bending moments to be transferred without endangering the residual femur.

In section 6.3 it was explained that the microscopic contact between the bone and the implant was assumed to be 25%. There is no data available for the amount of bone apposing the implant for an ITAP implant, but data from retrieved hip prostheses have given a range of 31-56% in one study using five prostheses (Tonino et al. 1998) and in another, using 58 hips, 37±2% (Coathup et al. 2000). 25% was chosen because it gives a factor of safety of 1.5 for 37%. The amount of microscopic contact is linearly related to the strength in torsion, so by assuming 50% instead of 25% the predicted failure load would double. However the amount of bone attachment to the implant is unknown, and cannot be measured on a radiograph.

6.6.2 Effect of Changing Bone Diameter on Settings for the Fail-Safe

Based on the results in 6.4.1-6.4.3, figure 6.7 can be modified to take into account the bone diameter, bone-implant contact length and bone quality.

It was found in section 5.3 that the femur with quarter removed could be modelled with a tubular bone with a cylindrical implant. For the femur scanned for use in this study the tubular bone required a diameter of 26mm to represent the loads in the anatomical model. In figure 6.3 a reduction in bone diameter from 26mm to 22mm resulted in halving the strength of the implanted bone. From figure 6.2 the femur with quarter removed can withstand 120Nm bending moment, so by reducing the diameter by 4mm the maximum bending moment is halved to 60Nm. Similarly, by reducing the diameter by 2mm, the strength is reduced by 25% to 90Nm. These results are plotted in figure 6.9.

The femur with half removed could not be accurately represented using a cylindrical model however figure 5.15 shows the results to be similar, and the same method is used for predicting the effect of a reduction in bone diameter on the femur with half removed.

The torsional strength is not altered by the bone diameter because it is dependent on the strength of the bone-implant interface (as shown in figure 6.3 (b)) so only the bending moment is shown in figure 6.9.

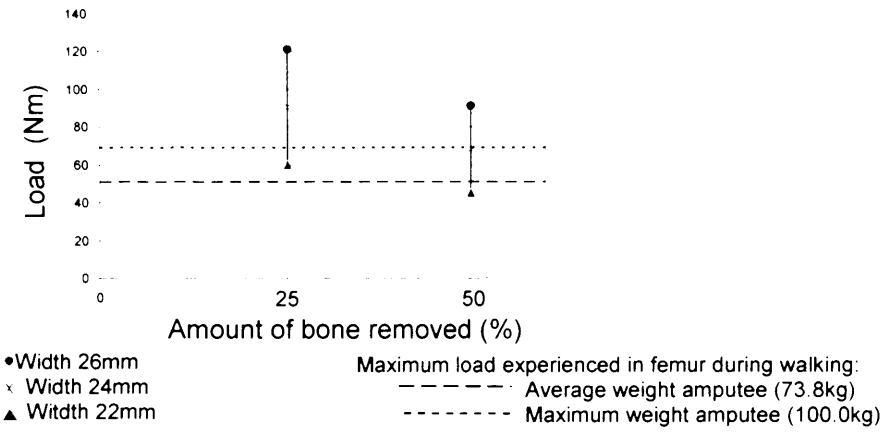

Figure 6.9 Maximum bending in bone for normal bone diameter, diameter reduced by 2mm and diameter reduced by 4mm

Some of these loads are lower than the predicted loads of normal use, marked with the dotted and dashed lines, and a fail-safe device set at these levels might cause the fail-safe to activate during walking or other normal activities. However, it is anticipated that the bone will remodel due to loading and that the shape of the bone will alter to withstand the daily loading. The diameter variable here is to be taken into account during early rehabilitation and the safeguards put in place to protect the smaller bone will no longer be applicable when the bone has substantially changed in shape.

6.6.3 Effect of Changing Bone-Implant Contact Length on Settings for the Fail-Safe

Reducing the length of bone-implant attachment by 50% reduces the torsional strength of the interface by 50% because the strength is proportional to the amount of bone attached. Figure 6.10 shows the reduction in strength of the implanted femur with 75% and 50% bone-implant contact. The bending strength is not affected by the length of contact over 30mm so the bending limit is not required to be altered for shorter lengths of bone attachment.

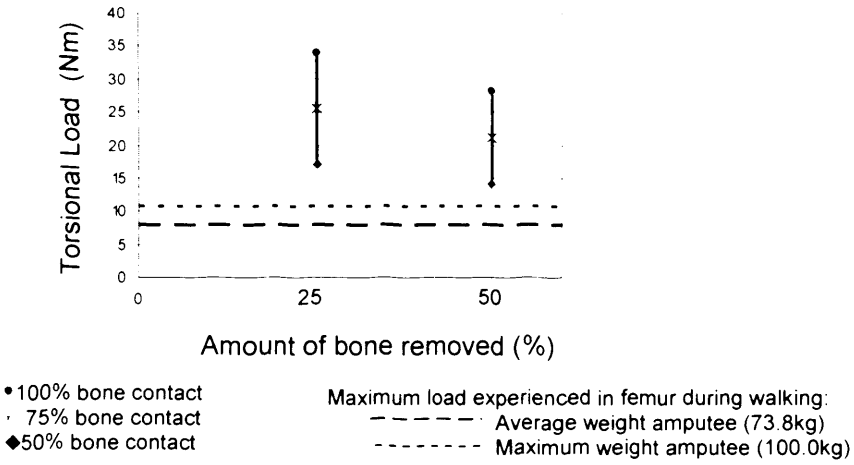

Figure 6.10 Maximum bending in bone for 100% bone contact, 75% contact and 50% bone contact with implant

The torsional strength does not go below the normal loads for walking with a reduction of bone-implant contact length, however for the bone with half removed the strength is close to the walking load for a maximum-weight amputee. The results in figure 6.9 and 6.10 will be discussed further in section 6.6.5.

6.6.4 Effect of Bone Density on Settings for the Fail-Safe

The osteoporotic femur of the transfemoral amputee who has used a socket prosthesis or no prosthesis at all is weaker than normal bone. It is anticipated that the bone will grow stronger, more like a normal femur, after a period of ITAP use. It is important to protect the bone during the early stages of the gradual loading regime until the bone increases in

density. In 6.3.3 the strength of the osteoporotic bone is 28% of the strength of the normal bone in bending and 53% in torsion. The strength of the bone-implant interface also increases with time after implantation. The fail-safe settings calculated in 6.6.1 are used as a basis for defining the initial settings for the fail-safe, and the initial settings are 28% of the bending setting and 53% of the torsional setting. These values are shown in table 6.2.

		Initial settings at commencement of loading (Nm)	Normal bone strength, geometry and 100% contact (Nm)
Bending	Quarter resected	22	80
	Half resected	18	65
Torsion	Quarter resected	13	25
	Half resected	9	18

Table 6.2 Settings for the fail-safe at the beginning and end of the loading regime.

Under normal circumstances the healing time for the bone-implant interface is about twenty weeks (Hing *et al.*, 1997), so the fail-safe settings should be increased over this period of time. The rate of healing of the bone implant interface has been shown in animal studies to be fast at first and to slow down as it reaches the optimum strength, and this pattern can be seen in figure 3.23. For simplicity, a linear increase in setting for the fail-safe will be used because there is no accurate data of the development of the interface in humans. Although some healing will occur before the loading regime begins, there is evidence to suggest that the quality of the interface reduces when the implant is first loaded and then increases in strength again after the first sessions of loading (Shao *et al.*, 2007) so the lowest values should be used until the development of the bone-implant interface is better understood.

6.6.5 Risk Groups

It might be simpler to regard these predicted failure loads in terms of risk: narrow bone or short implant contact length are markers for increased risk, and normal bone diameter and full implant contact would give a lower risk. The progress of the amputee could be checked against these risks by taking a radiograph and their fail-safe would be set according to the current risk factor.

To assign risks to each parameter the failure loads in figures 6.9 and 6.10 were put into groups of similar value and given risk designations. The group was designated low risk if the failure load were more than two times the maximum walking loads for an amputee of average weight, medium risk if the failure load were more than one and a half times the maximum walking loads for an amputee of average weight and high risk if less than one and a half times. The low risk group has a failure bending moment of over 101Nm and torsional strength of 21Nm, the medium risk group has a maximum bending load of over 77Nm and torque of over 16Nm and the high risk group includes bending strength of less than 77Nm and torsional strength of less than 16Nm.

Table 6.3 shows the predicted failure loads for the implanted bone for suggested settings for bones of different diameter and for shorter contact lengths. These data are taken from figures 6.9 and 6.10. The colours indicate the risk group to which each combination of geometric variables belongs: low risk is coloured green, medium risk is amber and high risk is red.

		Normal bone geometry and 100% contact	diameter smaller by 2mm	diameter smaller by 4mm	75% contact	50% contact
Bending	Quarter resected	121	90.75	60.5	121	121
	Half resected	91	68.25	45.5	91	91
Torsion	Quarter resected	34	34	34	25.5	17
	Half resected	28	28	28	21	14

Table 6.3 Failure loads for selected bone sizes and bone-implant contact lengths, the colours indicate the risk group (all values in Nm). Green represents low risk, amber represents medium risk and red represents high risk.

6.6.6 Combination of Risk Markers

It is possible, however, that an amputee may have both a narrow bone and less than 100% bone-implant contact, so a method for finding the risk level must be devised. Each risk marker (for example 75% contact) was given an index from 0 to 4 relating to the effect it has on the failure load for a particular model. The sum of these numbers can be used to allocate risk levels to the combination of features for a bone. These numbers are given in table 6.4.

Level of amputation	Quarter removed	0
	Half removed	2
Bone width	Normal	0
	less 2mm	2
	less 4mm	4
Bone-implant contact length	100%	0
	75%	1
	50%	3

Table 6.4 Risk indices for the geometric variables for allocating risk group

If the sum of the risk indices is 0 or 1 a low risk factor is allocated, a sum of 2 or 3 is medium risk and a sum of 4 or higher gives a high risk; for example, a bone with half removed (index 2), of normal thickness (index 0) and 75% contact (index 1) belongs to the medium risk category, with a sum of 3. The risk factors for the combinations of risk markers can be combined in graphical form, and are shown in figure 6.11.

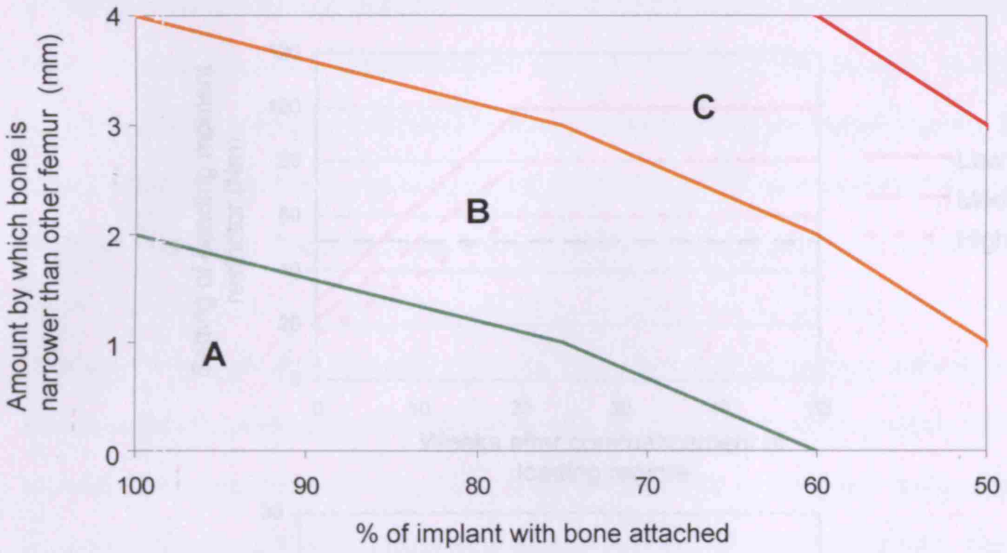

Quarter of femur resected: A = risk 0-1 = low risk
B = risk 2-3 = medium risk
C = risk 4-6 = high risk

Half of femur resected: A = risk 2-3 = medium risk
B = risk 4-6 = high risk
C = risk >6 = high risk

Figure 6.11 Chart for finding the risk group of an amputee depending on the level of amputation, thickness of the femoral shaft and length of bone-implant contact.

6.6.7 Recommended Settings for the Fail-Safe

Figure 6.12 shows the settings suggested for the fail-safe device in bending and torsion for the three different risk groups over time using a safety factor of 1.5 for each group. The black dashed line represents the maximum walking load for an amputee of average weight.

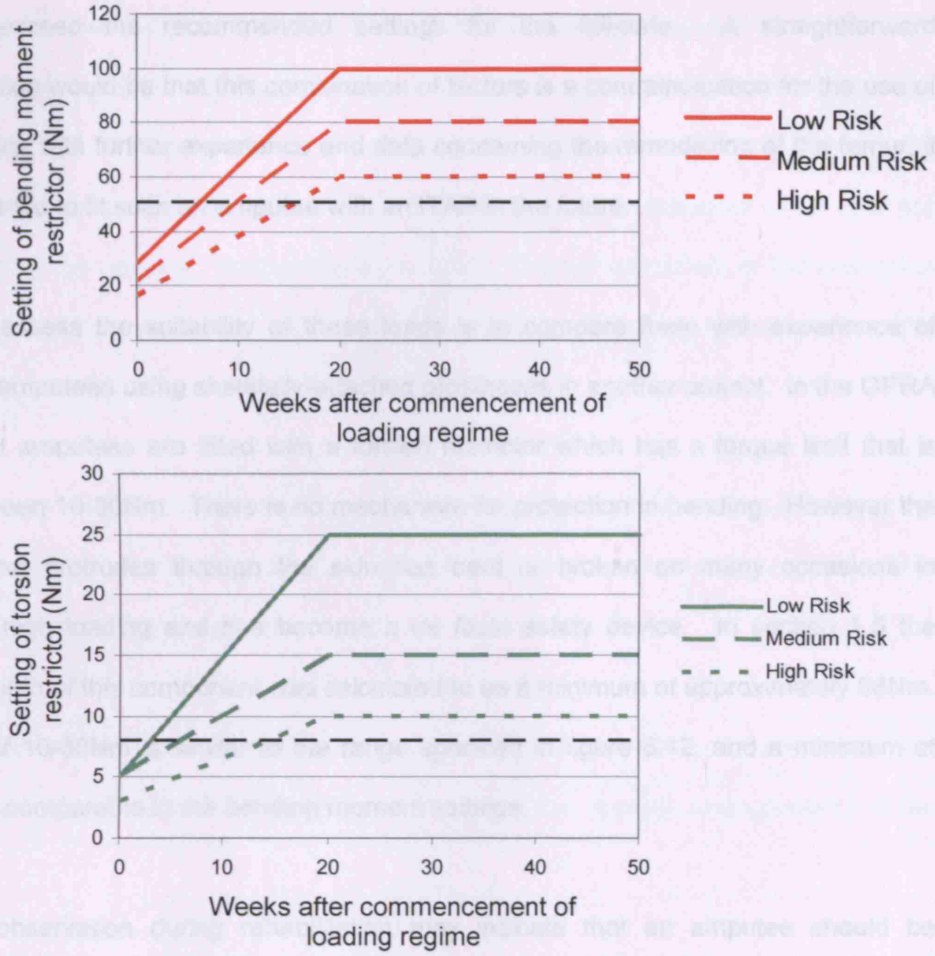

Figure 6.12 Settings for bending moment restrictor and torsion restrictor from the beginning of the implant loading regime.

The activation load of the fail-safe mechanism is low to begin with to protect the developing bone-implant interface and the osteoporotic bone, and is to be increased during rehabilitation.

The dotted line shows the maximum walking loads for an amputee of average weight (figure 6.6 can be used to find the walking loads for a particular amputee of different weight). When the fail-safe setting crosses this line it may be possible for them to apply their full weight to the prosthesis, and this can be used as a guideline for the rehabilitation supervisor in devising the exercise regime.

An amputee over 94kg who is in the 'high risk' group is expected to generate moments in the femur that exceed the recommended settings for the fail-safe. A straightforward recommendation would be that this combination of factors is a contraindication for the use of ITAP. However with further experience and data concerning the remodelling of the femur, it might be possible to fit such an amputee with an ITAP in the future.

One way to assess the suitability of these loads is to compare them with experience of transfemoral amputees using skeletally-attached prostheses in another project. In the OPRA technique the amputees are fitted with a torsion restrictor which has a torque limit that is variable between 10-30Nm. There is no mechanism for protection in bending. However the 'abutment' that protrudes through the skin has bent or broken on many occasions in response to high loading and has become a *de facto* safety device. In section 1.5 the bending strength of this component was calculated to be a minimum of approximately 58Nm. The torque of 10-30Nm is similar to the range specified in figure 6.12, and a minimum of 58Nm is also comparable to the bending moment settings.

Radiograph observation during rehabilitation may indicate that an amputee should be allocated a different risk factor. This should be monitored, and the fail-safe should be adjusted to match the amputee's current risk factor.

6.7 Conclusions

Settings have been recommended for a fail-safe mechanism to be situated distal to the residual limb of an ITAP patient using three risk groups that take into account the amount of bone removed, the thickness of the femoral shaft and the amount of bone in contact with the implant. It is recommended that the fail-safe settings be low to begin with and be increased over time to protect the developing bone-implant interface.

The settings have been devised using cautious values for bone strength, and higher values might need to be used, especially as the bone remodels and the amputee becomes more active, to prevent activation during weight bearing. Factors that affect the strength of the implanted bone that are not measurable in standard clinical practice such as bone density and amount of microscopic attachment to the implant have been assumed to be of a low value in devising the settings. If accurate bone density can be measured, or the amount of bone in contact with the implant at a microscopic level more accurately estimated, then the settings for the fail-safe can be adjusted accordingly.

An amputee over 94kg that falls in the 'high risk category might require the fail-safe to be set at loads lower than those experienced during normal activities, and so should not, at this time, be fitted with an ITAP prosthesis.

It is not recommended that an amputee with three quarters or more of the bone removed use a straight implant as modelled in this project because of the strength and geometry of the bone.

7 Design and Testing of a Fail-Safe Mechanism to Protect the Femur

7.1 Introduction

In the previous chapters it has been established that the femur securing the ITAP prosthetic system is at risk of breaking under loads associated with falling and traffic accidents, and that the strength of the interface between the bone and implant increases as the patient rehabilitates. There is therefore a need for some kind of protection for the bone which can be adjusted during the rehabilitation programme. This chapter documents the process carried out to design, fabricate, and test a fail-safe mechanism to be part of the prosthetic componentry.

This chapter includes the research that went into the design and a list of requirements for the device followed by a description of the design process. The device was then tested to ensure it functioned correctly and was further tested to the relevant British and International Standards. During the tests improvements were necessary to ensure that the device complied with the standards, and these are also explained.

Figure 7.1 shows the design process that was used to create the fail-safe component. The italicised numbers show the relevant sections in this chapter.

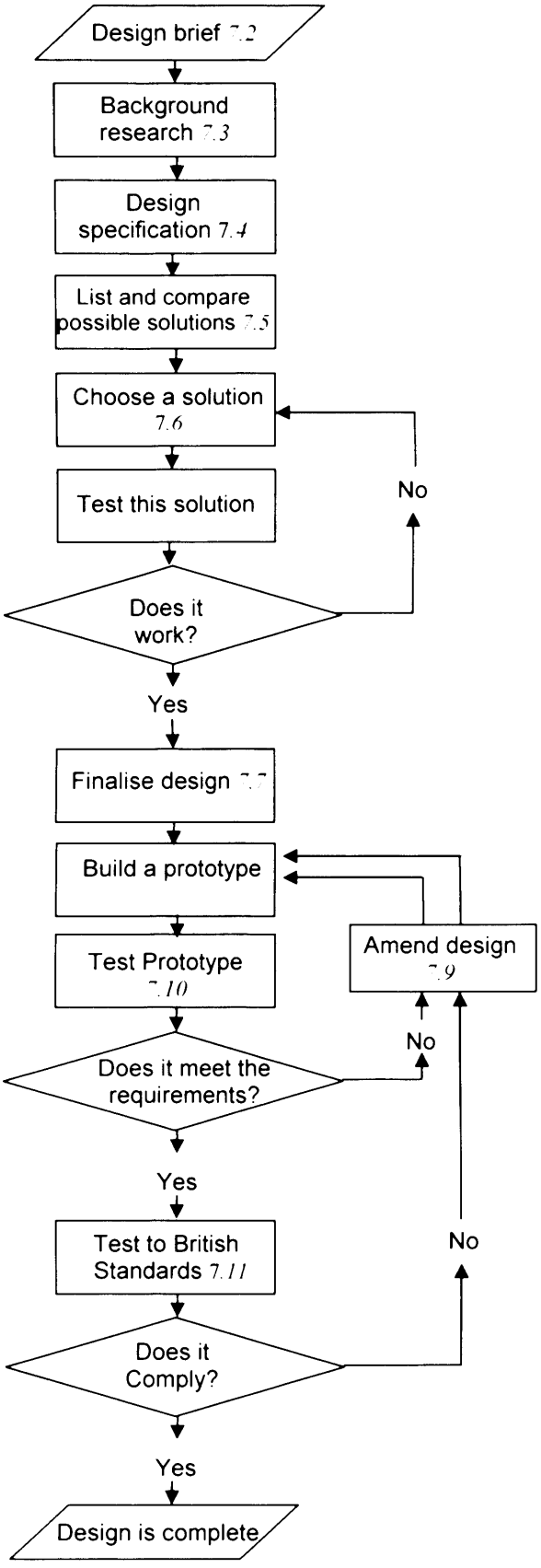

Table 7.1 A flow chart of steps carried out to design a fail-safe device to protect the femur. The numbers in italics refer to the section of this chapter in which each step is documented.

7.2 Design Brief

The design brief is a statement that describes requirements of the design. The designer must refer to it continually during the design process to ensure that the purpose of the project is being addressed by the design.

> "Design a structural component for the prosthetic leg that prevents potentially damaging loads being experienced by the femur when attached to an ITAP prosthesis."

In section 7.4 more detailed requirements of the design are listed after background research is carried out in section 7.3.

7.3 Background Research

The research that went into the design includes an investigation of the behaviour of an implanted bone and the loading of the prosthesis (chapters 2-6 of this document), discussions with rehabilitation professionals who are involved in the ITAP project, and research of the relevant International Standards for safety.

7.3.1 Load Levels

In the previous chapters, calculations of stress levels and computer models were used to find the magnitude and direction of applied forces that (a) should be allowed and (b) must be prevented by the fail-safe. Recommendations were made in figure 6.12 for the settings of the fail-safe. These ranged in value between 18 and 100Nm in bending and between 4 and 25Nm in torsion.

7.3.2 Variation of Activation Loads

One projected benefit of the ITAP over the OPRA system is that the rehabilitation time will be shorter. This means that the amputee will be wearing the prosthesis sooner than the eighteen months currently prescribed for OPRA. The load sustainable by the implant and bone will increase during the time after implantation. Firstly the bone will grow onto the implant and the pull-out force of the implant will increase. It is anticipated from the literature that it will take about twenty-one weeks for the shear strength of the interface to reach its maximum value (Cook *et al.* 1986). When the implant is loaded the surrounding bone will gradually remodel, resorbing in places, and increasing in density, strength and volume in others.

If the interface is disturbed the healing may be jeopardised, or soft tissue may grow between the implant and bone, causing loosening and preventing a rigid interface for transmitting loads to the femur. It is therefore proposed that the loading at which the fail-safe is to trigger should be variable. In discussion with other members of the ITAP team it has been decided that the rehabilitation supervisor should be able to vary the activation load during out-patient appointments. It has also been decided that the amputee should not be able to change the activation loads easily, so that the rehabilitation can be monitored.

It was advised by a consultant in rehabilitation medicine that the fail-safe should be easily removable from the prosthesis or be able to be locked to make it a purely structural component to give the greatest flexibility during trials.

7.3.3 Position of the Fail-Safe on the Prosthesis

The fail-safe device must be distal to the level of the skin because the skin attachment to the implant must not be disturbed. The most proximal component of a transfemoral leg prosthesis is the knee mechanism. A number of different knee mechanisms are in use by

amputees: there are simple mechanisms that lock when standing and flex to sit, but this type is unlikely to be used by amputees chosen for clinical trials of ITAP; the most common type of knee mechanism in the UK flexes during the swing phase of gait and locks using a friction-drum when load is applied to it; some amputees use a knee with an electronic chip to regulate the rate of extension during walking, such as the *C Leg* made by Otto Bock GmbH. The two later types of knee allow flexion during gait and may affect the way in which loads are transferred to the bone because they are able to flex, so a mechanism that is placed proximal to the knee will be more effective.

It was also considered to be important to situate the fail-safe device as near to the bone as possible. It is proposed that the fail-safe be situated above the knee mechanism and incorporate the facility to don and doff the prosthesis.

7.3.4 Size

The fail-safe will be between the knee and the stump in the 'thigh' region of the prosthesis. In order to fit between the knee and the stump it must not be too long if amputees with longer stumps are not to be prevented from using the ITAP technique. It is therefore important to make the mechanism as short as possible.

A prosthesis is usually covered by a cosmesis which is a non-structural foam covering for the structural components with an outer shape which is carved to resemble the other leg. The thigh region, being naturally bulky with muscle, is usually quite large in cross-section, so the cross-sectional size of the mechanism is less restricted than the length.

7.3.5 International Standards

Section 4.4.1 of ISO 22523:2006, 'External limb prostheses and external orthoses – requirements and test methods', states that a lower limb prosthetic device "shall have the

strength to sustain the loads occurring during use by amputees [...] in the manner intended by the manufacturer for that device according to his written instructions on its intended use". In order to assess the conformity of a structure to this requirement, BS EN ISO 10328:2006, 'Structural testing of lower limb prostheses – requirements and test methods', provides methods for determining the strength in fatigue and under an occasional severe event.

BS EN ISO 10328 was developed after a number of meetings organised by the International Society for Prosthetics and Orthotics in the nineteen seventies. The aim was to give manufacturers "confidence in designing [prosthetic components] secure in the knowledge that the prosthesis will be durable and, more important, that the patient will not be exposed to dangerous failures" (McKenzie, 1977). A consensus was reached in 1977 and a draft specification for structural testing was submitted to the International Standards Organisation (ISO). It is important that this consensus be respected and that new prosthetic components are designed to conform to the standards of safety set by the ISO. The structural tests required are under both static and cyclic loads to represent the repetitive loading of walking and the high loads caused by a single event.

The purpose of the fail-safe mechanism is to prevent the forces and moments that pose a risk being transferred to the femoral bone. At lower loads the fail-safe mechanism is to function as a structural component of the prosthesis, and must conform to the International Standard, as would any other structural component.

7.4 Design Specification

In section 7.3 a number of features of the device to be developed were discussed. The following is a summary of the factors important in the design of a fail-safe device. The requirements listed here are important factors to be considered throughout the design process.

7.4.1 Performance

The device must:

- protect the body from damaging forces and moments,
- act as a rigid structural component below the level of activation,
- have a variable activation load between 18Nm and 100Nm in bending and between 4Nm and 25Nm in torsion,
- have a mechanism that can be fully locked, if required during rehabilitation, so it does not have to be removed,
- not endanger the wearer when activated,
- be re-settable after activation.

7.4.2 Maintenance

The device will be maintained by the prosthetist. Any part of the device that is adjustable is to be operated in outpatient appointments with the prosthetist.

7.4.3 Materials

The materials should not be corrosive or likely to cause an allergic reaction.

7.4.4 Size

The device needs to be small enough to fit on the prosthetic leg between the stump and the knee mechanism, and to allow for various different levels of bone resection.

7.4.5 Standards

The standard ISO 22523:2006, 'External limb prostheses and external orthoses – requirements and test methods' states that a partial structure of a prosthetic leg should be tested to BS EN ISO 10328:2006, 'Structural testing of lower limb prostheses – requirements and test methods'.

7.4.6 Testing

The device should be tested to ensure it meets the requirements in 7.4.1 and 7.4.5.

7.4.7 Service Life

The Standards specify that the device should be tested for a service life of two years.

7.4.8 Safety

The device should be able to pass the requirements for CE marking.

7.4.9 Quantity

During the first stage of the clinical trial fewer than twenty devices are required. The design should take the quantity requirement into account.

7.5 Alternative Solutions to Fulfil Design Specifications

There are two methods by which a fail-safe can prevent application of an excessive load to the bone: (a) to disengage the implant from the prosthesis, or (b) to allow the prosthesis to swing or turn in the direction of the applied load, dissipating the energy of the blow through the heat of friction or deformation of a material.

If the prosthesis were allowed to disengage from the implant (option a, above) this could place the amputee in a hazardous situation by removing the support of the prosthesis and causing them to fall. Therefore the method of protection that was chosen was option (b), the deformation of the fail-safe component to dissipate the energy and remove the ITAP from the source of impact. To fulfil this design the device should comprise an attachment to the part of the ITAP implant that protrudes through the skin, an attachment to the prosthetic leg, and a coupling mechanism that articulates when the load is dangerous to the implanted bone. A number of possible mechanisms for activation were considered after brainstorming and some are represented in the sketches in figure 7.1.

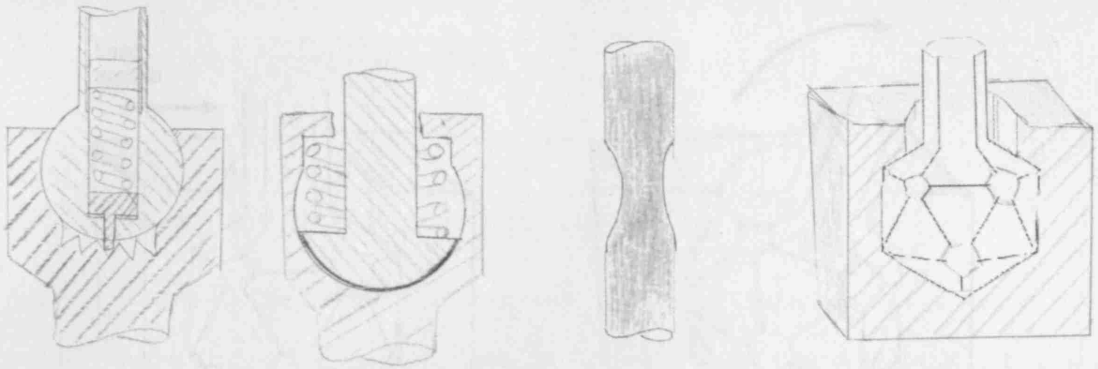

(a) Spring-plunger (b) friction clutch (c) bar of material that bends (d) resistance material

Figure 7.1 Sketches of possible solutions to remove the load from the femur.

7.6 Testing the Design Principle

The options outlined in figure 7.1 were considered and 7.6.1 and 7.6.2 outline two mechanisms that were tested. These are options (a) and (d) in figure 7.1. Options (b) and (c) were not chosen because it was considered to be too difficult to comply with the specification to allow a different activation load in bending and torsion.

7.6.1 Resistive Material

The first concept to be chosen was a shaped bar housed in a cavity in a block of a different material, (d) in figure 7.1. The material of the second part would have a lower Young's Modulus than the first material and the device would be activated when the softer material deformed to allow the bar to turn. For example, the bar in figure 7.2 has a bending force applied to it and, at a point dictated by the cup material, the bar rotates thirty degrees.

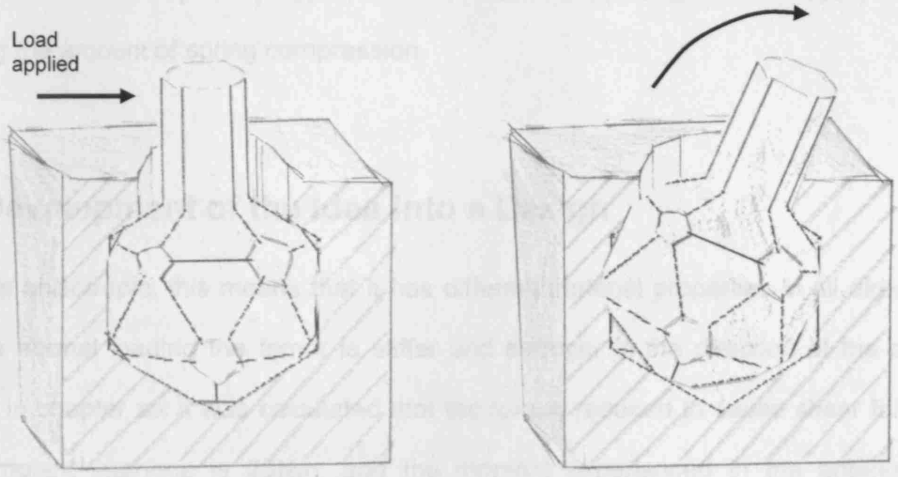

Figure 7.2 Sketch of the resistance material idea. The right-hand image shows how the icosahedron turns in the cup of resistance material.

This idea was tested with a number of different materials. An octagonal bar was sandwiched between two blocks of a softer material in a materials testing machine and the torsional moment was gradually increased until the bar moved. There was a wide variation in the load required to turn the bar. After trying both metallic and polymeric materials with different surface finishes, all giving variable results, the decision was made not to continue with this principle and to choose another method of disengagement.

7.6.2 Spring Plunger

The second idea pursued was the spring plunger (a) in figure 7.1. To test this idea a cylindrical plunger was abutted into a conical indentation by a spring. The load required to slide the plunger out of the indent was measured using the materials testing machine and the same method was used test the concept as before.

The results of this test were much more reliable, and this method was chosen for the fail-safe device. The spring plunger idea is consistent with the design requirements set out in

section 7.4 and is especially appropriate because the activation load is easily adjusted by varying the amount of spring compression.

7.7 Development of the Idea into a Design

Bone is anisotropic, this means that it has different material properties in all directions. To sustain normal loading the femur is stiffer and stronger in the direction of the axis of the bone. In chapter six it was calculated that the torque required to cause shear failure at the bone-implant interface is 25Nm, and the moment experienced in the anterior-posterior direction by the femur during walking for a person of average weight is about 51Nm. If a fail-safe mechanism were designed to activate below 25Nm, to protect the femur in torsion, it would activate during walking in the anterior-posterior direction. For this reason it was decided to control the activation load for the bending and torsion load separately and with different mechanisms.

It was decided in section 7.5 that to reduce the risk of injury to the patient by losing balance the device should not allow the prosthesis to disengage completely from the implant. There must, therefore, be a method of allowing the prosthesis to swing or turn out of the way of a moment or force while allowing the amputee to bear at least some weight on the prosthesis.

7.7.1 Mechanism for Protection in Bending

The mechanism must be rigid in torsion so that protection from excessive torque can be provided by a different mechanism. A method of providing rigidity in torsion is to use the gimbal concept in the form of a 'universal joint', pictured in figure 7.3. A universal joint is used to allow a shaft to transmit a torque around a corner. This concept was considered to be a good way of enabling the fail-safe to flex in bending and still allow the torque to be governed by a separate mechanism.

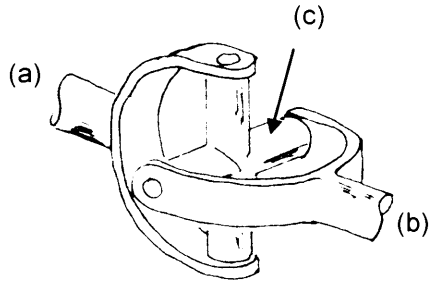

Figure 7.3 A universal joint.

A number of ways of fitting the spring-plunger idea in with the universal joint were considered but each seemed flimsy and unlikely to sustain the loading of a prosthetic leg; observe the narrow hinges in figure 7.3 that are required to allow the two shafts (a) and (b) to rotate independently of component (c).

The action of each of the two parts of the shaft (a) and (b) in the universal joint is to describe an arc at ninety degrees to the other which, combined, allow motion around any arc on a sphere. This action is preserved if component (b) is rotated 180 degrees about its hinges to be coincident with component (a). Figure 7.4 shows the way that the shaft components were configured to describe arcs perpendicular to each other, with two sliders that move in directions indicated by A, P, M and L.

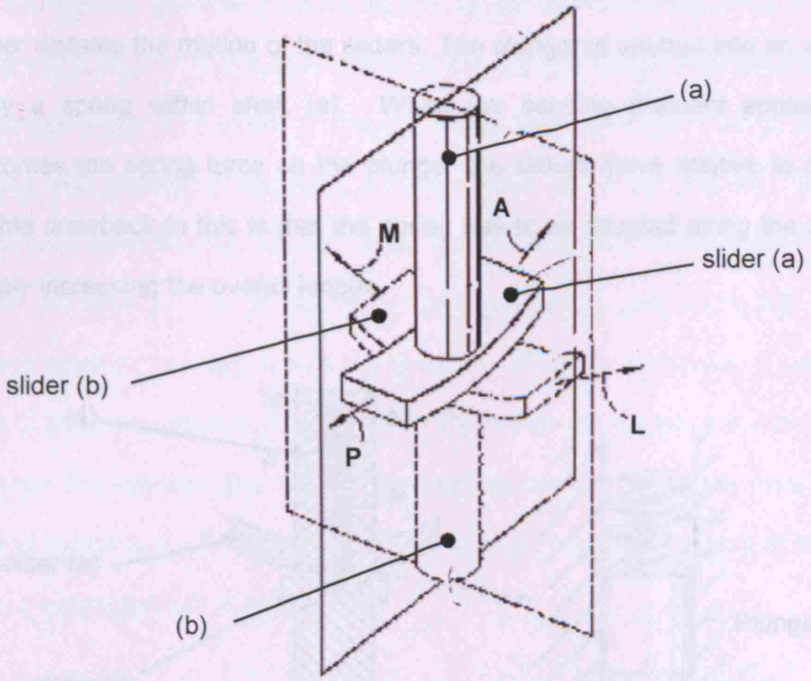

Figure 7.4 Configuration of the shafts with perpendicular sliders. Adapted from patent WO 0405530.7

Slider (a) is attached to the proximal part of the mechanism and slider (b) is attached to the distal part of the mechanism. To allow the plates to slide in this way they are sandwiched between three bearing plates made of nylon containing a solid lubricant. The bearing plates are machined to the dimensions of the sliders to prevent rotational movement between them. Figure 7.5 shows the sliders moving within the bearing plates which are red in colour. The sliders and bearings were kept together within a cage with gaps to allow the sliders to move.

In neutral position slider (a) activated slider (b) activated

Figure 7.5 Sliders and bearing rings before and after activation

Figure 7.6 is from the patent that was granted for the design and shows how the spring plunger dictates the motion of the sliders. The plunger is abutted into an indentation in shaft (b) by a spring within shaft (a). When the bending moment applied to either slider overcomes the spring force on the plunger the sliders move relative to one another. One possible drawback to this is that the spring has to be situated along the axis of the device, possibly increasing the overall length.

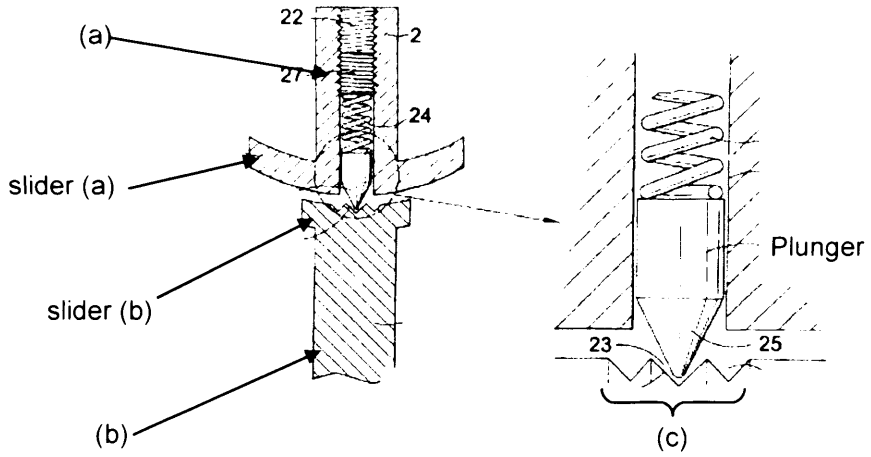

Figure 7.6 A drawing of the way in which the spring plunger prevents and allows motion in the lateral loading restrictor. Adapted from patent WO 0405530.7.

It was planned that there would be a series of grooves (marked (c) in figure 7.6) for the plunger to fall into, so that the fail-safe would allow a small amount of movement and then if the load were still being applied, it would move again. A benefit of having just one indentation instead is that it is easier to find the neutral position to re-set it after activation. With one notch there would be protection from the same level of loading and instead of moving step-by-step it would smoothly slide in the event of activation. The grooves (c) in figure 7.6 were replaced with one indentation.

7.7.2 Mechanism for Protection in Torsion

Torsional loading presents a particular risk for the bone structure and the interface between the bone and implant (Porta et al. 1997) so it is important to restrict the torque. The first idea for a torque limiter was similar to the one tested in section 7.6.2, and is shown in figure 7.7. A spring was situated horizontally abutting a ball into radial grooves. In the event of the torque restrictor activating, the ball would be pushed against the spring until it was allowed to fall into the next groove. If the torque continued to be applied the ball would fall into the following groove. In order to vary the activation torque by compressing the spring there was a hole in the side opposite the grooves. The image on the left is a working sketch used to determine the number and type of bearings required to bear the body weight and allow torsional movement. The drawing on the right is of the outer casing of the device showing the grooves for the ball to abut.

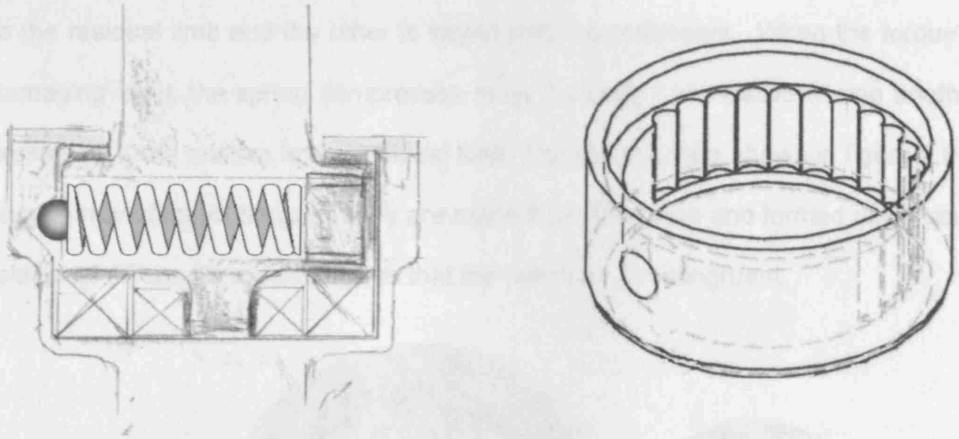

Figure 7.7 Torque restrictor with horizontal spring.

This design was manufactured but there were two main drawbacks to it: the length and diameter of the spring were limited by the total size of the device, and the grooves could not go all the way around, limiting the function to 180 degrees of movement. It was decided to discontinue this idea and devise an alternative design that was more compatible with the bending moment restrictor, was more compact and had greater flexibility for the size of the spring.

A clutch was considered for the torque restrictor, with two roughened surfaces which are pushed together with variable pressure. The torque at which the plates move relative to one another would be governed by the friction between them and the pressure. The idea was modified to make it easier to re-set the torque restrictor after activation by using congruent corrugated plates instead of friction surfaces.

The congruent plates could be in the form of rings with a cavity inside for the spring from the bending restrictor to be situated, therefore saving space and solving the problem stated at the end of section 7.7.1 that a long spring may be required for the bending moment restrictor. It is also possible to situate the springs concentrically, further reducing the length. The torque mechanism consists of two 'slip rings' which are congruent and are pressed together by a spring. One of the slip rings is keyed with the part of the mechanism attached to the residual limb and the other is keyed with the prosthesis. When the torque reaches a damaging level, the spring compresses to let the rings turn relative to one another and the prosthesis turns relative to the residual limb. The slip rings are shown in figure 7.8. They are easy to manufacture because they are made from one piece and formed using spark erosion (electrical discharge machining) so that the two rings are congruent.

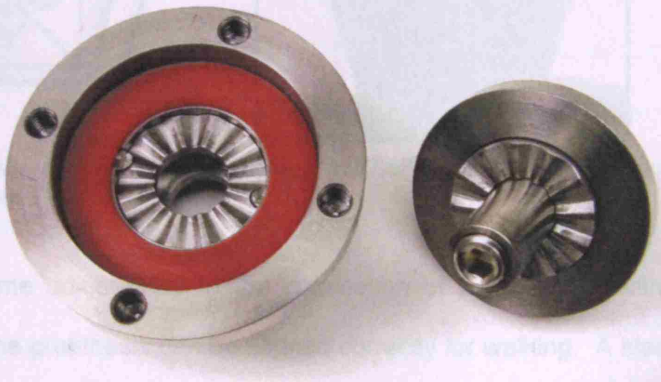

Figure 7.8 Slip rings for torque restrictor inside the fail-safe.

7.7.3 End Attachments

It was decided in section 7.3.4 that the fail-safe mechanism must be as near to the bone as possible and so the means by which the amputee dons and doffs the prosthesis should be integral to the fail-safe mechanism.

A cup was made part of the top slider of the bending moment restrictor to accept the part of the implant protruding from the amputees stump. A slight taper gives a secure feeling to the amputee as soon as they don the prosthesis. The connection is then secured with a grub screw. When this design was manufactured it was discovered that the taper connection was so effective that it prevented removal and another screw was required to aid the disassembly of the connection. A cross-sectional view and an image of the finished design can be seen in figure 7.9.

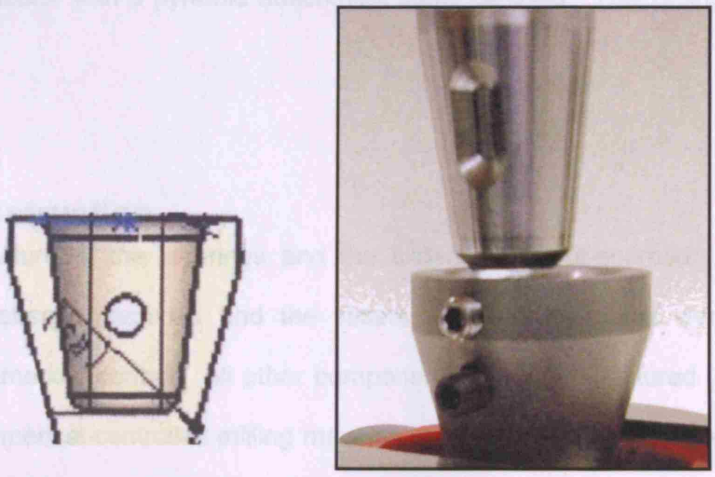

Figure 7.9 A cross-section of the cup for attaching the ITAP implant and an image of the cup and peg attached to the implant.

There must be some adjustability in the connection of the fail-safe with the rest of the prosthesis so that the prosthesis can be aligned correctly for walking. A standard connection between components of a prosthetic leg is the 'pyramid adapter', patented by prosthesis manufacturer Otto Bock GmbH (Patent Number DE1922619, 1969), but widely used and regarded as a standard component. It requires an Allen key to operate and gives ten degrees of angular adjustment in any direction between prosthetic components. Figure 7.10 shows the pyramid adapter and the adjustment available.

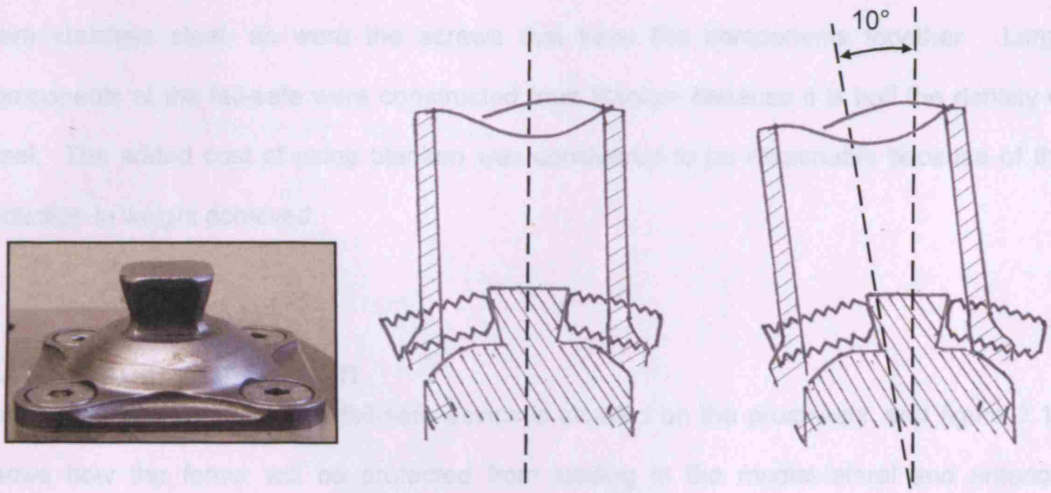

Figure 7.10 Pyramid adapters showing angular adjustment. Adapted from Patent DE1922619

During the testing of the fail-safe the structure of the distal end was cylindrical so that a tubular connector with a pyramid attachment could be used. This is shown, later, in figure 7.24.

7.7.4 Construction

The manufacture of the slip-rings and the sliders were out-sourced: the slip-rings were electrical-discharge-machined and the sliders and bearing plates were machined using computer numerical control. All other components were manufactured using a lathe and a computer-numerical-controlled milling machine in the workshop at the Centre for Biomedical Engineering. All surface finishes were left 'as machined' in the first instance. In future versions of the fail-safe other surface finishes were explored and this is documented in section 7.9.2.

7.7.5 Materials

The design requirements did not specify a particular weight for the component. However it was perceived that the weight should be kept as low as possible to keep the metabolic cost of walking with the prosthesis low. The bearing plates were made from a solid-lubricant-filled

nylon which is 1.1g/cm^3, about seven times lighter than steel (about 7.5g/cm^3). The slip-rigs were stainless steel, as were the screws that keep the components together. Large components of the fail-safe were constructed from titanium because it is half the density of steel. The added cost of using titanium was considered to be reasonable because of the reduction in weight achieved.

7.8 Summary of Design

Figure 7.11 shows where the fail-safe device is situated on the prosthesis, and figure 7.12 shows how the femur will be protected from loading in the medial-lateral and anterior-posterior directions and in torsion.

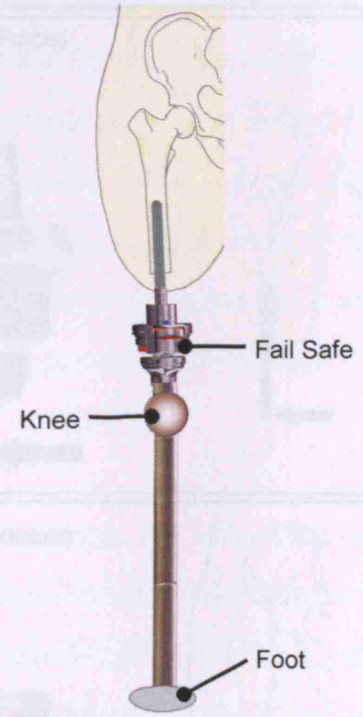

Figure 7.11 Position of fail-safe in the prosthesis.

Figure 7.12 shows how the prosthesis moves in relation to the bone when the fail-safe activates. The bending moment restrictor allows movement in the medial-lateral direction and in the anterior-posterior directions and also any other direction with combined movement

of both of the sliders. In torsion the prosthesis rotates relative to the bone. In figure 7.12 the blue button represents the anterior direction.

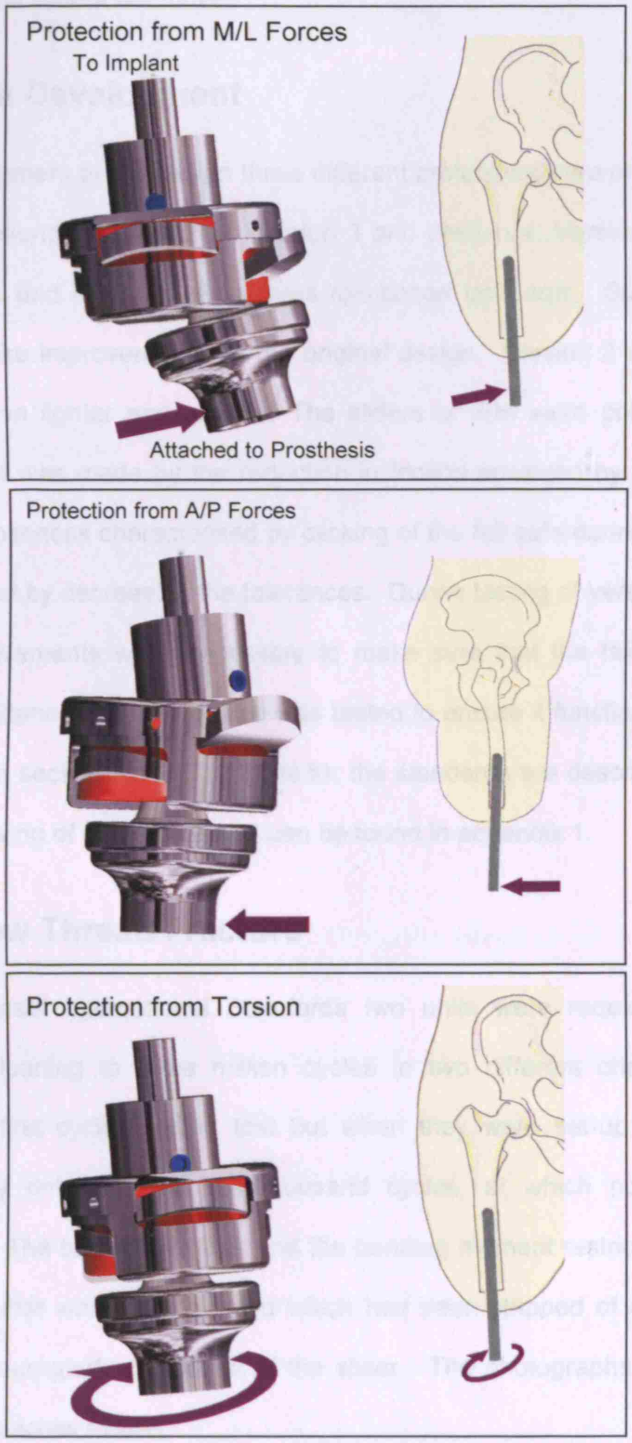

Figure 7.12 Images to explain the action of the fail-safe mechanism.

If the bending load is applied in the anterior-posterior plane only the top slider will activate and in the medial-lateral plane the bottom slider will activate and if the load is applied at any other angle both sliders will move.

7.9 Design Development

During development of the design three different prototypes were created. They were called version 1, versions 2(a) and 2(b), version 3 and version 4. Version 1 is pictured in figures 7.11 and 7.12 and includes all features mentioned until now. Subsequent versions were created to make improvements on the original design. Version 2 was improved by making the construction lighter and smaller. The sliders of 2(b) were polished to investigate the difference that was made by the reduction in friction achieved by polishing. In version 3 a problem of looseness characterised by clicking of the fail-safe during load bearing in version 2 was removed by decreasing the tolerances. During testing of versions 2(a) and 2(b) and 3 various improvements were necessary to make sure that the fail-safe complied with the International Standards. The device was tested to ensure it functioned correctly, and this is documented in section 7.10. The tests for the standards are described in section 7.11. An assembly drawing of the final design can be found in appendix 1.

7.9.1 Screw Thread Fracture

In order to meet International Standards two units were required to be tested under compressive loading to three million cycles in two different orientations. The devices survived the first cyclic loading test but when they were set-up for the second loading condition they only survived ten thousand cycles, at which point one of them failed substantially. The torque restrictor and the bending moment restrictor were connected by a screw thread that was too short and which had been stripped of its threads and also had fractured the surrounding material of the slider. The photographs in figure 7.13 show the damage to the screw thread.

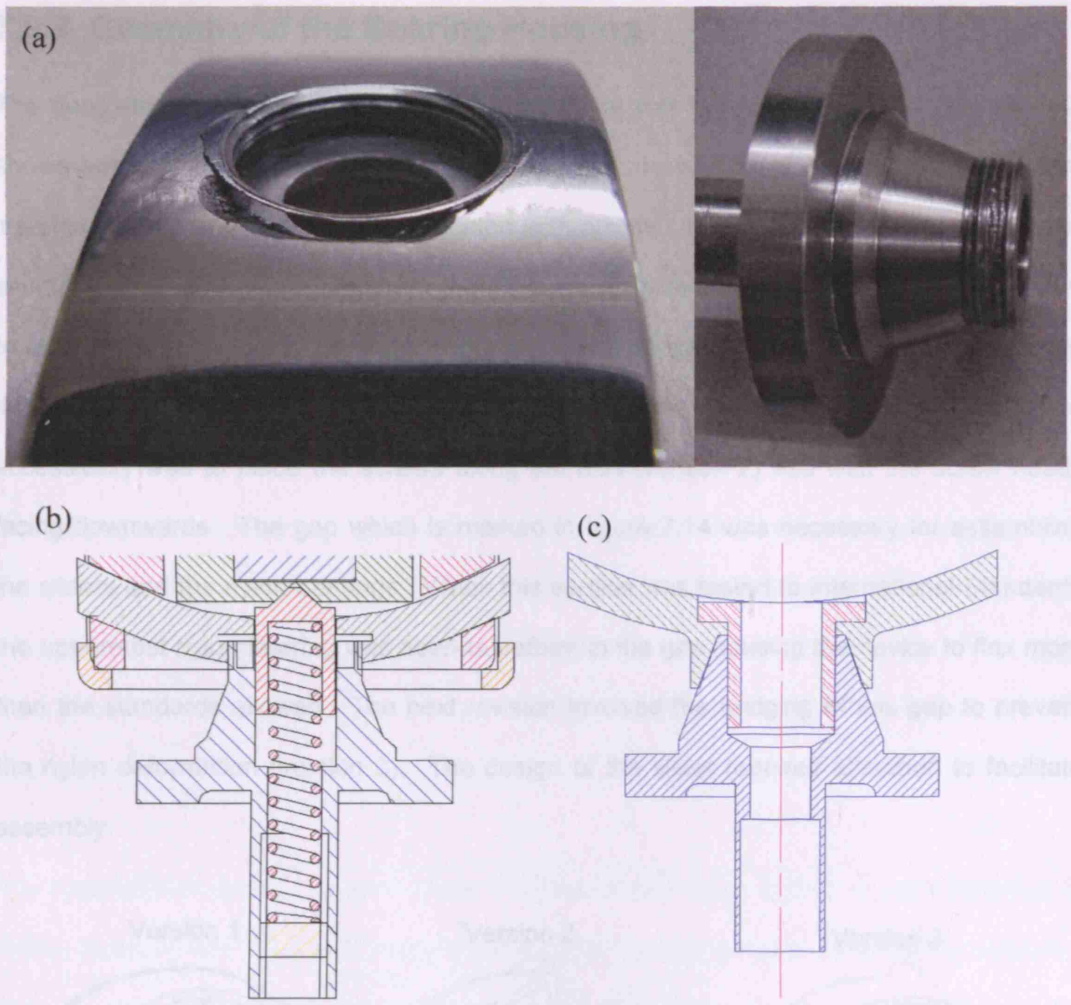

Figure 7.13 (a) Damaged screw thread. (b) Connection design for version 1, 2 and 3 (c) Solution: connection design for version 4 Pink hatching is bolt component

The conclusion was made that the screw thread was too short and a solution was designed that involved the two components being bolted together as opposed to screwed together. In addition to making the connection stronger, it made this part of the device stiffer.

7.9.2 Geometry of the Bearing Housing

The geometry of the housing for the nylon bearings was gradually improved. Figure 7.14 shows some of the versions that were developed. In version, 1 assembly screws were inserted radially from the outside, indicated with arrows. It was suggested that the screws should be less accessible to prevent the amputee disassembling the device. Also, in order to allow the screws to have enough depth the whole component needed to be made larger, this made it quite bulky. The solution to the problems regarding the screw depth and accessibility was to place the screws along the axis (version 2) and with the screw heads facing downwards. The gap which is marked in figure 7.14 was necessary for assembling the sliders and the nylon bearings. When this version was tested to International Standards the uppermost nylon bearing was seen to deform in the gap causing the device to flex more than the standards allowed. The next revision involved the bridging of this gap to prevent the nylon deformation (version 3). The design of the slider required alteration to facilitate assembly.

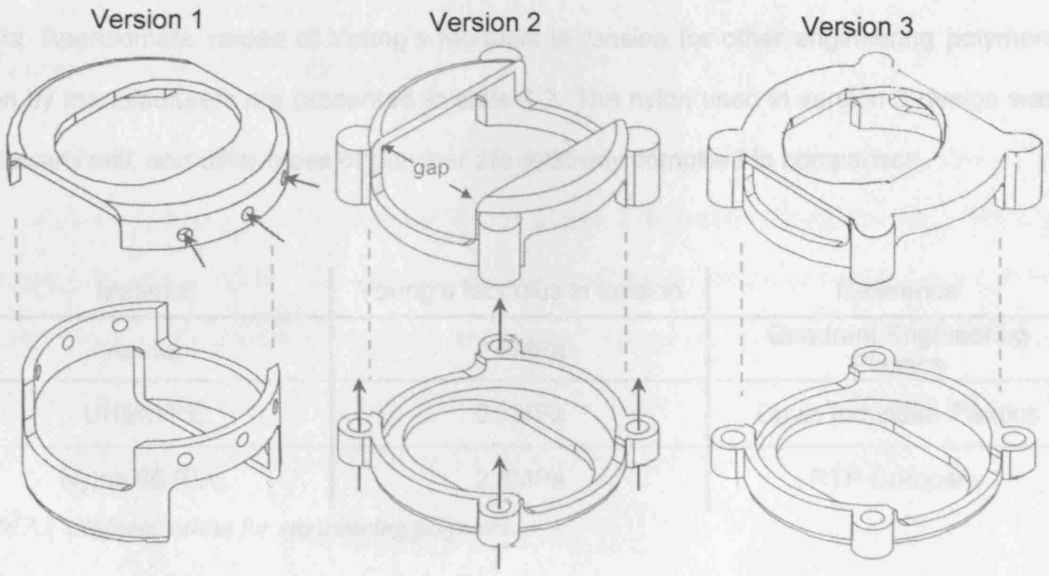

Figure 7.14 Three stages in the design of the bearing housing for prototype versions 1, 2 and 3.

7.9.3 Material of the Bearings

When version 3 was tested the fail-safe device was still flexing more than allowed by the standards and the bottom nylon bearing ring was visibly deforming. Two options that were available were to further improve the rigidity of the housing, as described in 7.9.2, or to make the bearing rings out of a different material. Improving the containment of the housing, as before, would have made only a small difference because the nylon bearing plate was deforming under the load.

The requirements for a new material for the bearing plates were that it must be stiffer than the nylon used in version 3, it must have a low coefficient of friction against titanium, and it should have a low density to keep the weight as low as possible. The strength of the nylon in version 3 was sufficient so the new material for the bearing plates did not need to be any stronger.

The material that used in version 3 was a self-lubricating nylon with a Young's Modulus of 4MPa. Approximate values of Young's Modulus in tension for other engineering polymers given by manufacturers are presented in table 7.2. The nylon used in version 3 design was particularly stiff, and other types of polymer are relatively compliant in comparison.

Material	Young's Modulus in tension	Reference
Acetal	3.6MPa	Quadrant Engineering Plastics
UHMWPE	0.7MPa	Davis Industrial Plastics
Nylon 66 (PA)	2.8MPa	RTP Company

Table 7.2 Stiffness values for engineering polymers.

One way to increase the stiffness of a polymer is to reinforce it with a much stiffer material. This creates a composite material, which is defined as 'any multiphase material that exhibits the properties of both constituent phases for a better combination of material properties'

(Callister, 1997). In this case, the polymer is the primary phase of the material (the matrix) and the reinforcing material is the secondary phase (the filler).

An example of the increase in stiffness that can be gained by reinforcing nylon with glass fibres is shown in figure 7.15. Materials with a higher filler ratio are more expensive and more difficult to machine.

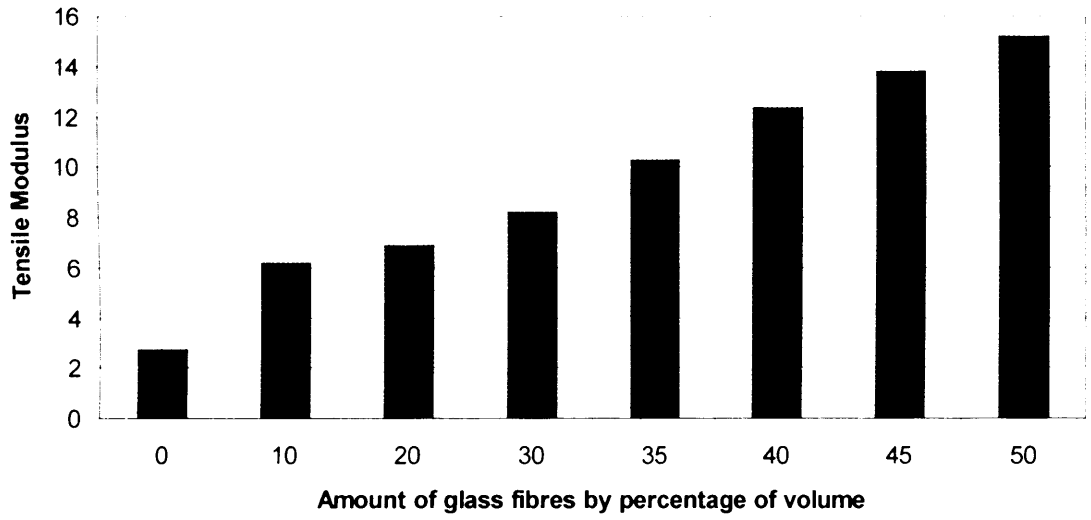

Figure 7.15 Tensile modulus for reinforced nylon containing different amounts of glass fibre (from data sheets supplied by RTP Company).

Possible materials for the reinforcement of engineering polymers are glass, carbon and mineral fibres (such as Kevlar). Carbon fibre reinforcement makes the composite stiffer and stronger than glass fibres and mineral fibres increase the toughness of the composite. Mineral fibres are more expensive and much rarer than carbon and glass fibres and are therefore not appropriate for this application. Although carbon fibre reinforcement creates a stiffer material it is also more expensive so the cost and the material properties need to be taken into account.

Using long, narrow, fibres of the second phase material is the most common form. Alternatively, the filler material can also take the form of spherical beads creating an isotropic composite, in this way the strength and stiffness are increased equally in all orientations.

This type of composite would be used if homogeneity were an important requirement. However the Young's Modulus for a bead composite is the same as in the transverse direction of a fibre composite and quarter of the stiffness in the longitudinal direction for a fibre composite of the same volume ratio (Kardos, 1985). The tensile strength of a bead-filled composite is about double that of a fibre filled composite in the transverse direction. There is therefore only benefit in paying the extra charge for a bead composite if the strength in the transverse direction is a concern for a fibre filled composite.

A short-fibre-glass-filled nylon was chosen to replace the nylon bearings in fail-safe version 4, and the volume of glass fibre was 30%. This material doubled the Young's Modulus to 8.2MPa.

7.10 Testing the Design for Function

Tests were carried out on fail-safe version 1 to check that the principle of operation worked. It was loaded perpendicular to the femur axis in three directions: in the anterior-posterior direction, the medial-lateral direction and at forty five degrees, using a materials testing machine (Zwick 2300). The three different directions were used to eliminate the effects of different frictional characteristics of the two sliders. Testing was also carried out to ensure that the device fulfilled the design requirement to have a variable activation load. The configuration is pictured in figure 7.16. The prototype was tested in torsion by attaching a lever arm to the proximal end and using the materials testing machine to apply a load until the fail-safe turned relative to its anchor.

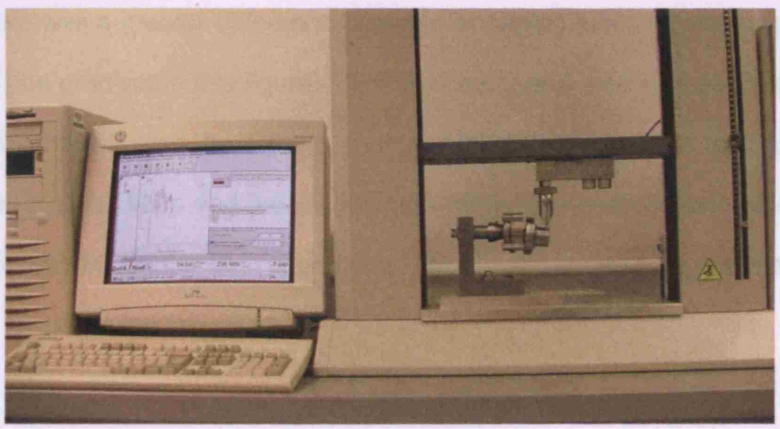

Figure 7.16 Testing set-up for calibration of bending moment activation

7.10.1 Testing of Version 1

Figures 7.17 and 7.18 show the levels at which the mechanism triggered in bending and in torsion. Each test was carried out five times and a straight line of best-fit applied to the data.

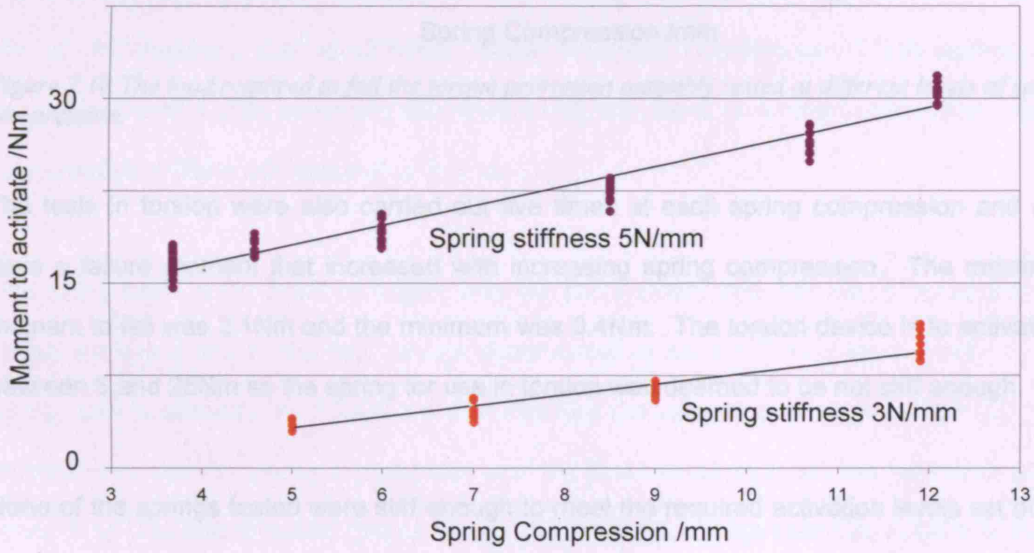

Figure 7.17 The load required to fail the lateral loading protection assembly containing two different springs, tested at different levels of spring compression.

The bending mechanism was tested with two different springs: the purple points in figure 7.17 are for a spring of 5N/mm stiffness and the orange points are the results for a spring of 3N/mm stiffness. The bending mechanism containing the stiffer spring activated at higher

loads and there was a greater difference between activation loads for an increase in spring compression (the gradient in this figure). The maximum and minimum bending moments to activate the mechanism with the 5N/mm spring were 28Nm and 18Nm, and for the 3N/mm spring the maximum is 9Nm and the minimum is 3Nm. The settings recommended for the fail-safe, calculated in chapter six, range from 18Nm to 100Nm so both of the springs tested are too weak for use in the fail-safe.

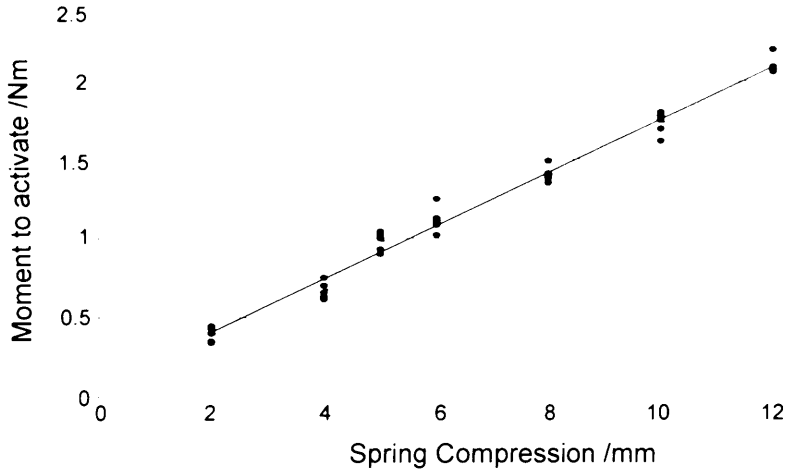

Figure 7.18 The load required to fail the torque protection assembly tested at different levels of spring compression.

The tests in torsion were also carried out five times at each spring compression and also gave a failure moment that increased with increasing spring compression. The maximum moment to fail was 2.1Nm and the minimum was 0.4Nm. The torsion device is to activate at between 5 and 25Nm so the spring for use in torsion was deemed to be not stiff enough.

None of the springs tested were stiff enough to meet the required activation levels set out in chapter six so stiffer springs were ordered from the supplier for the tests on fail-safe version 2.

7.10.2 Testing Subsequent Prototypes

The initial prototype (version 1) was found to be too large and changes were made to the design to make it shorter by reducing the length of the spring containers for the springs and

by reducing the thickness of the sliders and nylon bearings. Then two prototypes of the new, smaller, design were made for testing. These are fail-safe version 2(a) and version 2(b).

The sliders of the new prototypes were initially left 'as machined' and during initial testing there was high friction between the sliders and the nylon housing. To investigate the effect of the surface properties one of the sets of sliders was polished (version 2(b)). One effect of this was to allow motion between the slider and the nylon as a result of making the slider smaller, creating a slight rattling of the assembly. A small movement was observed in the other unit as well and indicated the need for creating the sliders slightly larger and with a closer tolerance. This change was made for version 3.

7.10.2.1 Performance of Version 2(a)

The first unit had sliders as-machined. It was tested in the A-P direction, the M-L direction, and at 45 degrees, and at different levels of spring compression. The spring was compressed with a grub screw and the levels used here were: no spring compression, spring compression of 3mm, of 6mm and of 8.5mm.

The spring used in the initial prototype was not stiff enough, and the device would activate during walking if one of the two springs documented in section 7.10.1 were used. A new spring, with a stiffness of 11.73N/mm (Lee Springs Ltd spring number LHL 375B 03), was ordered and used for the new prototypes and the loads required to fail the assembly are in figure 7.19. The two different colours of marking on the chart represent an initial test (blue) and one after disassembly and reassembly of the entire unit (pink).

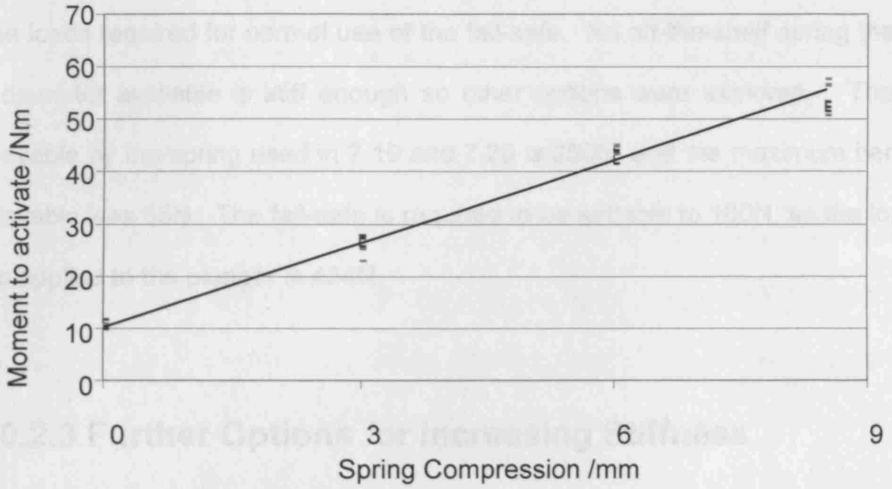

Figure 7.19 The bending moment required to fail version 2(a) at different compressions of spring of stiffness 11.73N/mm. Points in pink represent testing after disassembly and reassembly.

7.10.2.2 Performance of Unit 2(b)

The second unit had polished sliders. This activated at a lower load, possibly because of the lower coefficient of friction of the polished sliders, and was tested at the same levels of spring compression. The loads required to activate this mechanism are in figure 7.20.

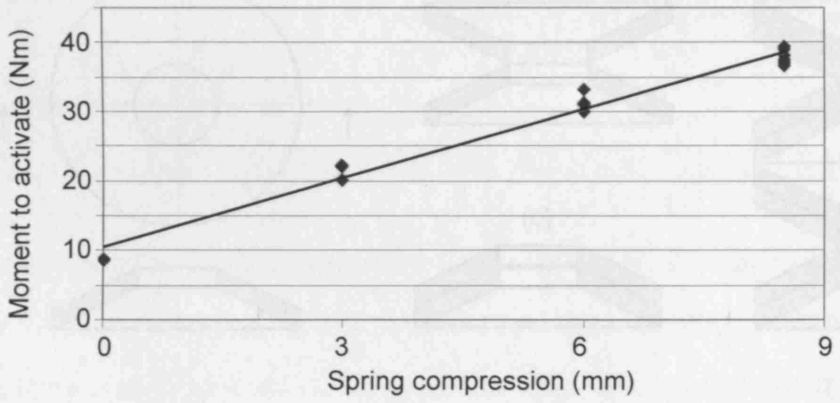

Figure 7.20 Load to activate version 2(b) in bending at different compressions of spring of stiffness 11.73N/mm.

The spring chosen for these tests was also not stiff enough to allow the fail-safe to activate at the loads required for normal use of the fail-safe. No off-the-shelf spring that will fit within the diameter available is stiff enough so other options were explored. The highest load achievable by the spring used in 7.19 and 7.20 is 250N, and the maximum bending moment achievable was 55N. The fail-safe is required to be settable to 100N, so the load that needs to be applied to the plunger is 454N.

7.10.2.3 Further Options for Increasing Stiffness

Spring washers (or bell washers) have the capacity to apply a greater force than a coil spring within the same geometric limits. The possibility of using spring washers has been investigated as it provides the possibility for increasing the bending limit of the fail-safe. Figure 7.21 shows how spring washers can be combined to increase stiffness and the amount of deflection. If all washers are the same dimensions, the combination in (b) has double the maximum deflection of one spring washer, (c) has double the stiffness and (d) has four times the maximum deflection and double the stiffness. It is possible to combine spring washers to provide the load and the amount of deflection required for the fail-safe.

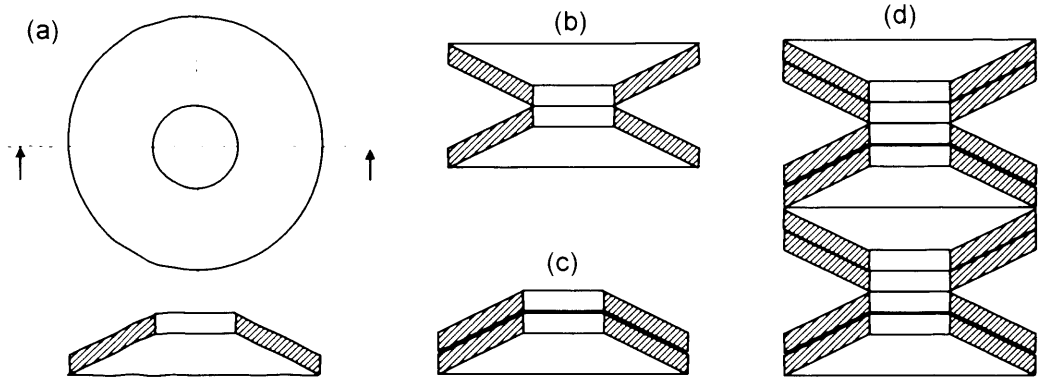

figure 7.21 Spring washers (a) top view and cross-section (b) combination for increased deflection (c) combination for increased stiffness (d) combination for increased stiffness and deflection.

7.10.3 Load Rate

The lateral loading restrictor was tested before and after complete disassembly and reassembly of fail-safe version 2(a) because there was concern that the friction characteristics might be different if the assembly were loosely or tightly assembled and figure 7.19 shows that there was little difference between the two tests. Another variable that was investigated was the rate of loading. The graph in figure 7.22 shows that at a higher loading rate there is less scatter in the bending moment required to activate the mechanism. The load required to activate the mechanism also appears to decrease with higher loading rates. The previous tests were all carried out at 10mm/min. In this test the rate was varied from 5mm/min to 500mm/min (the machine's maximum rate).

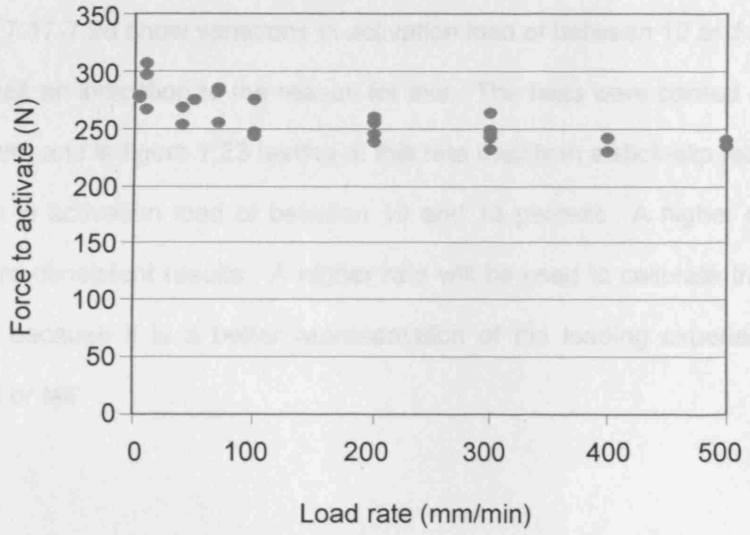

Figure 7.22 The force required to activate the bending moment restrictor at different rates of loading.

The force applied by the testing machine to the fail-safe at different rates of loading is plotted in 7.23 where it appears that the lower load speeds are affected more by friction. The stick-slip effect is much reduced in the higher load rates giving a smoother plot.

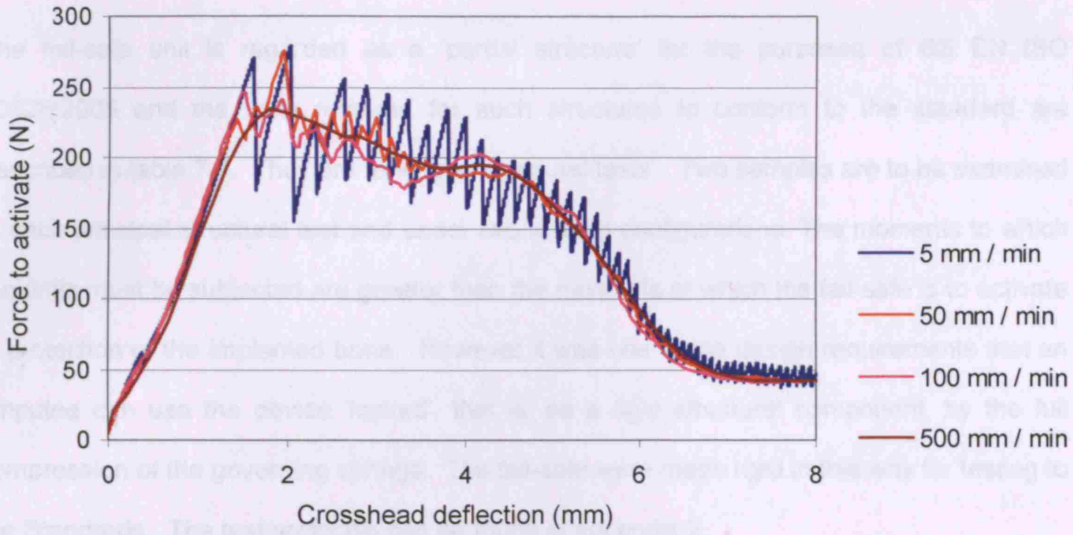

Figure 7.23 The force applied by the testing machine during testing at different load rates.

Figures 7.17-7.20 show variations in activation load of between 10 and 20 percent, but figure 7.23 gives an indication to the reason for this. The tests were carried out at the lowest rate (5mm/min) and in figure 7.23 testing at this rate results in a stick-slip relationship that gives a variation in activation load of between 10 and 15 percent. A higher rate of loading would give more consistent results. A higher rate will be used to calibrate the final version of the fail-safe because it is a better representation of the loading experienced during a traffic accident or fall.

7.11 Testing of the Design to British and International Standards

In addition to testing the fail-safe for function, it must also pass certain strength requirements in order to be sold for use as a prosthetic component. BS EN ISO 10328:2006, as discussed in subchapter 7.3.5, was created to give instructions for testing separate components of a prosthetic leg and was adhered to for testing the fail-safe.

7.11.1 Tests Required

The fail-safe unit is regarded as a 'partial structure' for the purposes of BS EN ISO 10328:2006 and the tests required for such structures to conform to the standard are described in table 7.3. They are 'principal structural tests'. Two samples are to be examined in each principal structural test and under two loading configurations. The moments to which the units must be subjected are greater than the moments at which the fail-safe is to activate in protection of the implanted bone. However it was one of the design requirements that an amputee can use the device 'locked', that is, as a rigid structural component, by the full compression of the governing springs. The fail-safe were made rigid in this way for testing to the Standards. The test protocols can be found in appendix 2.

Name of test	Description	Performance Requirement
Static Proof Test	Application of a static load which represents a severe loading condition but does not affect the component's ability to function.	to sustain 2065N (1811N) for 30s and deform < 5mm
Fatigue Test	A cyclic load is applied at a level expected of normal, daily, loading. The component must withstand the load for a specific number of cycles.	to sustain cyclic loading between 50N and 1230N (1035N) for 3 million cycles followed by 2065N (1811N) for 30s
Ultimate Static Test	A single, very high, load which the component must sustain but may be unusable afterwards.	to sustain 4130N (3626N) without failing or 3098N (2717N) without loss of structural integrity
Separate Static Test in Torsion	A torsional moment is applied which must be sustained by the component.	To sustain 50Nm torque and one end of the component must have twisted less than 3°

Table 7.3 The test required of BS ISO 10328:2006 the forces specified are those for 'loading condition 1', and 'loading condition 2' are in parentheses.

7.11.2 Loading Configurations

The static and cyclic tests were to be carried out in two different loading conditions. One represents a high load state near the beginning of the stance phase of gait and the other a high load state near the end of the stance phase. The force vector for testing in each condition is defined by points in three-dimensional space representing the position of the 'top of the prosthesis', knee and ankle. The level of amputation was assumed to be at the level

defined as 'top of prosthesis' in the Standard, 150mm above the knee, and the load applied at an offset to the fail-safe components using lever-arms.

7.11.3 Connection of the Lever-Arms

The Standard states that the fail-safe units must have end connections with 'mechanical characteristics similar to those of the intended adjacent components' (BS EN ISO 10328:2006). Proximally, the fail-safe mechanism is attached to the implant in the bone daily by the wearer using the attaching cup. An abutment is provided for the testing which is rigidly attached to the offset arms and is designed to imitate the abutment of the implant, being identical in shape to the peg seen in figure 7.9. It is intended that the fail-safe device be connected, distally, to a tubular component with a split-ring connection which, in turn, connects to the knee component with a pyramid attachment. Figure 7.24 (b) shows the component that is used in the testing, an Otto Bock 'tube clamp adapter' catalogue reference 4R82.

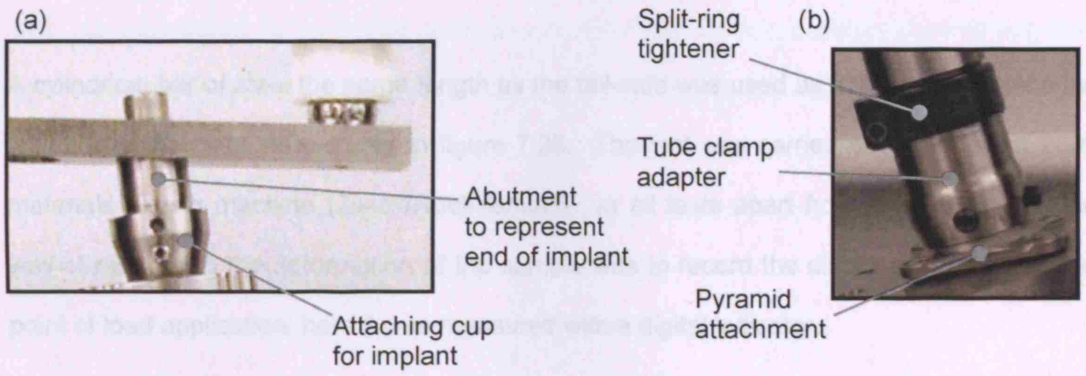

Figure 7.24 End-attachments for Standards tests (a) proximal attachment, (b) distal attachment.

7.11.4 Test Reports

The following sections describe the tests that were carried out on the fail-safe devices to the International Standards. The test reports are in appendix 2.

7.11.4.1 Proof Test of Attachments

The proof test of the attachments was to confirm that the jig used to apply loads to the test pieces was not too flexible. If it were, the loading regime would vary throughout the cyclic test. The proof test of the attachments was to be carried out in the worst-case alignment *i.e.* the one with the largest lever arm (as specified in paragraph 13.2.1.2.2 of BS EN ISO 10328).

Prior to the commencement of tests the 2006 version of the standards was published and changes had to be made to the offset attachments to comply with the new standards. The 1996 version of the standard stated that the attachments must flex less than 2mm for a load application of 5000N but the force-application levers would have to be substantial in size to conform to this requirement and may increase the stress load on the sample due to inertial effects. The new regulations require the same flexion under a force of 2478N for the static proof test and the cyclic test.

A cylindrical bar of steel the same length as the fail-safe was used as a 'blank' to replace the fail-safe for this test, as pictured in figure 7.25. The test was carried out on a Zwick 2000 materials testing machine (Zwick/Roell GmbH). In all tests apart from the torsion test the way of measuring the deformation of the sample was to record the distance travelled by the point of load application; here it was measured with a digital indicator.

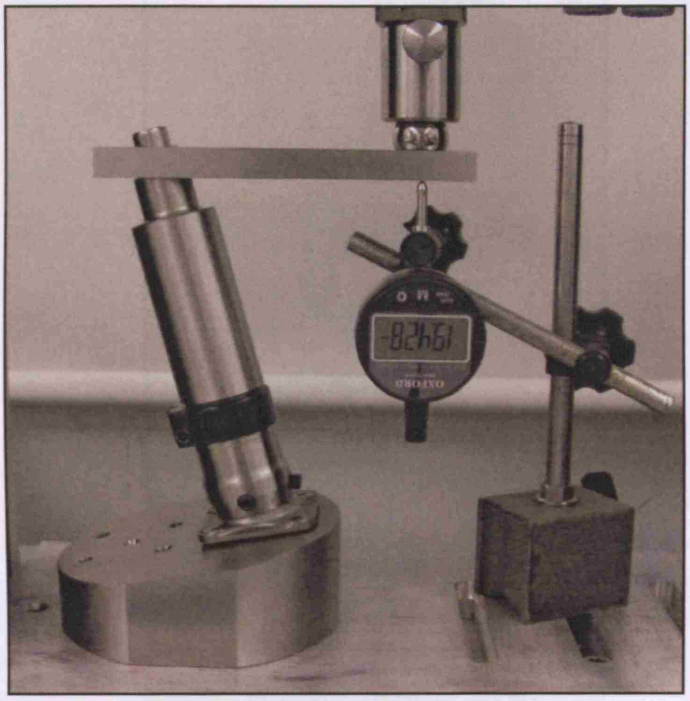

Figure 7.25 Proof test of attachments in loading condition 1

The test reports for the proof test of attachments for both loading conditions are in appendix 3. The attachment devices passed the stiffness requirement which was for the load application point to move less than 2mm. The first unit tested flexed 1.977mm and 1.001mm in the first and second loading conditions respectively and the second unit flexed 1.776mm and 1.057mm in the two loading conditions.

7.11.4.2 Static Proof Test

In this test a single, high, load was applied to the component and the difference between the position of the load-application point after the test was to be no more than 2mm away from its position at the beginning of the test. Figure 7.26 shows the fail-safe undergoing this test.

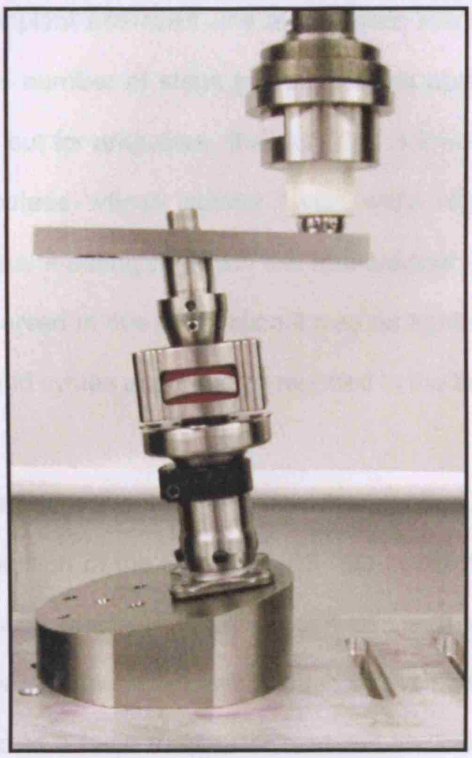

Figure 7.26 Static Proof Test in loading condition 2

The test reports can be found in appendix 3. The fail-safe passed the static proof tests in both loading conditions, the first unit deflected 0.076mm and 0.602mm and the second unit deflected 0.630mm and 0.711mm in the first and second loading conditions respectively.

7.11.4.3 Cyclic Load Tests

During the cyclic tests the samples were subjected to loads equivalent to normal loading over a period of about five years. After the application of the cyclic load the device was to pass the static proof test again in order to comply with the Standard.

Paragraph 16.3.1.2 in the International Standard states that, during the cyclic test, "specific parts shall be replaced when the number of cycles has reached a value at which such replacement is indicated by the manufacturer". No such replacements are required for this component but, during normal use, the component shall be donned and doffed daily so the

connection between the implant abutment and the fail-safe mechanism is tightened about once a day. The average number of steps per day for the able-bodied population is just under 9000 (Miller, 2004), but for amputees, the daily rate is lower: an average of 2377 and 3288 steps for two amputees whose activity levels were regarded as 'average' in a submission to the consensus meeting on which this International Standard is based (Dewar, 1977). If loosening is observed in this connection it may be tightened by hand but not more frequently than five thousand cycles and must be reported in the test report.

No frequency was designated for this test. 2Hz was chosen because that was the frequency specified in the previous edition of the Standard (BS ISO 10328:1996). The machine used was a hydraulic cyclic testing machine (RDP Howden Ltd) with six stations, each applying the same force to whatever is placed under it. Three of the stations were blocked of with blanks, one applied a load to a force transducer, and two stations applied loads to the two fail-safe devices.

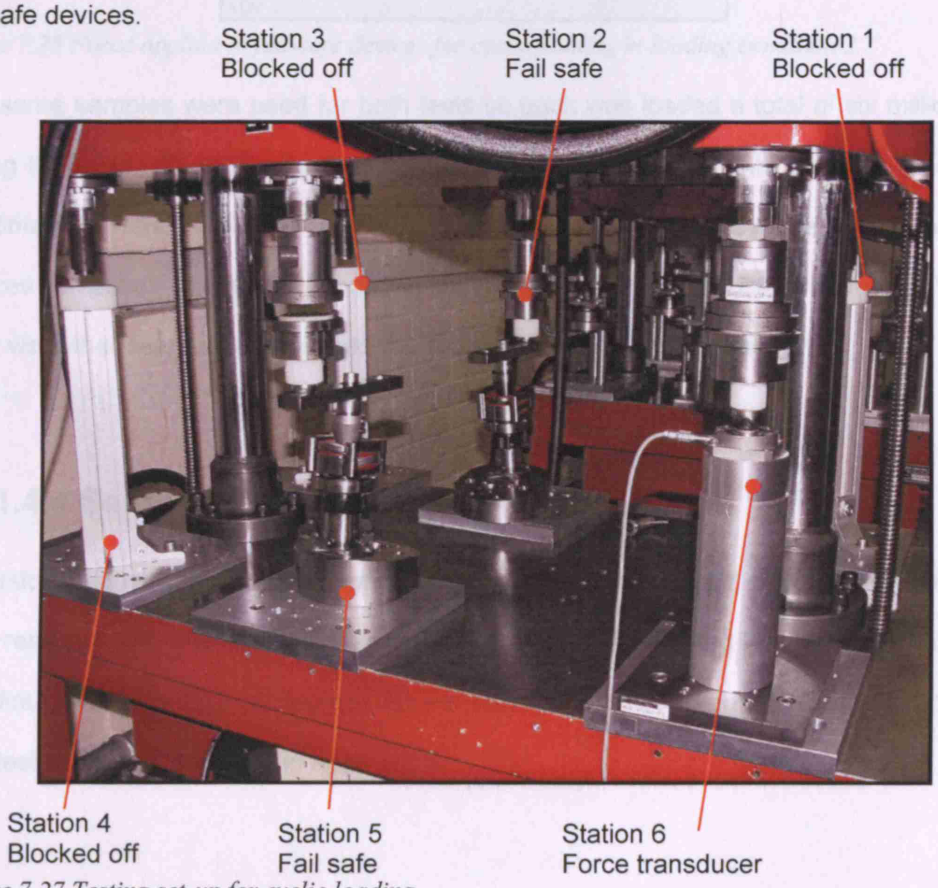

Figure 7.27 Testing set-up for cyclic loading.

The force transducer was attached to a voltmeter which was calibrated with the testing machine to give a continuous readout of the load during the first part of the test. The requirement for the test was for the load to vary sinusoidally and be 'smooth with no overshoot spikes'. Figure 7.28 shows the display on the voltmeter showing the pattern from the force transducer in loading condition 2. The reading has small variations but no departure from the sinusoidal curve overshoots the maximum or minimum value and this was acceptable for the test.

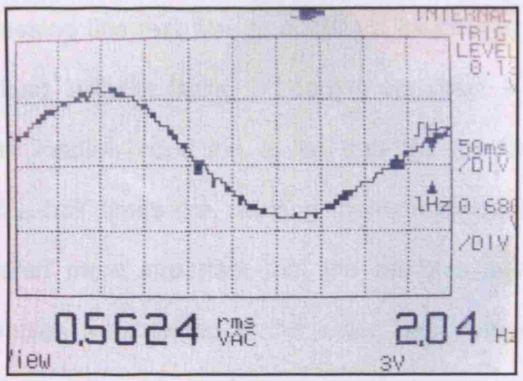

figure 7.28 Force applied to fail-safe devices for cyclic loading in loading condition 2

The same samples were used for both tests so each was loaded a total of six million times during the tests. The fail-safe devices did not pass the requirements for cyclic loading the first time they were tested and a number of improvements had to be made to ensure that the devices complied. These improvements were described in section 7.9. The revised fail-safe units were then retested and passed the requirements for the Standards.

7.11.4.4 Separate Static Test in Torsion

In torsion a similar method was employed to the static proof test, 50Nm was applied and then removed and one end of the component was to have rotated less than three degrees. The final rotation was 2.34 degrees for the first unit and 1.98 degrees for the second unit. The test report can be found in appendix 3.

7.11.4.5 Ultimate Static Test

All tests apart from the torsion test were to be carried out in both loading conditions using two samples, however it would have been permissible to use a different sample for each test. Two units were prepared for testing and the manufacture of more was an option throughout. The ultimate failure test carried a risk of rendering the sample unusable, so was left until the end.

The requirement for passing this test was to sustain a lower load without 'loss of structural integrity' or a higher load 'without failing'. Loading condition 1 used a higher force and greater lever-arm than loading condition 2, so that the bending moment applied was equivalent to two and a half times the bending moment in loading condition 2. For this reason it was considered more important that the samples pass the test under loading condition 1. Both samples were tested to the lower load in loading condition two before being subjected to the high failure load in loading condition one.

Both units sustained the lower load in loading condition two without loss of structural integrity. They were subsequently subjected to the highest loading in loading condition one, and fulfilled the requirement not to fail, withstanding the maximum load for thirty seconds. After the test were completed the units looked normal. When the springs were loosened the torsion restrictor worked and the sliders moved normally within the bearing housing.

Two fail-safe samples met the requirements of BS EN ISO 10328:2006. All of the test record sheets can be found in appendix 3, they include charts showing displacements and measurements from the tests.

7.12 Conclusions

A component for a prosthetic limb has been designed to protect the femur from loads applied to a skeletally-attached transfemoral prosthesis. This fail-safe device works by sliding or turning the prosthesis relative to the bone. Figure 7.29 shows the parts of the fail-safe device. The patent granted for this design can be found in appendix 3.

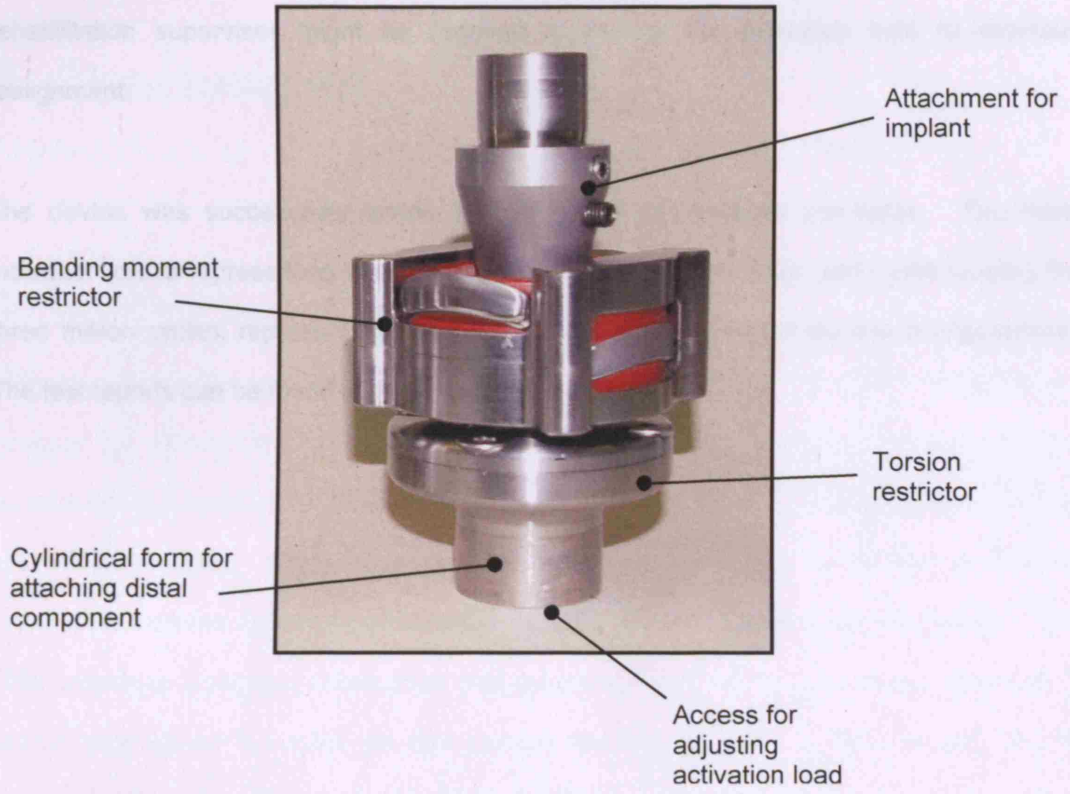

Figure 7.29 fail-safe device showing the different functions.

The fail-safe device includes the mechanism for attaching the prosthesis to the implant that protrudes from the residual limb so it is situated immediately distal to the stump. This ensures that whenever a prosthesis is attached to the ITAP implant the fail-safe is used.

The load at which the fail-safe device triggers is variable to protect the healing bone.

The activation load should only be altered by the rehabilitation supervisor. Disassembly of the adjacent component of the prosthesis is required to gain access to the means for adjusting the fail-safe and a special key is required to make the adjustment.

One of the design requirements was for the fail-safe to be re-settable after activation. It is possible that the amputee will be able to reposition the prosthesis after activation but the rehabilitation supervisor might be required to reduce the activation load to facilitate realignment.

The device was successfully tested to British and International Standards. The tests included: forces representing severe loading episodes, torsion tests, and cyclic loading for three million cycles, representing five years of use, in two different loading configurations. The test reports can be found in appendix 2.

8 Conclusions

8.1 Summary

Many leg amputees are unable to use a prosthetic limb because of skin problems or because the shape of the residual limb makes it difficult to attach a normal socket prosthesis. Attachment of a prosthetic limb to the bone is a solution for these amputees because it does not rely on a socket. It is necessary to have a permanent breach of the skin to make a connection between the bone and an external limb, which presents a risk of infection. The ITAP prosthesis translates information from a natural analogue, the deer antler, to create a dermal seal around the metal pin that crosses the skin boundary. Other benefits of this system are the ability to feel vibrations through the implant and greater range of movement than with a socket prosthesis. A need to protect the bone from external loads is identified and it has been concluded that a failsafe capability is required in the prosthesis and that it should protect the bone and implant under loading in bending and in torsion. To design a device to protect the implanted bone two sets of loading data were required: the normal loads encountered during daily activities, which should be allowed to transfer to the bone, and loads that might cause the bone to break, which must be prevented.

The normal loading expected in the implanted femur has been calculated (chapter two). Data based on normal subjects give unrealistic loads because of the high muscle forces that are present in the normal leg, so a recent laboratory study of the loads measured in transfemoral amputees fitted with bone-anchored prostheses has been examined, which gives values of loading for walking, stair negotiation, ramp walking and walking around a circle (normal activities) (Lee *et al.*, 2007 (a)). In order to find loading values for other activities the geometry of the leg, angle of the knee and ground-reaction force data have been used to predict loads for jogging, running and cycling. By combining the calculated and measured data, maximum loads in all directions were derived, as shown in figure 8.1.

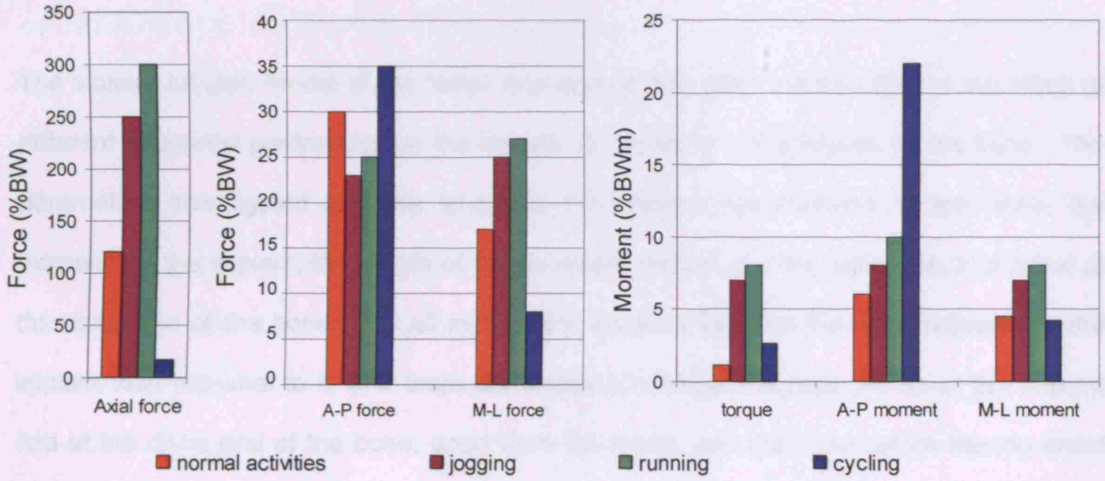

Figure 8.1 (also appears as figure 2.10) Maximum forces and moments at the mid femur during different activities.

After finding the normal loading in the femur the loads that risk the integrity of the implanted bone need to be calculated. Finite element analysis has been employed to investigate the effect of altering the bone geometry and material properties on the stresses experienced by the bone. Two finite element models have been used, a tubular representation of the femur and an anatomical model created from a CT scan of a femur. To create and analyse the finite element models the material properties of the femur are required.

An investigation into the elastic properties of bone was carried out, and by gathering data from published work the material properties for a tubular finite element model (chapter four)

have been defined. The material properties for the anatomical model were calculated from CT data using a mathematical relationship to convert the intensity of colour in the CT image to bone density and then Young's Modulus. The failure properties of the femur have been investigated (chapter three), and the Tsai-Wu failure criterion for composite materials has been chosen because it takes into account the anisotropic nature of bone. The situations and loads in which whole femurs are known to fracture have been investigated to show the loads that might present a danger. The strength of the bone-implant interface has been researched using published data from *in vivo* animal studies, and found to increase gradually over time.

The simple, tubular, model of the femur and implant has been used to assess the effect of different geometric parameters on the transfer of stress from the implant to the bone. The parameters investigated are: the length of the implant, the diameter of the bone, the diameter of the implant, the length of bone-implant contact and the presence of a collar at the distal end of the bone. For all models the stress is lower in the bone adjacent to the implant than proximal to it, and there are stress concentrations near the tip of the implant and at the distal end of the bone, apart from the model with the collar which has no distal stress concentration. It has been concluded that a collar at the distal end of the bone is desirable for the implant because it removes a high stress concentration at this point. There is no difference in stress in the bone for implants of different length, but shorter than 30mm the stress concentrations are higher. Reducing the diameter of the bone and reducing the diameter of the implant increases the stress in the bone. Creating a model with the bone material properties of an amputee altered the stress distribution only slightly, but the reduced strength of the bone needs to be taken into account.

The tubular model is not adequate to investigate the load transfer in short residual femurs because its symmetrical geometry is unlike that of the proximal femur. Therefore, the stresses in the bone due to different levels of amputation have been investigated using the

anatomical model. Three levels of amputation have been modelled: a femur with one-quarter removed, with half removed and with three-quarters removed. The stresses in the femur with three-quarters removed match the stresses in the tubular femur model. The femur with half removed match the tubular model until the implant is proximal to the diaphysis, where the bone thickens and has a larger cross-section, so the stresses are lower. However the implant is not in contact with cortical bone here and the cancellous bone that surrounds it is weaker. The bone with three-quarters removed has a different pattern of stress transfer to the bone because the geometry is different. It was concluded that the implanted bone can be modelled for finite element analysis using a tube if the implant does not extend beyond the diaphysis, with the outer diameter being equal to the thickness of the bone as measured on a radiograph taken in the medial-lateral direction.

The results have been collated to find appropriate levels for a fail-safe device to protect the femur from external loading. Three possible failure modes have been ascertained which depend on the strength of the bone and the shear strength of the bone-implant interface. It is predicted that different failure modes would govern the failure at different levels of resection and it is proposed that an amputee with three quarters of the bone removed should not be fitted with a cylindrical implant as modelled here. Variables that were considered important - the bone quality, the bone thickness, and the length of implant in contact with cortical bone - were assessed for their contribution to the strength of the bone. It is found that a reduction in thickness of four millimetres or cortical bone contact of fifty percent reduces the strength by half. The variables examined have been used to define risk groups into which each amputee could be placed for the purposes of setting a fail-safe device to protect the bone (figure 8.2). Settings for a fail-safe device have been recommended for each risk group taking into account the normal loads, the development of the implanted bone over time, and the failure models (figure 8.3).

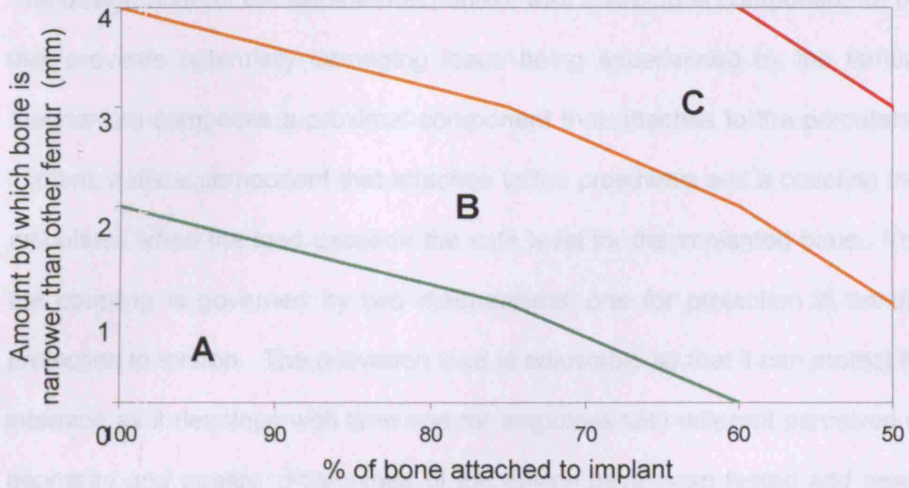

Quarter of femur resected: A = risk 0-1 = low risk
B = risk 2-3 = medium risk
C = risk 4-6 = high risk

Half of femur resected: A = risk 2-3 = medium risk
B = risk 4-6 = high risk
C = risk >6 = high risk

Figure 8.2 (also appears as figure 6.11) Chart for finding the risk group of an amputee depending on the level of amputation, thickness of the femoral shaft and length of bone-implant contact.

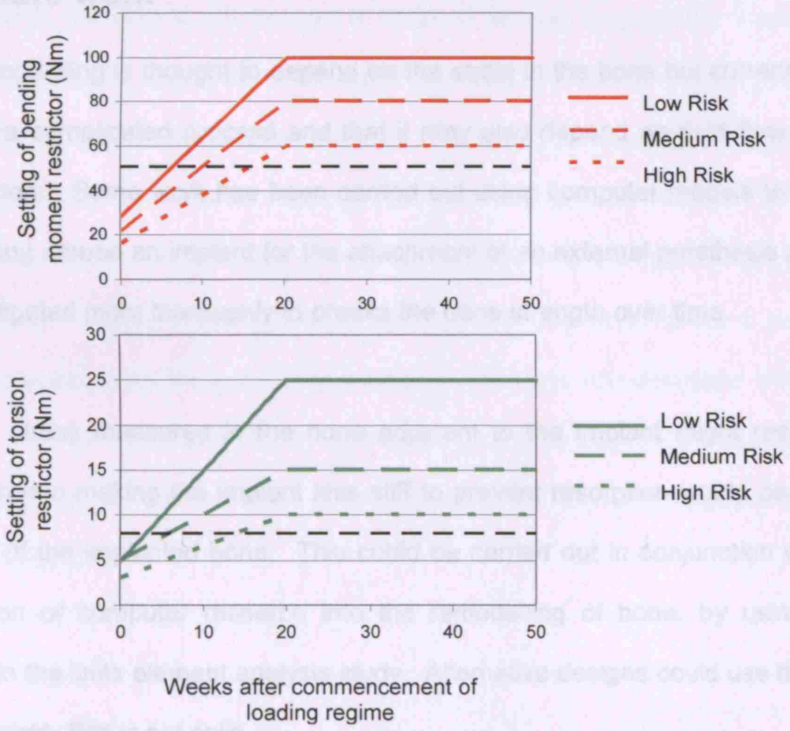

Figure 8.3 (also appears as figure 6.12) Settings for bending moment restrictor and torsion restrictor from the beginning of the implant loading regime. The black dashed line represents the maximum walking load for an amputee of average weight.

The design brief for the failsafe mechanism was a structural component for the prosthetic leg that prevents potentially damaging loads being experienced by the femur. The fail-safe mechanism comprises a proximal component that attaches to the percutaneous part of the implant, a distal component that attaches to the prosthesis and a coupling mechanism which articulates when the load exceeds the safe level for the implanted bone. The articulation of the coupling is governed by two mechanisms: one for protection in bending and one for protection in torsion. The activation load is adjustable so that it can protect the bone-implant interface as it develops with time and for amputees with different perceived risk due to bone geometry and quality. Prototypes of the device have been tested and passed the relevant British and International Standards. Copies of the test reports can be found in appendix 4. The design has been granted worldwide patent protection.

8.2 Future work

Bone remodelling is thought to depend on the strain in the bone but current research shows that it is a complicated process and that it may also depend on fluid flow in the bone and other factors. Some work has been carried out using computer models to predict the bone remodelling around an implant for the attachment of an external prosthesis and this needs to be investigated more thoroughly to predict the bone strength over time.

The low stress measured in the bone adjacent to the implant might result in resorption. Research into making the implant less stiff to prevent resorption would be beneficial to the strength of the implanted bone. This could be carried out in conjunction with the previous suggestion of computer research into the remodelling of bone, by using different bone designs in the finite element analysis study. Alternative designs could use different materials or a geometry that is not solid.

It has been shown in this thesis that there is a high stress concentration at the proximal end of the implant and that this stress concentration governs the failure of the bone in some cases. Making the proximal end of the implant less stiff would reduce this stress concentration and would mean that the permissive load could increase. For example a reduction in stress concentration by thirty percent would mean the fail-safe device could be set thirty percent higher in bending. One method reducing the stiffness of the proximal implant would be to perforate it or make it out of different materials. A hollow implant could have an increasing inner diameter toward the end of the implant, this so-called 'dove-tailing' would spread the stress concentration at the implant tip and so reduce the magnitude.

The design of the fail-safe mechanism is complicated, and requires machining by computer numerical control. A simplification of the design would have financial benefits. It would also be beneficial to reduce the weight of the fail-safe device. The weight could be reduced by making it smaller or by choice of materials. The design was intentionally made to be highly adjustable in bending and in torsion in order to be able to gradually increase the strength during rehabilitation, and to allow for a different level of protection to be used if required, and also to be re-set easily after activation. The fail-safe could be replaced by a simpler mechanism such as a bar of material that bends or breaks that can be easily replaced. However it would have to pass the design requirement set out in chapter seven to 'not endanger the wearer when activated', so there would need to be a secondary support mechanism that takes the body weight when the fail-safe has activated; it would be required to 'have a variable activation load', so a method of changing the activation load would have to be included; and 'be resettable after activation', so the safety feature would need to be easy to replace.

Analysis of the model created for the most proximal level of amputation showed that the cylindrical implant used in this study was not adequate to transmit the torsional loads to the bone, and it was suggested that a different design of implant be used for proximal amputations. Following discussion with surgeons and implant designers there should be further research into the best design of implant to use for amputees with short residual femurs.

Appendix 1

Assembly Drawing of Fail-Safe

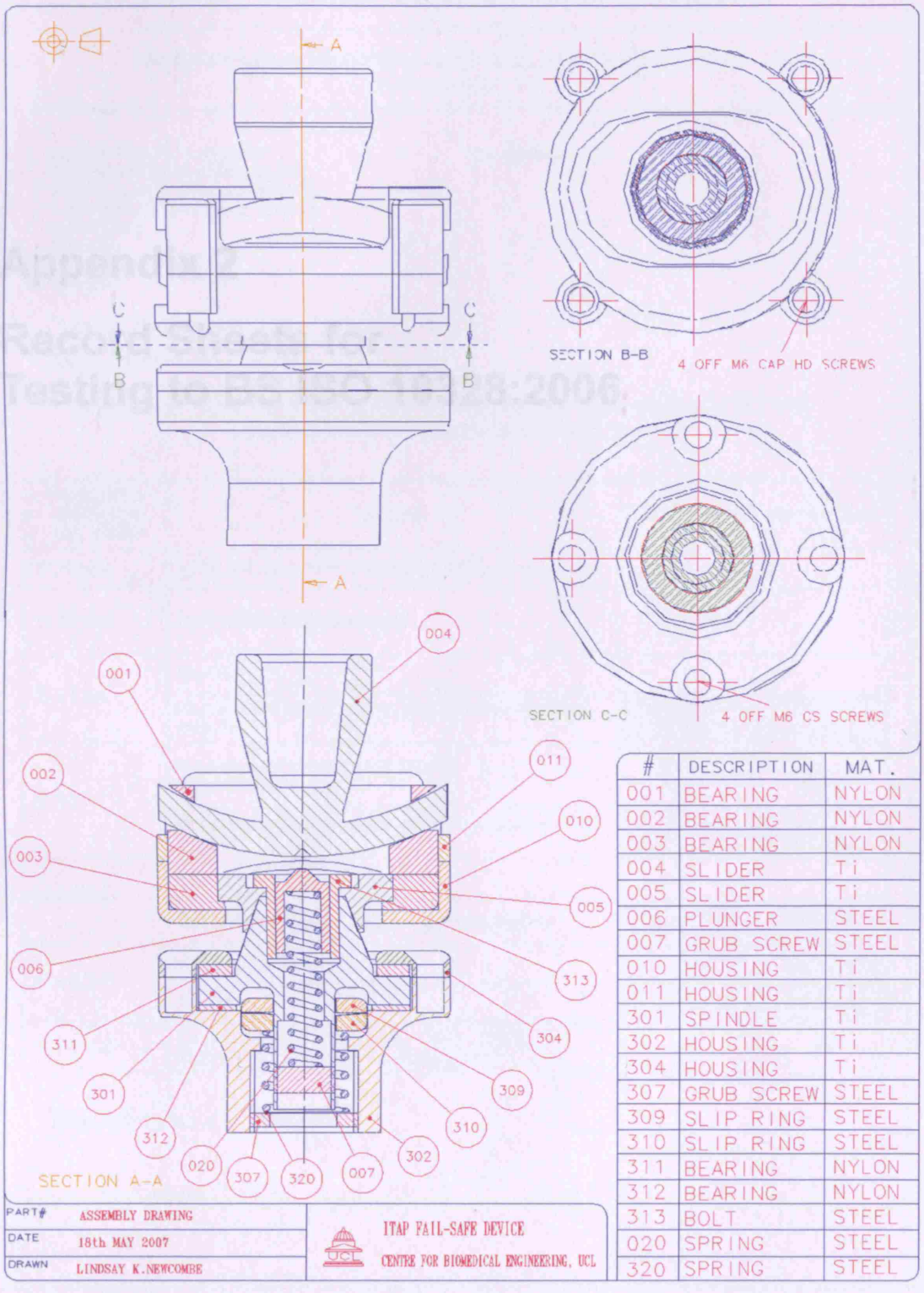

#	DESCRIPTION	MAT.
001	BEARING	NYLON
002	BEARING	NYLON
003	BEARING	NYLON
004	SLIDER	Ti
005	SLIDER	Ti
006	PLUNGER	STEEL
007	GRUB SCREW	STEEL
010	HOUSING	Ti
011	HOUSING	Ti
301	SPINDLE	Ti
302	HOUSING	Ti
304	HOUSING	Ti
307	GRUB SCREW	STEEL
309	SLIP RING	STEEL
310	SLIP RING	STEEL
311	BEARING	NYLON
312	BEARING	NYLON
313	BOLT	STEEL
020	SPRING	STEEL
320	SPRING	STEEL

Appendix 2

Record Sheets for Testing to BS ISO 10328:2006

Appendix 2

BS EN ISO 10328:2006
Prosthetics – Structural Testing of Lower Limb Prostheses

Test Report – Proof Test of End Attachments in Loading Condition 1
Section 13.2.1

Prepared by L.K. Newcombe
Centre for Biomedical Engineering,
Institute of Musculoskeletal Science,
Royal National Orthopædic Hospital,
Brockley Hill,
Stanmore,
Middlesex,
HA& 4LP.

Tel. 020 8954 2300

Tested on 22nd November 2006

Test load level P4

Performance requirements: to deform < 2mm under the application of 2478N and experience a permanent deformation of < 1mm

Paragraph of BS EN ISO 10328:2006	Direction	End attachment set no.1	End attachment set no.2
13.2.1.2.4	Assemble test sample to Loading Condition 1 orientation	✓	✓
13.2.1.2.5	Apply 1024N for 30±3 seconds	✓	✓
13.2.1.2.6	Apply 50N	✓	✓
	Measure displacement of the moving load application point, δ_1.	δ_1= 1.767	δ_1= 2.354
13.2.1.2.7	Increase force smoothly to 2478N at between 100-250 N/s.	Approx. 200N/s	Approx. 200N/s
	Measure displacement of the moving load application point, δ_2.	δ_2=3.744	δ_2= 4.130
13.2.1.2.8	Reduce force to 50N.	✓	✓
	Measure displacement of load application point, δ_3.	δ_3= 1.933	δ_3= 2.469
13.2.1.2.9	$D_1 = \delta_2 - \delta_1$	D_1= 1.977	D_1= 1.776
	$D_2 = \delta_3 - \delta_1$	D_2= 0.166	D_2= 0.115
13.2.1.2.10	Do not use if D_1 > 2mm or if D_2 > 1mm. Do end attachments comply with the requirements?	yes	yes

Signature of tester: *L K Newcombe*

Date: *22 / 11 / 06*

Appendix 2

BS EN ISO 10328:2006
Prosthetics – Structural Testing of Lower Limb Prostheses

Test Report – Proof Test of End Attachments in Loading Condition 2
Section 13.2.1

Prepared by L.K. Newcombe
Centre for Biomedical Engineering,
Institute of Musculoskeletal Science,
Royal National Orthopædic Hospital,
Brockley Hill,
Stanmore,
Middlesex,
HA& 4LP.

Tel. 020 8954 2300

Tested on 22nd November 2006

Test load level P4

Performance requirements: to deform < 2mm under the application of 2173N and experience a permanent deformation of < 1mm

Paragraph of BS EN ISO 10328:2006	Direction	End attachment set no.1	End attachment set no.2
13.2.1.2.4	Assemble test sample to Loading Condition 2	✓	✓
13.2.1.2.5	Apply 828N for 30±3 seconds	✓	✓
13.2.1.2.6	Apply 50N	✓	✓
	Measure displacement of the moving load application point, δ_1.	δ_1= 20.788	δ_1= 20.750
13.2.1.2.7	Increase force smoothly to 2173N at between 100-250 N/s.	Approx. 200N/s	Approx. 200N/s
	Measure displacement of the moving load application point, δ_2.	δ_2=21.789	δ_2= 21.820
13.2.1.2.8	Reduce force to 50N.	✓	✓
	Measure displacement of load application point, δ_3.	δ_3= 20.807	δ_3= 20.807
13.2.1.2.9	$D_1 = \delta_2 - \delta_1$	D_1= 1.001	D_1= 1.057
	$D_2 = \delta_3 - \delta_1$	D_2= 0.019	D_2= 0.057
13.2.1.2.10	Do not use if D_1 > 2mm or if D_2 > 1mm. Do end attachments comply with the requirements?	yes	yes

Signature of tester: *L K Newcombe*

Date: *22 / 11 / 06*

Appendix 2

BS EN ISO 10328:2006
Prosthetics – Structural Testing of Lower Limb Prostheses

Test Report – Principal Static Proof Test in Loading Condition 1
Section 16.2.1

Prepared by L.K. Newcombe
Centre for Biomedical Engineering,
Institute of Musculoskeletal Science,
Royal National Orthopædic Hospital,
Brockley Hill,
Stanmore,
Middlesex,
HA& 4LP.

Tel. 020 8954 2300

Tested on 19th April 2008

Test load level P4

Performance requirements: to sustain 2065N for 30s and deform < 5mm

Paragraph of BS EN ISO 10328:2006	Direction	Sample 1	Sample 2
16.2.1.1.2.	Assemble test sample to 16 degrees.	✓	✓
16.2.1.1.3.	Apply 944N for 10-30 seconds then remove load and record time elapsed.	20 seconds	20 seconds
	Wait 10-20 minutes.	10 minutes	17 minutes
16.2.1.1.4.	Apply 50N and record lever arms.	✓	✓
16.2.1.1.5.	Top offset with application of 50N	68mm	68mm
	Bottom offset with application of 50N	50mm	50mm
16.2.1.1.6.	Measure displacement of the moving load application point, δ_4.	δ_4=0.231	δ_4=0.243
16.2.1.1.7.	Increase force smoothly to 2065N at between 100-250 N/s.	Approx. 150N/s	Approx. 150N/s
	Maintain 2065N for 30±3 seconds.	✓	✓
	Record whether or not sample has sustained 2065N for 30s.	yes	yes
16.2.1.1.8.	Reduce force to 50N.	✓	✓
	Measure displacement of load application point, δ_5 within 5 minutes and note time interval after decreasing force to 50N.	δ_5=0.307 at 20s	δ_5=0.873 at 15s
16.2.1.1.9.	$D_3 = \delta_5 - \delta_4$	D_3=0.076	D_3=0.630
16.2.1.1.10.	If D_3 > 5mm sample does not comply. Does sample comply?	yes	yes

Signature of tester: *L K Newcombe*

Date: *19/4/08*

Appendix 2

BS EN ISO 10328:2006
Prosthetics – Structural Testing of Lower Limb Prostheses

Test Report – Principal Static Proof Test in Loading Condition 2
Section 16.2.1

Prepared by L.K. Newcombe
Centre for Biomedical Engineering,
Institute of Musculoskeletal Science,
Royal National Orthopædic Hospital,
Brockley Hill,
Stanmore,
Middlesex,
HA& 4LP.

Tel. 020 8954 2300

Tested on 8th May 2008

Test load level P4

Performance requirements: to sustain 1811N for 30s and deform < 5mm

Paragraph of BS EN ISO 10328:2006	Direction	Sample 1	Sample 2
16.2.1.1.2.	Assemble test sample to 6 degrees.	✓	✓
16.2.1.1.3.	Apply 828N for 10-30 seconds then remove load and record time elapsed.	20 seconds	20 seconds
	Wait 10-20 minutes.	12 minutes	10 minutes
16.2.1.1.4.	Apply 50N and record lever arms.	✓	✓
16.2.1.1.5.	Top offset with application of 50N	68mm	68mm
	Bottom offset with application of 50N	50mm	50mm
16.2.1.1.6.	Measure displacement of the moving load application point, δ_4.	δ_4=28.974	δ_4=28.913
16.2.1.1.7.	Increase force smoothly to 1811N at between 100-250 N/s.	Approx. 130N/s	Approx. 130N/s
	Maintain 1811N for 30±3 seconds.	✓	✓
	Record whether or not sample has sustained 1811N for 30s.	yes	yes
16.2.1.1.8.	Reduce force to 50N.	✓	✓
	Measure displacement of load application point, δ_5 within 5 minutes and note time interval after decreasing force to 50N.	δ_5=29.580 at 10s	δ_5=29.624 at 15s
16.2.1.1.9.	$D_3 = \delta_5 - \delta_4$	D_3=0.602	D_3=0.711
16.2.1.1.10.	If D_3 > 5mm sample does not comply. Does sample comply?	yes	yes

Appendix 2

BS EN ISO 10328:2006
Prosthetics – Structural Testing of Lower Limb Prostheses

Test Report – Principal Static Proof Test in Loading Condition 2
Section 16.2.1

Notes:

Chart to show the variation of force with test time during the static proof test to LC2

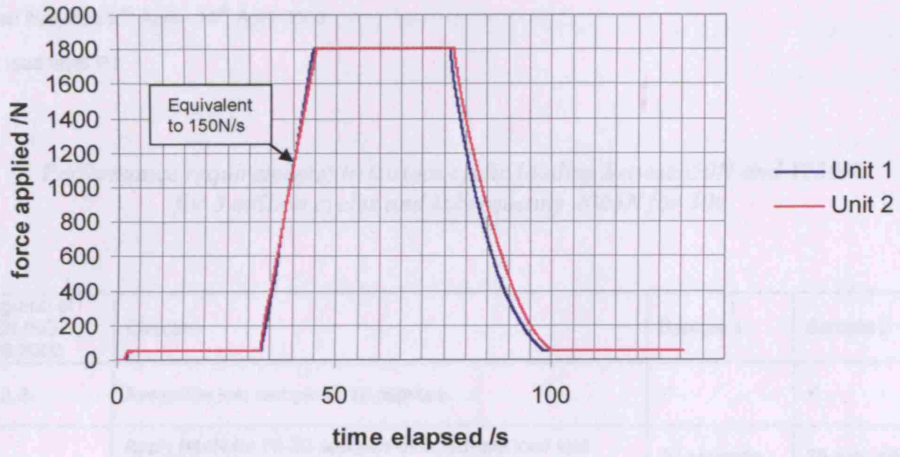

Static Proof Test in Loading Condition 2 showing displacement of testing machine crosshead

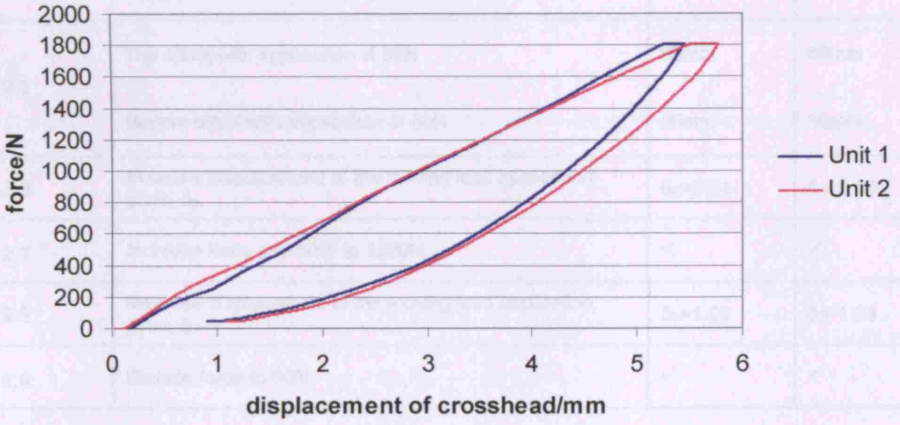

Signature of tester: *L K Newcombe*

Date: *8 / 5 / 08*

Appendix 2

BS EN ISO 10328:2006
Prosthetics – Structural Testing of Lower Limb Prostheses

Test Report – Principal Cyclic Test in Loading Condition 1
Section 16.3.2

Page 1/2

Prepared by L.K. Newcombe

Tel. 020 8954 2300

Centre for Biomedical Engineering,
Institute of Musculoskeletal Science,
Royal National Orthopædic Hospital,
Brockley Hill,
Stanmore,
Middlesex,
HA7 4LP.

Tested between 2nd April– 19th April 2008

Test load level P4

Performance requirements: to sustain cyclic loading between50N and 1230N for 3 million cycles and subsequently 2065N for 30s

Paragraph of BS EN ISO 10328:2006	Direction	Sample 1	Sample 2
16.3.2.2.	Assemble test sample to 16 degrees.	✓	✓
16.3.2.3.	Apply 944N for 10-30 seconds then remove load and record time elapsed.	20 seconds	20 seconds
	Wait 10-20 minutes.	10 minutes	10 minutes
16.3.2.4	Apply 50N and record lever arms.	✓	✓
16.3.2.5	Top offset with application of 50N	68mm	68mm
	Bottom offset with application of 50N	50mm	50mm
16.3.2.6.	Measure displacement of the moving load application point, δ_6.	δ_6=0.04	δ_6=0.06
16.3.2.7	Increase force smoothly to 1230N.	✓	✓
16.3.2.8	Measure displacement of the moving load application point, δ_7.	δ_7=1.00	δ_7=1.33
16.3.2.9	Reduce force to 50N.	✓	✓

Appendix 2

BS EN ISO 10328:2006
Prosthetics – Structural Testing of Lower Limb Prostheses

Test Report – Principal Cyclic Test in Loading Condition 1
Section 16.3.2

16.3.2.10	Apply cyclic force between 50N and 1230N. Check that the waveform is within 50±25N and1230±37N. Ensure waveform is smooth with no overshoot spikes.	✓ ✓ ✓	✓ ✓ ✓
16.3.2.11	Increase force smoothly to 1230N. Measure displacement of the moving load application point, δ_8.	✓ δ_7=1.805	✓ δ_7=1.430
16.3.2.12	apply 50N	✓	✓
16.3.2.13	Apply pulsating force between 50N and 1230N as before Check that the waveform complies with description in 16.3.2.10. Record the frequency of the waveform	✓ ✓ 2.05Hz	✓ ✓ 2.05Hz
16.3.2.17	Continue for 3 million cycles	✓	✓
16.3.2.18	Increase force smoothly to 2065N at between 100-250N/s. Maintain 2065N for 30±3 seconds.	✓ ✓	✓ ✓
16.3.2.19	Record whether or not sample has sustained the cyclic load for 3 million cycles followed by 2065N for 30s.	passed	passed

notes:

graph showing displacement of moving load application point throughout 3 million cycles

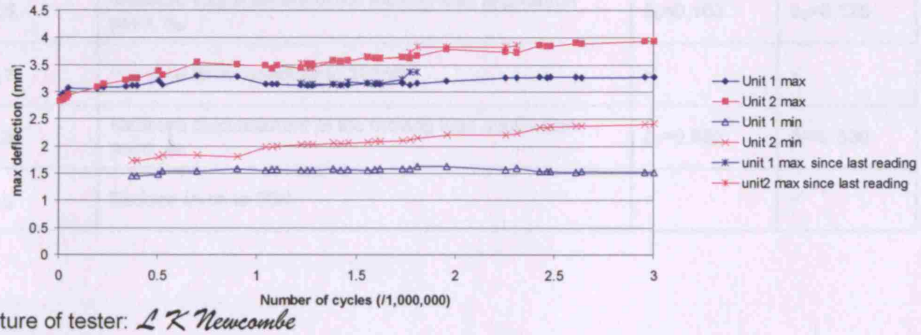

Signature of tester: *L K Newcombe*

Date: *19/4/08*

Appendix 2

BS EN ISO 10328:2006
Prosthetics – Structural Testing of Lower Limb Prostheses

Test Report – Principal Cyclic Test in Loading Condition 2
Section 16.3.2

Prepared by L.K. Newcombe
Centre for Biomedical Engineering,
Institute of Musculoskeletal Science,
Royal National Orthopædic Hospital,
Brockley Hill,
Stanmore,
Middlesex,
HA& 4LP.

Tel. 020 8954 2300

Tested between 21st April– 8th May 2008

Test load level P4

Performance requirements: to sustain cyclic loading between50N and 1035N for 3 million cycles and subsequently 1811N for 30s

Paragraph of BS EN ISO 10328:2006	Direction	Sample 1	Sample 2
16.3.2.2.	Assemble test sample to 6 degrees.	✓	✓
16.3.2.3.	Apply 828N for 10-30 seconds then remove load and record time elapsed.	20 seconds	20 seconds
	Wait 10-20 minutes.	16 minutes	16 minutes
16.3.2.4	Apply 50N and record lever arms.	✓	✓
16.3.2.5	Top offset with application of 50N	68mm	68mm
	Bottom offset with application of 50N	50mm	50mm
16.3.2.6.	Measure displacement of the moving load application point, δ_6.	δ_6=0.103	δ_6=0.126
16.3.2.7	Increase force smoothly to 1035N.	✓	✓
16.3.2.8	Measure displacement of the moving load application point, δ_7.	δ_7=0.882	δ_7=0.530
16.3.2.9	Reduce force to 50N.	✓	✓

Appendix 2

BS EN ISO 10328:2006
Prosthetics – Structural Testing of Lower Limb Prostheses

Test Report – Principal Cyclic Test in Loading Condition 2
Section 16.3.2

16.3.2.10	Apply pulsating force between 50N and 1035N. Check that the waveform is within 50±25N and1035±31N. Ensure waveform is smooth with no overshoot spikes.	✓ ✓ ✓	✓ ✓ ✓
16.3.2.11	Increase force smoothly to 1035N. Measure displacement of the moving load application point, δ_8.	✓ δ_7=0.141	✓ δ_7=-.277
16.3.2.12	apply 50N	✓	✓
16.3.2.13	Apply pulsating force between 50N and 1035N as before Check that the waveform complies with description in 16.3.2.10. Record the frequency of the waveform	✓ ✓ 2.02Hz	✓ ✓ 2.02Hz
16.3.2.17	Continue for 3 million cycles	✓	✓
16.3.2.18	Increase force smoothly to 1811N at between 100-250 N/s. Maintain 1811N for 30±3 seconds.	✓ ✓	✓ ✓
16.3.2.19	Record whether or not sample has sustained the cyclic load for 3 million cycles followed by 1811N for 30s.	passed	passed

Notes:
Test paused at 1,629,000 for repairs to testing machine. Displacement of load application point throughout cyclic test:

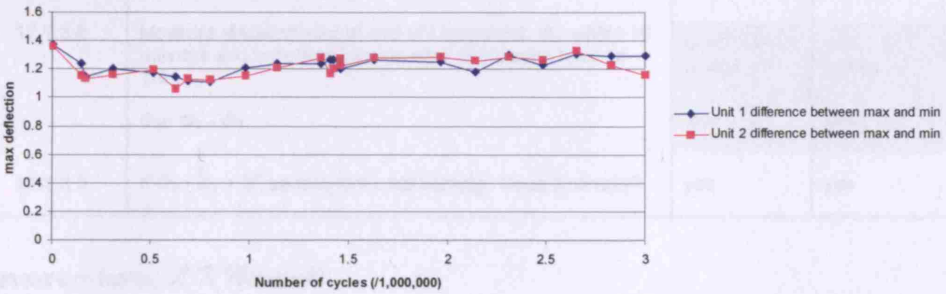

Signature of tester: *L K Newcombe*

Date: *8/5/08*

Appendix 2

BS EN ISO 10328:2006
Prosthetics – Structural Testing of Lower Limb Prostheses

Test Report – Separate Static Test in Torsion
Section 17.1.3

Prepared by L.K. Newcombe
Centre for Biomedical Engineering,
Institute of Musculoskeletal Science,
Royal National Orthopædic Hospital,
Brockley Hill,
Stanmore,
Middlesex,
HA& 4LP.

Tel. 020 8954 2300

Tested on 27th June 2008

Performance requirements: to sustain 50Nm for 30s and twist < 3°

Paragraph of BS EN ISO 10328:2006	Direction	Sample 1	Sample 2
17.1.3.3	Fix the sample in the neutral position at one end of the test sample.	✓	✓
17.1.3.4	Apply 3Nm for 10-30 seconds then remove load and record time elapsed.	20 seconds	20 seconds
	Wait 10-20 minutes.	11 minutes	14 minutes
17.1.3.5	Apply 1Nm and record angle of twist of sample relative to fixed end	✓	✓
17.1.3.6	Angle of twist of sample, Φ_1	Φ_1=1.20°	Φ_1=0.93°
17.1.3.7	Increase force smoothly to 50Nm at no greater than 4 Nm/s.	2.5Nm/s	2.5Nm/s
	Maintain 50Nm for 30±3 seconds.		
	Record whether or not sample has sustained 50Nm for 30s	✓	✓
	Reduce force to 1Nm.	✓	✓
17.1.3.8	Measure displacement of end of component, Φ_2, within 10 minutes and note time interval after decreasing force to 1Nm.	Φ_2=3.54° at 40s	Φ_2= 2.91° at 60s
	$\Phi_3 = \Phi_2 - \Phi_1$	Φ_3= 2.34°	Φ_3=1.98°
17.1.3.9	If $\Phi_2 - \Phi_1 > 3°$ sample does not comply. Does it comply?	yes	yes

Signature of tester: *L K Newcombe*

Date: *27 / 6 / 08*

Appendix 3

Patent Number WO 2005/087145:

Prosthetic Limb Attachment

Appendix 3

Prosthetic Limb Attachment

Field of the Invention

The present invention concerns improvements in and relating to prosthetic limb attachment.

Background to the Invention

In recent years procedures have been developed in which a limb prosthesis (artificial arm or leg) is attached by a bone implant directly to the bone of an amputee's residual limb. As an example of such a procedure, the present applicant's own UK patent application GB-A-2,365,355 describes and illustrates the use of an intra-osseous transcutaneous implant that is secured at a distal end to a limb prosthesis or severed limb and that attaches at a proximal end directly to the bone of the patient's residual limb through the skin. The implant is differentially surface treated, having coatings (e.g. of hydroxy apatite and/or a protein such as laminin or fibronectin to encourage fibrous in-growth) at its proximal end to promote optimal integration with the bone, ligament and skin tissues of the residual limb while having a very low surface energy at its distal (external) end deterring bacterial colonisation at the implant's external skin interface.

The transcutaneous bone implants of GB-A-2,365,355 are relatively securely held in place to the patient's native tissue and are less prone to infection than prior transcutaneous implants. However, in use of these or other direct bone implants for attachment, the attachment can still pose mechanical problems in use. In particular, the joint of the prosthesis to the bone generally has no give and there is a substantial risk that a bending or torsional force applied to the prosthetic limb may either break the bone or cause the bone implant to become detached from it.

The present invention seeks, amongst other objectives, to provide means for addressing the shortcomings of the existing attachments and the bone implant differential coating technology of GB-A-2,365,355 suitably is used in combination with the present invention.

Appendix 3

Summary of the Invention

According to a first aspect of the present invention there is provided an apparatus for attaching a prosthetic limb to the bone of a patient, the apparatus comprising:

i) a proximal component to mount to a bone implant ;

ii) a distal component to mount to a prosthetic limb ; and

iii) a coupling body coupling together the proximal and distal components with freedom to articulate when, in use, a bending and/ or torsional force is applied to the prosthetic limb only when the force exceeds a threshold level whereby the force may be accommodated by articulation within the attachment apparatus.

The attachment apparatus thus functions as a fail-safe articulation mechanism protecting the bone of the patient. Suitably it is first attached to the bone implant component and then has the prosthetic limb attached to it. However, it may be incorporated into the bone implant component or the prosthetic limb and may be, in part or wholly, integrally formed or assembled with the bone implant or the limb prosthesis.

Preferably the coupling body has a clutch mechanism to rotationally couple the prosthetic limb to the bone implant in use but which automatically disengages, rotationally decoupling the prosthetic limb from the bone implant, when torque applied to the prosthetic limb exceeds a predetermined threshold.

The apparatus suitably has a resilient biasing means whereby the clutch mechanism is resiliently biased to the rotationally coupled state and whereof the biasing force applied to the clutch mechanism by the resilient biasing means in use determines the threshold level of torque on the prosthetic limb that will cause disengagement of the clutch mechanism.

Preferably the apparatus has adjustment means whereby the threshold level of torque on the prosthetic limb that will cause disengagement of the clutch mechanism may be increased or decreased. In the case that the apparatus has the aforesaid resilient biasing means, the adjustment means may comprise a screw adjustment

Appendix 3

means that suitably is screw-threadedly adjustable axially toward or away from the clutch mechanism.

Preferably the clutch mechanism has opposing sets of co-operating clutch teeth whereof the teeth are substantially symmetrical in profile whereby the clutch mechanism may be disengaged in either rotational direction of torque, clock-wise or anti-clockwise, applied to the prosthetic limb.

Suitably the clutch mechanism is on the proximal component. This is particularly useful when used in tandem with an automatically disengageable connector to allow tilting, since it will remain effectively operable even when the tilting connector is actuated to tilt. Preferably it is configured to be located external to the patient's skin in use so that there will be no tearing of the patient's skin when the clutch mechanism disengages.

Preferably the coupling body has an automatically disengageable connector that couples together the proximal and distal components so that one is in a fixed angle relation to the other (e.g. axially aligned with or at a fixed angle of incline to the axis of the other) in normal use but with freedom to articulate away from the fixed angle relation when, in use, a bending force is applied to the prosthetic limb only when the force exceeds a threshold level.

The apparatus with disengageable connector suitably has a resilient biasing means whereby the disengageable connector is resiliently biased to the coupled state and whereof the biasing force applied to the disengageable connector by the resilient biasing means in use determines the threshold level of bending force on the prosthetic limb that will cause disengagement of the disengageable connector.

Preferably the disengageable connector comprises a pin mounted to one of the proximal and distal components and co-operating with a socket in the other of the proximal and distal components. Suitably the pin is mounted to be movable back and forth axially of the component to which it is mounted and biased forwardly. Preferably the pin is concentrically mounted within the component.

Appendix 3

Preferably the pin has a domed (e.g. ball-shaped) or pointed tip and the socket is of a corresponding concave shape whereby a bending force applied to the prosthetic limb in use will cause the tip of the pin to ride outwardly up the socket wall.

Suitably the shape of the tip is domed or substantially conical to facilitate disengagement of the disengageable connector whichever radial orientation the bending force is applied from. Preferably such an arrangement is combined with the disengageable connector being configured to allow universal articulation, substantially in the manner of a ball joint, when it disengages.

In one preferred embodiment the disengageable connector comprises a T-shaped formation at the end of one or both of the proximal and distal components that are adjacent each other, the head of the or each T-shaped formation being curved/ arcuate to facilitate tilting of one component relative to the other. Suitably the T-shaped formations substantially nest one against the other and suitably they are accommodated in the coupling body or a further coupling body, to tilt within the coupling body. Amongst special benefits from the use of a disengageable connector of this type in contrast to, say, a ball-in-socket connector, is that the fulcrum about which the distal component tilts is better distanced from the bone implant, further reducing risk of trauma to that area.

Preferably the coupling body has slots therethrough, through each of which a respective end of a head of a T-shaped formation extends and whereby the end may protrude to a greater or lesser extent as the component tilts, whereby the coupling body provides a captive articulated joint with a restricted degree of tilting freedom of movement.

Suitably one T-shaped formation is oriented in the coupling body with its head substantially orthogonal to the head of the other, whereby through tilting of each relative to the other an approximately universal or gyrating articulation may be achieved.

Preferably a coupling part of the apparatus further comprises a shear pin means whereby the apparatus will uncouple at the coupling part through shearing of the shear pin means if an excess tensile/distracting force is applied to it. Suitably the coupling part here is formed at or in the proximal component and the shear pin is

Appendix 3

demountable or retractable whereby the apparatus and prosthesis conveniently may be demounted by the user while the main part of the apparatus and prosthesis remain coupled to each other. Thus the shear pin may serve a dual function, allowing daily mounting and demounting of the prosthesis and failsafe assembly while providing for tensile force failsafe.

Brief Description of the Drawings

A preferred embodiment of the present invention will now be more particularly described, by way of example, with reference to the accompanying drawings, wherein :

Figure 1 is a schematic perspective view of the attachment apparatus of the preferred embodiment;

Figure 2 is a view similar to Figure 1 but with a clutch mechanism part omitted to show the parts of the attachment responsible for bending articulation;

Figure 3 is a view similar to Figure 2 but with a connector body of the attachment removed to show the co-operating ends of the proximal and distal components and how they may move relative to each other;

Figure 4 is a schematic section through the apparatus taken in plane 14 in Figure 3;

Figure 5 is a schematic section through the apparatus taken in plane 16 in Figure 3;

Figure 6 is a detail section corresponding to Figure 4 but showing the latching detail of the coupling that resists bending at the coupling until excessive force is applied;

Figure 6A is a close-up view of the latching detail in Figure 6;

Figure 7 is a view similar to Figure 1 but with the parts of the attachment responsible for bending articulation omitted to highlight the rotation mechanism part;

Appendix 3

Figure 8 is a cut-away view corresponding to Figure 7 and showing the construction of the clutch mechanism that rotationally couples the proximal component for axial rotation with the distal component until excessive torque is applied; and

Figure 9 is a schematic long sectional view of a modified embodiment of the attachment device in which the proximal component is itself split into proximal and distal parts coupled together via a shear pin.

Description of the Preferred Embodiment

An overall view of the attachment apparatus is shown in Fig.1. The attachment apparatus 1 is approximately cylindrical in shape with an elongate proximal component 2 at the proximal end that attaches to the bone implant and an elongate distal component 3 at the distal end to which the prosthetic limb is attached. (In the figures these two components are also shown as cylindrical for convenience, but in practice they may not necessarily be so.)

The apparatus 1 has two movement accommodating mechanisms: one to allow the prosthetic limb to tilt away from axial alignment (or other fixed angle relationship) with the bone implant/residual limb when excessively forced and the other to allow twisting/ axial rotation of the prosthetic limb without twisting/ rotating the bone implant when excessive torque is applied. The twisting/ axial rotation accommodating feature is suitably provided in a clutch unit 4 on the proximal component 2 while the tilting feature 5 is at the interface of the proximal component 2 and distal component 3.

An overall view of the bending/tilting feature 5 is shown in Fig.2. Starting from the position when the proximal and distal components 2 and 3 are in-line the mechanism allows the distal component 3 to tilt in four directions, 7 or 8 and 9 or 10, relative to proximal component 2. By a combination of these movements distal component 3 can therefore tilt (gyrate) in any direction (e.g. 11 is a combination of 7 and 9) without being able to rotate 12 about its own axis. Although in practice it is tilting of distal component 3 relative to proximal component 2 that is significant in terms of the operation of the device, for descriptive purposes it is easier to consider the movement of the components 2, 3 relative to coupling body 13 that couples the components 2, 3 together.

Appendix 3

In Fig.3 the coupling body 13 of the mechanism has been omitted to show the operation of the device. Relative to the body 13 (not shown in Figure 3) the proximal element 2 is constrained to rotate/tilt only in directions 7 or 8, i.e. in the plane 14, by the curved element 15. The distal element 3 is similarly constrained to rotate/tilt only in directions 9 or 10, i.e. in the plane 16 which is orthogonal to plane 14, by the curved element 17.

Fig.4 is a section through the tilting mechanism in the plane 14. The centre of rotation of the proximal element 2 is located at a point 18 proximal to the mechanism. The location of point 18 is determined by tne curvature of the element 15. Element 15 is constrained to move in an arc about the centre 18 by shaped slots 19 and 20 in the body of the mechanism 13.

Fig.5 is a section through the mechanism in the plane 16. In an identical manner to that for the proximal element 2, the distal element 3 is constrained to rotate about the centre of rotation 18. Because the curved element 17 is situated distal to the curved element 15 its radius of curvature is greater than that of element 15 so that the centres of rotation are coincident at point 18.

In the normal situation the elements 2 and 3 are prevented from moving relative to each other by the latching mechanism shown in Fig.6. A pin, here shown as a cylindrical element 21 which is free to slide in a hole 22 in the centre of element 2 has a conical tip which engages in a correspondingly shaped socket/depression 23 in the end of element 3. Pin 21 is kept in engagement with the depression 23 by compression of the spring 24 that biases the pin 21 forwardly.

The tilt fail-safe mechanism is activated when a force tending to tilt distal component 3 relative to proximal component 2 is sufficient to cause the tip 25 to slide up the angled side 26 of the depression 23, further compressing the spring 24. The magnitude of the force required to do this can be controlled by the amount of the compression of the spring 24. This in turn is controlled by the element 27 which is a threaded fit in the hole 22 and whose position can be changed by a screw adjustment. Once the tip 25 has been pushed out of the depression 23 it drops into a circular groove 28. Further angulation of proximal component 2 and/or distal component 3 is prevented by the physical limit imposed by the body 13.

Appendix 3

An overall view of the clutch/axial rotation mechanism unit 4 is shown in Fig.7. It couples (partial) axial rotation 12 of the distal component 3 with the proximal component 2 until the applied torque exceeds a safe level, at which point the two are uncoupled and the proximal component rotation is then able to occur.

The construction of the clutch mechanism 4 is shown diagrammatically in Fig.8. The radially serrated face 29 on the end of distal component 3 engages with a similarly serrated face 30 on the end of a cylindrical-shaped pin 31. Pin 31 is free to slide inside the hole 32 in the centre of proximal component 2 but is prevented from rotating relative to it by a key (not shown) which engages in longitudinal grooves in the outer wall of element 31 and in the inner wall of element 2. The faces 29 and 30 are held in engagement by the spring 33 exerting a distal force on element 30 while the outer case of the mechanism 34 exerts a proximal force on element 3. Compression of the spring 33 is controlled by screw adjustment of the cylindrical element 35 which is a threaded fit within the hole 32.

The axial rotation fail-safe mechanism triggered when a torque tending to rotate distal component 3 relative to proximal component 2 is sufficient to cause the sloping faces of the serrations of faces 29 and 30 to slide past one another, further compressing the spring 33.

As a further facility to failsafe against excessive forces (specifically tensile forces) the proximal component is suitably subdivided into proximal and distal parts 2a, 2b coupled together by a shear pin. Referring to Figure 9, the proximal part 2a of the proximal component 2 that mounts in the bone is coupled to the distal part 2b by extending into a socket in the distal part 2b and is held in place by shear pin 43 that extends through the wall of the socket in the distal part 2b and into co-operative engagement with a groove 44 formed in a lateral face of the proximal part 2a of proximal component 2. The shear pin 43 is threaded to enable it to be adjusted in its extent of projection into the socket and hence into the groove 44 of the proximal part 2a of proximal component 2 to lock the latter in place.

At the end of the shear pin 43 which co-operatively engages with the groove 44 there is provided a weakened neck zone 46 whereby that end of the shear pin 43 may break off when excessive tensile/pulling force is applied to the joint distracting

Appendix 3

the joint. Accordingly, the articulation of the attachment device of the present invention will generally protect the patient's residual limb from harm when excess torsional or lateral forces are applied to it and the shear pin coupling will protect the patient's residual limb from excessive tensile forces on the prosthetic limb.

The shear pin coupling usefully doubles as means for daily mounting and demounting of the prosthesis from the patient's residual limb as well as providing tensile failsafe, simply by demounting the shear pin 43 by unscrewing it from engagement with groove 44.

Appendix 3

Claims

1. An apparatus for attaching a prosthetic limb to the bone of a patient, the apparatus comprising:
a proximal component to mount to a bone implant ;
a distal component to mount to a prosthetic limb ; and
a coupling body coupling together the proximal and distal components with freedom to articulate when, in use, a bending and/ or torsional force is applied to the prosthetic limb only when the force exceeds a threshold level whereby the force may be accommodated by articulation within the attachment apparatus.

2. An apparatus as claimed in Claim 1, wherein the apparatus is incorporated into the bone implant component or the prosthetic limb , being in part or wholly, integrally formed or assembled with the bone implant or the limb prosthesis.

3. An apparatus as claimed in Claim 1 or Claim 2, wherein the coupling body has a clutch-like mechanism to rotationally couple the prosthetic limb to the bone implant in use but which automatically disengages, rotationally decoupling the prosthetic limb from the bone implant, when torque applied to the prosthetic limb exceeds a predetermined threshold.

4. An apparatus as claimed in Claim 3, wherein the apparatus has a resilient biasing means whereby the clutch mechanism is resiliently biased to the rotationally coupled state and whereof the biasing force applied to the cutch-like mechanism by the resilient biasing means in use determines the threshold level of torque on the prosthetic limb that will cause disengagement of the clutch.

5. An apparatus as claimed in Claim 3 or 4, wherein the apparatus has adjustment means whereby the threshold level of torque on the prosthetic limb that will cause disengagement of the clutch-like mechanism may be increased or decreased.

6. An apparatus as claimed in Claim 5 as dependent on Claim 4, wherein the adjustment means comprises a screw adjustment means that is screw-threadedly adjustable axially toward or away from the clutch-like mechanism.

Appendix 3

7. An apparatus as claimed in any of Claims 3, 4, 5 or 6, wherein the clutch-like mechanism has opposing sets of co-operating clutch teeth whereof the teeth are substantially symmetrical in profile whereby the clutch-like mechanism may be disengaged in either rotational direction of torque, clock-wise or anti-clockwise, applied to the prosthetic limb.

8. An apparatus as claimed in any of Claims 3, 4, 5, 6 or 7, wherein the clutch-like mechanism is on the proximal component but is configured to be located external to the patient's skin in use so that there will be no tearing of the patient's skin when the clutch-like mechanism disengages.

9. An apparatus as claimed in any preceding claim, wherein the coupling body has an automatically disengageable connector that couples together the proximal and distal components so that one is in a fixed angle relation to the other (e.g. axially aligned with or at a fixed angle of incline to the axis of the other) in normal use, but with freedom to articulate away from the fixed angle relation when, in use, a bending force is applied to the prosthetic limb only when the force exceeds a threshold level.

10. An apparatus as claimed in any preceding claim, wherein the apparatus with disengageable connector has a resilient biasing means whereby the disengageable connector is resiliently biased to the coupled state and whereof the biasing force applied to the disengageable connector by the resilient biasing means in use determines the threshold level of bending force on the prosthetic limb that will cause disengagement of the disengageable connector.

11. An apparatus as claimed in Claim 10, wherein the disengageable connector comprises a pin mounted to one of the proximal and distal components and co-operating with a socket in the other of the proximal and distal components.

12. An apparatus as claimed in Claim 11, wherein the pin is mounted to be movable back and forth axially of the component to which it is mounted and is biased forwardly.

Appendix 3

13. An apparatus as claimed in Claim 11 or 12, wherein the pin has a pointed or domed tip and the socket is of a corresponding concave shape whereby a bending force applied to the prosthetic limb in use will cause the tip of the pin to ride outwardly up the socket wall.

14. An apparatus as claimed in Claim 13, wherein the shape of the tip is domed or substantially conical to facilitate disengagement of the disengageable connector whichever radial orientation the bending force is applied from.

15. An apparatus as claimed in any of Claims 9 to 14, wherein the disengageable connector is configured to allow gyrating articulation or universal articulation, substantially in the manner of a ball joint, when it disengages.

16. An apparatus as claimed in any of Claims 9 to 15, wherein the disengageable connector comprises a T-shaped formation at the end of one or both of the proximal and distal components that are adjacent each other, the head of the or each T-shaped formation being curved/ arcuate to facilitate tilting of one component relative to the other.

17. An apparatus as claimed in Claim 16, wherein the T-shaped formations are accommodated in the coupling body, or a further coupling body, to tilt within the coupling body.

18. An apparatus as claimed in Claim 17, wherein the coupling body has slots therethrough, through each of which a respective end of a head of a T-shaped formation extends and whereby the end may protrude to a greater or lesser extent as the component tilts, whereby the coupling body provides a captive articulated joint with a restricted degree of tilting freedom of movement.

19. An apparatus as claimed in Claim 17 or 18, wherein one T-shaped formation is oriented in the coupling body with its head substantially orthogonal to the head of the other, whereby through tilting of each relative to the other an approximately universal or gyrating articulation may be achieved.

20. An apparatus as claimed in any preceding claim, wherein a coupling part of the apparatus has a shear pin means whereby the apparatus will uncouple at the

Appendix 3

coupling part through shearing of the shear pin means if an excess tensile distracting force is applied to it.

21. An apparatus as claimed in Claim 20, wherein the coupling part is formed at or in the proximal component and the shear pin is demountable or retractable whereby the apparatus and prosthesis may be demounted by the user.

Appendix 3

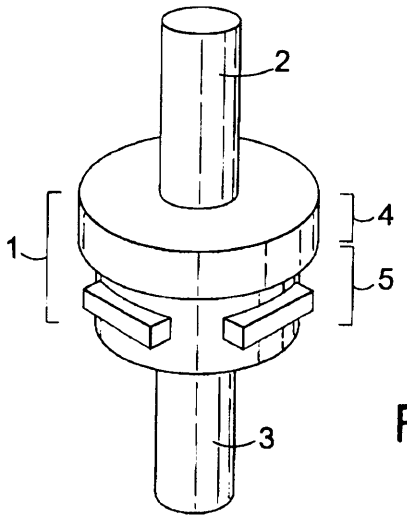

Fig. 1

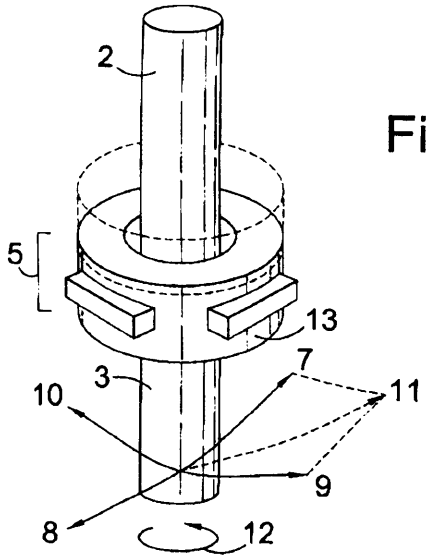

Fig. 2

Appendix 3

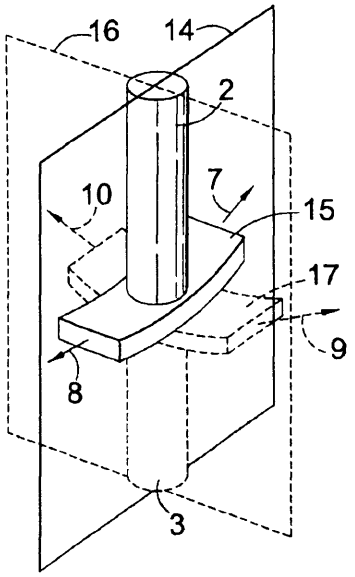

Fig. 3

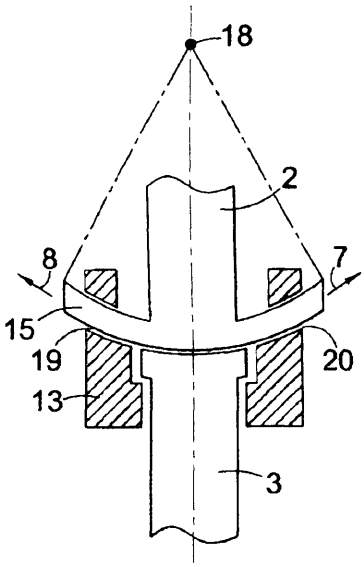

Fig. 4

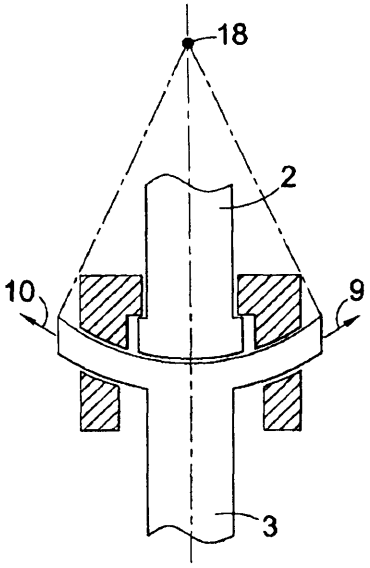

Fig. 5

Appendix 3

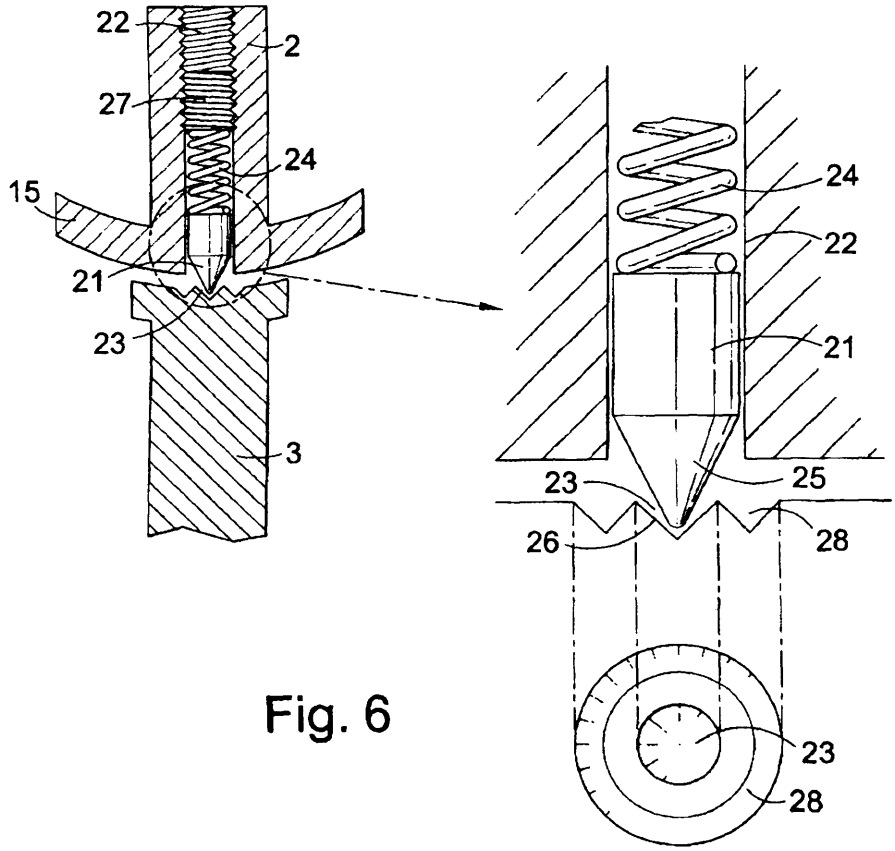

Fig. 6

Appendix 3

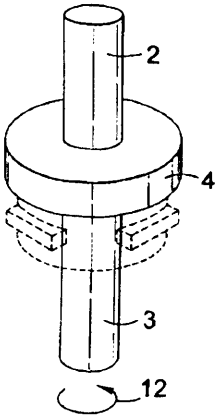

Fig. 7

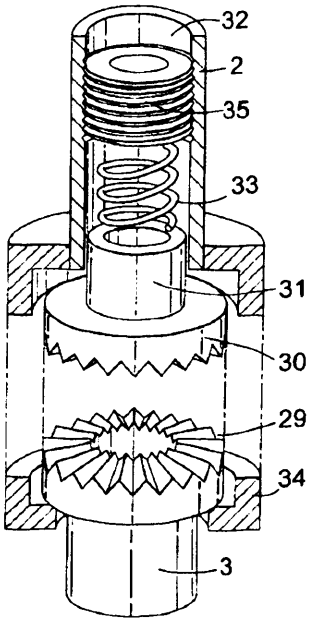

Fig. 8

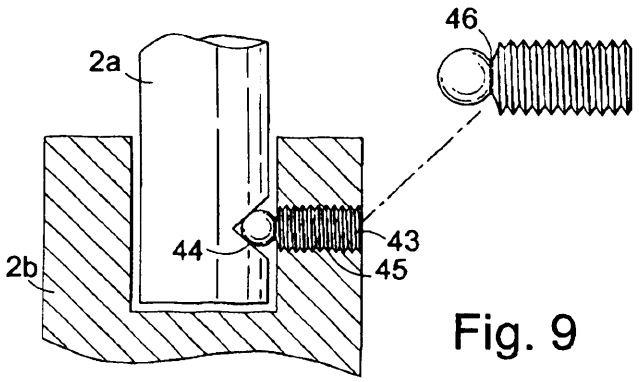

Fig. 9

References

Adell,R., Eriksson,B., Lekholm,U., Brånemark ,P.I., and Jemt,T. (1990) Long-term follow-up study of osseointegrated implants in the treatment of totally edentulous jaws. *Int.J.Oral Maxillofac.Implants.* **5,** 347-359.

Aebli,N., Krebs,J., Stich,H., Schawalder,P., Walton,M., Schwenke,D., Gruner,H., Gasser,B., and Theis,J.C. (2003) In vivo comparison of the osseointegration of vacuum plasma sprayed titanium- and hydroxyapatite-coated implants. *J.Biomed.Mater.Res.A* **66,** 356-363.

Aerssens,J., Boonen,S., Lowet,G., and Dequeker,J. (1998) Interspecies differences in bone composition, density, and quality: potential implications for in vivo bone research. *Endocrinology* **139,** 663-670.

Albrektsson,T., Jansson,T., and Lekholm, U. (1986) Osseointegrated dental implants. *Dent.Clin.North Am.* **30,** 151-174.

Arcuri,M.R. (1995) Titanium implants in maxillofacial reconstruction. *Otolaryngol. Clin.North Am.* **28,** 351-363.

Ashman,R.B. and Rho,J.Y. (1988) Elastic modulus of trabecular bone material. *J.Biomech.* **21,** 177-181.

Ax,E. Keynote Speech, the International SOciety for Prosthetics and Orthotics. 2004.

Barsby,P. (1995) Trans-femoral (above knee) Amputation. In *Amputee Management -- A Handbook* Pp. 180-202. Kings College School of Medicine and Dentistry, London.

Bassey,E.J., Littlewood,J.J., and Taylor,S.J. (1997) Relations between compressive axial forces in an instrumented massive femoral implant, ground reaction forces, and integrated electromyographs from vastus lateralis during various 'osteogenic' exercises. *J.Biomech.* **30,** 213-223.

References

Bauer,T.W., Geesink,R.C., Zimmerman, R., and McMahon,J.T. (1991) Hydroxy-apatite-coated femoral stems. Histo-logical analysis of components retrieved at autopsy. *J.Bone Joint Surg.Am.* **73,** 1439-1452.

Bell,G.H., Dunbar,O., Beck,J.S., and Gibb,A. (1967) Variations in strength of vertebrae with age and their relation to osteoporosis. *Calcif.Tissue Res.* **1,** 75-86.

Bergmann,G., Graichen,F., and Rohl-mann ,A. (1995) Is staircase walking a risk for the fixation of hip implants? *J.Biomech.* **28,** 535-553.

Black,J. and Hastings,G. (1998) *Handbook of Biomaterial Properties.* Chapman and Hall.

Blunn,G., Cobb,J.P., Unwin,P., and Goodship,A.E. Transcutaneous Pros-thesis. 0115381.6[GB 2 365 355 A]. 2001. United Kingdom Patent

Blunn,G.W., Briggs,T.W., Cannon,S.R., Walker,P.S., Unwin,P.S., Culligan,S., and Cobb,J.P. (2000) Cementless fixation for primary segmental bone tumor endoprostheses. *Clin.Orthop.Relat Res.* 223-230.

Brånemark ,P.I. (1997) Osseointegration: Biotechnological Perspective and Clinical Modality. In *Osseointegration in Skeletal Reconstruction and Joint Replacement* (Edited by Brånemark, P.I., Rydevik,B.L., and Skalak,R.) Pp. 1-24. Quintessence Books, London.

Brånemark,P.I., Hansson,B.O., Adell,R., Breine,U., Lindstrom,J., Hallen,O., and Ohman,A. (1977) Osseointegrated implants in the treatment of the edentulous jaw. Experience from a 10-yearperiod.*Scand.J.Plast.Reconstr.Surg. Suppl* **16,** 1-132.

Brånemark, R. and Skalak,R. (1998) An in-vivo method for biomechanical characterization of bone-anchored implants. *Med.Eng Phys.* **20,** 216-219.

Breme,J. and Biehl,V. (1998) Titanium and Titanium Alloys. In *Handbook of Biomaterial Properties* (Edited by Black,J. and Hastings,G.) Pp. 179-200. Chapman and Hall.

Brown,T.D., Pedersen,D.R., Gray,M.L., Brand,R.A., and Rubin,C.T. (1990) Toward an identification of mechanical parameters initiating periosteal remodeling: a combined experimental and analytic approach. *J.Biomech.* **23,** 893-905.

Buckley,J.G. (1999) Sprint kinematics of athletes with lower-limb amputations. *Arch.Phys.Med.Rehabil.* **80,** 501-508.

Buma,P., Elmans,L., and Oestricher,A.B. Changes in innervation of long bones after insertion of an implant: Immunohistochemical study in goats with antibodies to calcitonin gene-related peptide and B-50/GAP-43. Journal of Orthopaedic Research 13, 570-577. 1995.

Burkett,B., Smeathers,J., and Barker,T. (2003) Walking and running inter-limb asymmetry for Paralympic trans-femoral amputees, a biomechanical analysis. *Prosthet.Orthot.Int.* **27,** 36-47.

Burstein,A.H. and Wright,T.M. (1994) In *Fundamentals of Orthopaedic Biomechanics* (Edited by Williams and Wlikins) Pp. 34. New York.

Callister,W.D. (1997) *Materials Science and Engineering: an Introduction.* John Wiley and Sons Inc..

Carter,D.R. and Hayes,W.C. (1977) The compressive behavior of bone as a two-phase porous structure. *J.Bone Joint Surg.Am.* **59,** 954-962.

References

Cezayirlioglu,H., Bahniuk,E., Davy,D.T., and Heiple,K.G. (1985) Anisotropic yield behavior of bone under combined axial force and torque. *J.Biomech.* **18,** 61-69.

Cheal,E.J., Spector,M., and Hayes,W.C. (1992) Role of loads and prosthesis material properties on the mechanics of the proximal femur after total hip arthroplasty. *J.Orthop.Res.* **10,** 405-422.

Cheung,L.K. and Leung,A.C. (2003) Dental implants in reconstructed jaws: implant longevity and peri-implant tissue outcomes. *J.Oral Maxillofac.Surg.* **61,** 1263-1274.

Coathup,M.J., Blunn,G.W., Flynn,N., Williams,C., and Thomas,N.P. (2001) A comparison of bone remodelling around hydroxyapatite-coated, porous-coated and grit-blasted hip replacements retrieved at post-mortem. *J.Bone Joint Surg.Br.* **83,** 118-123.

Cook,S.D., Thomas,K.A., Kay,J.F., and Jarcho,M. (1988) Hydroxyapatite-coated titanium for orthopedic implant applications. *Clin.Orthop.Relat Res.* 225-243.

Cowin,S.C. (1984) Mechanical modeling of the stress adaptation process in bone. *Calcif.Tissue Int.* **36 Suppl 1,** S98-103.

Crismani,A.G., Bernhart,T., Schwarz,K., Celar,A.G., Bantleon,H.P., and Watzek,G. (2006) Ninety percent success in palatal implants loaded 1 week after placement: a clinical evaluation by resonance frequency analysis. *Clin.Oral Implants.Res.* **17,** 445-450.

Currey,J.D. (1984) Effects of differences in mineralization on the mechanical properties of bone. *Philos.Trans.R.Soc.Lond B Biol.Sci.* **304,** 509-518.

Czerniecki,J.M. and Gitter,A.J. (1995) Gait Analysis in the Amputee: Has it Helped the Amputee or Contributed to the Development of Improved Prosthetic Components? *Gait and Posture* **4,** 258-268.

Dahlstrom,L. (1999) A Summary of the work of Torgny Haraldson. In *Osseoperception and Musculo-skeletal Function* (Edited by Williams,E., Rydevik,B.L., Johns,R., and Brånemark, P.I.) Pp. 68-85. The Institute for Applied Biotechnology.

Dalby,M.J., Di Silvio,L., Harper,E.J., and Bonfield,W. (2001) Initial interaction of osteoblasts with the surface of a hydroxyapatite-poly(methylmethacrylate) cement. *Biomaterials* **22,** 1739-1747.

Davis,R.R. and Hull,M.L. (1981) Measurement of pedal loading in bicycling: II. Analysis and results. *J.Biomech.* **14,** 857-872.

Dempster,W.T. and Liddicoat,R.T. (1952) Compact bone as a non-isotropic material. *Am.J.Anat.* **91,** 331-362.

Ducheyne,P., De Meester,P., and Aernoudt,E. (1977) Influence of a functional dynamic loading on bone ingrowth into surface pores of orthopedic implants. *J.Biomed.Mater.Res.* **11,** 811-838.

Duda,G.N., Schneider,E., and Chao,E.Y. (1997) Internal forces and moments in the femur during walking. *J.Biomech.* **30,** 933-941.

Evans,F.G. (1973) Factors affecting the mechanical properties of bone. *Bull.N.Y.Acad.Med.* **49,** 751-764.

Gibson,L.J. (1985) The mechanical behaviour of cancellous bone. *J.Biomech.* **18,** 317-328.

References

Glabiszewiki,R. Justierbares Verbindungselement zwischen Prothesenteilen 'Connecting part between leg prosthesis components'. [DE1922619]. 1960. Patent

Gray,H. (1898a) Organs of digestion. In *Anatomy Descriptive and Surgical* Pp. 598-601. Robinson Publishing Ltd, London.

Gray,H. (1898) Osteology part 3: The Femur. In *Gray's Anatomy* Robinson Publishing Ltd, London.

Gray,H. (1898b) The Skeleton. In *Anatomy Descriptive and Surgical* (Edited by Parragon) Pp. 121-126.

Grundei,H. Transkutanes Lager fur ein Starres Implantat. 19931882.4-35[DE 19931882 C1]. 2001. Germany. Patent

Grundei,H. Subcutaneous, Intra-muscular Coupling for a Rigid Transcutaneous Implant. 10040590.8[WO 02 13729 A1]. 2002. Patent

Haberman,L.J. Silicone-Only Suspension (SOS) with Socket-Loc and the Ring for the Lower Limb. Journal of Prosthetics and Orthotics 7[1], 2-14. 1995.

Heimke,G., Stock,D., Busing,C.M., and von Mallinckrodt,D. (1989) Biomechanical considerations on some postoperative problems of directly anchored total hip replacements. *J.Biomed.Mater.Res.* **23,** 679-684.

Helgason,B., Viceconti,M., Runarsson,T.P., and Brynjolfsson,S. (2008) On the mechanical stability of porous coated press fit titanium implants: a finite element study of a pushout test. *J.Biomech.* **41,** 1675-1681.

Hench,L.L. and Paschall,H.A. (1973) Direct chemical bond of bioactive glass-ceramic materials to bone and muscle. *J.Biomed.Mater.Res.* **7,** 25-42.

Hernandez,C.J., Tang,S.Y., Baumbach,B.M., Hwu,P.B., Sakkee,A.N., van der,H.F., DeGroot,J., Bank,R.A., and Keaveny,T.M. (2005) Trabecular microfracture and the influence of pyridinium and non-enzymatic glycation-mediated collagen cross-links. *Bone* **37,** 825-832.

Hing,K.A., Wilson,L.F., and Buckland,T. (2007) Comparative performance of three ceramic bone graft substitutes. *Spine J.* **7,** 475-490.

Hodge,W.A., Fijan,R.S., Carlson,K.L., Burgess,R.G., Harris,W.H., and Mann,R.W. (1986) Contact pressures in the human hip joint measured in vivo. *Proc.Natl.Acad.Sci.U.S.A* **83,** 2879-2883.

Holgers,K.M., Thomsen,P., Tjellstrom,A., and Bjursten,L.M. (1995) Immunohistochemical study of the soft tissue around long-term skin-penetrating titanium implants. *Biomaterials* **16,** 611-616.

Huang,H.M., Chiu,C.L., Yeh,C.Y., Lin,C.T., Lin,L.H., and Lee,S.Y. (2003) Early detection of implant healing process using resonance frequency analysis. *Clin.Oral Implants.Res.* **14,** 437-443.

Huwiler,M.A., Pjetursson,B.E., Bosshardt,D.D., Salvi,G.E., and Lang,N.P. (2007) Resonance frequency analysis in relation to jawbone characteristics and during early healing of implant installation. *Clin.Oral Implants.Res.* **18,** 275-280.

References

Jansson,E., Kalltorp,M., Johansson,A., Tengvall,P., and Thomsen,P. (2001) On the formation of fibrous capsule and fluid space around machined and porous blood plasma clot coated titanium. *J.Mater.Sci.Mater.Med.* **12,** 1019-1024.

Kardos,J.L. (1985) Critical Issues in Achieving Desirable Mechanical-Properties for Short Fiber Composites. *Pure and Applied Chemistry* **57,** 1651-1657.

Keaveny,T.M. and Bartel,D.L. (1994) Fundamental load transfer patterns for press-fit, surface-treated intramedullary fixation stems. *J.Biomech.* **27,** 1147-1157.

Keaveny,T.M. and Hayes,W.C. (1993) A 20-year perspective on the mechanical properties of trabecular bone. *J.Biomech.Eng* **115,** 534-542.

Keaveny,T.M., Wachtel,E.F., Zadesky,S.P., and Arramon,Y.P. (1999) Application of the Tsai-Wu quadratic multiaxial failure criterion to bovine trabecular bone. *J.Biomech.Eng* **121,** 99-107.

Keller,T.S., Weisberger,A.M., Ray,J.L., Hasan,S.S., Shiavi,R.G., and Spengler,D.M. (1996) Relationship between vertical ground reaction force and speed during walking, slow jogging, and running. *Clin.Biomech.(Bristol., Avon.)* **11,** 253-259.

Klute,G.K., Kallfelz,C.F., and Czerniecki,J.M. (2001) Mechanical Properties of Prosthetic Limbs: Adapting to the Patient. *J.Rehabil.Res.Dev.* **38**.

Lasaygues,P., Pithioux,M., and Chabrand,P. An Alternative Ultrasonic Method for Measuring the Elastic Propertie of Cortical Bone. J.Biomech. 35[7], 961-968. 2002.

Lee,W.C., Frossard,L.A., Hagberg,K., Haggstrom,E., Brånemark, R., Evans, J.H., and Pearcy,M.J. (2007a) Kinetics of transfemoral amputees with osseointegrated fixation performing common activities of daily living. *Clin.Biomech.(Bristol., Avon.)* **22,** 665-673.

Lee,W.C., Frossard,L.A., Hagberg,K., Haggstrom,E., Gow,D.L., Gray,S., and Brånemark, R. (2007b) Magnitude and variability of loading on the osseointegrated implant of transfemoral amputees during walking. *Med.Eng Phys.*

Magyar,G., Toksvig-Larsen,S., and Moroni,A. (1997) Hydroxyapatite coating of threaded pins enhances fixation. *J.Bone Joint Surg.Br.* **79,** 487-489.

Mandell,J.A., Carter,D.R., Goodman,S.B., Schurman,D.J., and Beaupre,G.S. (2004) A conical-collared intramedullary stem can improve stress transfer and limit micromotion. *Clin.Biomech.(Bristol., Avon.)* **19,** 695-703.

Marks,L.J. and Michael,J.W. Artificial Limbs. Science, Medicine and the Future, Clinical Review. British Medical Journal 323, 732-735. 2001.

Martini,B. (2000) *Essentials of Anatomy and Physiology*. Prentice Hall.

Maruthainar,K., Dunstan,E.R., Hamilton,P.D., Unwin,P., Cannon,S.R., and Briggs,T.W. (2006) Massive endoprostheses for giant cell tumours of the distal femur: A 12-year follow-up. *Knee.* **13,** 378-381.

McKenzie,D.W. (1977) Standards for Lower-Limb Prostheses (Status of the Program).

References

Melnis,A.E. and Knets,I.V. (1981) Effect of the rate of deformation on the mechanical properties of compact bone tissue. *Mechanics of Composite Materials* **18,** 358-365.

Meredith,N., Shagaldi,F., Alleyne,D., Sennerby,L., and Cawley,P. (1997) The application of resonance frequency measurements to study the stability of titanium implants during healing in the rabbit tibia. *Clin.Oral Implants.Res.* **8,** 234-243.

Michael,J.W. (1989) Current concepts in Above-Knee Socket Design. In *Amputation and Prosthetic Management of the Lower Limb* Pp. 373-378.

Miller,Z., Fuchs,M.B., and Arcan,M. (2002) Trabecular bone adaptation with an orthotropic material model. *J.Biomech.* **35,** 247-256.

Moore,P. 2003.
Personal Communication

Moroni,A., Aspenberg,P., Toksvig-Larsen,S., Falzarano,G., and Giannini,S. (1998) Enhanced fixation with hydroxyapatite coated pins. *Clin. Orthop.Relat Res.* 171-177.

Murdoch,G. and Bennet Wilson Jr,A. Amputation. Surgical Practice and Patient Management. Gottschalk, F. A. and Jaegers, S. M. H. J. Transfemoral Amputation. 111-119. 1990. Butterworth Heinemann.

Natali,A.N. and Meroi,E.A. (1989) A review of the biomechanical properties of bone as a material. *J.Biomed.Eng* **11,** 266-276.

Natali,A.N. and Pavan,P.G. (2002) A comparative analysis based on different strength criteria for evaluation of risk factor for dental implants. *Comput.Methods Biomech.Biomed.Engin.* **5,** 127-133.

Orlic,D., Smerdelj,M., Kolundzic,R., and Bergovec,M. (2006) Lower limb salvage surgery: modular endoprosthesis in bone tumour treatment. *Int.Orthop.* **30,** 458-464.

Owens,L.J. Apparatus for Connecting a Prosthesis to a Bone. 559108[US 3947897]. 1976. Patent

Oxford English Dictionary . Oxford English Dictionary, Second Edition. 1989.

Peters,S. (1998) Introduction, Composite Basics and Road Map. In *Handbook of Composites(2nd Edition).*Pp.18. Springer-Verlag.

Pietruszczak,S., Inglis,D., and Pande,G.N. (1999) A fabric-dependent fracture criterion for bone. *J.Biomech.* **32,** 1071-1079.

Placzek,R., Ruffer,M., Deuretzbacher,G., Heijens,E., and Meiss,A.L. (2006) The fixation strength of hydroxyapatite-coated Schanz screws and standard stainless steel Schanz screws in lower extremity lengthening : a comparison based on a new torque value index: the fixation index. *Arch.Orthop.Trauma Surg.* **126,** 369-373.

Popovic,D., Oguztoreli,M.N., and Stein,R.B. (1995) Optimal control for an above-knee prosthesis with two degrees of freedom. *J.Biomech.* **28,** 89-98.

Porta,D.J., Frick,S.J., Kress,T.A., and Fuller,P.M. (1997) Production of spiral fractures in human cadaver long bones by use of a simple torsion machine. *Biomed.Sci.Instrum.* **33,** 418-422.

Porter,A.E., Patel,N., Skepper,J.N., Best,S.M., and Bonfield,W. (2003) Comparison of in vivo dissolution processes in hydroxyapatite and silicon-substituted hydroxyapatite bioceramics. *Biomaterials* **24,** 4609-4620.

References

Prendergast,P.J. (1997) Finite element models in tissue mechanics and orthopaedic implant design. *Clin.Biomech.(Bristol., Avon.)* **12,** 343-366.

Puelo,D.A. and Nanci,A. (1999) Understanding and Controlling the Bone-Implant Interface. *Biomaterials* **20,** 2311-2321.

Pugh,J.W., Rose,R.M., and Radin,E.L. (1973) A structural model for the mechanical behavior of trabecular bone. *J.Biomech.* **6,** 657-670.

Ramos,A. and Simoes,J.A. (2006) Tetrahedral versus hexahedral finite elements in numerical modelling of the proximal femur. *Med.Eng Phys.* **28,** 916-924.

Reilly,D.T. and Burstein,A.H. (1974) Review article. The mechanical properties of cortical bone. *J.Bone Joint Surg.Am.* **56,** 1001-1022.

Reilly,D.T. and Burstein,A.H. (1975) The elastic and ultimate properties of compact bone tissue. *J.Biomech.* **8,** 393-405.

Reilly,D.T., Burstein,A.H., and Frankel, V.H. (1974) The elastic modulus for bone. *J.Biomech.* **7,** 271-275.

Restwick,J.B., Mooney,V., Owens,L.J., and Bright,C.W. Prosthesis Coupling. 876438[US 4158895]. 1979.
Ref Type: Patent

Rho,J.Y., Hobatho,M.C., and Ashman,R.B. (1995) Relations of mechanical properties to density and CT numbers in human bone. *Med.Eng Phys.* **17,** 347-355.

Robinson,K.P. 2007.
Personal Communication

Rougraff,B.T., Simon,M.A., Kneisl,J.S., Greenberg,D.B., and Mankin,H.J. (1994) Limb salvage compared with amputation for osteosarcoma of the distal end of the femur. A long-term oncological, functional, and quality-of-life study. *J.Bone Joint Surg.Am.* **76,** 649-656.

Rubin,C.T., McLeod,K.J., and Bain,S.D. (1990) Functional strains and cortical bone adaptation: epigenetic assurance of skeletal integrity. *J.Biomech.* **23 Suppl 1,** 43-54.

Rush,P.J., Wong,J.S., Kirsh,J., and Devlin,M. (1994) Osteopenia in patients with above knee amputation. *Arch.Phys.Med.Rehabil.* **75,** 112-115.

Rydevik,B. (1997) Amputation Prostheses and Osseoperception in the Lower and Upper extremity. In *Osseointegration in Skeletal Reconstruction and Joint Replacement* (Edited by Brånemark, P.I., Rydevik,B.L., and Skalak,R.) Pp. 175-182. Quintessence Books, London.

Sanderson,D.J. and Martin,P.E. (1996) Joint kinetics in unilateral below-knee amputee patients during running. *Arch.Phys.Med.Rehabil.* **77,** 1279-1285.

Schindler,O.S., Cannon,S.R., Briggs,T.W., Blunn,G.W., Grimer,R.J., and Walker,P.S. (1998) Use of extendable total femoral replacements in children with malignant bone tumors. *Clin.Orthop.Relat Res.* 157-170.

Shahar,R., Zaslansky,P., Barak,M., Friesem,A.A., Currey,J.D., and Weiner,S (2007) Anisotropic Poisson's ratio and compression modulus of cortical bone determined by speckle interferometry. *J.Biomech.* **40,** 252-264.

Shao,F., Xu,W., Crocombe,A., and Ewins,D. (2007) Natural frequency analysis of osseointegration for trans-femoral implant. *Ann.Biomed.Eng* **35,** 817-824.

References

Sherk,V.D., Bemben,M.G., and Bemben,D.A. (2008) BMD and bone geometry in transtibial and transfemoral amputees. *J.Bone Miner.Res.* **23,** 1449-1457.

Shultz,T.R., Blaha,J.D., Gruen,T.A., and Norman,T.L. (2006) Cortical bone viscoelasticity and fixation strength of press-fit femoral stems: finite element model. *J.Biomech.Eng* **128,** 7-12.

Simon,M.A., Aschliman,M.A., Thomas,N., and Mankin,H.J. (1986) Limb-salvage treatment versus amputation for osteosarcoma of the distal end of the femur. *J.Bone Joint Surg.Am.* **68,** 1331-1337.

Stephenson,P. (1999) Direct skeletal fixation of an artificial limb for transfemoral amputees. A biomechanical evaluation. University of Leeds, dissertation for award of PhD.

Stephenson,P. and Seedhom,B.B. (1999) Cross-sectional geometry of the human femur in the mid-third region. *Proc.Inst.Mech.Eng [H.]* **213,** 159-166.

Stephenson,P. and Seedhom,B.B. (2002b) Estimation of forces at the interface between an artificial limb and an implant directly fixed into the femur in above-knee amputees. *J.Orthop.Sci.* **7,** 292-297.

Stephenson,P. and Seedhom,B.B. (2002a) Estimation of forces at the interface between an artificial limb and an implant directly fixed into the femur in above-knee amputees. *J.Orthop.Sci.* **7,** 292-297.

Strait,D.S., Wang,Q., Dechow,P.C., Ross,C.F., Richmond,B.G., Spencer, M.A., and Patel,B.A. (2005) Modeling elastic properties in finite-element analysis: how much precision is needed to produce an accurate model? *Anat.Rec.A Discov.Mol.Cell Evol.Biol.* **283,** 275-287.

Sullivan,J. 2007. Personal Communication

Sullivan,J., Uden,M., Robinson,K.P., and Sooriakumaran,S. Rehabilitation of the Tans-Femoral Amputee with an Osseointegrated Prosthesis: the United Kingdom Experience. Prosthetics and Orthotics International 27, 114-120. 2003.

Suzuki,S., Watanabe,S., and Homma,S. (1982) EMG activity and kinematics of human cycling movements at different constant velocities. *Brain Res.* **240,** 245-258.

Svehla,M., Morberg,P., Bruce,W., Zicat,B., and Walsh,W.R. (2002) The effect of substrate roughness and hydroxyapatite coating thickness on implant shear strength. *J.Arthroplasty* **17,** 304-311.

Taylor,S.J. and Walker,P.S. (2001a) Forces and moments telemetered from two distal femoral replacements during various activities. *J.Biomech.* **34,** 839-848.

Taylor,S.J., Walker,P.S., Perry,J.S., Cannon,S.R., and Woledge,R. (1998) The forces in the distal femur and the knee during walking and other activities measured by telemetry. *J.Arthroplasty* **13,** 428-437.

Taylor,S.J.G. and Walker,P.S. (2001b) Forces and Moments Telemetered from Two Distal Femoral Replacements During Various Activities. *Journal of Biomechanics* **34,** 839-848.

Taylor,W.R., Roland,E., Ploeg,H., Hertig,D., Klabunde,R., Warner,M.D., Hobatho,M.C., Rakotomanana,L., and Clift,S.E. (2002) Determination of orthotropic bone elastic constants using FEA and modal analysis. *J.Biomech.* **35,** 767-773.

References

Tonino,A.J., Therin,M., and Doyle,C. (1999) Hydroxyapatite-coated femoral stems. Histology and histomorphometry around five components retrieved at post mortem. *J.Bone Joint Surg.Br.* **81,** 148-154.

Tsai,S. and Wu,E. (1971) A General Theory of Strength for Anisotropic Materials. *Journal of Composite Materials* **5,** 58-80.

Turner,C.H. and Cowin,S.C. (1988) Errors induced by off-axis measurement of the elastic properties of bone. *J.Biomech.Eng* **110,** 213-215.

Viceconti,M., Bellingeri,L., Cristofolini,L., and Toni,A. (1998) A comparative study on different methods of automatic mesh generation of human femurs. *Med.Eng Phys.* **20,** 1-10.

Whittle.M. (1993) Normal Gait. In *Gait Anlysis, an Introduction* Butterworth Heinemann.

Willie,B.M., Bloebaum,R.D., Bireley,W.R., Bachus,K.N., and Hofmann,A.A. (2004) Determining relevance of a weight-bearing ovine model for bone ingrowth assessment. *J.Biomed.Mater.Res.A* **69,** 567-576.

Wirtz,D.C., Pandorf,T., Portheine,F., Radermacher,K., Schiffers,N., Prescher, A., Weichert,D., and Niethard,F.U. (2003) Concept and development of an orthotropic FE model of the proximal femur. *J.Biomech.* **36,** 289-293.

Wirtz,D.C., Schiffers,N., Pandorf,T., Radermacher,K., Weichert,D., and Forst,R. (2000) Critical evaluation of known bone material properties to realize anisotropic FE-simulation of the proximal femur. *J.Biomech.* **33,** 1325-30.

Wolff,J. (1986) *The law of bone remodelling / Julius Wolff ; translated by P.G.J. Maquet and R. Furlong.* Berlin; New York : Springer-Verlag .

Wong,M., Papa,A., Lang,T., Hodis,H.N., Labree,L., and Detrano,R. (2005) Validation of thoracic quantitative computed tomography as a method to measure bone mineral density. *Calcif.Tissue Int.* **76,** 7-10.

Wu (1972) Optical experimental Measurements of Anisotropic Failure Tensors. *J.Composite Materials.*

Xu,W., Crocombe,A.D., and Hughes,S.C. (2000) Finite element analysis of bone stress and strain around a distal osseointegrated implant for prosthetic limb attachment. *Proc.Inst.Mech.Eng [H.]* **214,** 595-602.

Xu,W., Xu, D.H. and Crocombe,A.D., (2006) Three-dimensional finite element stress and strain analysis of a transfemoral osseointegration implant. *Proc.Inst.Mech.Eng [H.]* **220,** 661-670.

Xu,W. and Robinson,K. (2008) X-ray image review of the bone remodeling around an osseointegrated trans-femoral implant and a finite element simulation case study. *Ann.Biomed.Eng* **36,** 435-443.

Yamada and Ed.Evans,F.G. (1970) *Strength of Biological Materials.* Williams and Wilkins.

Yang,Y.C. and Yang,C.Y. (2008) The influence of residual stress on the shear strength between the bone and plasma-sprayed hydroxyapatite coating. *J.Mater.Sci.Mater.Med.* **19,** 1051-1060.

Ysander,M., Brånemark, R., Olmarker,K., and Myers,R.R. Intramedullary Osseo-integration. Development of a Rodent Model and Study of Histology and Neuropeptide Changes around Titanium Implants. Journal of Rehabilitation Research and Development 38, 183-190. 2001.

References

Zhang,M., Turner-Smith,A.R., Roberts, V.C., and Tanner,A. (1996) Frictional action at lower limb/prosthetic socket interface. *Med.Eng Phys.* **18,** 207-214.

Zhou,Y., Jiang,T., Qian,M., Zhang,X., Wang,J., Shi,B., Xia,H., Cheng,X., and Wang,Y. (2008) Roles of bone scintigraphy and resonance frequency analysis in evaluating osseointegration of endosseous implant. *Biomaterials* **29,** 461-474.

Zioupos,P., Currey,J.D., Mirza,M.S., and Barton,D.C. (1995) Experimentally determined microcracking around a circular hole in a flat plate of bone: comparison with predicted stresses. *Philos.Trans.R.Soc.Lond B Biol.Sci.* **347,** 383-396.